X-band radar data and predictive management in urban hydrology

Abdellah Ichiba

Thèse présentée pour obtenir le grade de

Docteur de l'Université Paris-Est

Spécialité: Sciences et Techniques de l'Environnement

par

Abdellah Ichiba

Ecole Doctorale : Sciences, Ingénierie et Environnement

Données radar bande X et gestion prédictive en hydrologie urbaine

X-band radar data and predictive management in urban hydrology

Thèse soutenue le 01 Avril 2016 devant le jury composé de :

Peter Molnar	*Rapporteur*	École Polytechnique Fédérale de Zurich
Robert Moore	*Rapporteur*	Centre for Ecology and Hydrology Wallingford
Marie-Claire Ten Veldhuis	*Examinateur*	Delft University of Technology
Dong-In Lee	*President de jury*	Pukyong National University
Philippe Bompard	*Co-encadrant*	Conseil départemental du Val-de-Marne
Auguste Gires	*Co-encadrant*	École des Ponts ParisTech
Ioulia Tchiguirinskaia	*Co-directeur*	École des Ponts ParisTech
Daniel Schertzer	*Directeur de thèse*	École des Ponts ParisTech

Acknowledgements

First of all, I would like to express my sincere gratitude to my supervisors Daniel and Ioulia for their continued involvement and assistance throughout this work. Thank you very much for this great opportunity you offered to me. I would like also to thank Auguste and Philippe for their involvement for the success of this work. Thank you very much for your comments and suggestions which I'm sure helped me to improve this work.

I would also like to show my gratitude to my thesis committee, Professor Peter Molnar, Professor Robert Moore, Professor Marie-Claire ten Veldhuis and Professor Lee Dong-In. Thank you for giving of your time to report and to discuss this dissertation. I appreciated very much your comments and suggestions for improving this document.

My sincere thanks also go to all my colleagues from HM&CO unit for their support and the pleasant moments we spent during the three years. Thank you Catherine and Annick for being here for all kinds of support.

A special thanks to my family, mum, dad, sisters, brothers and to my fiancee Myriam. Thank you very much for your support. This work would not have been possible without your encouragements. I can not forget to thank all my friends who supported me, Abdessamade, Yassine, Hassan, Yacine, Zayed, Ayoub, Ismail, Yassine, Zouhair, Mohamad, Ali, ...Thank very much for your help, you were a great support to me.

Finally I would like to acknowledge the financial support of the County Council of Val-de-Marne (CD94), the ANRT association (http://www.anrt.asso.fr) and RainGain project (http://www.raingain.eu).

Abstract

The main goal of this thesis was to achieve a reliable management tool of storm water storage basins using high resolution X-band radar. It turned out that it required several research developments.

The analyzed case study is a 2.15 km^2 urban catchment located in Val de Marne county and equipped at its downstream with a stormwater retention basin of 10000 m^3. It has a twofold goal: storm water decontamination and flood protection by volume storage. Operationally the management strategies associated with these two aims are conflicting; hence, a predictive management has been set up: a routine exploitation of the basin in the anti-pollution mode, and a switch to the flood protection mode when needed. It should be based on reliable knowledge of short-term rainfall forecasts.

A common way to respond to operational needs of the predictive management is to set up a warning system based on the use of radar data. For example, the CALAMAR system relies on the use of single-polarization raw radar data, coming from Meteo-France radar network, being processed with the conventional conversion methods of radar reflectivity Z to rainfall intensity R followed by a calibration with rain gauge. However, the reliability of such warning systems has been subject to debate, often due to a questionable quality of the resulting radar rainfall estimates, compared to local rain gauges. Therefore a new methodology for more meaningful comparison of radar rainfall field products was developed during this PhD project. Being rooted to the multifractal theory, it allows a comparison of the structure and the morphology of rainfall fields in both space and time through scales. It was initially tested on CALAMAR and Meteo-France rainfall products before being applied for results confirmation on initial data from a X band radar, acquired by Ecole des Ponts ParisTech in the framework of the European project RainGain and providing data at higher resolution (up to 100 m in space and 1 min in time). The obtained results highlight the crucial influence of raw data processing on the scaling behavior, and permit to establish that the calibration used by CALAMAR may influence the quality of rainfall estimates. Such conditions would be very difficult to detect with widely used conventional methods, which rely on a very limited number of radar pixels (only those containing rain gauges). Further extensions of the proposed methodology open new horizons for the rainfall data merging.

While the scientific literature, notably around the TOMACS experiment in Japan and CASA one in the United States, highlights the operational benefits of higher resolution rainfall measurements thanks to X-band radars, its impact on the performance of hydrological models still remains a subject of debate. Indeed previous research, mainly based on conceptual hydrological models remains inconclusive. To overcome these limitations,

we used two models relying on two very distinct modeling approaches: CANOE (semi-distributed and conceptual) and Multi-Hydro (fully distributed and physically based research model developed at ENPC). An operational version of CANOE and a new much finer configuration, which increases the sensitivity of the model to spatio-temporal variability of small-scale rainfall, were used. Several extensions of the Multi-Hydro were developed, including an optimization of its resolution, which greatly improves its whole functionality. It appears from this work that by taking into account the spatial and temporal variability of small-scale rainfall, the performance of hydrologic models can be increased up to 20%.

Overall, we believe that this dissertation contributes to the development of new reliable and operational tools to use in their full extent the high-resolution X-band data.

Keywords

X-band radar, predictive management, hydrological modeling, rainfall variability, multifractal analysis.

Résumé

L'objectif principal de cette thèse était de parvenir à un outil de gestion fiable des bassins de rétention d'eaux pluviales en utilisant les données radar en bande X. Il s'est avéré que cela nécessite plusieurs développements de recherche.

Le cas d'étude considéré est un bassin versant urbain de 2.15 km^2, équipé à son aval d'un bassin de rétention des eaux pluviales d'un volume de 10000 m^3. Cet ouvrage assure un double rôle de traitement des eaux pluviales et de prévention des inondations par stockage du volume. Opérationnellement les modes de gestion associés à chacun de ces objectifs sont antagonistes si bien qu'une gestion prédictive a été mise en place ; exploitation routinière en mode anti-pollution et basculement vers le mode anti-inondation en cas de besoin. Il doit se faire sur la base d'une connaissance sûre de la situation pluvieuse prévue à court terme.

Une façon courante de répondre aux besoins opérationnels de la gestion prédictive est de mettre en place un système d'alerte basé sur l'utilisation de données radar. Le système CALAMAR par exemple, repose sur l'utilisation des données radar brutes à mono polarisation du réseau radar de Météo-France; traitées avec des méthodes classiques de conversion de la réflectivité radar Z en intensité de pluie R et une calibration avec des pluviomètres. Cependant, la fiabilité de ce système fait débat, notamment vis-à-vis de la qualité de la mesure radar obtenue. Une nouvelle méthodologie de comparaison de produits radar a été développée au cours de cette thèse. Elle repose sur le cadre théorique des multifractals et permet une comparaison de la structure et de la morphologie des champs de précipitations dans l'espace et le temps à travers les échelles. Cette méthode a d'abord été appliquée sur les produits CALAMAR et Météo-France, puis, pour confirmer certains des résultats, sur les premières données d'un radar bande X, acquis par l'Ecole des Ponts ParisTech dans le cadre du projet Européen RainGain et fournissant des mesures de précipitations à des échelles plus fines (jusqu'à 100m en espace et 1 min en temps). Les résultats obtenus mettent en évidence l'influence cruciale des méthodes de traitement des données brutes sur la variabilité spatio-temporelle à travers les échelles, et permettent d'établir que la calibration utilisée par CALAMAR peut amoindrir la qualité des mesures de pluie. Elles seraient très difficiles à détecter par les méthodes classiques largement répandues, n'impliquant qu'un nombre très limité de pixels radar (seulement ceux correspondants aux pluviomètres au sol). Des extensions de la méthodologie proposée ouvriront de nouveaux horizons pour la calibration des données de pluie.

Alors que la littérature scientifique, notamment autour des expériences TOMACS au Japon et CASA au Etats-Unis, souligne l'importance opérationnelle d'une mesure de

pluie plus détaillée grâce au radar en bande X, son impact sur les performances des modèles hydrologiques fait encore débat. Les recherches antérieures, basées pour la plupart sur des modèles conceptuels, ne sont pas concluantes. Ainsi pour dépasser ces limites, nous avons utilisé deux modèles impliquant des approches de modélisation différentes: CANOE (semi-distribué et conceptuel) et Multi-Hydro (distribué et à base physique; développé à l'ENPC). Une version opérationnelle de CANOE et une nouvelle configuration plus fine améliorant considérablement la sensibilité du modèle à la variabilité de la pluie ont été utilisées. Plusieurs développements ont été apportés à Multi-Hydro, y compris une optimisation de sa résolution, ce qui améliore grandement l'ensemble de ses fonctionnalités. Il ressort de ce travail qu'en prenant en compte la variabilité spatio-temporelle des précipitations à petite échelle, la performance des modèles hydrologiques peut être augmentée jusqu'à 20%.

Nous pensons que cette thèse a contribué à la mise au point de nouveaux outils opérationnels et fiables, ayant la capacité de prendre en compte les données en bande X haute résolution.

Mots Clés

Radar bande X, gestion prédictive, modélisation hydrologique, Variabilité de la pluie, analyse multifractale.

Contents

List of Figures

List of Tables

Abbreviations

QPE	**Q**uantitative **P**recipitation **E**stimation
QPF	**Q**uantitative **P**recipitation **F**orecast
DEM	**D**igital **E**levation **M**odel
GIS	**G**eographic **I**nformation **S**ystem
CD94	**C**onseil **d**epartemental du Val-de-Marne
ENPC	**E**cole **N**ationale des **P**onts et **C**haussées
BRGM	**B**ureau de **R**echerches **G**éologiaues et **M**inières
DSEA	**D**irection des **S**ervices de l'**E**nvironnement et de l'**A**ssainissement
HM&CO	**H**ydrology **M**eteorology & **Co**mplexity
WMO	**W**orld **M**eteorological **O**rganisation
DTM	**D**ouble **T**race **M**oment
TM	**T**race **M**oment
UM	**U**niversal **M**ultifractal
PRT	**P**ulse **R**epetition **T**ime
PRF	**P**ulse **R**epetition **F**requency

Symbols

R	rainfall intensity	(mm/h)
Z	radar reflectivity factor	$\mathrm{mm}^6\mathrm{m}^{-3}$
η	radar reflectivity	$dBzm^{-3}$
r	target distance from the radar	km
c	speed of light	km/s
G	radar antenna gain	dB
λ	wavelength	cm
θ	horizontal beam-width	rad
ϕ	vertical beam-width	rad
h	pulse length	m
PRT	pulse repetition time	s
PRF	pulse repetition frequency	Hz
$\|K\|^2$	complex index of refraction	
Z_e	equivalent radar reflectivity	$\mathrm{mm}^6\mathrm{m}{-}3$
σ	complex index of refraction	
Z_h	the horizontal reflectivity factor	dBz
Z_{DR}	the differential reflectivity	dBz
ϕ_{dp}	the differential phase	rad
ρ_{hv}	the correlation coefficient	
C_F	radar/rain gauge adjustment factor	
K_{dp}	the specific differential phase	rad/km

Introduction

Climate change and extensive urbanization are most pressing concerns of our everyday life. Environmental changes impact the hydrological processes sometimes at very fine scales, and we are more and more often facing an increased pluvial flood risk in European cities. Hence, the stormwater management is now also performed at smaller spatial scales (at the district or even at the street scale), putting on evidence the crucial necessity to have detailed knowledge on rainfall processes at these scales.

Rain gauges are traditionally used to measure precipitation, because they are cheap and provide direct and robust rainfall measurements. Their main shortcoming is that they represent a very limited space. Thus, even a dense network of rain gauge gives little information on the fine spatial distribution of precipitation. On the contrary, weather radars are used to characterize the precipitation over a large surface. However, unlike rain gauges, the radar does not measure the precipitation directly, but the "backscattering" by precipitation echoes of the transmitted signal. In radar meteorology, one of the main objectives is to provide estimates as accurate as possible of the precipitation rate R known as Quantitative Precipitation Estimation (QPE).

For many years, most of the national meteorological services have introduced networks with C band and S band radars to cover all concerned areas. However, these radars cannot easily be used by small entities and local authorities because of their price and their size. Indeed, the development of X band radars and their use for urban water management applications is growing over the years, following the increased demand for high-resolution QPE and more localized rainfall description.

The development of X band radars is further motivated by numerous scientific publications that discuss the results from operationally oriented experiments with X-band radars, including TOMACS experiment in Japan (https://www.wmo.int/pages/prog/arep/wwrp/new/documents/Doc4_6_TOMACS_RDP_proposal_20130704.pdf) and CASA experiment in the United States (http://www.casa.umass.edu/main/casa-nsf/) that highlight the multiple benefites from the more detailed rainfall information, in particular for improving forecasts and flood mitigation.

In the European level, a research project, INTERREG RainGain (http://www.raingain.eu/en/four-cities-gain-rain) involving 13 partners among them local authorities

and research institutions, was conducted in four European countries. The project aims to improve the prediction of pluvial floods in urban cities. It develops and tests innovative tools and practices based on the use of high resolution radars in four pilot cities: Leuven, London, Paris and Rotterdam. Two new X band radars were installed in the framework of this project in Paris and Rotterdam. The one installed in Paris has been acquired by Ecole des Ponts ParisTech and installed on its campus in Paris region. Since May 2015, this radar produces rainfall information at small space (up to 100 m) and time (up to 1 min) scales.

In Paris, the pilot study area is a 2.15 km^2 urban catchment located in Val-de-Marne County (Southeast of Paris). It includes in its downstream a retention basin of 10000 m^3 used for either storm water decontamination or flood protection by volume storage. These two objectives are conflicting and cannot be applied in real time using the traditional management approach. Therefore, a predictive management strategy has been set up for this site. It could be seen as a routine exploitation of the basin in the anti-pollution mode, while a switch to the flood protection mode remains possible and should be carefully evaluated on the basis of mostly reliable short-term rainfall forecasts.

An operational warning system based upon the use of radar data was set up to respond to operational needs of the predictive management. CALAMAR system relies mainly on the use of single-polarization raw radar data, coming from Meteo-France radar network, being processed with the conventional Z-R conversion methods. Hence, the reliability of this warning system has been subject to debate, often due to a questionable quality of the resulting radar rainfall estimates.

Framework and objectives

This work has been conducted in the context of a collaboration between HM&Co (Hydrology Meteorology & Complexity) research unit of Ecole des Ponts ParisTech and the County Council of Val-de-Marne (CD94) in the framework of the European research project RainGain. The main goal of this dissertation is to achieve a more reliable management tool for the storm water retention by using high resolution X-band polarimetric radar information. Hence, the first chapter of this dissertation presents key issues in urban flood risk management, mainly within the context of the Sucy-en-Brie catchment, which is one of the case studies of the RainGain project. Possible effects of climate change and the impact of urbanization process are discussed as well. The predictive

management strategy operated for the retention basin is presented with details on the functioning of CALAMAR forecasting system and the analysis of main issues encountered. The high rate of false early warnings was mainly related to wrong settings of the system and questionable quality of radar rainfall measurements. It finally turned out that long-range dissertation goals required several research developments that fall into three directions:

1. It was crucial at the fist stage of this work to identify specific needs in terms of reliable and high quality rainfall information that the predictive management requires. The analysis of the available radar products in Paris region and main issues encountered with the actual forecasting system CALAMAR is of huge interest as well. Indeed, an innovative comparison methodology was developed as a part of this work for more meaningful comparison of radar rainfall field products. Being rooted to the multifractal theory, the developed methodology allows a comparison of the structure and the morphology of rainfall fields in both space and time which would be difficult to achieve using the conventional radar - rain gauge comparison methods being largely used until now, when a very limited number of radar pixels (only those containing rain gauges) are involved. Hence, the second chapter focuses on rainfall data analysis. In fact, various investigations were performed to analyze the quality of rainfall radar products available in Paris region: Meteo France and CALAMAR use the same single polarization raw data coming from a C band radar but rely on different QPE algorithms. Thus, the new developed methodology was initially applied to perform a comparison between CALAMAR and Meteo-France rainfall products.

2. Exploration of hydrological responses at various space-time scales remains a crucial stage in approaching the cross-scale (or systemic) hydrological modeling of urban catchments. Indeed, various investigations were conducted in the framework of this dissertation about the needs of small-scale rainfall information for urban modeling applications. In fact, the impact of such detailed information on the performance of hydrological models still remains a subject of debate. Most of the former research carried out in this direction remains inconclusive about the advantage of such detailed rainfall information for modeling applications. Furthermore, most of these works involve only conceptually based models. Thus, two models that are based on two very distinct modeling approaches were used to wholly investigate the

impact of small-scale rainfall data on the performance of hydrologic models. Several improvements were implemented on these models following a deep reflection. Hence, the third chapter of this dissertation is entirely devoted to hydrological modeling of urban catchments. Three complementary studies were conducted in this context with the aim of providing answers to various questions related to the use of high resolution rainfall data for modeling applications. Two urban storm models were involved in this work and were implemented at various spatial scales for the needs of such investigations.

3. Finally, first X-band polarimetric radar data available from the dual polarization Doppler X- band radar were used to confirm some of initial findings of this work, in particular the spatio-temporal variability of rainfall information and the accuracy of the X-band polarimetric radar data. This accuracy was investigated as well using urban storm models.

Chapter 1

Sucy-en-Brie case study : Flooding risk and management strategy

The Sucy-en-Brie catchment was chosen as a case study for this work and to participate in international research studies conducted in the framework of RainGain project. This choice was motivated by the fact that this catchment represents a typical case study to show the operational interest of using radar data in real time for flooding management.

In fact, the Sucy-en-Brie catchment and in general the Val-de-Marne County are facing a major flooding risk due to their challenging local environment, and the high urbanization process that has been conducted in the past and increased their vulnerability to flood risk. The management strategy that was adopted to control flooding was based on the implementation of retention basins in critical catchments of the County, most of them ensure a double role, the protection against flooding by storing rainwater during extreme events and the decontamination of the stored water before its release into the natural environment. The management of 2 retention basins in Val-de-Marne County is performed using a forecasting system based upon on the use of radar data in real time.

However, first feedbacks from the use of the forecasting system are not entirely satisfactory due to some reasons that we will evoke later in this thesis. Consequently, the County Council of Val-de-Marne decided to participate with this case study in the European project RainGain with the aim of understanding difficulties surrounding the current

experience and to investigate possible improvements that the new high resolution and Dual polarization X-band radar bring to this experience.

1.1 Urban flooding risk

Urban environments have experienced big transformations over years in order to satisfy the human needs, the significant growth of urban population and migration issues increase pressure in urban areas and in the same time their vulnerability to flooding risk. The sustainable management of urban flooding risk is becoming an increasingly challenging task for urban communities and local authorities to address. On one hand the continuing urbanization process produces large runoff which the drainage networks cannot deal with, while on the other hand flooding are indeed increasing, both in terms of frequency and intensity.

The urban flooding risk can be defined according to Blong (1996), Crichton (2007) as a function of three important elements that reflect together the level at which the city is faced with flooding; (1) the impact of natural hazards, (2) the exposure of urban populations and infrastructures to flood and (3) the last one is related to the vulnerability of urban environments, each of these three elements will be detailed in the following points, with discussion about how they participate to the increase of flooding risk.

- **Natural hazards:** floods are the results of meteorological extremes that are usually aggravated by the hydrological behavior of urban catchments and human factors. Meteorological extremes consist on the increase of rainfall intensity and the frequency of severe events. This was noticed in many cities around the world.

  The possible effects of climate change in precipitation were subjects of several recent works (Alexander (2016), Moberg et al. (2006), Easterling (2008)) that are summarized in the Intergovernmental Panel on Climate change (IPCC) Fourth Assessment (AR4) Trenberth et al. (2007). Changes on precipitation concern the total amount, the rain intensity, the frequency of heavy events but also the type of precipitation. In general, a contrast was noticed in terms of the obtained conclusions.

Huffman et al. (2009) suggests that no trend was observed on precipitation since 1979, while Gu et al. (2007) confirms using the Global Precipitation Climatology Project (GPCP) data that the global change in precipitation is near zero but with variability between regions; weather is more rainy in America, Europe and Asia, and significantly much less rainy in southern Africa and South Asia (Indian subcontinent). According to (Mote (2003), Knowles et al. (2006)), more precipitation falls now as rain rather than snow. In terms of intensity, an increase of extreme flooding events was observed in the 20^{th} century (Milly et al. (2002), Karl and Trenberth (2003)) as a result of the increase of heavy rainfall in many areas around the world even in places where total precipitation is decreasing (Easterling et al. (2000), Peterson et al. (2002), Klein Tank and Können (2003), Groisman et al. (2005), Alexander et al. (2006), Groisman and Knight (2008)).

Royer et al. (2008b) analysed the output of climate models and noticed despite somehow conflicting tendency, an increase of rainfall extremes is expected in France. Hoang et al. (2014) analysed rain gauge time series from the Paris area and found an increase in extremes only at scales smaller than 1h. Trenberth et al. (2007) noticed that the precipitation season has become longer by up to 3 weeks in some regions over the last 50 years.

Hydrological factors reflect the natural vulnerability of the catchment prior to human intervention, they are linked to the capacity of the catchment to deal with the amount of water generated, and how its hydrological conditions can increase the flood risk. In fact the infiltration capabilities of the subsurface and the topography of the urban catchment are factors that can aggravate the urban risk by limiting the infiltration and promoting the urban runoff, the topography can lead to the increase of the runoff velocity and to the decrease of the catchment response time.

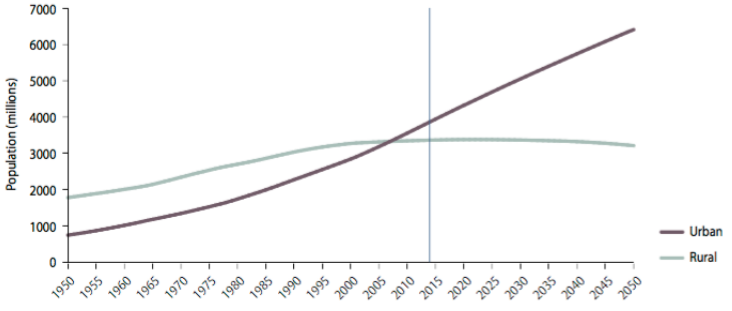

Figure 1.1: Distribution of the world population: the urban population is continually increasing and expected to be 66% in 2050 (United Nations (2014)).

In the meantime, human activities are changing the whole urban water cycle. The land use changes increase runoff and limit infiltration, the inefficiency of the drainage network and the absence of technical resources are factors that can contribute to flood disasters and increase damages.

The urbanization process is continually increasing following the increase of urban population, according to a recent United Nations report United Nations (2014) 54 per cent of the world population live actually in urban areas instead of only 30 per cent in 1950 and the ratio is projected to be 66 per cent in 2050 (Figure 1.1). The number of megacities (cities with more than 10 millions inhabitants) is increasing as well from 10 megacities in 1990 representing home for 153 million people to 28 megacities in 2014 representing home for 453 million people. This will participates on the creation of significant hazards.

The impact of urbanization and land use changes were studied in many case studies around the world (Nardi et al. (2015), Chen et al. (2015), Wibben (1976), Kang et al. (1998), Schulz and of Civil Engineering (1976), Hollis (1975), Ramesh (2013), Braud et al. (2013), Mulholland and Waikato (2006), Wheater et al. (2012), Ali et al. (2011)) in the purpose of understanding how they can affect the hydrological behavior of urban areas and increase flooding risk. These kind of works rely often on historical data available or in urbanization scenarios modeling.

Chen et al. (2015) observed in Xiaoqing catchment (located at the eastern end of the Yellow River basin in the province of Shandong, China) that the increase of build-up area from 19.1 % in 1995 to 40.5 % in 2008 has produced an increase of the peak discharge about 11.1 % and the total volume about 15.3 %. Ali et al. (2011) simulated the impact of a projected urbanization plan on Lai Nullah basin in Islamabad, their results show a possible increase of runoff by more than 51.6% as well as the peak discharge by more than 45.4%, while results coming from Braud et al. (2013) for a peri-urban catchment show an increase in impervious cover from 11% in 1960 to 44% in 2010, this change was accompanied by a decrease of the characteristic flood duration by 50% and an increase of the peak flow by over 400%.

The integration of new sustainable land use planning that integrates and interacts more and more blue and green spaces has emerged in recent years as a key solution to limit the urbanization effects (Barraqué (2014), Scolobig and Marchi, O'connell

et al. (2010), Newson (1991), Ferreira Carneiro and Gomes (2012), Clark et al. (1981))

- **Exposure:** the population explosion and cities expansion get people to build in river beds, or in zones known historically as flooding areas, this is what the exposure means, those houses and infrastructures are much more exposed to urban flood risk. In France, the 95-101 law of 2 February 1995 related to the protection of the environment recommends all cities to elaborate and publish a flood risk prevention plan (PPRI, Plan de Prevention des Risques Inondation).

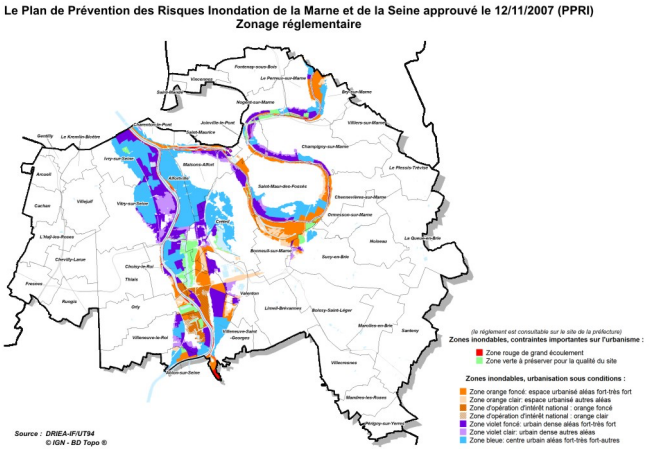

Figure 1.2: Flood risk prevention plan of Val-de-Marne County

This plan (example in Figure 1.2) must include a mapping of areas exposed to flood risk, and determine which construction rules should be considered when building in these areas. In practice, local authorities based on historical hazard map must define three zones:

- Red zone with high flood risk and where all constructions are prohibited.
- Blue zone where some rules are defined for all constructions, for example it may be required that the lowest floor level of the construction must be above the level observed during the historical flooding event.
- White area without risk of flooding, so no specific requirements for constructions built in this area.

Other zones can be defined as well by the local authority to adapt the given solution to the level of the flood risk.

- **Urban vulnerability:** The vulnerability is the last component of the flooding risk equation, it is considered as the extent of harm, which can be expected under certain conditions of exposure, susceptibility and resilience. Different approaches are used for the vulnerability assessment. The Flood Vulnerability Index (FVI) is expressed as function of exposure, susceptibility and resilience as follow (Balica and Wright (2010)):

$$Vulnerability = exposure + susceptibility - resilience \tag{1.1}$$

So the consequences of flooding depend on how vulnerable are people and facilities to flooding risk. This vulnerability can be reduced even in areas where the exposure is high by taking appropriate precautions in advance, knowing what should be done to limit the danger and by providing assistance during and after flooding. The vulnerability assessment allows to understand perception of risk, to quantify performance of resilience strategies taken into account and to support these kind of decisions.

1.1.1 Urban flooding damage

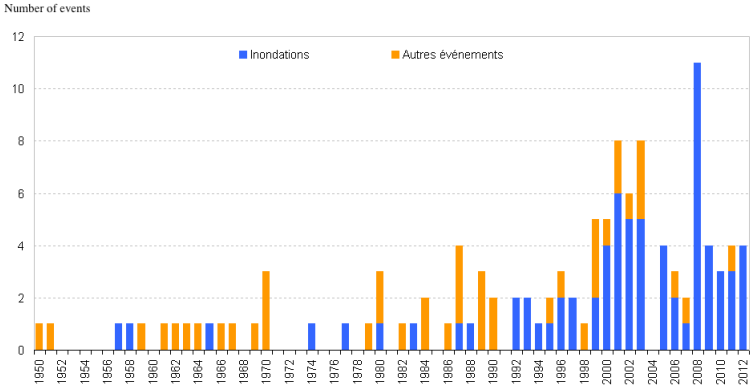

Figure 1.3: Severe natural events occurred in France between 1950 and 2012. Only events that caused more than 10 dead or over 30 million euros of damage are reported here (from Medde (DGPR), 2013)

Urban zones are increasingly exposed to natural disaster risk, especially floods. In France, flooding remains the first natural risk with 72% of decrees state of natural disaster issued between October 1982 and mid-November 2014. Figure 1.3 shows that

the number of flooding events occurred in France is increasing over the last 25 years. Some exceptional rainfall events listed below have caused considerable damages and losses especially in the south of the country:

- In 27 of February 2010, a violent windstorm Xynthia hits France and many European countries, it was accompanied by very strong winds up to 160 km.h^{-1} and very heavy flooding. It caused the death of 59 people in Europe, most of them in France (47 people were killed). Material damages were estimated to 2.5 billion Euros.

- The flood occurred in 2010 in the Var County is known as one of the largest the country has experienced in recent years; heavy rainfall generates between 150 mm to 397 mm in the area making a total of 26 dead and over a billion euros of material damages.

- In June 2013, the South West region was further hit by severe floods, balance sheet; 3 dead and 2 000 inhabitants had to leave their homes before the rising of water level. The state of natural disaster was declared and damages were estimated to 500 million euros.

- More recently, during the 2015 summer, 17 people died due to flooding following violent and unpredicted storms that hit 32 towns in the Alpes-Maritimes. 180 mm of water which represents 10% of the normal annual precipitation of the region fall between 19h and 22h. Insurers estimated damage to more than 500 million euros.

This increase on flooding intensity and frequency has consequences on the economic and social costs. A recent work (Jongman et al. (2014)) estimated floods cost in the European level averaged 4.9 billion euros per year between 2000 and 2012, 12 billion euros just for the June 2013 flooding event as is it considered as the most expensive natural catastrophe. According to Jongman et al. (2014), these average losses could increase to 23.5 billion euros by 2050.

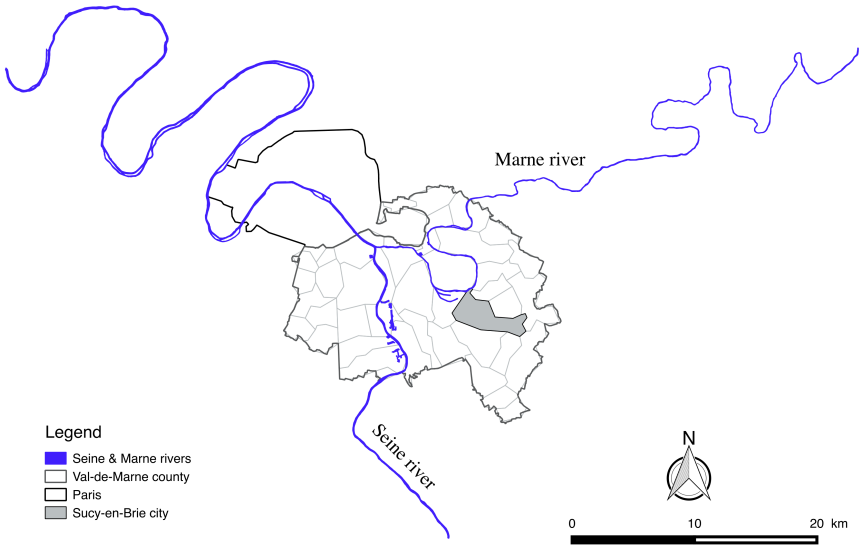

Figure 1.4: Localisation of Sucy-en-Brie City in the southeast of Paris

The Val-de-Marne County (Figure 1.4) is one of 8 counties of the Greater Paris region, its surface is 245 km^2 and its population is more than 1.35 millions. The County has experienced significant and rapid urbanization process starting from the 1900s (Figure 1.5) due to its proximity to Paris, its pleasant living environment and the consequences of the demographic explosion noticed during the last decade. The city of Sucy-en-Brie as example saw its population goes from few thousand people in the 1950s (8570 in 1954) to more than 25 000 in the 1990 (25 839 in 1990), this has a direct consequences on the increase of flooding risk.

The flooding risk is even more significant because of the presence of two main rivers in Paris region that cross the County over 15 km for the Seine river and 10 km for the Marne river. So any increase of the water level in these two rivers will have dramatic and disaster consequences on an important part of the County. The County has experienced several flooding events in the past, the reference and most disaster occurred in 1910 (Figure 1.6). If such exceptional situation should occur, more than 250 000 people of Val-de-Marne will be flooded, without forgetting material damages (cut in electricity, potable water, transport, ...). Other events were recorder later in 1924, 1955 and 1982 as well as a series of flood between 1999 and 2001.

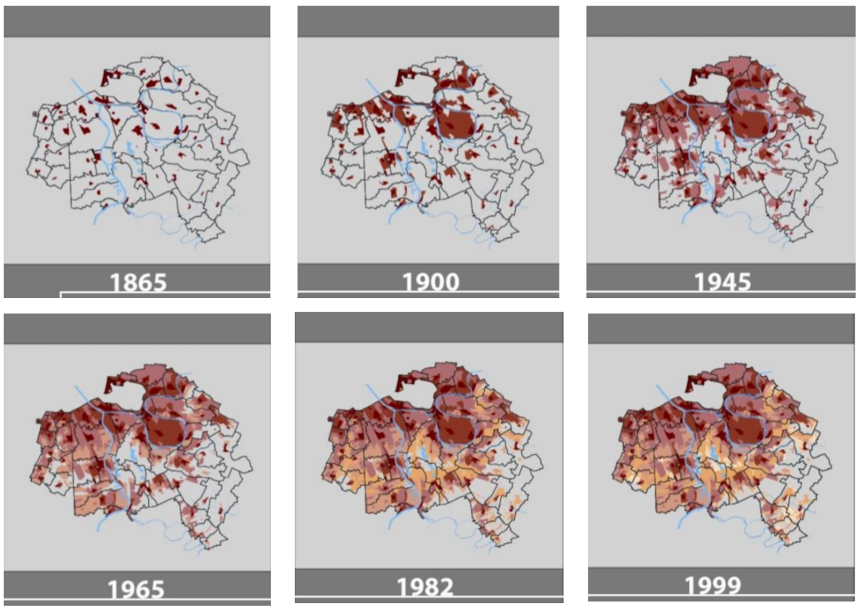

Figure 1.5: Urbanization development in Val-de-Marne County (1865-1999)

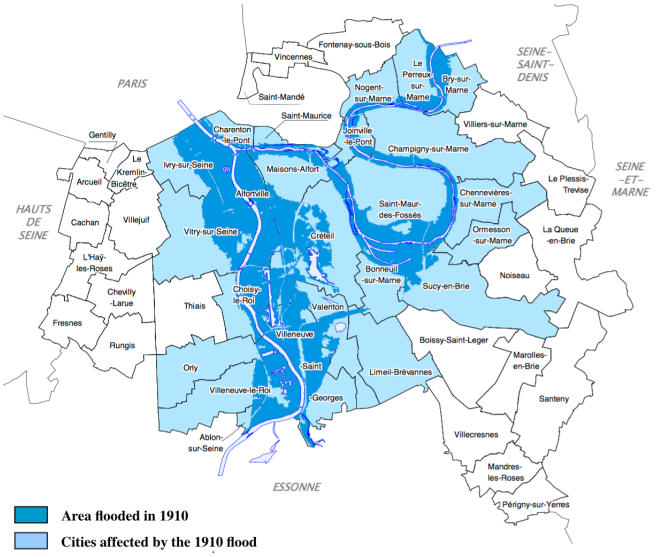

Figure 1.6: Area affected by the 1910 flood event

1.1.2 Urban pollution risk

In addition to the flood risk, urban areas are also facing a major pollution risk. In fact, several activities in urban environments generate significant pollution. Road traffic, industrial activities and soil erosion are often pointed out as main sources of pollutants that can have disastrous consequences on the quality of the receiving water bodies. Several investigations and works (Kittinger et al. (2013), Qureshi, Goonetilleke et al.

(2005), Lee (2000), Makepeace et al. (1995), Scuri et al. (2006), Borja et al. (2004), Sands and Galizzi (2006), Kaika (2003)) were carried out recently in order to list all contaminants that can be found in storm water and the possible relation between rainfall intensity and storm water pollutant load.

Makepeace et al. (1995) presented a literature review that identify and quantify contaminant data available on storm water, listing their specific chemical, physical, and biological parameters. Goonetilleke et al. (2005) investigate and found a relationship between the duration, intensity and amount of rainfall and the occurrence of peak microbial populations.

Certain measures were considered in the European level to investigate and preserve the physical, chemical and biological quality of aquatic systems. The European Water Framework Directive (THE EUROPEAN PARLIAMENT AND THE COUNCIL OF THE EUROPEAN UNION (2000)) adopted in 2000 goes in this direction. It obligates all European countries to control the quality of storm water before its release into water bodies and set a target of reaching a good ecological status of all aquatic systems.

Consequently, all technical solutions that were developed to control flooding in urban areas should also integrate a minimum level of water decontamination in their goal. This makes managing storm water in urban areas even more complex, and obligates urban water managers to consider new flood management processes that are more optimal and smart. The case study we presenting in this thesis is a perfect example of such management techniques that must rely on powerful tools including real time management systems and radar forecasting.

1.1.3 Urban flooding management

Several management techniques were developed and implemented in urban areas in order to cope with both the increased flooding and pollution risks. Their objective is to protect people from flooding and the natural environment from urban pollution sources by ensuring a minimum level of storm water decontamination. Theses techniques can be classified in three approaches depending on their goal and how they treat flooding situation. (1) The first approach is to locate all the effort at the outlet of the catchment, by implementing hard engineering structures. (2) The second one, which is more

sustainable is based on a distributed approach that relies on smaller constructions distributed over the catchment in order to control storm water volumes at their sources. In addition to these structural solutions, there are also (3) a non-structural approach that emerged in recent years, which is based on resilient strategies that showed their crucial interest in crucial situations.

The local traditional engineering approach regarding storm water management focuses only on building huge systems that can be part of a long-term solution. The most common practice is the detention and retention basins (Bergue and Ruperd (2000), Robinson et al. (2010), Travis and Mays (2008)), which are highly effective in controlling the peak flows but expensive to construct and to maintain. The main goals of all these techniques is to attenuate the possible effect of heavy rainfall on the downstream and to avoid the overflow of the sewer network. But, they are also the best candidates to implement storm water decontamination processes and to control thus the quality of all urban pluvial water generated at the catchment scale (Scherger and Davis (1982), Sébastian et al. (2014)).

Recently, a growing interest in adopting more sustainable techniques to control both the quality and the quantity of storm water runoff (Ellis and Revitt (2010), Ellis (2013), Strecker et al. (2004), Förster et al. (2004), O'connell et al. (2010), Clark et al. (1981), Jha et al. (2012), Martin et al. (2007)) has emerged. These systems are designed for source control in the framework of a distributed approach and are constructed taking into account the estimation of post-development stormwater flows and the catchment water balance. Alternative techniques can be better solutions from economic and environmental aspect. Their goal is to retain pluvial water and promote its infiltration , instead of leading it to the sewer system like conventional systems have done so far.

The new Low Impact Development (LID) approach aims to preserve or replicate the natural, pre-developed water cycle to maximize the on-site storm water control. In the USA and some other countries, they adopted the term Low Impact Development (LID) for techniques which are used to maintain the current peak flow below or equal to the peak flow that existed in the same area before the urbanization process for a given return period. In the UK the term Sustainable Urban Drainage System (SUDS) is adopted, while in Australia the term is Water Sensitive Urban Design (WSUD).

LID management practices include among others green roofs, dry wells, filter strips,

vegetated buffers and other multifunctional landscapes areas (the use of areas which have other primary functions, such as parking or sport fields as detention basins in case of flooding), wetlands, level spreaders, infiltration trenches, rain barrels and cisterns.

All these techniques are not applicable in all sites but this approach has some advantages towards the conventional one. They minimize the need for very large detention basins in the downstream as well as the pollutant loading by protecting pluvial water from pollution sources, they are more efficient, better aesthetically and they have a lower possibility of overall system failure.

Recent research works advocate the use of these three approaches together in urban catchment where the risk of flooding is high. Both alternative techniques and retention basins allow to handle the volume of water generated up to certain return period rainfall event, while resilience strategies (Gupta (2007), Su (2015), Dasgupta et al. (2015), Serre et al. (2012)) are used in emergency situations to limit damages and to promote a quick and safe return to the normal state of the catchment.

1.2 Sucy-en-Brie case study

Sucy-en-Brie city is located at the Southeast of Paris, in Val-de-Marne County which is a part of the big region of Île-de-France (Figure 1.4), its surface is 10.43 km^2 with a population of 25 900 inhabitants (2012 report). The city is connected to Paris with a train at the Sucy-Bonneuil station (30 min travel time to the center of Paris). Known historically as an agriculture area, the city is now highly urbanized with an imperiousness coefficient around 35%. The city is bounded at the north by the Marne river (one of the two main rivers in Paris region).

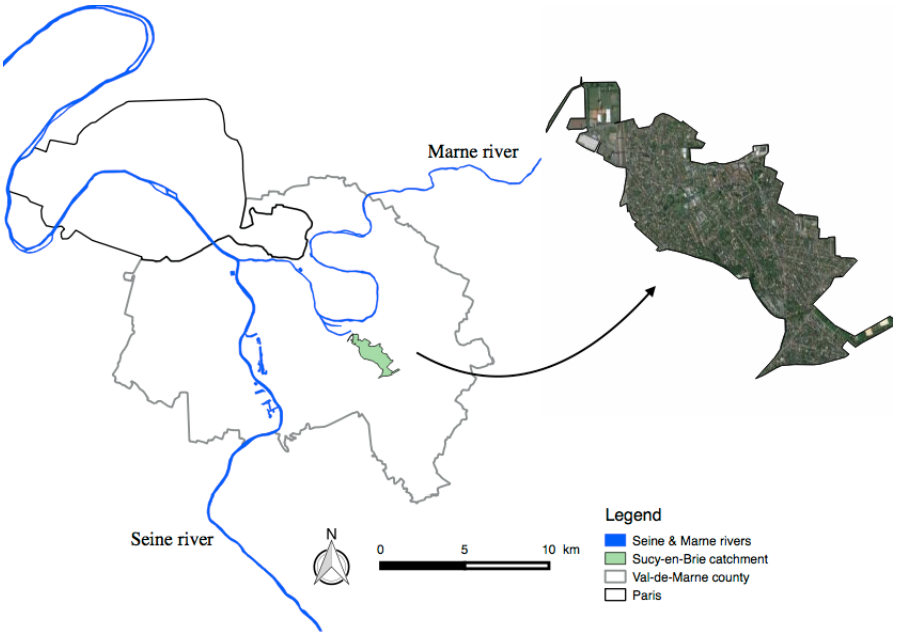

Figure 1.7: Localisation of the Sucy-en-Brie case study in Val-de-Marne County at the Southeast of Paris

The case study we study in this work is a part of the Sucy-en-Brie city. It is a 2.45 km^2 urban catchment (Figure 1.7), the area has suffered in the past from several flooding events as a consequence of: (1) the very steep slope ($\backsimeq$34m/km) that increases water speed and causes overflows in the downstream pluvial network and (2), the increase of imperiousness areas (34%) combined with a soil structure that limits infiltration to the subsurface. The sewer system in this area is a separate one and storm water is routed to the Marne River.

The County Council of Val-de-Marne manages and controls the main sewer system and is in charge of protecting people and facilities against flooding, as well as of protecting the natural environment from pollution sources. According to the topography, three areas can be identified in the Sucy-en-Brie catchment: (1) a plateau in the upstream with an elevation of approximately 100 m, (2) an alluvial plain in the downstream near the Marne river with an elevation of 32 m and between them there is (3) a hillside with a steep slope. The plateau and the hillside are housing areas (collective at 10% and individual at 90%) surrounded by green spaces, the plain is occupied by an industrial area and some sports fields, the Sucy Bonneuil train station is located in this area as well.

1.2.1 Data set

Data collection was performed at the beginning of the thesis by identifying needs for this study and contacting the various services that can provide them. The data was then analyzed and validated before being used in the various studies conducted as a part of this work. At the end of this step, a large and complete data set was available for this case study, including all geophysical data (land cover, topography, ...) in GIS (Geographic information system) format, different types of rainfall data and flow measurements as well.

- **GIS data :** GIS data is used in this study mainly to set up hydrological models. It is also used to describe the hydrological behavior of the catchment and to understand the challenging flooding risk in this urban area. It was made available by different institutes in the framework of a research collaboration with Ecole des Ponts ParisTech.
  - **Topography :**

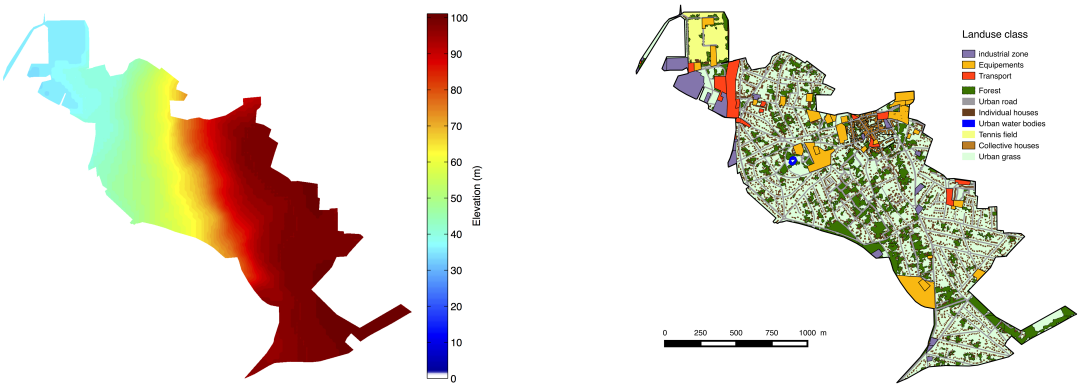

(a) **(b)**

Figure 1.8: Topography and land use for the Sucy-en-Brie catchment

The Digital elevation model (DEM) of the catchment was obtained from the IGN institute (French National Institute of Forest and Geographic Information), the spatial resolution of the data is 25 m, which is far from meeting the needs of studies conducted in the framework of this work. Linear interpolation was conducted to obtain data at a better resolution (between 5 m and 10 m).

According to the Digital Elevation Model (DEM) (Figure 1.8a), one can notice the very steep slope of this urban catchment. In fact, the altitude ranges

from 100 m at the upstream to just 32 m at the downstream (≃18 m/km), the slope is steeper (≃34 m/km) at the hillside in the center of the catchment, where the elevation goes from 90 m to 40 m. This has dramatic consequences on the hydraulic behavior of the catchment. Indeed, the topography promotes the urban runoff with high water velocity and limits infiltration into the subsurface, the catchment response time is very short (less than 15 min), which increases the pressure on the downstream pluvial sewer and explains the fact that the downstream is historically known as a flooding area.

– **Land use :** GIS data describing the landscape was obtained from the DSEA 94, the quality of this GIS data was very good with a precision up to 50 cm, but we had to deal with one land use class named "Other" in the original data, this class was just unknown and introduces a missing data. A comparison work with satellite images has been done in order to determine with which land use class can we correctly fill this missing data.

The city of Sucy-en-Brie has experienced big transformations over years, it is highly urbanized at the present time even if it includes several green areas. In terms of land use occupation (Figure 1.8b), at the downstream, there is a commercial zone around the Sucy-Bonneuil train station, an industrial area and some sport fields. Most of the surface of the city is occupied by individual housing, surrounded by green spaces, the collective housing area is located at the middle east of the catchment. The upstream includes a part of the great Notre-Dame forest, which is a 2050 ha forest that extends between the Val-de-Marne and the Seine-et-Marne counties.

– **Sucy-en-Brie subsurface structure :**

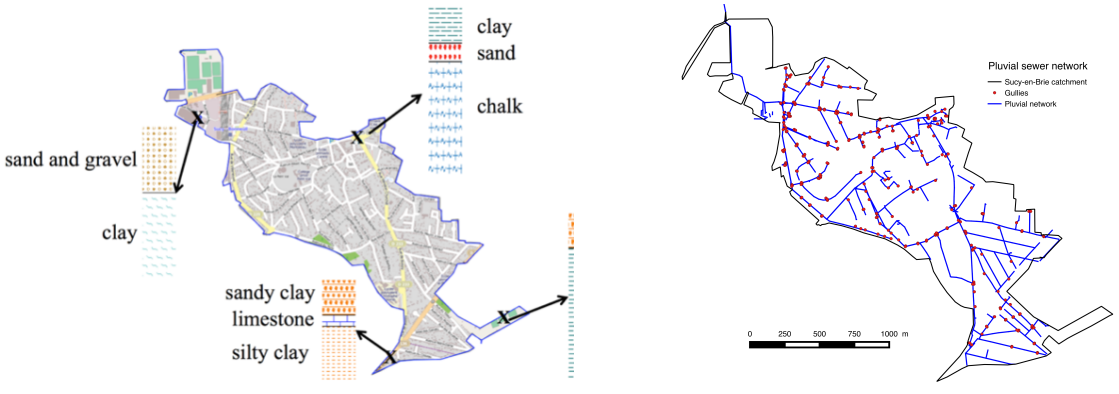

(a) **(b)**

Figure 1.9: The pluvial sewer system and soil data for Sucy-en-Brie catchment

The subsurface structure was elaborated using data obtained from the BRGM database (Office of Geological and Mining Research) related to the soil investigations done in the past before some construction works and archived in the BRGM database. The data (Figure 1.9a) clearly indicates that a layer of clay mixed in some places with sand dominates the majority of the catchment subsurface. In the downstream, near the river, we found a layer of sandy soil, so more permeable. This shows the complexity of this urban catchment from an hydrological point of view, in fact, infiltration in this catchment is very limited as well due to the subsurface structure. Physical parameters of soil needed for modeling were obtained from the literature and no measurements were done to verify or to estimate these parameters.

- **Sucy-en-Brie pluvial sewer system :** The sewer system in this catchment (Figure 1.9b) is a separate one, the pluvial one is routed in the downstream to the Marne river. The DSEA 94 of Val-de-Marne County (Direction des Services de l'Environnement et de l'Assainissement) is the service in charge of the control and the management of this system. Data describing the sewer system in this area is a very detailed one. It consists on 2030 nodes and 1015 elements of pipes representing a total length of 25 km, the average slope noticed is around 0.052.

- **Rain gauge data :**

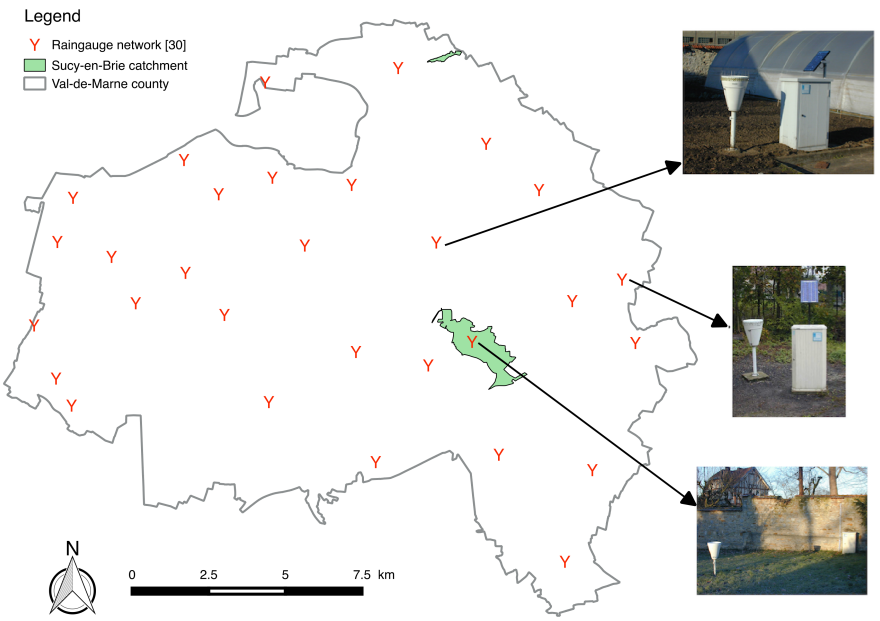

Figure 1.10: 30 rain gauges are deployed in the Val-de-Marne territory (245 km^2), most of then are operated in real time.

Point measurements data is coming from the rain gauge network of the County Council of Val-de-Marne (Figure 1.10). Thirty tipping bucket rain gauges with a 0.2 mm resolution are deployed in the Val-de-Marne County (245 km^2); most of them provide measurements in real time. The rain gauge located in the center of the study area is primary used to get rainfall information for modeling use, but it is not fully operated in real time due to some technical issues related to its local environment (real-time synchronization issues). Another rain gauge, that is 1 km away from the case study, can be used. Rain gauge data coming from the CD94 network is used both for modeling purposes and to perform a real time adjustment of the forecasting radar system CALAMAR. The data is validated by the CD94 services, but also by CALAMAR system based on a radar-rain gauge comparison performed in real time. Data used in this work was processed by the CD94 and sampled at 5 min temporal resolution, which is more convenient since radar data and flow measurements are available at 5 min as well.

Uncertainties related to point measurements will be discussed in the next chapter, and should not be neglected when used as reference data, especially during high rainfall rate where tipping bucket rain gauges tend because of their measurement principle to underestimate the rain intensity.

The entire times series recorded in 2013 and 2014 by the Sucy-en-Brie rain gauge were made available by the DSEA 94 as well as some events occurred in 2010, 2011, and 2012.

- **Radar data :**

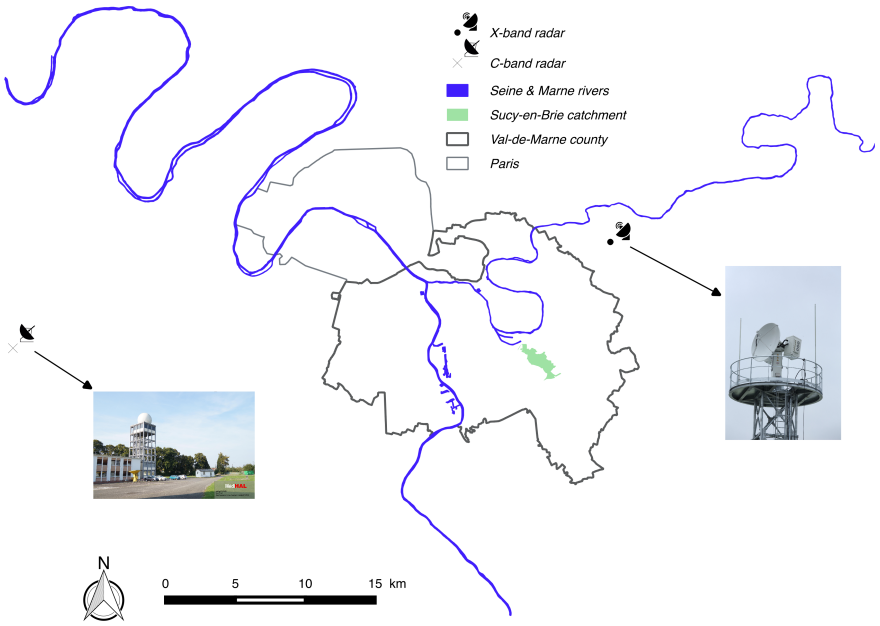

Figure 1.11: Location of the two radar available in Paris region: C-band radar located in Trappes (37 km west from the catchment) and the new X-band one located 10 km northeast of the catchment. ©Météo France & Rosa Vicari / HM&Co - ENPC

Two radars are available in Paris region, their location and main technical characteristics are given in Figure 1.11, Table 1.1 and Table 1.2 respectively:

  - **The C-band radar :** was installed in 2004 in the west of the Paris region in Trappes. It is one of 24 radars of the French national network ARAMIS. It has a dual polarization and Doppler capabilities. It is a fully operational radar and its final rainfall product is integrated within the French mosaic radar rainfall image. The data resolution is 1 km^2 in space and 5 min in time. The processing chain used by Météo France to process the data will be presented in the next chapter. However several products available in Paris region use the same raw data coming from the C-band radar of Trappes, but use different algorithms for data processing. CALAMAR forecasting system is one of them, its processing chain will be presented in chapter 2.
  - **The X-band polarimetric radar :** was installed in late 2014 and inaugurated in June 2015, in the east of Paris region. It is a Dual polarization and

C-band radar technical characteristics	
Manufacturer	SELEX
Geographical position	48.7758N, 2.0098E
Wavelength	5.31 cm
Polarization	H/V
Beam diameter	1.18
Antenna diameter	3.7 m
Pulse width	2 μs
Frequency	5.640 GHz
Range resolution	240 m

Table 1.1: Technical characteristics of the C-band radar of Trappes, operated by Météo France and 37 km west from the case study.

X-band radar technical characteristics	
Manufacturer	SELEX
Geographical position	48.8425510N, 2.588710E
Wavelength	3.16 cm
Polarization	H/V
Beam diameter	1.47
Antenna diameter	1.9
Pulse width	0.33 - 2 μs
Frequency	9.36 - 9.38 GHz or 9.30 - 9.35 Ghz
Range resolution	50 - 500 m

Table 1.2: Main technical characteristics of the newly installed X-band polarimetric radar, the radar is just 10 km northeast from the case study

Doppler radar installed in the framework of INTERREG RainGain project. The radar data is for now processed using the processing chain of SELEX, see Chapter 2 for more details. However important work should be conducted in the future around this radar platform in order to improve the data processing and to develop QPF product oriented for urban hydrology applications.

- **Flow measurement data :** In the Val-de-Marne County, several real time flow sensors are installed in the network. They are used in the real time management of the sewer network as well as in hydrological modeling studies. Two of them are located in Sucy-en-Brie Catchment, one in the entrance of the retention basin and the other one is in the outlet.

1.2.2 The hydrological behavior of the urban catchment

In urban hydrology, a good knowledge of the hydrologic behavior of the catchment is essential to understand flooding issues and to guarantee a correct management of sewer networks. Several research works were conducted in order to address urban catchments behavior based either on their geometric features or by analyzing the hydrograph obtained at the outlet of the catchment.

In this section we will analyze the hydrological response of the Sucy-en-Brie catchment to a given rainfall situation. Main characteristics of the catchment as well as the main flow direction are presented in Figure 1.12 and Table 1.3 respectively. The behavior will be addressed from two important points of view; first of all in terms of the water balance and the rainfall runoff relationship, then in terms of the response time and its consequences on the flooding management.

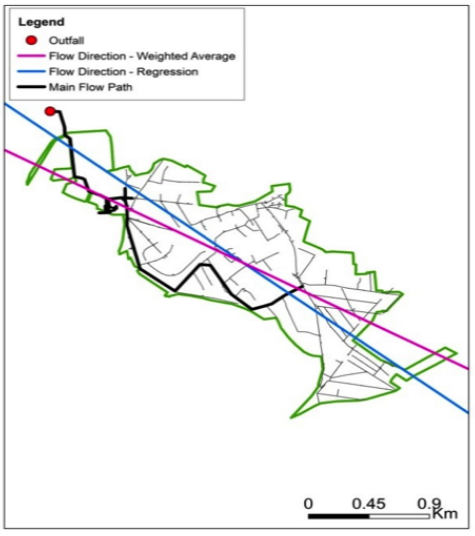

Figure 1.12: Sucy-en-Brie catchment and flow directions

Table 1.3: Main characteristics of the Sucy-en-brie catchment

Sucy-en-Brie catchment main characteristics	
Catchment area	235 ha
General slope(m/m)	0,006200
Catchment length	4,02
Catchment width	0,67
Shape factor	0,17
impervious areas	34%
Population density (persons/ha)	24,83
Sewer system	Separate one
Number of nodes	2030
Number of pipes	1015
Total pipe length (km)	25
Pipe slopes (m/m)	0,0116

- **Rainfall runoff relationship :** The relationship between rainfall and the generated runoff is very important especially in the case of Sucy-en-Brie, where the flooding risk is located in the downstream of the catchment and where the main aim of the retention basin is to handle this volume generated. So having an estimation of the expected water volume based on rainfall information is the basis of the basin management. Such relationship depends on rainfall characteristics (intensity, distribution, duration ...) and on the catchment physiography (size, shape, slope, land use, soil type ...) and will be determined here based on real rainfall and

sewer flow measurements. Data coming from 18 rainfall events (Table 1.4) were used to establish the rainfall runoff relationship between the precipitation depth R(mm) and the water volume V (m^3) measured in the entrance of the retention basin. Based on this data the relationship V=381.R was retrieved (Figure 1.13). This relationship gives an idea about the huge amount of water generated during rainfall events. As example 30 mm rainfall accumulation will generate about 10000 m^3 while 40 mm will generate 15000 m^3 that can be difficult to handle. The same rainfall-runoff relationship was retrieved by RHEA and used to define the warning thresholds of the forecasting-warning system CALAMAR.

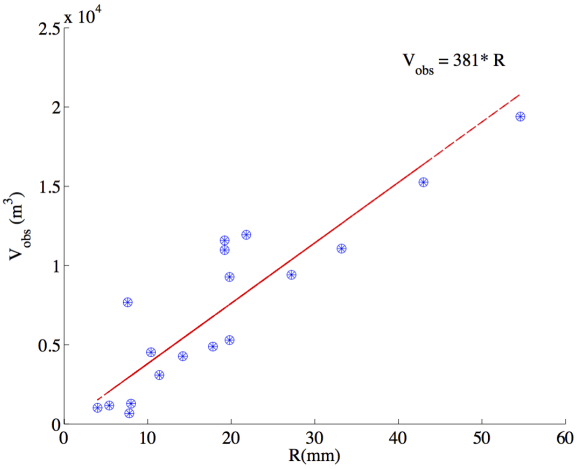

Figure 1.13: The rainfall runoff relationship of Sucy-en-Brie catchment

Table 1.4: 18 rainfall events that were selected to retrieve the rainfall runoff relationship

Event	Total depth R(mm)	$V_{obs}(m^3)$
E1	14.2	4279
E2	54.6	19395
E3	4.0	1019
E4	10.4	4524
E5	11.4	3089
E6	7.8	674
E7	27.2	9418
E8	43.0	15259
E9	19.8	5297
E10	8.0	1288
E11	17.8	4889
E12	5.4	1166
E13	33.2	11073
E14	21.8	11947
E15	7.6	7683.7
E16	19.2	10986
E17	19.2	11591
E18	19.8	9278.1

- **Time parameters of the catchment :** Time parameters are important in urban hydrology. The knowledge about time characteristics of the catchment response is of extreme importance in water management and flooding mitigation, especially during critical situations. The most frequently used time parameters are the time of concentration T_c and the lag time K. Several definitions do exist for these parameters and various formulas are used to estimate them based mainly on the catchment characteristics (slope, flow path, shape,...) :

- **Time of concentration T_c :** time of concentration is widely used in urban hydrology, and defined as the time required for a particle of water to flow from the most distant point in the catchment to the outlet, it varies depending upon slope, land use and the flow path of the urban catchment.
- **Lag time :** the time interval from the center of mass of rainfall excess to the peak of the resulting hydrograph.

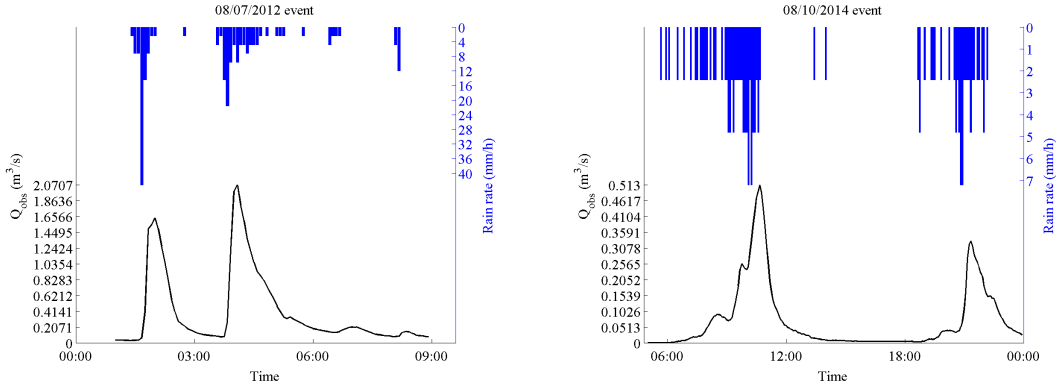

Figure 1.14: Hyetograph and hydrograph recorder for; a) 08/07/2012 and b) 08/10/2014 events

In Figure 1.14 are presented, the hyetograph and hydrograph observed at the outlet of the Sucy-en-Brie catchment for two rainfall events. One can notice the very weak response time of the catchment. The lag time is less than 15 min meaning that urban water managers only have few minutes to react from the beginning of rainfall and the necessity to have information about the rainfall forecast.

1.3 Retention basin and management strategies

After several flooding events that have affected the Sucy-en-Brie city, particularly in 2000 and 2001, where the train station was flooded and blocked for a time, the County Council of Val-de-Marne, made a decision to built a retention basin in the upstream of the catchment near the train station. The retention basin was designed from the beginning in order to achieve two roles. The main one is to protect the city from flooding by storing rain water during the peak flow and the second role is to decontaminate the rainwater stored before its release into the natural environment (the Marne river).

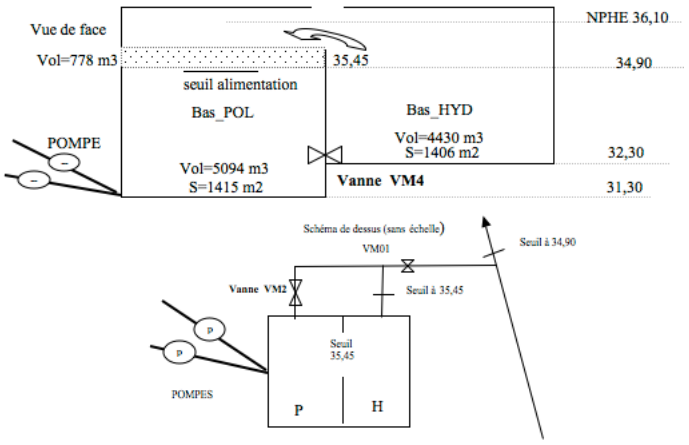

Figure 1.15: The Sucy-en-Brie retention basin

To ensure these two roles, the constructed basin has a total volume about 10 000 m^3 and was divided into two compartments that can be connected through a bottom valve (Figure 1.15) :

- The hydraulic compartment has a volume about 5200 m^3 and allows to avoid flooding for up 10 years return period rainfall event.
- The antipollution compartment has a volume about 5000 m^3 and allows the decontamination of 6 months return period rainfall event.

The decontamination process is simple and involves three steps: a pre-treatment step used to remove solid objects such as branches, plastics through a mechanical process of screening operated immediately upon admission of water into the basin. the second stage consists on a primary treatment of the pluvial water through a settling process operated in the basin to remove suspended matters. The efficiency of this treatment depends mainly on the time that water stays in the basin. The third step is achieved using a lamellar settling device, to facilitate the settling and removal of suspended solids.

The basin is fed by a pipe of 1.5 m diameter controlled by a valve V2 and can be evacuated using two pumping stations: the first one P1 is operated within a rate of 250 l/s which is recommended for better efficiency of the lamellar settling process. The second station P2 is operated within a rate of 500 l/s and used exceptionally in case of emergency.

1.3.1 The static management mode

The traditional static management mode of the retention basin is operated based on the period of the year and does not need an indication of the rainfall situation in real time:

- **The antipollution mode :** is operated during the period between October and April where there the flooding risk is very limited. Under this mode, the basin is operated as follow:
  - Emptying the basin is done at rate of 250 l/s to promote the decontamination process.
  - The Valve V1 is closed, the two compartments do not communicate.
  - The valve V2 is opened, the antipollution compartment continues to be fed until a volume of 5000 m^3
- **The anti flooding mode :** is operated during the period between April and October, where the flooding risk is high due to the extreme rainfall events occurred often in this period and particularly in the summer. The decontamination of a maximum volume of 3500 m^3 is guaranteed even during this period where the retention basin is operated primary to avoid flooding :
  - Emptying the basin is done at rate of 250 l/s
  - The Valve V1 is closed, the two compartments do not communicate.
  - The valve V2 is opened, the antipollution compartment continues to be fed until a volume of 3500 m^3

With this static management, the retention basin can avoid flooding for up 10 years return period events and decontaminate a maximum volume of 5000 m^3. Or the DSEA 94 (Direction des Services de l'Environnement et de l'Assainissement) in charge of the management of the basin hope to increase both the decontamination capability of the basin to a volume of 8000 m^3 and also to be able to avoid flooding caused by 15 to 20 years return period rainfall events.

1.3.2 The predictive management

The solution that was made is to connect the two compartments by opening the bottom valve V1, in order to use the basin with its full capacity both for flooding protection and rainwater decontamination.

In terms of management, this purpose is a challenging one, because operators need to know when they have to switch between this two gesture modes. In a simple way they need reliable information about the rainfall situation forecast in order to be able to empty the basin in case of oncoming extreme rainfall event. This is what the predictive management means.

To answer this question, a decision tool was set up for the predictive management of the retention basin. Its a forecasting system combined with a warning system that generates based on the actual and the expected rainfall situation two levels of warning indicating each, a level of flooding risk and the need to take decision up to the complete empty of the basin.

The Enterprise (RHEA) behind the forecasting system CALAMAR has conducted several works between 2004 and 2006 in order first of all to understand the local authority needs and also to set up the new forecasting-warning system and to define new predictive management modes that go with it.

As outcomes of this work, four new predictive management modes were set up, the choice of the mode is not based any more on the period of the year, but on the actual and the predicted rainfall situation described with the warning system:

- **The predictive antipollution mode B3 :** is defined as follow:
  - The valve V1 is open, so the two compartments can communicate.
  - The valve V2 is open as well, so the basin can continue to be filled until the the volume of 8750 m^3
  - The pumping station is operated with a rate of 250 l/s
- **The predictive anti-flooding mode B4 :**
  - The valve V1 is open, so the two compartments can communicate.
  - The valve V2 is open as well.

  - The pumping station is operated with a rate of 750 l/s in order to free the needed volume in the basin as quickly as possible. Water evacuated at this rate is considered as not decontaminated even if has been already pre-treated during the first two treatment steps.

- **The predictive anti-flooding mode B4bis :** This mode aims to have 6700 m^3 free storage available in the basin, so it is characterized as follow:
  - if the free storage available in the basin is less than 6700 m^3:
    - The valve V1 is still opened (the two compartments can communicate)
    - The valve V2 is closed (the basin can not receive additional water volume)
    - The pumping station is operated within a rate of 750 l/s until the basin regains a storage capacity of 6700 m^3
  - if the storage capacity available is more than 6700 m^3:
    - The valve V2 is closed
    - the pumping station is operated within a rate of 250 l/s, to decontaminate rain water

- **The predictive anti-flooding mode B4ter :** this mode aims to empty the whole basin as quickly as possible:
  - The valve V2 is closed.
  - The pumping station is operated within a rate of 750 l/s.

The predictive management of the retention basin depends only on the real time rainfall conditions. The switch between the antipollution management mode to the anti-flooding mode is made on the basis of the current rainfall situation and that one expected in the next hour. hence the necessity to set up a warning system that will indicate to the operator when to switch from one mode to another. This system should be sufficiently reliable to avoid both false warnings and non detection situations. Because on one hand do not empty the basin to ensure the storage volume required to avoid flooding due to a non-detection of the warning is very disastrous and can leads to significant damages, on the other hand, emptying the basin after a warning which is not confirmed later is also disastrous because non decontaminated water will be ejected into the natural environment.

Both These situations were studied by RHEA, and finally two levels of warning were set up for the Sucy-en-Brie retention basin.

1.3.3 The warning system

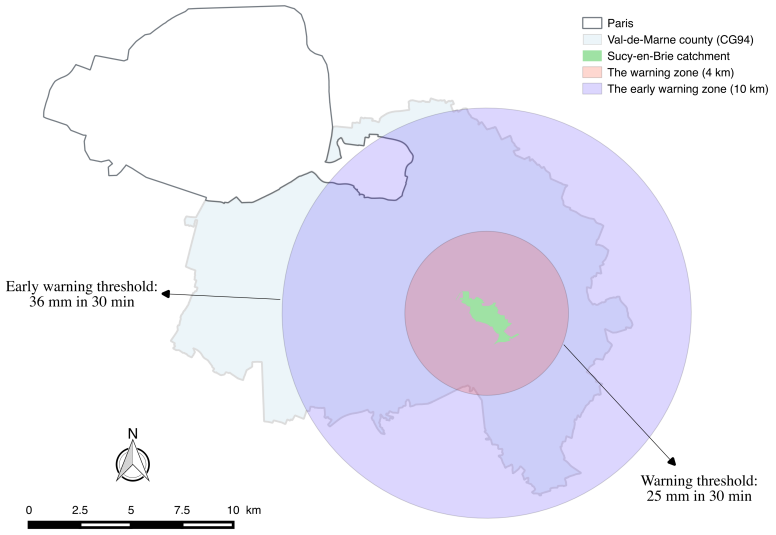

Figure 1.16: CALAMAR warning system

1.3.3.1 The early warning indicator

The early warning indicator was set up in order to inform the operator as soon as possible of the approach of a rainy situation that could cause a risk of overflow in the downstream of the sewer network (near the train station) if the available capacity in the basin is not sufficient to ensure the storage function.

The system generates an early warning when it detects within a 10 km radius around the center of the catchment (Figure 1.16), a storm cell with a minimum size of 4 km^2 (4 radar pixels) and leading to a cumulative rainfall over 36 mm in 30 min. The verification of the early warning threshold crossing is made on 4 cumulative 30 min rainfall defined as follow:

- t_0 - 15 min $\mapsto$ t_0 + 15 min, so 15 min of measurement and 15 min of forecast
- $t_0 \mapsto t_0$ + 30 min, so 30 min of forecast starting from t_0
- t_0 + 15 min $\mapsto$ t_0 + 45 min, so 30 min of forecast starting from t_0 + 15 min

- t_0 + 30 min $\mapsto$ t_0 + 60 min, so 30 min of forecast starting from t_0 + 30 min

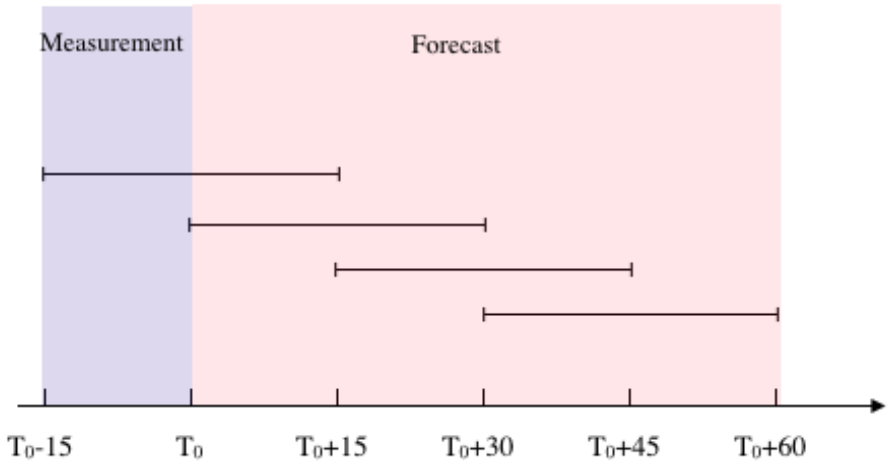

Figure 1.17: CALAMAR warning system

From Figure 1.17, one can notice that only 15 min of rainfall measurement is used to check any exceed of the early warning threshold, the other 60 min corresponds to the forecasting rainfall for the next 60 min. So the early-warning threshold is more based on the rainfall forecast than on the effective rainfall measurement. In fact, the consequence of an early warning on the management of the basin is based upon the storage capacity that still available in the basin and also on the reliability of the forecasting estimation. Indeed, an indicator of the reliability of the forecast was set up and integrated within the CALAMAR window, which allow the operator to judge the best decision to make in real time situation.

According to the decision tree that was set up for the predictive management of the basin, the operator must compare the duration of a reliable rainfall forecast D_r to the time D_v needed to empty the basin with a maximum pumping rate (750 l/s) in order to have a storage capacity of 6700 m^3.

If D_r is higher than D_v, then the operator should wait to have a reliable forecast before making a decision, if not, the basin switch to the anti-flooding mode, and the pumping stations are operated within the maximum rate in order to evacuate the stored rainwater.

If the early-warning is triggered, it remains active during 1h before updating the state of warning on the basis of CALAMAR calculations.

1.3.3.2 The warning indicator

The warning indicator was set up in order to indicate to the operator the immediate presence of an exceeding of the critical risk threshold. it is calculated based on 10 min of rainfall measurement and 2h of forecast. The warning is triggered if a rain cell with a minimum size of 4 km^2 that generates a cumulative 30 min rainfall that exceeds 25 mm is detected within 4 km radius around the center of the catchment (Figure 1.16). The verification of the warning threshold crossing is made on 6 cumulative 30 min rainfall defined as follow:

- t_0 - 10 min $\mapsto$ t_0 + 20 min, so 10 min of measurement and 20 min of forecast
- t_0 + 10 min $\mapsto$ t_0 + 40 min, so 30 min of forecast starting from t_0 +10 min
- t_0 + 30 min $\mapsto$ t_0 + 60 min, so 30 min of forecast starting from t_0 + 30 min
- t_0 + 50 min $\mapsto$ t_0 + 80 min, so 30 min of forecast starting from t_0 + 50 min
- t_0 + 70 min $\mapsto$ t_0 + 100 min, so 30 min of forecast starting from t_0 + 70 min
- t_0 + 90 min $\mapsto$ t_0 + 120 min, so 30 min of forecast starting from t_0 + 90 min

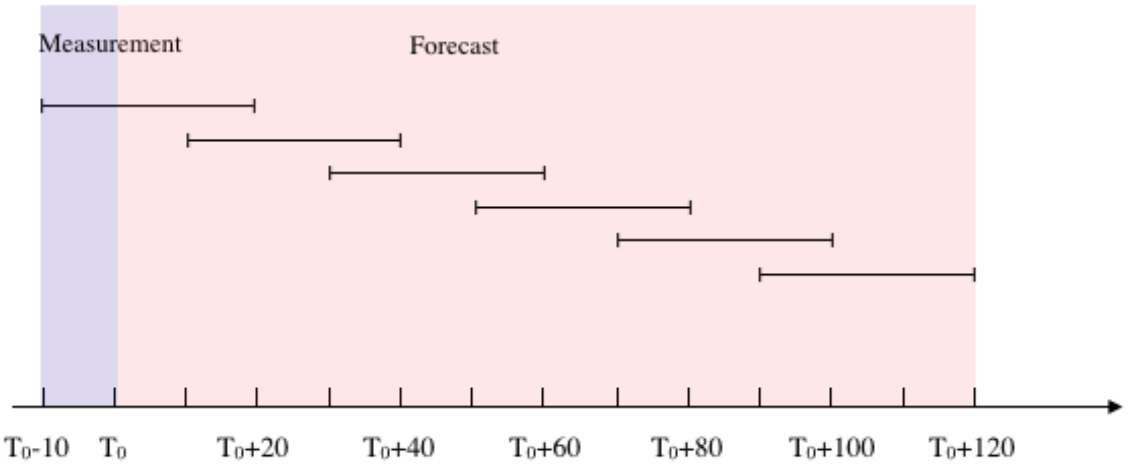

Figure 1.18: The verification of the warning threshold crossing is made on 6 cumulative 30 min rainfall and based on 10 min measurements and 2h of forecast

From Figure 1.18, one can notice that the warning indicator is based only on 10 min rainfall measurement and 2 h rainfall forecast. Hence the need to set up in addition to these two level warning indicators another one showing the reliability of the used rainfall

forecast. The real time decision that can be taken by the operator should be based on both the warning and the reliability indicators in order to avoid critical situations. The reliability of radar-based QPF was investigated for years, and results coming out show that extrapolation QPF techniques have good skills at lower lead time (1-2 h) which is the case here. However, it is important to note that uncertainties of radar forecast can have two main sources of errors: uncertainties on the radar rainfall measurements themselves and uncertainties related to the forecasting technique used. On one hand an overestimation for example of the rainfall rate will leads to an overestimation of the obtained rainfall forecast since rainfall intensities remain unchanged, while on the other hand, the radar-based techniques often consist on the simple extrapolation of rain cells movements without any changes on their intensity, their shape, and their movements, which is far from being correct. In fact many studies show that the life time of a given rain cell is around 20 min which is not taken into account wen computing the 2h forecast.

1.3.3.3 CALAMAR system feedback

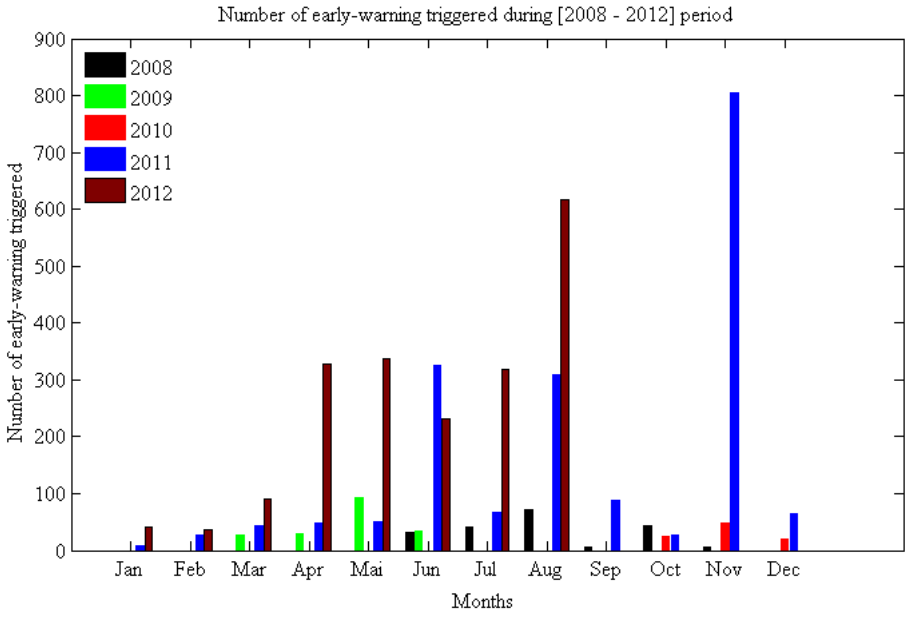

Figure 1.19: Number of early-warning triggered during (2008 - 2012) period

The feedback of the use of CALAMAR system for the predictive management of the Sucy-en-Brie retention basin was not as expected. In fact, the DSEA 94 noticed a high rate of early-warnings triggered per year, the frequency of early-warning is even more higher in the summer in such way that the predictive management has become impossible

and was abandoned by the CD94. So the retention basin is operated currently using the static management mode and based on the period of the year.

Figure 1.19 shows statistics about the number of early warning triggered during the period between 2008 and 2012. The state of the early warning indicator is reported every 15 min.

As a results of our investigations, RHEA confirms after verification that the system was not correctly set: an early warning threshold defined over 20 km around the basin was discover instead of 10 km originally set. The 20 km area includes some zones in Paris with high building, so high effect of ground clutters which leads according to RHEA to the triggering of the early-warning. In addition to that, RHEA evokes the possible effect of the anomalous propagation not corrected in the actual version of CALAMAR used by the CD94.

Following this exchange with RHEA and because of this finding, we decided to conduct several analysis on CALAMAR product data in order to further investigate processes used by the system for the data processing and rainfall forecasting and to understand causes of this issue and which improvements should be taken in order to establish the predictive management of the retention basin.

1.4 First investigations on the early warning threshold

Various investigations were conducted in the framework of this work in order to understand issues encountered with CALAMAR system. The first one consists on the verification of early warnings triggered and whether or not they are justified.

Event	Date	Number of early-warning triggered	Max 30 min cumulative observed (mm) in radar measurements
E1	2011/02/19	16	14.4333
E2	2011/08/26	12	12.45
E3	2011/03/26	24	12.575
E4	2012/06/21	32	20.75
E5	2012/03/23	17	82.7667
E6	2012/01/03	8	6.1
E7	2012/02/22	8	4.625
E8	2011/06/04	12	91.775
E9	2012/06/10	13	15.6
E10	2012/05/21	24	10.0583

Table 1.5: Characteristics of 10 rainfall events selected : the number of early warning triggered per event and the maximum cumulative 30 min rainfall observed on rainfall measurements

10 rainfall events occurred between 2011 and 2012 have been selected, the common point between them is that at least one early warning was triggered by CALAMAR system. However only measurements were used here, CALAMAR does not allow the extraction of forecast data. Indeed, the analysis will be based on only one 30 min cumulative rainfall map computed for each time step as follow:

t_0 - 15 min $\mapsto$ t_0 + 15 min, so 30 min of measurement instead of 15 min of forecast and 15 min measurements used for the early warning threshold.

Table 1.5 gives characteristics of 10 rainfall events selected : the number of early warning triggered per event and the maximum cumulative 30 min rainfall observed on rainfall measurements. One can notice that 8 of the 10 selected events should not give place to an early warning if it was only based on 30 min measurements. The cumulative 30 min rainfall computed only on measurements is very weak than the 36 mm needed to trigger an early warning. So no exceed of the early warning threshold was noticed within the 10 km radius the catchment, not even within the 20 km around the catchment. This lead as to make two hypothesis, the first one and the most probable one is that the threshold

exceeding was detected for a previous rain cell that we don't see in this data and that was extrapolated to at least the 20 km area around the center of catchment. The second one is that CALAMAR system overestimates the rainfall forecast intensity leading to an exceed of the early warning threshold. Both hypotheses are difficult to verify without having QPF estimation data. But it is clear that the issue for this 8 events is not due to a wrong setting of the early warning threshold.
Now, Lets analyze the two events for which the early warning was justified if we considered the whole radar image (32 km radius around the center of the catchment).

- **2012/03/23 event :**

	The maximum cumulative 30 min rainfall R_{max} and the number of pixels N exceeding the threshold (36 mm) :					
	The whole radar image (32 km around the basin)		Within 10 km around the basin		Within 20 km around the basin	
Time	R_{max}	N	R_{max}	N	R_{max}	N
00:30	1.625	0	0.066667	0	1	0
00:45	0.85833	0	0	0	0.85833	0
01:00	0.75833	0	0	0	0.75833	0
02:30	2.0083	0	0.066667	0	2.0083	0
02:45	2.4667	0	0.066667	0	2.4667	0
03:00	1.8917	0	0	0	1.55	0
03:15	10.1917	0	0	0	1.125	0
05:15	5.7167	0	0.11667	0	4.175	0
05:30	0.55833	0	0	0	0	0
05:45	1.9917	0	0.15	0	0.55833	0
06:00	3.1167	0	0.50833	0	1.3	0
06:15	19.5833	0	0.59167	0	19.5833	0
06:30	47.2167	2	0.5	0	47.2167	2
06:45	65.3083	3	0.81667	0	65.3083	3
07:00	82.7667	6	1.0417	0	82.7667	5
07:15	50	2	0.5	0	50	2
07:30	1.1083	0	0.19167	0	0.19167	0

Table 1.6: Characteristics of the 17 early warnings triggered the 2012/03/23 between 00:30 and 07:30, the max cumulative rainfall and the number of pixels that exceed the early warning threshold observed within the whole radar image (64*64 km2), within 20 km from the center of the catchment and within 10 km from the center

For the 2012/03/23 event, 17 early warnings were triggered between 00:30 and 07:30 and the maximum 30 min cumulative rainfall observed in measurements is 82.76 mm, which is a very high 30 min cumulative rainfall and exceeds largely the early warning threshold. However, still to verify whether or not the early warning threshold exceeding was observed within the 10 km area around the center of the

catchment as it was originally set or within the 20 km around the center of the catchment in the wrong setting of the threshold.

In Table 1.6 are reported the exact time of the early warnings, the max cumulative rainfall and the number of pixels that excess the early warning threshold observed within the whole radar image (64*64 km2), within 20 km from the center of the catchment and within 10 km from the center.

Results show that no exceed was observed between 00:30 and 06:15 and that all pixels identified with an exceed between 06:30 and 07:15 are within the 20 km area around the catchment, which confirm that there was effectively a wrong setting of the threshold. However when looking at the given cumulative maps in Figure 1.20 observed at 06:45 and 07:00, we notice that it not even a rainy moment, and that exceeds of the threshold were observed for pixels corresponding to ground clutter echoes that were not removed during data processing step. The ground clutter in the top left is recognized as the one corresponding to the business district of la Defense known for its high towers.

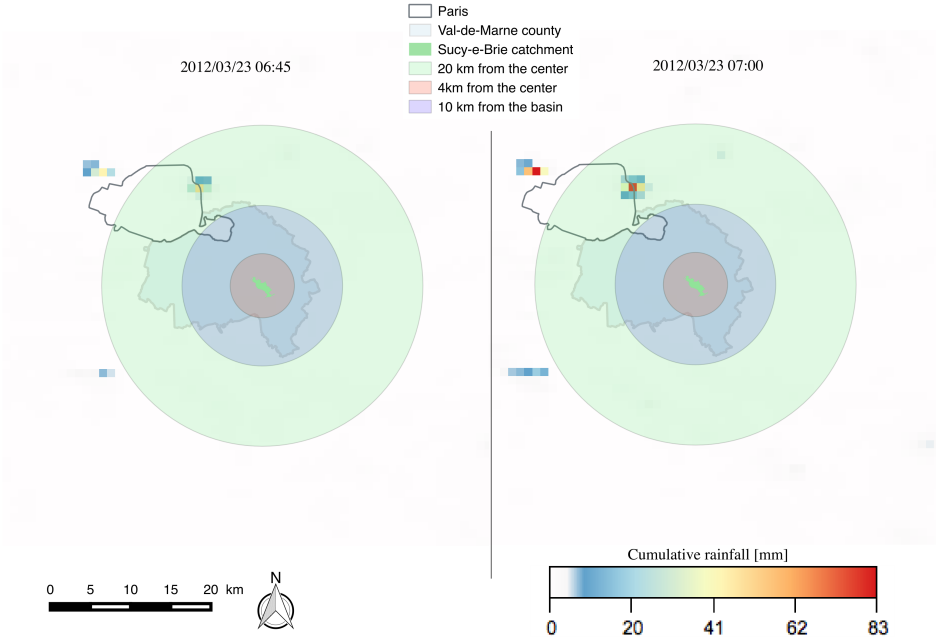

Figure 1.20: 30 min cumulative rainfall maps observed the 2012/03/23 at 06:45 in the left and at 07:00 in the right

- **2011/06/04 event :** For the 2011/06/04 event, 12 early warnings were triggered between 21:00 and 23:45 and a maximum 30 min cumulative rainfall about 91.7 mm was identified. In Table 1.7 are reported as for the previous event the exact

time of the early warnings, the max cumulative rainfall and the number of pixels that exceed the early warning threshold observed within the whole radar image (64*64 km2), within 20 km from the center of the catchment and within 10 km from the center.

Results show that only three early warnings triggered at 21:45, 22:00 and 22:15 are justified. However all pixels exceeding the early warning threshold are within the 20 km area around the catchment and not the 10 km confirming thus the wrong setting of the threshold that was corrected recently (25 pixels that exceed the threshold are identified at 21:45, 44 at 22:00 and only 4 at 22:15, Figure 1.21).

	The maximum cumulative 30 min rainfall R_{max} and the number of pixels N exceeding the threshold (36 mm) :					
	The whole radar image (32 km around the basin)		Within 10 km around the basin		Within 20 km around the basin	
Time	R_{max}	N	R_{max}	N	R_{max}	N
21:00	61.4333	2	0.24167	0	8.625	0
21:15	42.55	3	3.8417	0	16.8583	0
21:30	41.4417	5	16.6583	0	22.825	0
21:45	58.0167	32	24.975	0	58.0167	25
22:00	91.775	63	28.6917	0	91.775	44
22:15	56.8917	49	14.1583	0	38.2083	4
22:30	41.4667	11	3.375	0	16.4083	0
22:45	32	0	3.4917	0	6.725	0
23:00	15.5667	0	3.2333	0	3.2333	0
23:15	5.375	0	3.1583	0	3.3917	0
23:30	7.9167	0	2.925	0	4.2333	0
23:45	13.0917	0	5.0917	0	5.125	0

Table 1.7: Characteristics of the 12 early warnings triggered the 2011/06/04 between 21:00 and 23:45, the max cumulative rainfall and the number of pixels that exceed the early warning threshold observed within the whole radar image (64*64 km2), within 20 km from the center of the catchment and within 10 km from the center

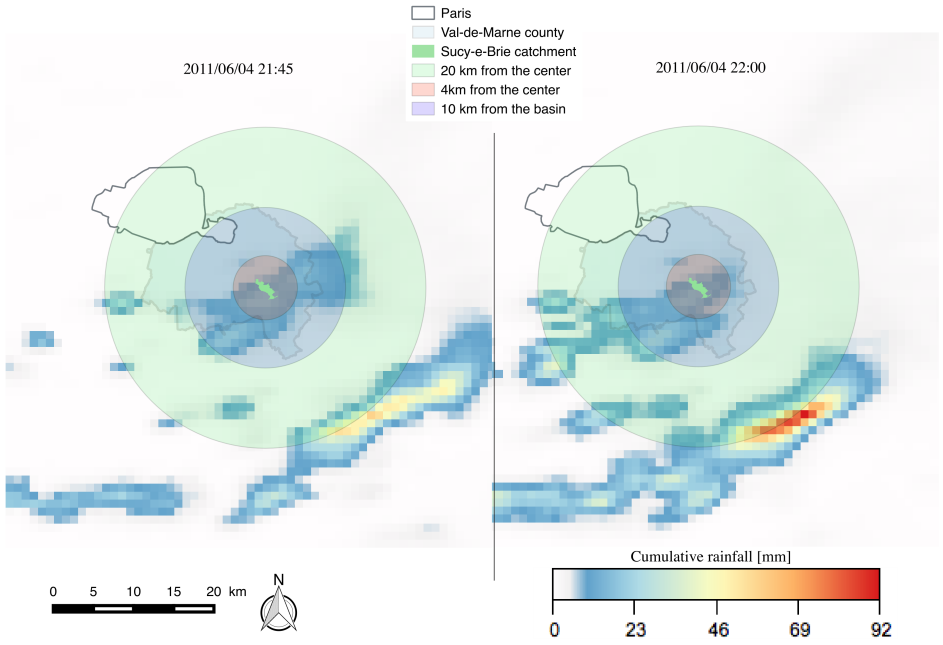

Figure 1.21: 30 min cumulative rainfall maps observed the 2011/06/04 at 21:45 in the left and at 22:00 in the right

As a summary: from the 10 rainfall events selected without setting any criterion except that they all give place to early warnings. Early warning triggered for 8 events were not justified using the measurements data we have (no exceed was reported in the 30 min cumulative rainfall), they may be due to previous rain cells that we don't see in this data or may be due to an overestimation of the forecasted rainfall intensity. For one event, the early warning was triggered due to the bad quality of the rainfall measurement (two ground clutters were not removed form the radar data) while for the last event, early warnings were triggered because of the wrong setting of the threshold (20 km radius around the center of the catchment was found instead of 10 km originally set).

These first level investigation results pushed us to go further on CALAMAR data analysis, in order to set the quality of the data and consequences of the static treatment of ground clutters as well as the radar-rain gauge adjustment process performed in real time. A morphological comparison between CALAMAR and Meteo-France rainfall products will be performed in the next chapter using the Universal Multifractal framework.

1.5 Intermediate conclusions on Chapter 1

Elements included in this chapter demonstrate some aspects of urban flooding risk in relation with the challenging context of climate change and the ongoing urbanization process that increased further more the pressure on urban areas and increased their vulnerability to flooding. Several engineering solutions were developed over the years and implemented in urban areas to control the flooding risk and to limit its effects on the concerned populations and public authorities.

In France, various management techniques were developed and implemented in urban areas in order to cope with both the increased flooding and pollution risks. They rely on most cases on the combination of hard engineering structures like retention basins and the implementation of sustainable techniques to control both the quality and the quantity of the pluvial water. A retention basin was implemented in Sucy-en-Brie in the downstream of the catchment, it was designed to achieve two roles, the protection from flooding by volume storage and the decontamination of pluvial water before its release into the natural environment. However, using the retention basin to achieve both purposes is challenging and cannot be reached with the classical management strategies. The predictive management of Sucy-en-brie retention basin is very ambitious strategy to handle issues of both flooding risk and water decontamination. The implementation of such strategy should be increased in the future following the increase of flooding risk and derived by advances noticed in terms of radar data availability.

However, this kind of strategy is highly demanding on data quality and reliability. Issues encountered with CALAMAR system especially the high rate of false early warnings is an example of the complexity of such management. First investigations performed in the framework of this work show that some of issues encountered are in fact due to the questionable quality of radar measurements provided by CALAMAR system. Further analysis will be conducted in the next chapter to analyze the structure and the morphology of radar data involved in this case and improvements that the new X-band polarimetric radar can bring in terms of data quality and variability of rainfall information.

Chapter 2

Rainfall data analysis

This chapter is entirely dedicated to rainfall data analysis. Various analysis were performed in the framework of this thesis and involve several radar products as well as rain gauges data.

A significant part of this dissertation has been devoted to the development of a new methodology for more meaningful comparison of radar rainfall field products, including with point measurements by rain gauges. Being rooted to the multifractal theory, the developed methodology allows a comparison of the structure and the morphology of rainfall fields in both space and time. It has also the advantage of exploring all data pixels constituting the radar image. This method was initially applied to perform a comparison between CALAMAR and Meteo-France rainfall products. Finally, first X-band polarimetric radar data available from the dual polarization Doppler X-band polarimetric radar were used to confirm some of initial findings of this dissertation, in particular the spatio-temporal variability of rainfall information and the accuracy of the X-band polarimetric radar data.

This chapter is organized as follow:

1. The first section addresses precipitation measurements in urban areas, with details on the several measurement methods and instruments involved, it will be discussed the accuracy and representativeness of the data obtained in relation with the spatial and temporal variability. Main issues and sources of errors related to rainfall measurements are discussed as well.

2. The second section is devoted to radar rainfall products available in Paris region: Meteo France and CALAMAR products are presented with details about the data processing they involve. The forecasting algorithm used by CALAMAR system is detailed as well.

3. In the third and the fourth sections, the new developed methodology for radar products comparison is used to perform a comparison between CALAMAR and Meteo France rainfall products for five rainfall events. The methodology is fully based on the Universal Multifractal framework and allow a deep analysis of rainfall field from various points of view. Indeed, the scaling behavior of radar products is analyzed in both space and time, the structure and the morphology is analyzed as well.

4. In the last section, first X-band polarimetric radar data available is analyzed following the new methodology developed in this work. A comparison is performed in this context between C band and X-band polarimetric radar data.

2.1 On rainfall measurement

Precipitation is the quantity of the liquid or solid water reaching the ground, it includes rain, hail and snow. This section focuses on the liquid part of precipitation. Rainfall measurement can be expressed in terms of the vertical depth of water generally in mm or in terms of the amount of rainwater collected per unit time interval generally in $mm.h^{-1}$. Point measurements of precipitation and more recently weather radars and satellite are used for rainfall estimation. National weather networks usually integrate all these three sources of precipitation data. This part does not discuss neither devices which attempt to characterize the rain drop size distribution like disdrometers nor satellites because they're not commonly used for urban applications. So only rain gauges and weather radars devices are presented and discussed in this section.

2.1.1 Rain gauges

Rain gauges are the ground-based direct measurement most used devices, they have been extensively developed and implemented in urban environments because of their low cost and ease of installation and use compared to the radar technology. Rain gauges give rainfall measurements at a given point of the catchment, their spatial resolution is assumed to be very weak, the data is only representative of a limited area that depends on the local topography and the heterogeneity of the region. Their temporal resolution is related to the sampling methodology and to the measurement principle used by each type of rain gauge.

In urban modeling, rain gauge data has served as the primary source of rainfall data, urban models have been adapted to the use of this point measurements data and many interpolation methodologies were developed to get a spatial distribution of rain gauges information at the catchment scale. However, ground measurement of precipitation is particularly sensitive to the local environment of the gauge, and many sources of errors like wind, turbulence and evaporation may affect the gauge record and should be considered when using this data.

Many types of rain gauge are available, such as weighing bucket gauges, capacitance gauges, optical gauges, and tipping-bucket (TB) gauges. The commonly used one is the tipping bucket rain gauge which data used in this work coming from.

2.1.1.1 Tipping bucket rain gauges

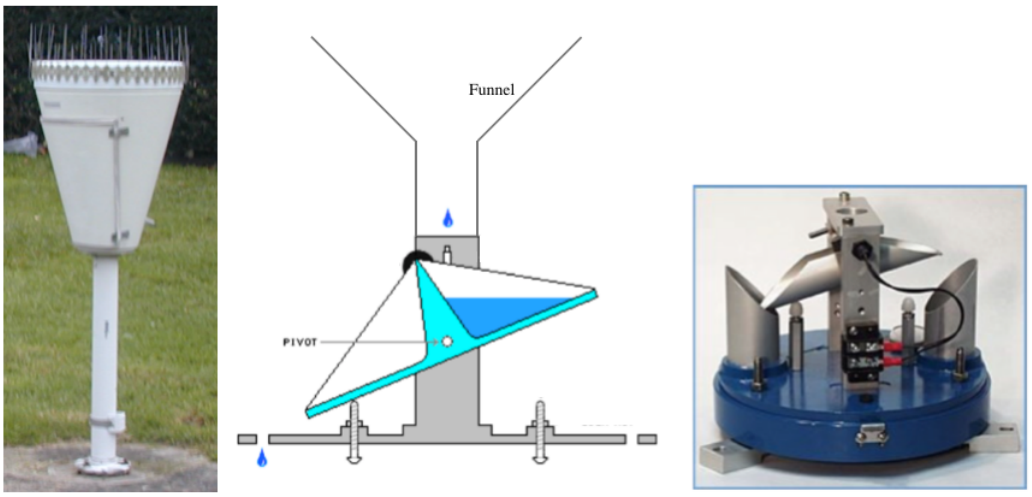

Figure 2.1: Tipping bucket Rain gauge. (©WeatherShack.com and http://i4weather.net/stationhistory.html

Tipping bucket rain gauges have become the standard device for measuring rainfall intensity in urban hydrology. The measurement principle of a tipping bucket rain gauge (Figure 2.1) consists on collecting precipitation that falls into the funnel and directs it to one of the two small compartments below that can collect water in turn thanks to a pivoting bucket system. When a determined weight of water (typically 0.1 or 0.2 mm) falls, the tipping bucket changes position, the first lever tips, dumping the collected water while the second begins to fill. Each switch over is recorded automatically indicating the measurement of 0.1 or 0.2 mm of rain. The minimum rain rate that can be measured by this type of rain gauge is indeed determined by the size of the bucket. Due to their measurement principle, tipping bucket rain gauges give measurement with high time resolution during high rainfall intensity, but information about the intensity distribution at low rainfall rates is poor. In addition to that, the exact start and end time of the rainfall event are uncertain due to the partial filling of the bucket.

2.1.1.2 Rain gauge network design

While radar based techniques are becoming increasingly spread in recent years, the estimation of the areal precipitation from operational rain gauge sensor network still widely used in urban hydrology, for modeling needs as well as for radar adjustment, it is also used as the only source of information in areas with no radar coverage(Messer

et al. (2006), Vogl et al. (2012), Price et al. (2014)). However, the ability to infer spatially distributed data from point measurements is strongly dependent on the number of gauge stations used, their location and reliability of measurement (Girons Lopez et al. (2015)). In fact, spatial precipitation estimation from point measurements is subject to two main sources of uncertainties, the errors with the measurements themselves and the estimation of the spatial and temporal precipitation variability (McMillan et al. (2012), Girons Lopez et al. (2015)) using interpolation methodologies (for example, Kriging method, Thiessen polygons method, Trend surface analysis, see Haberlandt (2011) for a review). The problem of rain gauge network design has been the subject of research over the years, many of them were focusing on establishing the effect of the gauge network density on the accuracy of the obtained areal estimation, and the possible effect on hydrological models outputs though it is commonly admitted that the areal precipitation estimation is more accurate with more gauges distributed in the area (Chen et al. (2010)). Anctil et al. (2006) showed that model performance reduced rapidly when the mean areal rainfall was computed using a number of precipitation gauges less than a certain threshold. Wood et al. (2000), Goodrich et al. (1995) show that precipitation interpolation uncertainties increase with increasing interpolation resolution due to the higher precipitation variability especially at the smallest scales (McMillan et al. (2012)). Xu et al. (2013) found for their study that the error range for rain gauge precipitation estimates when increasing network densities reaches a threshold beyond which no considerable improvements are seen. According to all studies, it is difficult to derive a universal method for the design of rain gauge networks. The density of gauges required in any region depends on the size of the area and the type of precipitation (convective, stratiform).

2.1.1.3 Point measurements uncertainties

Point measurements rainfall are subject to the effect of several systematic errors due to their siting and their local environment, errors due to the static calibration, but also to some random errors that cannot be linked to any particular cause. In cities, gauges are subjected to complex exposure changes, and can be influenced by wind, evaporation, and local turbulence or nearest obstacle (Sevruk and Hamon (1984)). This is why it is important to have the gauge sited and positioned correctly. Following the World Meteorological Organization (WMO 1965) recommendations, the gauge should be

installed at 1 m above the ground level and all gauges in a given catchment should be the same height and in an open area away from obstructions like trees or building. In urban hydrology, TB rain gauges are less and less considered as "ground truth" they are mostly affected by some local environment errors including wind, turbulence, tipping bucket losses especially during high rainfall rates and sampling errors (Habib et al. (2001), Fankhauser (1998), Ciach (2003a), Emmanuel et al. (2012)). Habib et al. (2001) showed that the dynamic calibration and wind effects can cause differences in estimating runoff volumes in the range of 4 to 10% and 6 to 18% respectively. The impact on predicting runoff peaks was also significant 2 to 12% for dynamic calibration effect, and 2 to 18% for wind effect. An underestimation of rainfall volumes and intensities have been noticed as well due to the measurement principle, some rainfall is missed between successive tips of the bucket. This underestimation increases with the increase of rainfall rates Niemczynowicz (1999), Humphrey et al. (1997), Luyckx and Berlamont (2001). Legates and Willmott (1990), Yang et al. (1998) developed an empirical formula to estimate correction factors as a function of wind speed while Nešpor and Sevruk (1999) developed a formula to estimate wind errors as a function of wind velocity, rainfall intensity, and raindrop size distribution. In addition to these systematic errors, TB measurements are also affected by local random errors (Fankhauser (1997), Yu et al. (1997), Nystuen et al. (1996)). These errors are mainly related to the discrete sampling method of the TB gauge. Habib et al. (2001), Fankhauser (1998), Ciach (2003a) showed that such random errors have significant magnitudes, mainly at small rainfall intensities and short time scales, they are reduced as rainfall records are averaged to coarser resolutions. Habib et al. (2008) developed a formula to describe the error dependence on the time resolution of rainfall measurements and on the rain gauge volume and temporal sampling resolution.

2.1.2 Weather radars

Rain gauges are traditionally used to measure precipitation, because they are cheap and provide direct and robust rainfall measurements. Their main shortcoming is that they represent a very limited space (Ciach (2003a)). Thus, even a dense network of rain gauge gives little information on the fine spatial distribution of precipitation. On the contrary, weather radars used to characterize the precipitation over a large surface. However,

unlike rain gauges, the radar does not measure the precipitation directly, but the "reflection" by precipitation echoes of the transmitted signal. In radar meteorology, one of the main objectives is to provide estimates as accurate as possible of the precipitation rate R known as Quantitative Precipitation Estimation (QPE).

The radar reflectivity Z and the precipitation rate R depends both on raindrops distribution. It has been found that these variables may be linked by empirical relationships called Z-R relationships (Marshall and Palmer (1948), Uijlenhoet (2001), for example). But the great variability of rainfall and the complexity of the raindrop size distribution involve a large number of possible Z-R relationships. The Z-R relationship appears to be associated with different types of precipitation, different geographic locations or different seasons (Battan (1973), Fišer (2004)).

Precipitation estimation based on radar measurements are subject to many sources of errors such as calibration of the radar itself, attenuation of the radar signal, contamination by ground clutters and the anomalous propagation of the radar beam, etc. (Krajewski et al. (2010b), Porter et al., Chandrasekar (1987), Villarini and Krajewski (2010)).

For many years, the majority of radars used to measure rainfall operate at a wavelength in such way to limit partially or totally the attenuation of the radar signal by the atmosphere or the precipitation (S and C band radars). These radars can therefore have a very large range (about 200 km). Thus, most of the national meteorological services are equipped networks with such radars to cover all concerned areas. However, these radars cannot easily be used by small entities and local authorities because of their price and their size.

But for several years, demand for high-resolution QPE and more localized rainfall description is growing. The use of such data are more targeted by local authorities and urban water managers. The X-band radars (lower wavelength) meet these requirements. However, their main shortcoming is the high attenuation of their signal at this wavelength (Berne and Uijlenhoet (2006), Chandrasekar and Bringi (1988), Snyder et al. (2010), Eccles and Mueller (1971), Wanyu Li et al.). That is why they have been little used in the past, but with recent improvements of radar technology, the X-band radars are excellent candidates for many applications of rainfall measurements in hydrology and urban small catchments for modeling needs as well as short term forecasting.

In order to improve the QPE, radars have known in recent years many innovations and evolution of both the hardware and the algorithms used. So many radar have now the ability to measure the velocity of the precipitation targets thanks to their Doppler capability. The measurement of raindrops velocity provides valuable information on the dynamic of rainfall structure (Bringi et al. (2003), Marquis et al. (2008), French et al. (2008)) and it is also used to improve the complex process of ground clutters identification and removal as their velocity is zero (Berenguer et al. (2006)). In addition to that, it was established that raindrops are generally not spherical, the reflected signal amplitude must be different depending on whether the polarization is horizontal or vertical. Thus, the Dual polarization capability is used to provide information on raindrop size and allows a more accurate estimation of precipitation (Illingworth and Blackman (2002)). In practice, various polarimetric parameters such as the differential reflectivity or the specific differential phase are provided by Dual polarization radars and can be used to replace the Z-R relationships in order to better take into account the extreme variability of precipitation (Brandes et al. (2002)).

The term radar is an acronym for RAdio Detection And Ranging and means that this remote sensing device is designed to detect and locate precipitation targets using radio waves. Radars were developed in the 1940s for military purposes and used during the Second World War to detect aircraft. Their use was very disturbed at the time by precipitation echoes. The attenuation of the signal by raindrops was seen as an obstacle rather than a scientific discovery. But when war ends up, scientists began to think how to connect the signal reflected by rain echoes to rainfall intensity. Therefore, David Atlas and J. Stewart Marshall participated on the development of first meteorological radars in US and Canada. At the late 20th century, first national radar networks were built (NEXRAD in US, ARAMIS in France and the Canadian weather radar network).

In the following part, it will be presented in a simplified way the mathematical basis of rainfall measurement by weather radar. it was elaborated from WMO (2008), Bringi and Chandrasekar (2001), Sauvageot (1994), Uijlenhoet (2001), Yuter (2003), Wilson and Brandes (1979), Cyr (2014). Readers should refer to these documents for further details.

2.1.2.1 Measurement principle

A radar is composed of three main elements: a transmitter, an antenna and a receiver. The transmitter generates at regular time intervals, an electromagnetic energy pulses, with high power and very short duration but with a high frequency. The antenna focuses the energy in a beam in a specific space direction. The energy is then partially absorbed and re-emitted by all kinds of targets present in the beam. The energy portion returned towards the radar is captured by the receiver and is called the radar echo. To scan a volume of space (Figure 2.2b), the antenna changes direction vertically (to perform an elevation scan) and horizontally (to perform an azimuth scan), its size is larger as the wavelength is large in order to be able to locate the radar beam. Over short distances, it is considered that the electromagnetic waves propagate in a straight line at a constant speed (the speed of light). Then the orientation of the antenna and the delay between the transmission of the radar signal and the reception of the returned echo are used to estimate both the direction and the distance of the target. Moreover, the radial velocity of the target can be estimated from the difference observed between the phase of the transmitted signal and the backscattered one. Finally, polarimetric radars provide information about the shape of the target by emitting the signal in several polarizations. In case of raindrops, this is used to estimate their size knowing the fact that more their size increase, they flatten, so their horizontal dimension is large compared to the vertical one.

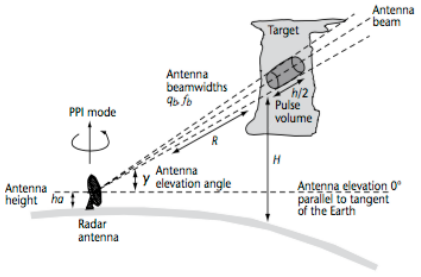

(a) Propagation of electromagnetic waves through the atmosphere for a pulse weather radar (WMO (2008))

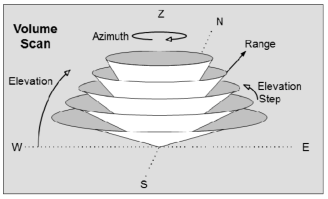

(b) The volume scan performed by the radar antenna (©SELEX)

Figure 2.2

2.1.2.2 The radar equation

The distance r of the target is determined by measuring the time delay t between the transmission of the signal and the receive of the corresponding energy reflected:

$$r = \frac{c.t}{2} \tag{2.1}$$

Where c is the speed of light and the factor 2 is used in the formula to take into account the go and back trip. Furthermore, this relation defines also the radar range r_{max}, which is determined by the time interval T between two radar pulses:

$$r_{max} = \frac{c.T}{2} \tag{2.2}$$

So, targets located beyond the distance r_{max} reflect a negligible signal.
It was established through several considerations that power received back to the radar $P(r)$ is related to the radar reflectivity $\eta(r)$ through Equation 2.3, called the radar equation:

$$P(r) = \left[\frac{P_e G^2 \lambda^2 \theta \phi h}{1024\pi^2 \ln 2}\right] . \frac{\eta(r)}{r^2} \tag{2.3}$$

Where P_e is the transmitted power; G is the gain of the antenna; λ is the wavelength of the transmitted signal; θ is the horizontal beam-width and ϕ the vertical one; r is the distance of the target from the radar and h is the pulse length in space. The part between brackets is constant and depends only on the characteristics of the radar in use. It is called the constant of the radar and the denoted C.
The radar reflectivity factor $Z[mm^6 m^{-3}]$ is the sixth-order moment of the raindrop size distribution $N(D)$:

$$Z = \int_0^{+\infty} N(D) D^6 dD. \tag{2.4}$$

A common practice is to express the reflectivity factor in a logarithmic scale or dBZ units which is numerically defined as:

$$[dBZ] = 10 \log(Z[mm^6 m^{-3}]) \tag{2.5}$$

Under the Rayleigh approximation (the size of droplets reflecting the radar signal is assumed to be much more smaller than the radar wavelength ($D \ll \lambda$)), the radar reflectivity factor Z is simply proportional to the radar reflectivity $\eta(r)$ through the

relationship:

$$\eta = \frac{\pi^5}{\lambda^4}|K|^2 Z. \tag{2.6}$$

Where $|K|^2$ is the complex index of refraction,it is 0.93 for water and 0.197 for ice. However, the Rayleigh approximation is no longer valid for the radar using a wavelength λ less than 10 cm or for non-spherical particles. In this case, Equation 2.6 remains valid on the condition of taking into account the equivalent radar reflectivity factor Z_e instead of the reflectivity factor Z.

$$\eta = \frac{\pi^5}{\lambda^4}|K|^2 Z_e. \tag{2.7}$$

Z_e is defined as the reflectivity factor of a population of liquids and spherical particles satisfying the Rayleigh approximation conditions and producing a signal of the same power. It is no longer the sixth-order moment of the raindrop size distribution and it is defined by Equation 2.8:

$$Z_e = \frac{\lambda^4}{\pi^5|K|^2}\int_0^{+\infty} N(D)\sigma(D)dD \tag{2.8}$$

Z_e depends now on the wavelength of the radar used. $\sigma(D)$ is the effective section of backscattering for a spherical drop.

In meteorology, several wavelengths are used, the three most used ones for precipitation estimation are cited below :

- **S band :** S-band radars use the greatest wavelength (8 - 15 cm), so lower frequency (2 - 4 GHz). They need a very impressive antenna (4 to 8 m) to focus the emission into a convenient beam for rainfall measurement (about 1°). They are therefore huge and difficult to install in urban environments but practically not affected by the attenuation and may have a very long range up to 500 km.

- **C band :** C-band radars are widely used by national meteorological services, they use a wavelength between 4 and 8 cm, their frequency is between 4 and 8 GHz and they use a big antenna size. C-band radar are affected by attenuation, their range is up to 200 km.

- **X band :** X-band radars use a short wavelength (2.5 to 4 cm) and high frequency (8 - 12 GHz). The antenna size is generally between 1 and 2 m, so their are easily transportable and their short pulses allow to obtain a very good radial resolution

(tens of meters). However, this low wavelength used makes that their signal is highly attenuated by raindrops and they have therefore a short range.

Other (Table 2.1) high frequency ranges (K-band and W-band) are used as well in meteorology especially for the characterization of clouds.

Designation	frequency band	wavelength range	applications
S-band	2 - 4 GHz	8 - 15 cm	Precipitation
C-band	4 - 8 GHz	4 - 8 cm	Precipitation
X-band	8 - 12 GHz	2.5 - 4 cm	Precipitation
K-band	18 - 27 GHz	1.2 - 1.7 cm	Clouds
W-band	75 - 110 GHz	0.27 - 0.4 cm	Clouds

Table 2.1: Radar frequency used in meteorology and the corresponding wavelength range used.

The Equation 2.8 shows that the equivalent radar reflectivity factor Z_e depends on the wavelength used. Indeed, it is clear that the radar technology used and its applications are very different depending on the frequency at which the radar operates and the wavelength used. The choice of the wavelength influences mainly on three parameters:

- **On the size of the radar antenna :** The opening angle θ of an antenna of diameter d is $\theta = 70\lambda/d$. We can therefore acknowledge the existing dependence between the antenna diameter d and the wavelength λ. In fact, if we want to keep the opening angle small as it is required for precipitation estimation (between 0.5°and 1°) we should increase the antenna size d as the wavelength λ increases. This is why S band and C band radars have huge radar antenna while X-band ones rely often on small antenna.

- **On the reflectivity factor Z :** Under the Rayleigh approximation the Equation 2.6 shows that for the same rainfall intensity (same radar reflectivity factor Z), the radar reflectivity η strongly depends on the wavelength λ. Thus, more the wavelength is greater, the radar reflectivity will be low. In an other way, shorter

wavelengths are more sensitive to low radar reflectivity factors Z and makes it possible to detect non-precipitating clouds (K and W bands).

- **On the attenuation intensity :** The attenuation of the radar signal is a big issue for radar meteorology, and still a challenging problem for radar specialists to overcome. The choice of the radar technology and the wavelength used are crucial and usually made in order to limit the effects of attenuation. In fact, the attenuation intensity is highly dependent on the wavelength λ and the diameter of the raindrops D. The attenuation is weak and can be neglected for a radar operating with a 10 cm wavelength, while it is important in case of a radar operating with a small wavelength $\lambda \leq 5cm$.

2.1.2.3 Uncertainties of radar measurements and sources of errors

Radar-based rainfall measurements are subject of several sources of errors that were widely reported in the literature (AghaKouchak et al. (2010), Krajewski et al. (2010a), Villarini et al. (2008), Ciach and Krajewski (1999), Wilson and Brandes (1979)). According to Wilson and Brandes (1979), the numerous sources of uncertainties associated with radar-based rainfall estimates can be classified on three categories; 1) uncertainties on measuring the radar reflectivity factor, 2) uncertainties related to variability in $Z-R$ relationship and 3) uncertainties related to the sampling differences between radar and rain gauge.

Uncertainties on estimating the radar reflectivity factor include calibration of the radar itself, attenuation of the radar signal especially at lower wavelength (Lahaie and Lecours, Otto and Russchenberg (2010), Berne (2005), Hamilton (1960)), bright band, anomalous propagation, beam blockage by obstacles near the radar site (Zhang et al. (2011), Lang et al. (2009), Bech et al. (2003)), and ground clutter (Sánchez-Diezma et al. (2001), Hubbert et al. (2009)).

Several studies investigated the variability of raindrop size distribution (DSD) and it influence on the $Z-R$ relationship (Cyr (2014), Puhakka (1974), Mapiam and Sriwongsitanon (2008)).Wilson and Brandes (1979) listed some physical processes that can affect the drop size distribution while Fišer (2004) investigated the use of different $Z-R$ formulas. Some weather radar services may use double Z-R relationship, for example

$Z = 200R^{1,6}$ for stratiform rain and $Z = 486R^{1.37}$ for convective rain (Badoche Jacquet et al. (1994)). Other works try to derive the $Z - R$ relationship using disdrometers and gauges (Cyr (2014)).

In spite all progress for radar data correction, some of these uncertainties remain and often propagate to hydrological models outputs and radar-based forecast and can have significant consequences in the context of hydrological applications Stransky et al. (2007a), Wu et al. (2014)).

However, recent advances noticed in the radar technology and the understanding of physical basis of rainfall processes enhances the capability of weather radars to provide quantitative estimates of precipitation. There is a huge work in quantifying errors in radar rainfall estimates. In the mean time, the correction often relies on the radar-rain gauge adjustment using different techniques. However, rain gauge network are also subject to different sources of errors that should be taken into account, in addition to that, the quality of points measurements areal estimation as reported in (Section 2.1, Section 2.1.1) decreases with increasing area size, increasing time period, increasing gauge density, and increasing rainfall amount.

2.2 Radar rainfall products available in Paris region

2.2.1 The French National weather radar network

The French National weather radar network ARAMIS (Application Radar à la Météorologie Infra Synoptique) has known huge transformations in the past few years. The network is in continuous growth and development both on the number and the technology of radars deployed, but also on the algorithm chain used for the data processing. In 1991 the French network consists of 8 C band radars and 3 S band ones and it was so far from covering the whole French territory. In 2012 (Figure 2.3) the network was significantly improved with more new radars installed (24 C band and S-band radars and 4 X-band radars), the network contains several dual polarization radars (13 of the 24 radars are polarimetric). The projected configuration of the network at 2017 shows a dense network with 24 C-band and S-band radars, most of them (19 radars from 24) are dual polarization and 8 X-band radars.

The algorithm chain used by Meteo France services for radar processing has been improved as well in the aim of integrating new radar processing techniques and the enhancements offered by new radar capabilities like the Dual polarization and Doppler. Improvements are widely described in scientific papers (Delrieu et al. (2000), Tabary et al. (2007), Tabary (2007), Tabary et al. (2011), Figueras i Ventura and Tabary (2013), Emmanuel et al. (2012), Figueras i Ventura et al. (2012)).

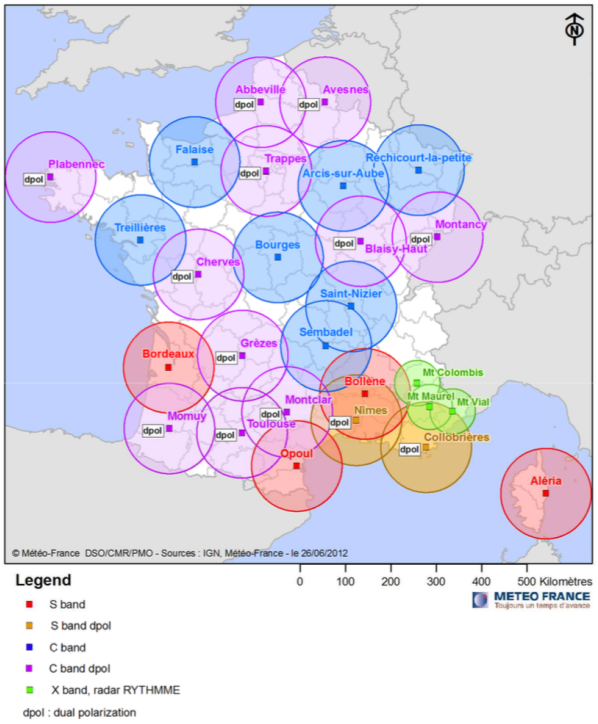

Figure 2.3: The French National Weather network ARAMIS in 2012

Some of the radar data used in this work are derived from the French National Network (ARAMIS) and was therefore processed using Meteo France chain algorithm. This is why we found it important to present in the following points the major processing steps used to correct, convert and adjust the raw radar data to obtain the final radar rainfall product.

The French network combines polarimetric and non-polarimetric radars. Indeed, the operational radar rainfall product is used to process both data, it includes two chains: one for the single polarization radars and the other one for polarimetric radars. The processing chain of the conventional single polarization radar was described in detail in (Tabary (2007), Tabary et al. (2007)). The first version (Figure 2.4) of the polarimetric chain operational since late 2011 is described in Figueras i Ventura et al. (2012) and

uses polarimetry only to correct attenuation and filter out clear-air echoes. The second version (Figure 2.5) of the polarimetric chain that will be operational in 2017 extends the use of polarimetry, in particular for the reflectivity to rain rate conversion (Figueras i Ventura and Tabary (2013)). Below some important steps of the processing chain will be summarized below. Readers should refer to Tabary (2007), Tabary et al. (2007), Figueras i Ventura et al. (2012), Figueras i Ventura and Tabary (2013) for further details.

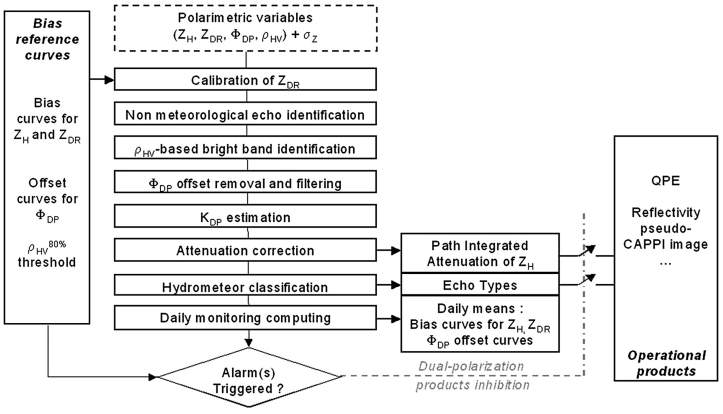

Figure 2.4: The first version of the polarimetric processing operated since 2011(Figueras i Ventura et al. (2012))

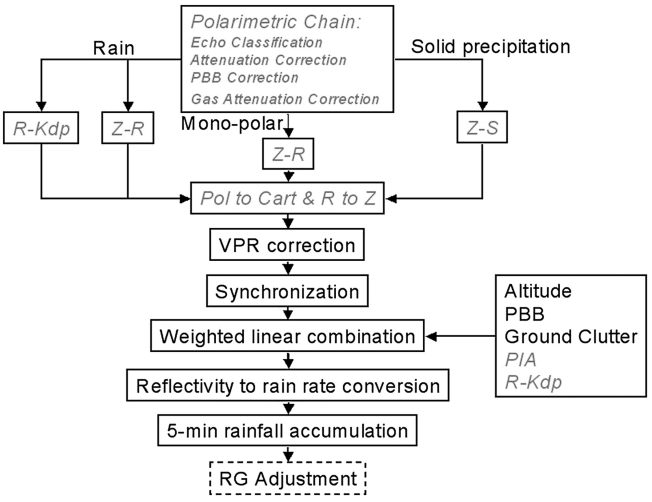

Figure 2.5: The new version of the polarimetric processing that will be operational in 2017 (Figueras i Ventura and Tabary (2013))

The new Meteo France processing chain uses polarimetric radar outputs, mainly; the horizontal reflectivity factor Z_h, the differential reflectivity Z_{DR}, the differential phase ϕ_{dp}, the correlation coefficient ρ_{hv} and the pulse-to-pulse fluctuation of the radar reflectivity σ_z in the correction of the data.

- **Ground clutter correction :** In the single polarization chain (Tabary (2007), Tabary et al. (2007)) ground clutter (GC) identification is performed using the pulse-to-pulse fluctuation of the radar reflectivity σ_z (Sugier et al. (2002)). The threshold level σ_{z0} is set to be around 1 dB in ground-clutter areas, 5 dB in rain, and 3 dB in snow. So the distinction between all forms of echoes is done quite satisfactory (Tabary (2007)).

  In the first version of the polarimetric chain (Figueras i Ventura et al. (2012), Figure 2.4), a new condition has been added based on the Doppler velocity of the targets, in case of a low velocity the echo is considered to be a ground clutter one. Moreover the pixels adjacent to a pixel identified as ground clutters are further analyzed. If no pixel adjacent to those pixels is valid they are classified as well as ground clutters. Otherwise their reflectivity value is substituted by the average reflectivity of the surrounding valid pixels. In the new polarimetric chain (Figueras i Ventura and Tabary (2013), Figure 2.5), a static ground clutters map is used as well, and a threshold (15 dB signal-to-noise ratio) was set up for the use of polarimetry. In fact, Meteo France assumes that below this threshold, polarimetric variables are not usable because of hardware or data transmission problems or because the signal-to-noise ratio (SNR) is too low.

- **Attenuation correction :** The attenuation correction is not performed in the single polarimetric chain.

  In the first version of the polarimetric chain, attenuation by rain is corrected using the differential phase ϕ_{dp}. In fact, the attenuation by rain is assumed to be linearly proportional to ϕ_{dp}. The coefficient of proportionality is set to be 0.08 dB for C band radars, 0.04 dB for S-band radars and 0.28 dB for X band radars.

- **Radar raingauge adjustment :** The processing chain used for the single polarization radars does not perform any real time radar rain gauge adjustment. This adjustment was introduced in the polarimetric chain. Rain gauge data are then used to correct the whole 5-min rainfall accumulation image. Indeed, one single-bias adjustment factor (C_F) is computed using data of the preceding hours, this factor is applied to the 12 next 5min radar images and updated at the end of the current hour. The C_F factor is calculated from ratios between rain gauges and the corresponding radar pixels using the formula given in (Tabary et al. (2011)).

- **Reflectivity Z to rain rate R conversion :** In the single polarization radars, the Z–R relationship used to convert radar reflectivity $Z(mm^6.m^{-3})$ to rain rate $R(mm.h^{-1})$ is the Marshall–Palmer relationship (Marshall and Palmer (1948)):

$$Z = aR^b \tag{2.9}$$

where a=200 and b=1.6. No distinction between stratiform and convective storm is used in this step.

In the new polarimetric chain, the rainfall rate is estimated differently according to the echo type. Solid precipitation (snow, ice, etc.) is estimated using a $Z - R$ relationship where Z_h has been attenuation corrected. The quantification of rain depends on a K_{dp} threshold. If K_{dp} is above a certain threshold, then the $K_{dp} - R$ relationship (Equation 2.10) is used otherwise the $Z - R$ Marshal-Palmer relationship is used. For S and C-bands radars, the K_{dp} threshold is set to $1°km^{-1}$ ($30mmh^{-1}$), in this case $m = 129$ and $n = 0.85$, while for X-band radars, the threshold is set to $0.5°km^{-1}$ with $m = 132.44$ and $n = 0.791$ Tabary (2007), Tabary et al. (2007), Figueras i Ventura et al. (2012), Figueras i Ventura and Tabary (2013).

$$R = m(\frac{K_{dp}}{f})^n \tag{2.10}$$

where K_{dp} is the specific differential phase and f is the central frequency in gigahertz.

2.2.2 CALAMAR forecasting system

CALAMAR is a forecasting system developed by a private company RHEA in 1992 following works of Neumann (1991) and Einfalt et al. (1990), Einfalt (1988) and protected by three patent documents Raay and Thevenet Leprevost Amelie (2008), Badoche Jacquet and Blanchet (1994), Badoche Jacquet et al. (1994). CALAMAR is widely used in France to manage urban pluvial water sewer networks. It is based on the use of radar/rain gauge data in real time and can be combined with a warning system for flooding mitigation applications. Therefore, the product is targeted towards the anti- flood services, urban water managers and especially local authorities. In Paris area, it is used by the County

Council of Val-de-Marne for the predictive management of the Sucy-en-Brie retention basin, it is also used by the General Council of Seine-Saint-Denis county (CG93) and by SIAVB (Syndicat Intercommunal d'Assainissement de la Vallèe de la Bièvre) for real time flow management of the BIEVRE catchment.

Several investigations were conducted in the framework of this thesis to understand issues encountered with CALAMAR system and possible improvements that can be proposed in order to enhance the reliability of the system and to re set up the predictive management strategy of the Sucy-en-Brie retention basin.

Of course understanding a private and well-protected system was not an easy task. In fact, no technical or scientific papers describing in details the functioning of the system exists despite two thesis published in 1991 and 1988 and some patents documents that have been protected for a long time before becoming public recently (no longer protected by the patent, so can be consulted by the public). However, information included in such documents are not as detailed as it is the case of scientific papers and we do not have any details about improvements or modifications done since the publication of these documents. So all information given in this thesis about algorithms and methods used by CALAMAR system were elaborated from the documents we hold and a lot of investigations were performed on CALAMAR data to understand further more and also confirm algorithms used by the system.

2.2.2.1 CALAMAR data processing

CALAMAR system uses the same raw data coming from the C-band Dual polarization and Doppler radar of Trappes (37 km West from the case study), managed by Meteo-France. However CALAMAR has no access to dual polarization and Doppler outputs (like K_{dp}, ϕ_{dp}, the velocity maps,...), so it relies on a single polarization algorithm scheme for data processing.

No explication is available about the reason behind this choice and whether it is motivated by economic reason (Dual polarization data should clearly be more expensive than the single one), or if it is the consequence of the competition in this field. In fact, the

demand for the use of this kind of forecasting system is growing in France and Meteo-France started recently (in 2011) commercializing it own forecasting system developed specifically for urban applications.

The processing chain used by CALAMAR is based on three important steps; (1) reflectivity correction, (2) reflectivity to rain rate conversion and (3) radar-rain gauge adjustment.

1. **Reflectivity correction :**

   As discussed in the state of the Art (chapter 0, section 1), radar reflectivity is subject to several sources of errors and should be carefully corrected. In fact the returned signal can be derived from a precipitation echoes as it can be from a non precipitated echoes like ground clutter echoes (building,...) or air-echoes (targets that).

   For the treatment of ground clutters, CALAMAR uses the static method for the identification and the removal of ground clutter echoes, this method is applied in real time for every single radar image according to either or not it corresponds to a rainy time. If the image is representative for a dry weather time, then all pixels with high reflectivity are assumed to be ground clutter echoes, and therefore they are identified and marked in a specific clutter echoes map. If on the contrary the image corresponds to a rainy weather then all pixels previously identified on the clutter echoes map will be removed from the current radar image and replaced by extrapolation of rain cells or by zeros. RHEA confirms that no interpolation with adjacent pixels is done at this stage to replace the removed ground clutter echoes pixels.

   The distinction between dry and rainy weather is based mainly on the ratio of pixels detected with significant reflectivity. Indeed, if this ratio is below a certain threshold (3% for example) then the image will be considered as representing a dry weather, otherwise it will be considered as representing a rainy weather. The extrapolation of rain cells that serves to replace ground clutter echoes pixels is represented in section 2.

2. **Reflectivity to rain rate conversion :**

   CALAMAR system uses Marshall–Palmer relationship for the reflectivity $Z(mm^6m^{-3})$

to rain rate $R(mmh^{-1})$ conversion (Equation 2.9) with a =200 and b =1.6 for stratiform rain and a=486 and b=1.37 for convective rain. The switching from one to the other can be made during the same rainfall event.

3. **Radar-rain gauge adjustment :**

   CALAMAR system has access in real time to point measurements coming from the 30 rain gauges available within the Val-de-Marne network (Figure 1.10). This data is used to perform a rigorous real time adjustment for the radar product. The adjustment is used to correct the radar calibration issues and to overcomes estimation errors of the Z-R relationship parameters. RHEA evokes the necessity to have a sub rain gauge network with a minimum gauge distance between 2 and 4km, this has the ability to catch all significant rain cells for which the size is 4 km by 4 km, the velocity is around 40 km/h and a 20 min lifetime.

   The adjustment is performed in real time using a single calibration factor CF to adjust the entire 5 min radar image, the CF is computed as the ratio between rain gauges and the corresponding radar pixels. CALAMAR forecasting system (Badoche Jacquet et al. (1994)) computes the adjustment factor every 15 min and it is used to adjust the next 3 radar images.

2.2.2.2 CALAMAR forecasting algorithm

To meet the increased urban flooding risk, sewer networks have been largely evolved in the past few years. They are certainly more complex now, but they incorporate considerable technical capabilities that allow an optimal management of urban flooding and real time decision-making. In fact, even automated management systems have been set up and are able to simulate and propose management scenarios based on continuous monitoring of the sewer network state.

In addition to that, resilience strategies were developed and designed to protect important infrastructure from flooding in order to ensure a safe return to the normal state of the catchment as quickly as possible. However, small urban catchment of a few km^2, characterized by a short response time [10 min - 30 min] are much more challenging because all these strategies cannot be applied without information about the rainfall forecast. Indeed, radar based forecast constitutes a valuable input information in near

real time and provides emergency management authorities sufficient time to respond to the warning and take adequate decisions to avoid flooding.

Many radar-based forecasting methods were developed over the years (Kyznarová and Novák (2009), Rosenfeld (1987), Germann and Zawadzki (2002), Mecklenburg et al. (2000), Berenguer et al. (2005), Bellon et al. (2010), Novák et al. (2009), Brémaud and Pointin (1993)) and used for urban hydrology applications (Einfalt et al. (1990), Berenguer et al. (2005), Burlando et al. (1996), Pessoa et al. (1993), Bell and Moore (1998), Einfalt et al. (2004), Löwe et al. (2014), Schellart et al. (2009), Einfalt et al. (1990)). The basic idea for a radar-based forecast is the spatial extrapolation of the precipitating echoes. This extrapolation can be performed in two manners that are extensively described in the literature: area tracking methods (Figure 2.6a,Mecklenburg et al. (2000), Reyniers (2008)) and cell or centroid tracking methods (Figure 2.6b, Einfalt et al. (1990)) as it can be performed using a global approach.

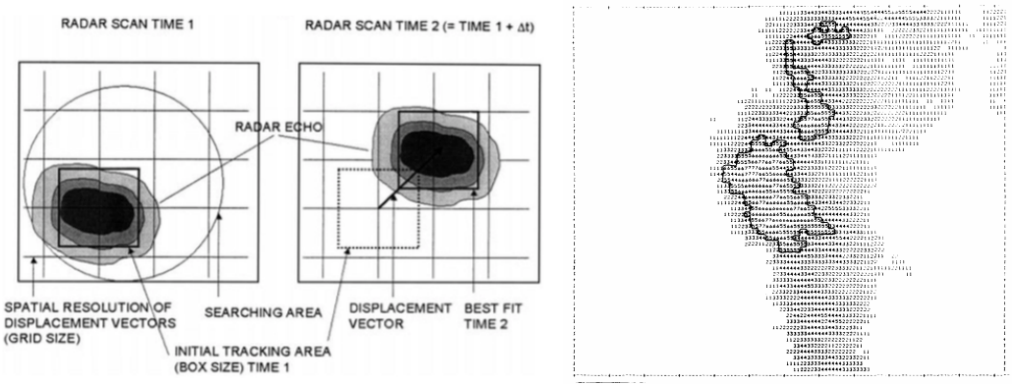

(a) Area tracking forecasting method (Mecklenburg et al. (2000), Reyniers (2008))

(b) Cell tracking forecasting method (Einfalt et al. (1990))

Figure 2.6: Area tracking and Cell tracking forecasting method

The global approach of QPF is based on the extrapolation of the entire radar image using a mean velocity vector computed based on the successive radar images comparison. This basic approach made an assumption about the displacement of rain cells inside the radar image, which are not taken into account. The area tracking method (Mecklenburg et al. (2000), Reyniers (2008)) divides the radar image on several blocks and each block is then extrapolated using the global approach. A new-sophisticated method exists (Einfalt et al. (1990)) and it is based on individual cell tracking or centroid tracking. This structural method relies often on four steps: 1) identification of rain cells in the current radar image, 2) matching step to identify identical cells on consecutive images by

performing a cross-correlation of two successive radar images, 3) characterization of rain cells by computing typically their centroid coordinates, the area, their velocity vector and 4) the extrapolation of rain cells movements. Technical details of the tracking algorithms, and the skill of the corresponding forecasts, have been reported in the literature for a single-radar domain to continental scale (Rosenfeld (1987), Reyniers (2008), Mandapaka et al. (2012), Novák et al. (2009)).

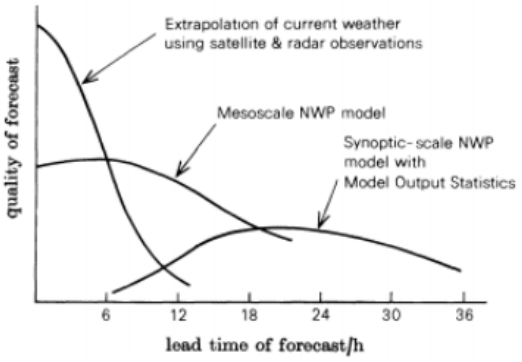

Figure 2.7: Quality comparison of three QPF methods as function of the forecast lead time (Browning (1980), Reyniers (2008))

The extrapolation-based forecasts were shown to have good skill up to lead times of 1–2 h (Figure 2.7). However, their skill decreases rapidly with lead-time because they do not account for the initiation, growth, and dissipation of precipitation patterns (Bellon and Austin (1984), Mandapaka et al. (2012)). To improve the accuracy of QPF for larger lead time, various studies (Burlando et al. (1996), He et al. (2013), Sokol (2006)) have focused on the combination of both extrapolated radar-based techniques and Numerical Weather Prediction models (NWP) which are assumed to give better accuracy for larger lead time since they integrate information about physical and meteorological processes.

A new methodology developed by Seed (2003) has emerged in recent years , it is based on the decomposition of the radar reflectivity field into a cascade of structures of different scales, each cascade is predicted separately taking into account an estimation of its life time. Macor et al. (2007b) worked on a Multifractal method applied to rain forecast using radar data.

The forecasting algorithm used by CALAMAR is based on the structural extrapolation of rain cells. It is performed for every single radar image and allow to get QPF estimation

for short lead lime up to 2h used for the warning system verification. The algorithm is based on four important steps:

1. **Identification of rain cells :**

   The basic step of CALAMAR forecasting system is the identification of rain cells observed in the current radar image. This identification has been set up by Einfalt et al. (1990), Einfalt (1988) and consists on grouping radar pixels to form entities called rain echoes or rain cells. This identification is based on two thresholds, one for the radar reflectivity threshold r_{min} set up in order to limit the number of rain cells and the second one is the maximum distance d_{max} that defines whether or not a single pixel can be considered as a part of the nearest rain cell.

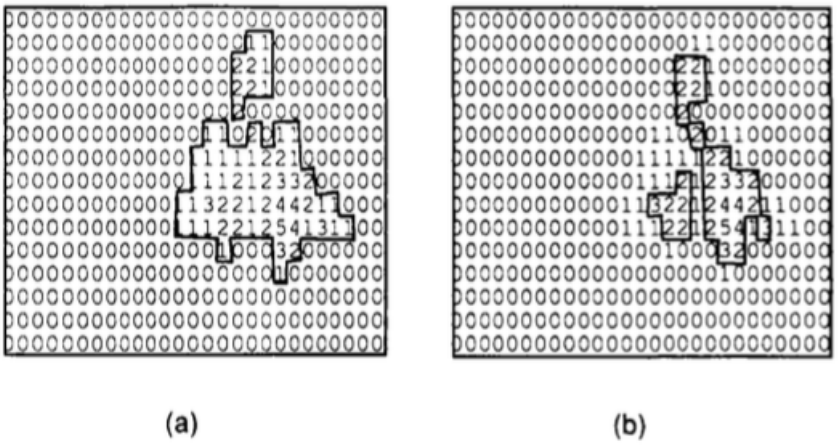

Figure 2.8: Rain cells identification when considering : a); $r_{min} = 1$ and $d_{max} = 1$ and b) $r_{min} = 2$ and $d_{max} = 1.5$ (Neumann (1991))

   Neumann (1991)) proposes r_{min} =25 dBZ and $d_{max} = 1.5$ in its work. Furthermore, two other parameters (one for the size of the rain cell and the other one for its mass) were used to limit even more small rain cells with no flooding risk. It is important to note that we don't have information about exact values of these threshold used in the actual version of CALAMAR system.

   Figure 2.8 obtained from Neumann (1991) shows rain cells identification when considering : a); $r_{min} = 1$ and $d_{max} = 1$ and b) $r_{min} = 2$ and $d_{max} = 1.5$.

2. **The matching step :**

   The aim of the matching step is to identify selected rain cells in previous radar

images in order to characterize their movements. So previous radar scans are selected to obtain potential matching cells.

Neumann (1991) developed an automatic method based on the artificial intelligence concept to determine the matching cells based primary on their characteristics comparison and modifications observed on previous radar images. This method relies also on the type of the rainfall event and the radar image characteristics.

Several extrapolation based techniques perform the matching step using a cross correlation between successive radar images. Indeed, the current radar image is compared with several displaced realizations of the previous radar image. The most correlated realization defines the most probable matching. However, this method shows some limits during specific weather conditions.

3. **Characterization of rain cells :**
   According to Badoche Jacquet et al. (1994), various characteristics are retrieved for selected rain cells. Mainly, their size (km^2), their mass defined as the product of their size and their mean intensity (m^3/h), their mean and max intensity (mm/h), the variance observed in their intensity, their center coordinates and the most important is the velocity and direction of their movements. In addition to these characteristics the mean vector velocity is computed as well and will be applied for the extrapolation of rain cells for which no individual velocity vector was retrieved for some reasons among them the matching step failure.

4. **Extrapolation of rain cells movements :** The extrapolation step performed by CALAMAR consists on the simple extrapolation of rain cells movements following their vector velocity retrieved in the previous step and without performing any change in their characteristics (form, intensity,...). Each selected rain cell will be displaced individually which offer better representation of these movements heterogeneity comparing to the global extrapolation approach.

2.3 Multifractal theory

The comparison methodology of this thesis has been developed in the framework of multifractals. This is not surprising because precipitation has been very inspiring for the development of multifractals. It was indeed argued (Schertzer and Lovejoy (1987a)) that

the complex structure of rainfall and clouds presumably result from coupled cascades of turbulent wind and water content and mutlifractals are the generic output of cascade processes. Furthermore the basic phenomenology of multifractal fields does correspond to that of precipitation: higher and higher activity of these fields is concentrated on smaller and smaller fractions of the embedding space. But with multifractals, this behavior can be quantified: "smaller" that means "smaller fractal dimension". This manner of quantifying intermittency, a basic feature of precipitation that has remained illusive for quite a while, already explains the mushrooming interest in multifractals (see Lovejoy and Schertzer (1992) for an early review) on various aspects of precipitations, for instance : extremes Hubert et al. (1993), Schertzer et al. (2006), Bernardara et al. (2007), Schertzer et al. (2010) , climate Royer et al. (2008a), Lovejoy and Schertzer (2013), prediction Marsan et al. (1996), Schertzer and Lovejoy (2004), Macor et al. (2007b), data interpolation and merging Salvadori et al. (2001), data quality Hoang et al. (2012), radar data Tessier et al. (1993), Lovejoy et al. (1996), Lilley et al. (2006), satellite data Pflug et al. (1992), Pecknold et al. (1996), Lovejoy et al. (2008), discharge data Pandey et al. (1998), Labat et al. (2013), Tchiguirinskaia et al. (2014), topography data Lavallée et al. (1993), urban hydrology Gires et al. (2012a, 2015). However, the interest of multifractals, in particular for urban hydrology, is more general because multifractals have placed precipitation in a theoretical framework where many questions can be now formalized as problems of statistical physics instead of being only analyzed with the help of a few case studies. For instance, the question of extremes can be related to multifractal phase transitions Schertzer and Lovejoy (1992), the number of relevant parameters to stochastic universality Schertzer and Lovejoy (1987a, 1997), the forecast limitations to intrinsic predictability limits Schertzer and Lovejoy (2004) and the type of involved chaos Schertzer et al. (2002b). Readers interested in the most recent developments of multifractal formalism are referred to Schertzer and Lovejoy (2011), Schertzer and Tchiguirinskaia (2015). The general idea of the method, that we develop and present in detail in Section 2.4 corresponds to the comparison of two multifractal fields, i.e. those corresponding to the precipitation field estimated by two different sensors and/or two different retrieval algorithms. This is more easily achieved in a parametric approach,, i.e. by comparing the relevant parameters of these fields. It is therefore important to consider of universal multifractals Schertzer and Lovejoy (1987a, 1997) that broadly generalise the central limit theorem to multiplicative processes and have only a few relevant parameters that are furthermore physically meaningful (see

Section 2.4 for discussion). Readers familiar with multifractals can skip Section 2.3 that gives an overview of the concepts of fractals and multifractals that are used in our methodology.

2.3.1 Fractal Geometry

Fractal geometry has been introduced by Mandelbrot (1983) and used to describe geometrical sets that represent a given level of complexity, i.e. they are too irregular to be easily described with the help of basic Euclidean concepts (e.g. a river is not a straight line), but can be described with the help of simple and repetitive processes. Fractal geometry exhibits scale invariance, which means that similar structure will be observed at any scale. In practice, the number of pixels $N_{\lambda,A}$ needed to cover the set (A) at a given resolution λ, which is defined as the ratio between the outer scale l_0 and the observation scale l ($\lambda = \frac{l_0}{l}$), follows a power-law:

$$N_{\lambda,A} \approx \lambda^{D_f} \tag{2.11}$$

where the exponent D_f is the fractal dimension and is the asymptotic slope of $N_{\lambda,A}$ vs. λ in in log-log plot. The fractal dimension can be therefore defined as follows:

$$D_f = \lim_{l \to 0} \frac{ln(N_{\lambda,A})}{ln(l)} \tag{2.12}$$

2.3.2 Codimension concept

To address the fractal behavior of random sets the codimension concept is useful (Feder (1988), Barnsley and Hurd (1989), Mandelbrot (1977, 1967)). The definition of the codimension c of a fractal set of dimension D_f is based on the same equality as for classical vector sub-spaces: $c = D - D_f$, where D is the dimension of the embedding space, e.g. the Euclidean space R^D. In fact, as discussed below, the codimension is more useful for random multifractal fields than the dimension. A first hint is that it corresponds to the scaling exponent of the probability that a given pixel will cover/intersect the fractal set A Schertzer et al. (2002a):

$$N_{\lambda,A} \approx \lambda^{D_f};\ N_\lambda \approx \lambda^D \Rightarrow \frac{N_{\lambda,A}}{N_\lambda} \approx \lambda^{D_f - D} = \lambda^{-c} \tag{2.13}$$

2.3.3 Codimension function $c(\gamma)$ and the scaling moment function $K(q)$

There had been long debate about the potential and limitations of fractal geometry to grasp the heterogeneity of fields that cannot be reduced to geometrical sets, i.e. to be binary valued function like the set indicator function. It turned out that instead of considering a unique fractal set, one has to consider an infinite hierarchy of embedded fractal sets Schertzer and Lovejoy (1983), Hentschel and Procaccia (1984), Benzi et al. (1984), Halsey et al. (1986), Mandelbrot (1989), each of them corresponding to a given level of activity, hence the term 'multifractal' coined by Parisi and Frisch (1985). This is the common fundamental feature of various multifractal formalisms. As argued by Schertzer and Lovejoy (2011), the most general one is a stochastic multifractal formalism where the level sets of activity S_λ at resolution λ of a field P_λ are defined by a scaling threshold λ^γ, where γ takes arbitrary values: $S_\lambda = \{P_\lambda \geq \lambda^\gamma P_1\}$. γ is called 'singularity' because when positive, it measures the algebraic rate of divergence of P_λ for higher and higher resolution λ. Due to Equation 2.13, it is expected that:

$$Pr(S_\lambda) = Pr(P_\lambda \geq \lambda^\gamma P_1) \approx \lambda^{-c(\gamma)} \tag{2.14}$$

where $c(\gamma)$ is a codimension that depends on the given singularity γ and is therefore called the codimension function of the field P_λ. It is worthwhile to note that whereas this codimension function is scale invariant, this is not the case of the probability itself. It can be also demonstrated with the help of the Mellin transform Schertzer et al. (2002a) that the scaling of the probability (Equation 2.14) is equivalent to that of the statistical moments:

$$\langle P_\lambda^q \rangle \approx \lambda^{K(q)} \tag{2.15}$$

where q is the moment order and $K(q)$ is the scaling moment function. Furthermore, it can be shown that the Mellin transform boils down to a Legendre transform for the exponents $K(q)$ and $c(\gamma)$:

$$K(q) = \max_\gamma(q.\gamma - c(\gamma)) = q.\gamma_q - c(\gamma_q) \tag{2.16}$$

$$\Leftrightarrow \quad c(\gamma) = \max_q(q.\gamma - K(q)) = q_\gamma.\gamma - K(q_\gamma) \tag{2.17}$$

where γ_q is defined by $c'(\gamma_q) = q$ and q_γ by $K'(q_\gamma) = \gamma$.

The symmetry of these relations, first obtained in the restrictive case of deterministic multifractals Parisi and Frisch (1985), is due to the fact that the Legendre transform is involutive and more precisely that one curve is the envelope of the tangents of the other one. It ensures the duality/equivalence of the characterization of multifractals either with the help of codimension function/probability or the scaling function/statistical moments. A product of this duality is that both $c(\gamma)$ and $K(q)$ are convex: this is fairly easy to demonstrate for $K(q)$ and this property is then transferred to $c(\gamma)$ with the help of the Legendre transform.

2.3.4 Universal multifractals

The aforementioned property that $c(\gamma)$ and $K(q)$ are both convex is the main constraint on these statistical functions. This means that they both depend in a general manner on an infinite number of parameters. However, Schertzer and Lovejoy (1987b, 1997) demonstrated that there is a broad generalisation of the central limit theorem to multiplicative processes instead of the classical additive case. Loosely speaking, the universal multifractals correspond to a generalisation of the classical Gaussian variables that are fully characterised by their two first statistical moments, e.g. mean and variance. This results from the fact that Gaussian variables are attractive and stable for renormalised sums of independently identically distributed (i.i.d.) variables having a finite variance. Although universal multifractals are strongly non Gaussian, they possess similar properties for renormalised products of i.i.d. fields. They are also characterized by only two parameters, but they are directly related to intermittency:

- C_1 characterises the mean intermittency, i.e. the intermittency of the mean field. It is both the singularity of the mean field and its codimension ($C_1 = c(C_1)$) for a conservative field ($< P_\lambda >=< P_1 >$). $C_1 = 0$ corresponds to an homogeneous field.

- α is the multifractality index ($0 \leq \alpha \leq 2$). It measures how fast the intermittency evolves when considering singularities slightly different from the average field singularity. $\alpha = 0$ corresponds to a uni-/mono- fractal field, i.e. a field characterized by a unique fractal dimension.

Both parameters are defined for any multifractal field and characterize it locally, i.e. around the mean field ($q = 1$ or $\gamma = C_1$). But in the case of universal multifractals this characterization becomes global, i.e. for any q or any γ. α and C_1 are thus often called Universal Multifractal parameters and the corresponding parametric approach Universal Multifractal analysis , in short UM parameters and UM analysis, respectively. Precisely, the scaling function $K(q)$ and codimension function $c(\gamma)$ of universal multifractals have the following analytical expressions (up to a critical order q_D or corresponding critical singularity γ_D) :

$$K(q) = \begin{cases} \frac{C_1}{(\alpha-1)}(q^\alpha - q) & \alpha \neq 1 \\ C_1 q \ln q & \alpha = 1 \end{cases} \tag{2.18}$$

$$c(\gamma) = \begin{cases} C_1(\frac{\gamma}{C_1.\alpha'} + \frac{1}{\alpha})^{\alpha'} & \alpha \neq 1 \\ C_1.exp(\frac{\gamma}{C_1} - 1) & \alpha = 1 \end{cases} \tag{2.19}$$

where $\frac{1}{\alpha'} + \frac{1}{\alpha} = 1$.

2.3.5 Universal Multifractal data analysis techniques

The aim of the Universal Multifractal analysis is to estimate the two UM parameters α and C_1. There are two methods widely used for such an analysis, the trace moment analysis (TM) and the double trace moment analysis (DTM).

2.3.5.1 Trace moment analysis:

The trace moment analysis (TM Schertzer and Lovejoy (1987a)) yields estimates of $K(q)$ first and then of α and C_1 based on Equation 2.15 and successive upscaling of the observed field; i.e degrading its resolution λ . Indeed, for any $q \geq 0$ four steps are performed :

- For each resolution λ, the moment of order q is evaluated by summing the values of P_λ^q over all the pixels (of resolution λ):

$$\langle P_\lambda^q \rangle = \frac{\sum P_\lambda^q}{\lambda^D} \tag{2.20}$$

The P_λ field is obtained by upscaling (averaging) the original data to the resolution λ.

- The logarithm of $\langle P_\lambda^q \rangle$ is plotted versus the logarithm of λ (Figure 2.9a).
- A linear regression is performed and the slope $K(q)$ is retrieved (Figure 2.9b).

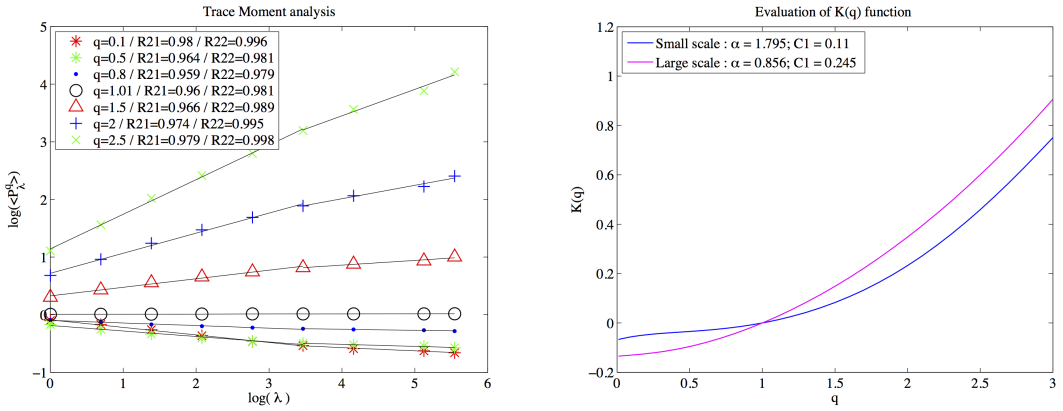

(a) **(b)**

Figure 2.9: Trace moment analysis: In a) the logarithm of $\langle P_\lambda^q \rangle$ is plotted versus the logarithm of λ (Equation 2.15). In b) K(q) is plotted as function of q in a log-log plot and the UM parameters α and C_1 estimated.

UM parameters can be then estimated by different techniques, e.g. obtaining nonlinear fitting of the estimated $K(q)$ with the help of its analytical expression (Equation 2.18) or in a simple manner with the help of the estimates of the first two derivatives of $K(q)$ that should satisfy: $K'(1) = C_1$ and $K''(1) = \alpha.C_1$

2.3.5.2 Double Trace moment analysis:

The Double Trace moment analysis analysis (DTM, Lavallée et al. (1992)) yields a somewhat more direct estimation of the UM parameters α and C_1 for a conservative and multifractal field P. Loosely speaking it corresponds to perform a TM analysis on various powers η of the field, hence its name. It is convenient to first introduce the normalized η^{th}-power of a multifractal field P:

$$P_\lambda^{(\eta)} = P_\lambda^\eta / \langle P_\lambda \rangle^\eta \tag{2.21}$$

which is also multifractal:

$$\langle P_\lambda^{(\eta)q} \rangle \approx \lambda^{K(q,\eta)};\ K(q,\eta) = K(\eta.q) - qK(\eta) \tag{2.22}$$

it is straightforward to check that for universal multifractals:

$$K(q,\eta) = \eta^\alpha K(q) \tag{2.23}$$

It can be then shown that the normalized η-power of the field $P_\lambda^{(\eta)}$ merely corresponds to the upscaling to the resolution λ of the η^{th} power of the field P_Λ^η observed at its highest resolution Λ. Consequently, the DTM analysis is performed following two steps:

- For each selected η values, proceed to the TM analysis of P_Λ^η that yields an estimate of $K(q,\eta)$ (Figure 2.10a).
- For given q value(s), $K(q,\eta)$ is plotted versus η in a log-log plot. α is the slope a of the linear portion of the graph and C_1 is related to the intercept b (Figure 2.10b).

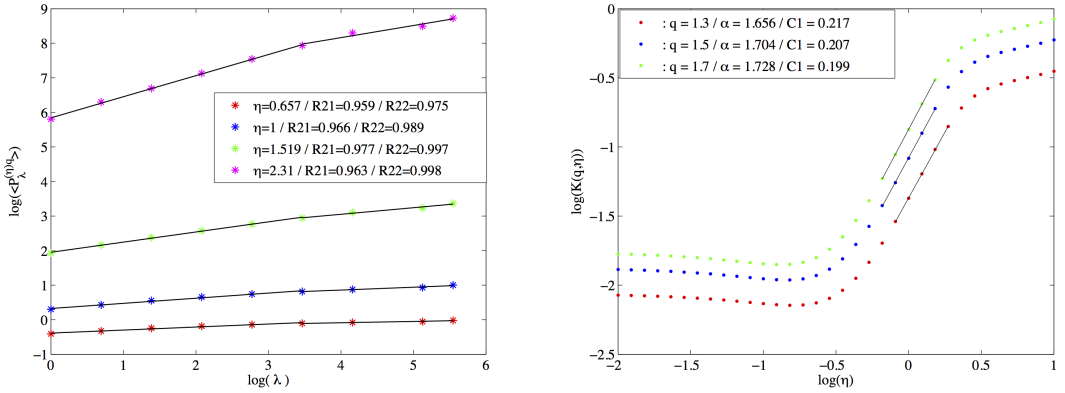

(a) **(b)**

Figure 2.10: Double Trace moment analysis: In a) the logarithm of $\langle P_\lambda^{(\eta)q} \rangle$ is plotted versus the logarithm of λ for different values of η (Equation 2.22). In b) $K(q,\eta)$ is plotted as function of η in a log-log plot for different values of d and the UM parameters α and C_1 estimated.

2.4 Multifractal comparison of two operational radar products

Various operational radar products are available over the Paris area. This part suggests a comparison between two operational products provided by Meteo-France and RHEA. Meteo-France is the French meteorological office that operates and maintains a network of 24 radars (18 C band, 6 S band) distributed over the French territory (see Section 2.2.1). CALAMAR is the forecasting system developed by a private company RHEA and used by the County Council of Val-de-Marne for the predictive management of Sucy-en-Brie retention basin (see Section 2.2.2).

The aim of this section is to perform an innovative morphological comparison between the two radar products using the Universal Multifractal framework. This comparison will help to characterize differences between the algorithms employed by each product, especially regarding the treatment of ground clutters and the adjustment phase. The multifractal analysis of radar data (spectra analysis, trace moment and double trace moment analysis) has been extensively implemented in previous studies for various purposes such as characterizing rainfall spatio-temporal variability, comparing radar data and rainfall output of numerical weather predictions (Macor (2007), Gires et al. (2011b), Dimitriadis and Koutsoyiannis (2015)). The innovative aspect of this work is that the Multifractal framework is used here to compare and validate two radar products, that use the same raw radar data but process it with the help of different Quantitative Precipitation Estimates (QPE) algorithms. Such comparison still relies in most cases on standard scores comparison with raingauges (Figueras i Ventura and Tabary (2013), Tabary et al. (2011), Figueras i Ventura et al. (2012), Gires et al. (2014b), Sebastianelli et al. (2010)). It is important to note that preliminary results of such comparison demonstrated that the real time calibration between CALAMAR and rain gauges was not performed correctly (some raingauges were not available for real time calibration due to synchronization issues during severe storms). The CALAMAR provider also discovered a wrong setting of the system, e.g., a 20 km radius around the basin for triggering an early warning was noticed, instead of a 10 km one, and rainfall thresholds were differing from those initially planed. Hence, we decide to "replay" the adjustment process using the rain gauge data provided by the CD94. All the actually available rain gauge data was imported into the system, and the calibration process has been replayed

using CALAMAR system in a delayed mode). The purpose behind replaying this adjustment process is also that we want to analyze differences between adjusted and not adjusted CALAMAR radar data in order to describe the effect of radar calibration on the morphology of the final radar product.

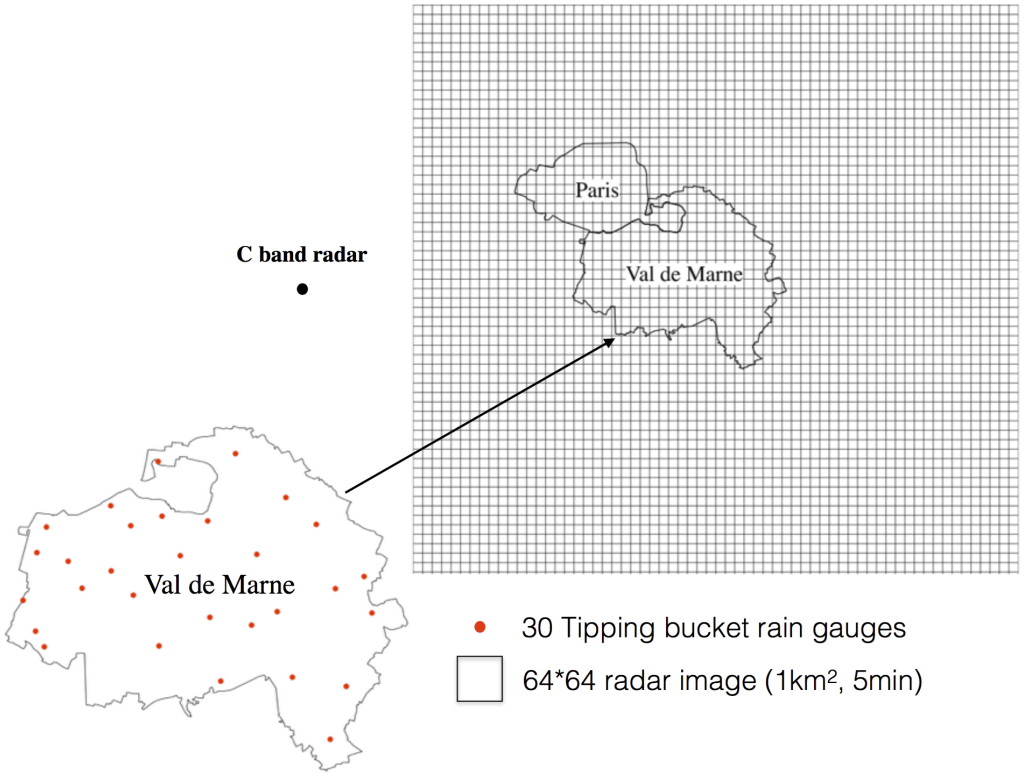

Figure 2.11: The C band radar sites, the whole radar image (64*64) and raingauge network (30) used in this study

Figure 2.11 displays the location of the 30 rain gauges available over the Val-de-Marne County and the 64*64 km^2 radar image used in this study (pixel sizes are $1km^2$). As a consequence three radar products will be compared in this study: Meteo-France data, non-adjusted (not adj.) CALAMAR and adjusted (adj.) CALAMAR data. It is important to note that in this study, neither the radar data nor rain gauge data are considered to be "ground truth", each of these devices are affected by different sources of errors; radar errors include attenuation, contamination by soil echoes, the anomalous propagation, beam blockage and radar range effects (Gebremichael et al. (2006), Vignal and Krajewski (2001), Seo et al. (2000), Sebastianelli et al. (2010), Krajewski et al. (2011)), while rain gauges are mostly affected by some local environment errors including wind,

turbulence, tipping bucket losses especially during high rainfall rates and sampling errors (Habib et al. (2001), Fankhauser (1998), Ciach (2003b), Emmanuel et al. (2012)). The two radar products and their corresponding QPE algorithms were presented in the previous section. The Multifractal theory as well as the five rainfall events selected for this comparison, and the methodology will be presented in the following subsections.

2.4.1 Material and methods

2.4.1.1 Selected rainfall events

Five rainfall events that occurred on 14th July 2010, 15th August 2010, 15th December 2011, 19th June 2013 and 16th October 2013, have been selected to perform the comparison. 30 tipping bucket rain gauges with a 0.2 mm resolution are deployed rather homogeneously over the Val-de-Marne County (245 km^2) and operated by the CD94. Most of them provide measurements in real time with 5 min time step, however only 27 raingauges were available for the events studied here. Indeed, Three of the 30 raingauges experiences some technical issues and were not validated by the CD94 for these five events. This data is available for the five events, as well as the three types of radar product (Meteo-France, CALAMAR adj. and CALAMAR not adj.) in a Cartesian 64x64 km^2 field format with a resolution of 1 km in space and 5 min in time. Table 2.2 summarizes the main characteristics of rainfall data calculated using the rain gauge network and the whole radar image, it clearly shows that maximal rain intensity observed in CALAMAR adj. field is almost twice greater than the one found in the other fields. Furthermore, the comparison of the two CALAMAR field characteristics shows that the calibration process yields overestimated rainfall rates.

		14 July 2010	15 August 2010	15 December 2011	19 June 2013	16 October 2013
Duration		7h 50min	27h	12h	6h 05min	8h 05min
$P^{max}(mm)$	Meteo-France	44.3	63.8	35.4	34.7	7.21
	CALAMAR adj.	80.2	63.8	38.8	116.9	9.95
	CALAMAR non-adj.	55.5	65.8	35.6	48.8	6.8
	Rain gauge	50.2	53	28.8	40.6	7.4
$I^{max}(mm/h)$	Meteo-France	119.2	45.5	78.4	207.7	9.7
	CALAMAR adj.	248.9	79.3	110	464.9	17.6
	CALAMAR non-adj.	136	47.4	98.1	153.4	11.9
	Rain gauge	132	43.2	81.6	151.2	9.6

Table 2.2: Main characteristics of rainfall data used in this study. P^{max} and I^{max} are respectively the maximum 5 min rainfall depth and the maximum rainfall intensity computed over the whole area.

2.4.1.2 Methodology

The purpose of this section is to quantitatively compare radar and rain gauges data (27 rain gauges were available) at various time scales. It consists in statistical comparison of each rain gauge's time series with the corresponding radar pixel by calculating at different time scales (5min, 15min, 30min and 1hour) some standard scores such as Nash-Sutcliffe coefficient ($Nash$) (Equation 2.24), $Correlation$ (Equation 2.25) and Root-Mean-Square Error ($RMSE$) (Equation 2.26), which are widely used when it comes to compare time series.

$$Nash = 1 - \frac{\sum_{t=0}^{T}(P_{Radar}^{t} - P_{RG}^{t})^2}{\sum_{t=0}^{T}(P_{RG}^{t} - \bar{P}_{RG}^{t})^2} \tag{2.24}$$

$$Correlation = \frac{\sum_{t=0}^{T}(P_{RG}^{t} - \bar{P}_{RG}^{t}) * (P_{Radar}^{t} - \bar{P}_{Radar}^{t})}{\sqrt{\sum_{t=0}^{T}(P_{RG}^{t} - \bar{P}_{RG}^{t})^2} \cdot \sqrt{\sum_{t=0}^{T}(P_{Radar}^{t} - \bar{P}_{Radar}^{t})^2}} \tag{2.25}$$

$$RMSE = \sqrt{\frac{1}{T} \cdot \sum_{t=0}^{T}(P_{Radar}^{t} - P_{RG}^{t})^2} \tag{2.26}$$

where P_{RG}^{t} and P_{Radar}^{t} are the cumulative rainfall observed respectively in rain gauge data and the corresponding radar pixel, T is the number of time steps.

Nash criterion (Nash and Sutcliffe (1970)) is commonly used in urban hydrology to evaluate the quality of a prediction with respect to the observed value (Merz and Blöschl (2004)). A value of 0.7 may be taken as an indicator of a good fit (Mc Cuen et al. (2006)). It is used here to assess the quality of radar estimations with respect to rain gauge measurements. The correlation is used in general to show whether two variables follow the same trend or not, it ranges from -1 to 1, a value of 1 indicates a perfect correlation between the two variables (linear relation). The Root-Mean-Square Error quantifies differences between predicted and observed values; a value close to zero indicates a good match between the two variables.

This statistical comparison has been used in many other studies for different purposes, in (Figueras i Ventura and Tabary (2013), Tabary et al. (2011), Figueras i Ventura et al. (2012), Gires et al. (2014b)). More specifically, it has been used to assess the performance of different QPE algorithms used by Meteo-France by comparing the hourly rainfall accumulation obtained by the QPE algorithms against hourly rain-gauges; it has also been used to perform a comparison between radar and rain gauge data at different time scales (10 , 15 , 30 and 60 min) and at different distances from the radar location (Sebastianelli et al. (2013)).

Then both, spatial and temporal, multifractal analyses are performed. In the spatial case, the sample is a radar image (64 x 64 pixels) at a single time step; then the number of samples is the number of time steps. In the temporal case, the sample is a time series corresponding to a single radar pixel, meaning that there are 4096 (= 64 x 64) samples (see Figure 2.13). This technique introduced in Macor et al. (2007a) has been used in

Gires et al. (2011b) to perform a multifractal comparison between Meteo-France radar data and numerical simulations obtained with the help of the Meso-NH model.

The first step in a multifractal analysis consists in a spectral analysis to check of the scaling behavior of the data. A scaling field exhibits a power law relation between the power spectra and the wave number (in spatial analysis) or frequency (in temporal analysis):

$$E(f) = f^{-\beta} \tag{2.27}$$

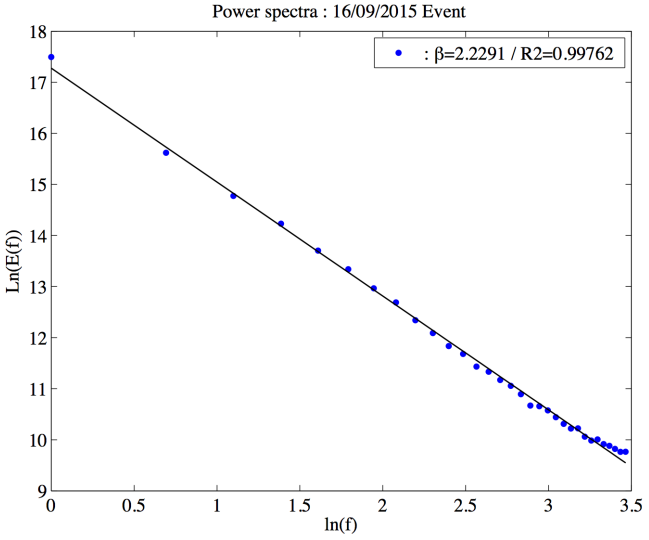

Figure 2.12: Spectral analysis (Equation 2.27). The scaling bhavior is confirmed over the whole range of scale available.

When plotted in a log-log scale, Equation 2.27 yields a straight line, as shown in the example from Figure 2.12. The spectrum exhibits a linear behavior, with a spectral slope $-\beta$. The spectral exponent β is linked to the degree of non-conservation H of the field ($H = 0$ for a conservative field) by the following relationship (Tessier et al. (1993)):

$$\beta = 1 + 2H - K(2) \tag{2.28}$$

where $K(2)$ is the second moment scaling function of the conservative part of the field (see definition below).

For a conservative field, the estimate of β is lower than the dimension D of embedding space ($D = 2$ for spatial analysis and $D = 1$ for temporal analysis). If $\beta > D$, then the field must be differentiated before implementing the multifractal analysis that assumes

a conservative field (Nykanen (2008)). A common approximation of this differentiation consists in analyzing the absolute value of the fluctuations of the field at the maximum resolution; the resulting rainfall fluctuations field is denoted $\Delta R - 2D$ in spatial analysis and $\Delta R - 1D$ in temporal analysis (Lavallée et al. (1993)).

The two UM parameters α and C_1 were estimated using UM analysis techniques presented in Section 2.3.5.

In addition to the two multifractal parameters, the fractal dimension D_F and the maximum singularity γ_s are also computed. γ_s is the maximum singularity that one can expect to observe in a field with a finite number of samples (Hubert et al. (1993)), it quantifies the extremes of a field. γ_s is estimated based on α and C_1 values following Equation 2.29 :

$$\gamma_s = C_1(\frac{\alpha}{\alpha - 1}) * ((\frac{1}{C_1})^{\frac{\alpha-1}{\alpha}} - \frac{1}{\alpha}) \tag{2.29}$$

The fractal dimension D_F (Section 2.3.1) characterizes the rainfall support in a scale independent way, it is related to the space needed to represent the data at a given resolution λ (Equation 2.11).

Figure 2.13 illustrates how the multifractal analysis is performed on the radar data, the scaling behavior is checked first with the help of spectral analysis and then confirmed by both TM and DTM analysis; the scaling regimes are also defined at this step. The two multifractal parameters α and C_1 are calculated for each sample using the DTM analysis; in the spatial analysis a couple of (α, C_1) is calculated for each single radar image and the temporal evolution of these parameters is analyzed with the help of other parameters such as the rate of zero values, the fractal dimension D_F and the maximum singularity γ_s. In the temporal analysis a couple of (α, C_1) is calculated for the time series of each radar pixel and maps describing the spatial variability of these parameters will be analyzed. For each type of analysis, ensemble estimates using all the samples at once (each sample is up-scaled independently and the average is taken in Equation 2.15 and Equation 2.23) are also computed.

Multifractal temporal analysis is performed also for the 27 raingauges data available. Similarly,the time series of each raingauge are first analyzed with the help of spectra, TM and DTM to check the scaling behavior, and then the UM parameters α and C_1 are computed and compared to the corresponding radar pixel parameters.

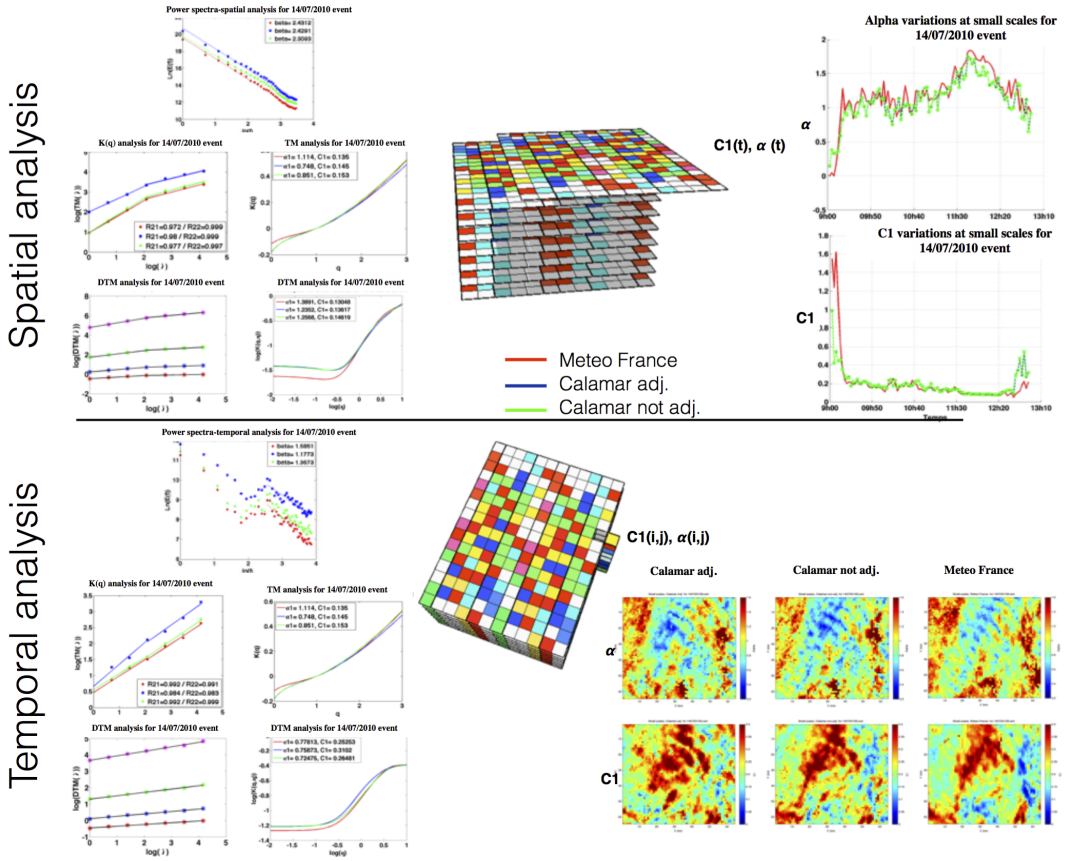

Figure 2.13: Implementation of the multifractal analysis. In spatial analysis, a point in the temporal evolution corresponds to a parameter calculated for a single radar image (the map of a time step). In the temporal analysis, a point in the map corresponds to a parameter calculated for the time series of a single radar pixel.

2.4.2 Results and discussion

2.4.2.1 Comparison with standard scores

Figure 2.14 summarizes results obtained when using the three types of radar data. It shows that for the first event, cumulative rainfall calculated using radar data are slightly lower than those calculated using data from rain gauges, we also noticed a clear over-estimation of the cumulative rainfall observed on CALAMAR adjusted data. Scores at 5 min scale confirm this remark, with a value of *Nash* and *Correlation* below 0.5 while *RMSE* error values are around 1.25. The comparison shows a correct agreement between radar and rain gauges data for the second and third events. Indeed, scores indicate that at 5 min time scale Meteo-France data is better correlated to rain gauges than both CALAMAR products while the three radar products show similar agreement with rain gauges data at 1h scale. The fourth event, exhibits the greatest disparities

in terms of cumulative depth, it was identified as an extreme event due to the high rain rates recorded (up to 200 mm/h) for some rain gauges and flooding observed in some areas. Rain rates recorded by rain gauges are much greater than those obtained by radar, especially for Meteo-France and CALAMAR not adj. The adjustment process used by CALAMAR improves radar estimations but parameters obtained show a clear disagreement between radar and rain gauges data even at 60 min scale. $Nash$ and $Correlation$ coefficients remain negative and the $RMSE$ error greater than 0.5 for all time scales. Scores obtained for Meteo-France are better than those calculated on CALAMAR product even if Meteo-France depth are much worse than CALAMAR ones. Results for the last event indicate that at 5 min scale, Meteo-France and CALAMAR non-adjusted radar data exhibit similar scores and are not well correlated to rain gauges; $Nash$ coefficients remain under 0.6, $Correlation$ coefficients are under 0.8 and the $RMSE$ errors are about 0.1. The adjustment process improves the correlation of CALAMAR data.

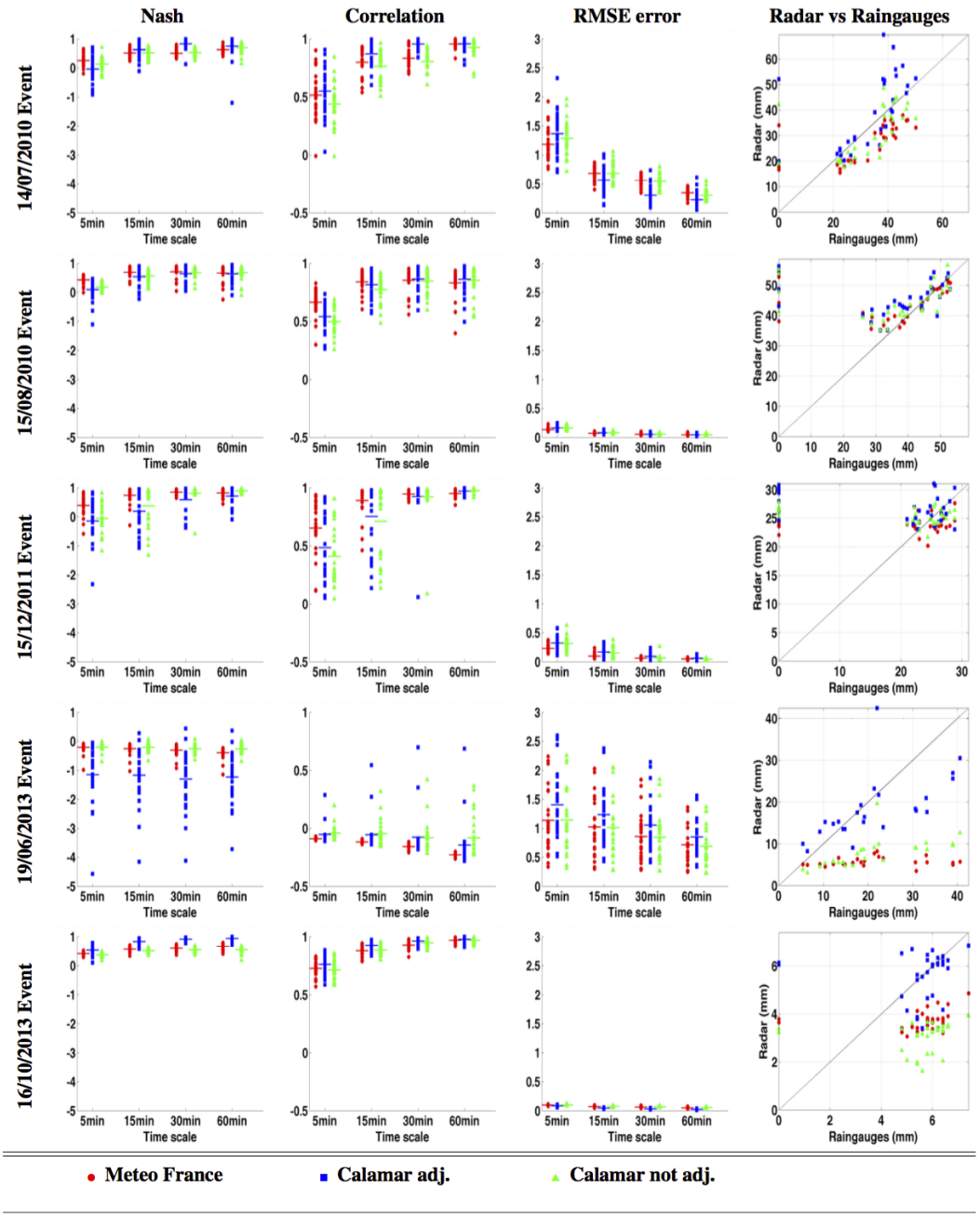

Figure 2.14: Standard scores obtained using 27 raingauges for the three types of radar data and the five rainfall events at different time scales (5, 15, 30 and 60 min), the black line represents the bisector

The comparison analysis between radar data and rain gauges given in Figure 2.14 suggests that at the original time scale Meteo-France data is better correlated in general (except for the last event) with rain gauges than both CALAMAR products. The quantitative evolution of the scores with time scale indicates a tendency to improve with greater time steps but not systematically and not in the same magnitude for each event.

A significant improvement of scores is observed (except for the last event) when increasing the time scale from 5 min to 15 min and then less significant when increasing from 15 min to 1 h. Disparities among points tend to decrease with greater time steps (except for correlation for second and the fourth events). This high scale dependency may be related to the presence of singularities. In fact the calibration process used by CALAMAR product is performed at each time step by calculating the average rate observed between radar and rain gauges without taking into account singularities and potential strong variability, which may explain the regular shift noted between the two CALAMAR products. Therefore, this calibration process seems to be adapted well when rain gauge measurements are close together (Events 3 and 5 as examples) and not so well when they are scattered (Events 4, 1 and 2 as examples).

The validation analysis presented here is widely used when it comes to validate radar data. It allows us to highlight the dependence on time scale and also the calibration issues encountered with CALAMAR product. It was helpful to judge the quality of radar adjustment, but it does not allow concluding on differences between the three types of radar data because of the very small number of pixels involved in this study (only 27 among 4096=64*64) and their position in the center of the radar image as shown in Figure 2.11. It is also important to note that rain gauge measurements are subjects to uncertainties as discussed in Ciach (2003b), Emmanuel et al. (2012), and that intrinsic small scale (sub-radar pixel size) rainfall variability also introduces a bias (Zhang et al. (2007), Emmanuel et al. (2012), Gires et al. (2014b)).

2.4.2.2 Rainfall analysis across scales

- **Power spectra analysis :** Figure 2.15 displays Equation 2.27 in log-log plot for the three fields in both spatial and temporal analysis. In spatial analysis (Figure 2.15, first column) straight lines are obtained. A break is noticed for the 2011 event at wave number $k \approx 7$ which corresponds to 9 km. The spectral exponent β estimates for small scales range from 2 to 2.8 with greater values for Météo-France fields suggesting shorter correlation ranges. We find β greater than the dimension of the field (2 here) meaning that it is non-conservative. The $\Delta R - 2D$ new fields still exhibit a scaling behavior with lower values of β in most of the cases (Figure 2.15, second column), a break is noticed for the last three

events around the wave number $k \approx 12$ which corresponds to approximately 6 km. β remains greater than 2 for the last three events except for CALAMAR adj. data. In the temporal analysis (Figure 2.15, third column), a scaling behavior is retrieved for the 15 August 2010, 19 June 2013 and 16 October 2013; and less clearly for the other events. Two distinct ranges of scales separated by a break at 18 min are visible for the 2011 event. For 14 July 2010 event it seems that we obtain three ranges (with two slope breaks) instead of the two usually observed (the second break is observed at $f \approx 13$ which corresponds to 36 min). However the short duration of the event limits samples length, and hence reduces the reliability of the analysis. In fact, spectral analysis, being a statistical property requires large amount of data to be properly observed. The spectral analysis is more sensitive to this issue than the TM and DTM (whose results are discussed in the following parts). Nevertheless the absence of a clear spectral slope highlights a lower quality of scaling for these events. In fact, it appears that the scaling behavior is better for the 15 August 2010 event for which we have 324 time step and worse for the other events that are shorter (only 94 time steps for the 14th of July 2010, 144 for the 2011 event, 73 for the 19th of June 2013 and 97 for the last event). Same as in the spatial analysis the spectral slope values are between 1 and 1.5 and therefore greater than the embedding dimension (1 in temporal analysis). The spectra of the rainfall fluctuations $\Delta R - 1D$ (Figure 2.15, last column) exhibits a sign change of the non-conservativeness parameter H, visible on the five events and the three fields (a clear break is observed between $f \approx 23$ for the first event, $f \approx 70$ for the August 2010 event and between $f \approx 26$ and $f \approx 33$ for the next three events, which corresponds to a time break between 18 min and 23 min). It would mean that over this range of scales fluctuations tend to flatten when averaging which is not the case for positive values of H. This makes the separation between small (up to 23 min) and large time scales of the rainfall event more evident confirming the existence of two distinct scaling regimes.

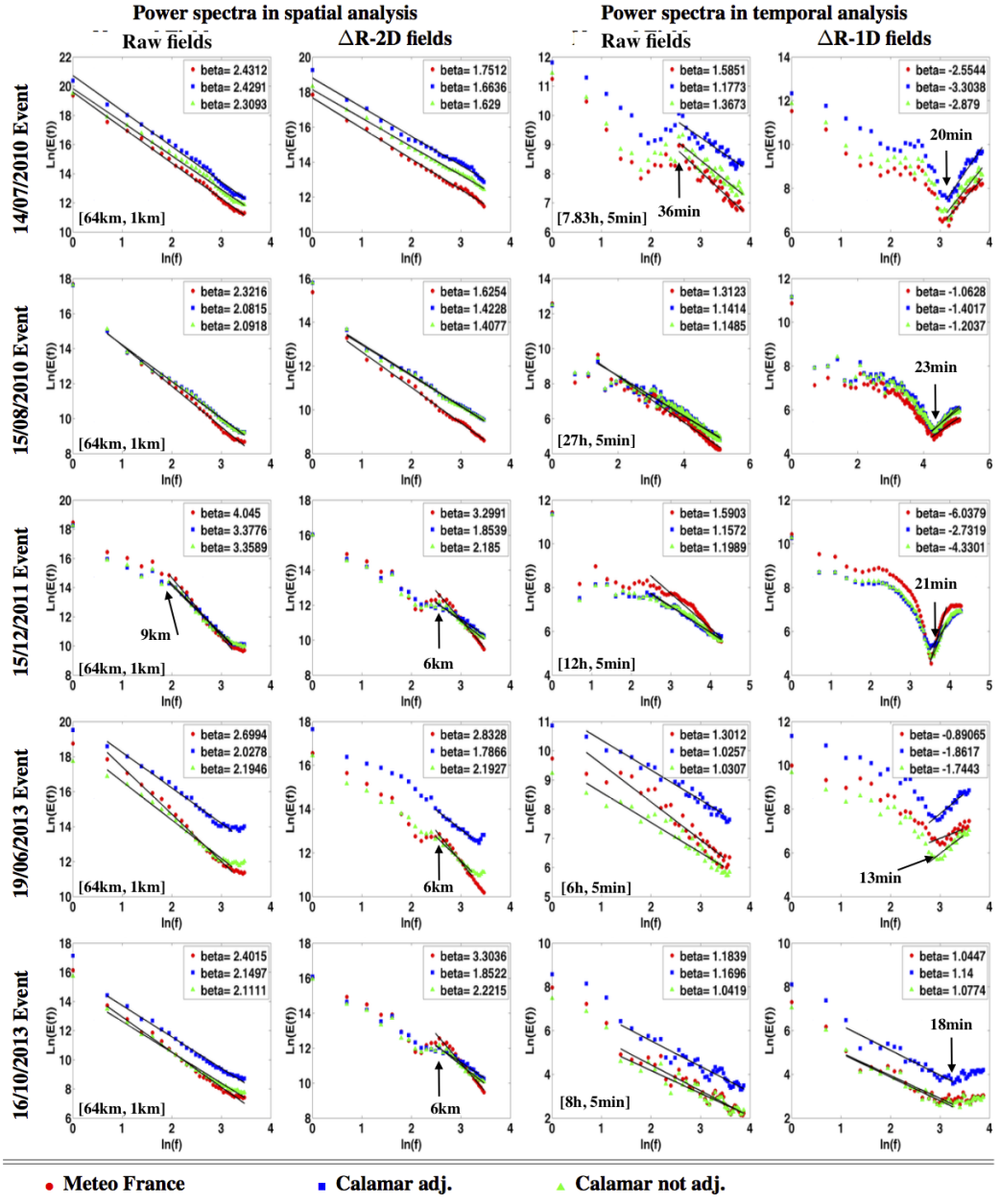

Figure 2.15: Power spectra in both spatial and temporal analysis with the spectral slope β obtained for small scales, the range of scale in which the power spectrum is considered linear is highlighted in black line

- **Trace moment analysis :** Figure 2.16 displays the Trace Moment (TM) analysis; i.e. (Equation 2.15) in a log-log plot for the rainfall fluctuations for $q = 1.5$ in both spatial and temporal analysis. In spatial analysis, the scaling behavior is very good with a break observed at roughly 8 km for all events (R^2 coefficient ranges between 0.98 and 0.99). In temporal analysis, the scaling behavior is good for all events with a break at 40 min for the first four events and 80 min for the last event (R^2 coefficient ranges between 0.96 and 0.99). These results are rather consistent

with the observations on the power spectra in time but not in space (unlike the power spectra analysis, the TM analysis shows clearly a break at 8 km in space). The coefficient of determination R^2 of the straight line whose slope gives $K(q)$ is greater than 0.98 for small scales. $K(q)$ estimated over the small-scale range in space([1 km – 8 km]) and time ([5 min – 40 min] for the four first events and [5 min – 80 min] for the last event) are displayed Figure 2.16. The curvature of the scaling moment function $K(q)$ reflects the multifractal nature of the studied field. In the spatial analysis, it appears that $K(q)$ for the CALAMAR fields is almost linear (especially visible for the August 2010 and 2011 events), meaning the algorithms used to obtain them tend to reduce the actual field fluctuations to a fractal process. From Figure 2.16 it can be seen that Meteo-France fields yield greater values of α and smaller values of C_1 than CALAMAR fields suggesting greater variability. If we focus on the two CALAMAR fields we observe that the adjustment process changes slightly in most cases α and C_1 parameters, inducing a change on both variability and heterogeneity of the field. The Trace moment analysis used here to estimate α and C_1 parameters is sensitive to the sample length and can be biased in case of a high percentage of zero values in the field. Indeed the introduction of numerous artificial zeros results in a multifractal phase transition that biases $K(q)$ for small $q \leq 1$ (Gires et al. (2012b)). This is visible in Figure 2.16 with the linear portion for small q whose influence extends to $q \geq 1$ for some CALAMAR events. This strongly affects the estimates made of UM parameters by computing the first and second derivatives of $K(q)$ around $q = 1$. It means that the reliability of the estimates is low (especially for the CALAMAR data) and the conclusions made on the basis of these results should be confirmed in the following part by the DTM analysis which is less affected by this bias.

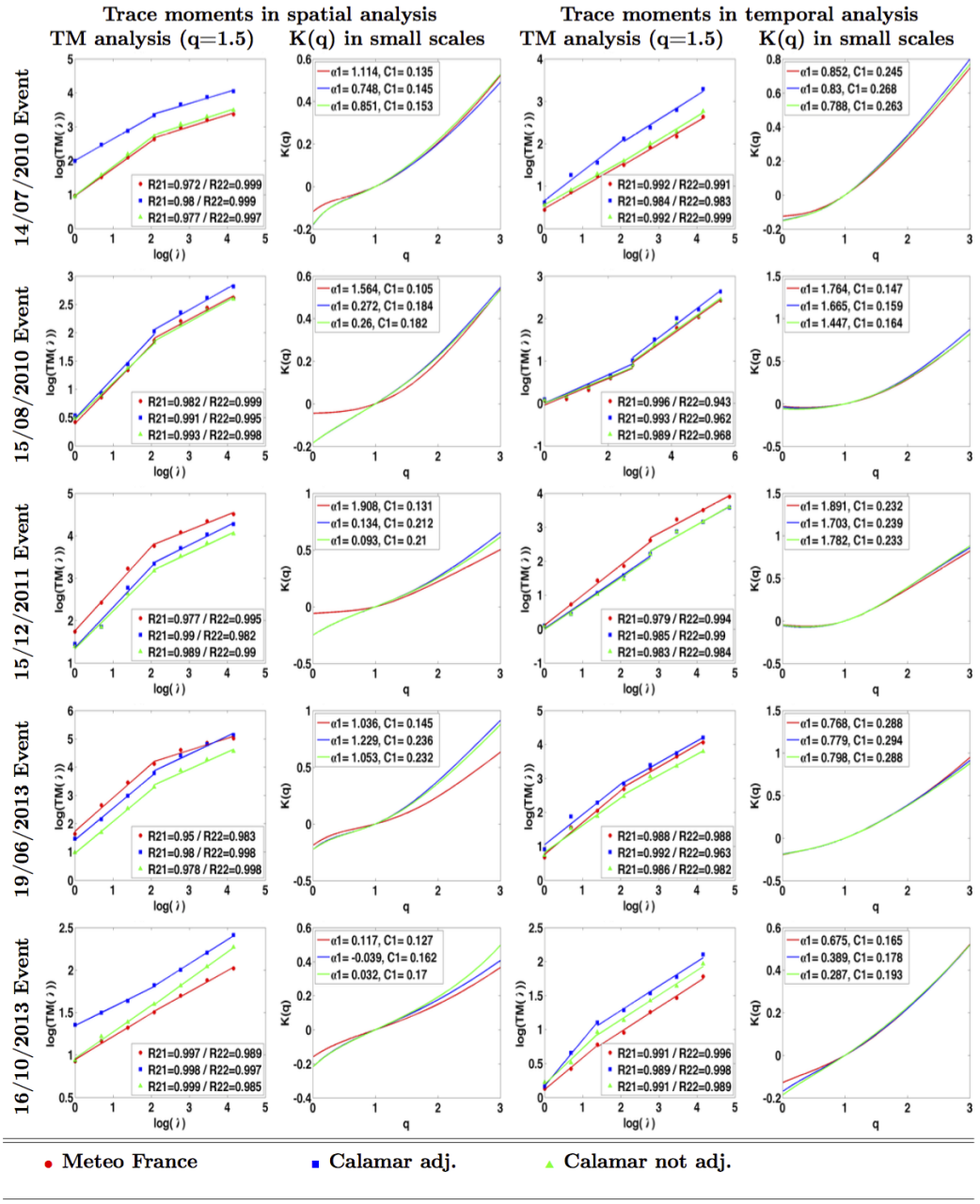

Figure 2.16: TM analysis (Equation 2.15 in log-log plot) for $q = 1.5$ and scaling moment function $K(q)$ for $\Delta R - 2D$ in spatial analysis and $\Delta R - 1D$ in temporal analysis. R^2 coefficients are indicated for small scales.

The event-based comparison of the parameters estimates over small scales in space and time demonstrates the profound difference between the Meteo-France and CALAMAR data. Indeed, the multifractality in space and time remains the same for Meteo-France data except for the last event (see Figure 2.16), which is expected in space-time framework (Macor et al. (2007b), Gires et al. (2011b)) $\alpha = 1.11$ for the event of 14 July 2010, $\alpha = 1.56$ for the event of 14 August 2010, $\alpha =$

1.90 for the event of 15 December 2011 and $\alpha = 1.03$ for the 19 June event but $\alpha = 0.11$ for the last event. Being much more sensitive to the sample size, the second parameter C_1 still remains in good agreement between space and time estimates. This agreement improves with the length of the rainfall episode, e.g., for the event of 14 August 2010. These results suggest that the parameters of an underlying conservative multifractal space-time flux have been identified for the first four Meteo-France rainfall events. It means that the prediction of the rainfall process could be significantly improved within the multifractal framework (Macor et al. (2007b), Schertzer and Lovejoy (1987b, 1997)). On the contrary, the rainfall fluctuations of CALAMAR fields expose mostly the fractal behavior ($\alpha \approx 0$) in space, while it remains multifractal in time with the α estimates of the same order as for the Meteo-France data. It could be that the CALAMAR procedure remains more sensitive to weak rainfall intensities, and, in particular to zeros of the rainfall fields.

- **Double trace moment analysis :** Figure 2.17 and Figure 2.18 show results of the double trace moment analysis performed in both spatial and temporal analysis. In spatial one, the scaling behavior is good for the first four events with a break at 8 km, confirming the trace moment analysis results and the need to take into account two scaling regimes (small scales [1 km, 8 km] and large scales [8 km, 64 km]). Estimates for Meteo-France are in range 1.3-1.7 for α and 0.1-0.15 for C_1 which is consistent with those found for rainfall fields in similar studies. Values of α and C_1 retrieved for CALAMAR data are respectively smaller and greater than for Meteo-France. The differences are less pronounced than with the TM analysis, but remain significant confirming the previously discussed interpretation. The adjustment process used by RHEA does not significantly affect the UM parameters.

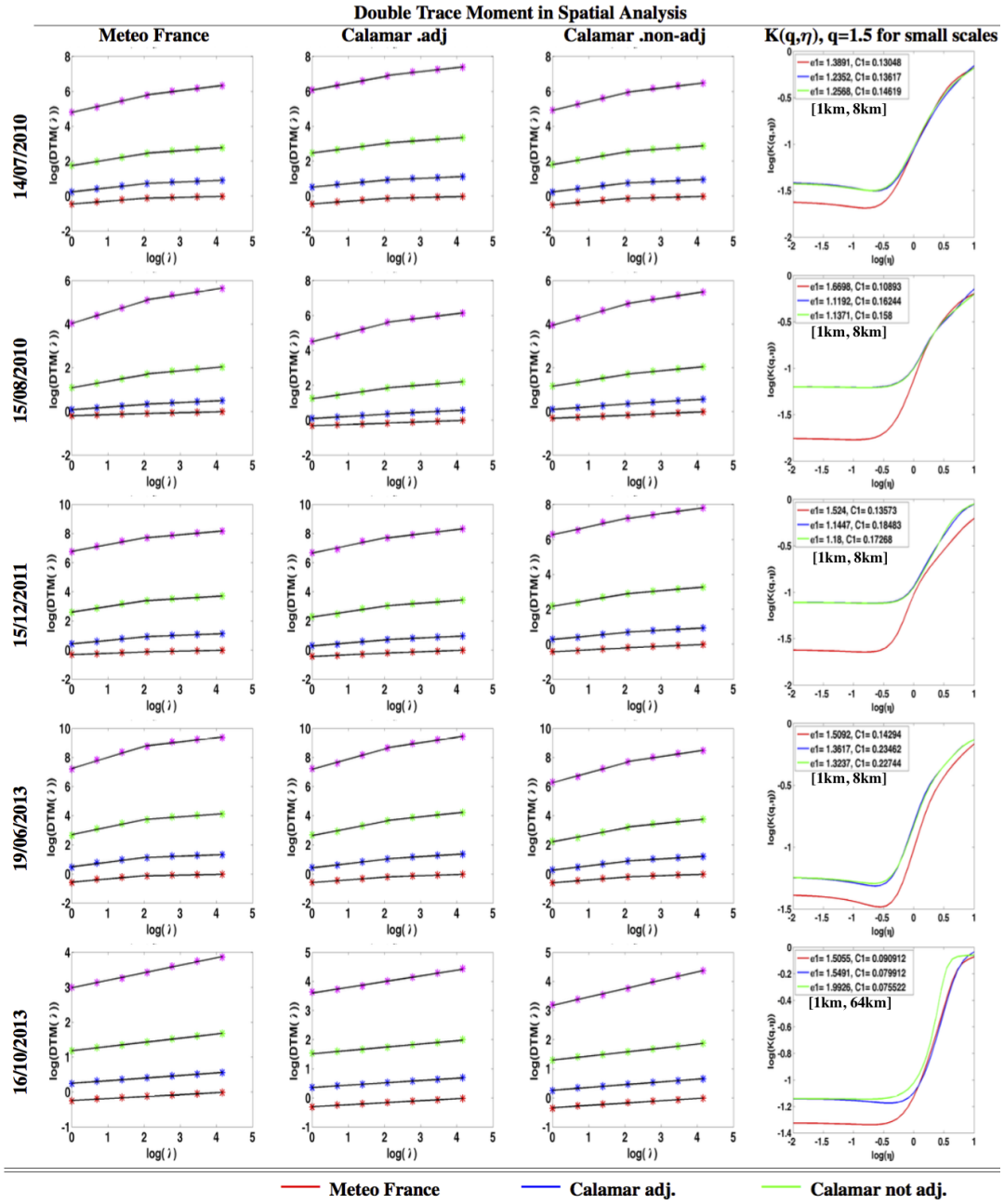

Figure 2.17: DTM analysis in spatial analysis for the three radar data and $K(q, \eta)$ function obtained in small scales

For the last event, the scaling behavior is confirmed and no break is noticed, hence a unique scaling regime [1km, 64km] will be considered. Values of α obtained are 1.50, 1.55 and 1.99, while those obtained for C_1 are 0.09, 0.08 and 0.07 respectively for Meteo-France data, CALAMAR adj. and CALAMAR non-adj data. There is no clear explanation why α is greater for CALAMAR non-adj than for the two other products for this event.

Figure 2.18 displays DTM analysis performed in temporal analysis. It shows a clear scaling behavior with no break for all events and for the three types of radar data, α values range from 0.7 to 2 while C_1 values range from 0.17 to 0.4. The 15 August 2010 and 15 December 2011 events yield the greatest values of α and C_1 reflecting events with extreme variability. Interestingly the discrepancies between the estimates for the three products are almost removed with regards to the spatial analysis, suggesting that this analysis is less sensitive to the bias associated with the numerous artificial zeros introduced in the CALAMAR product.

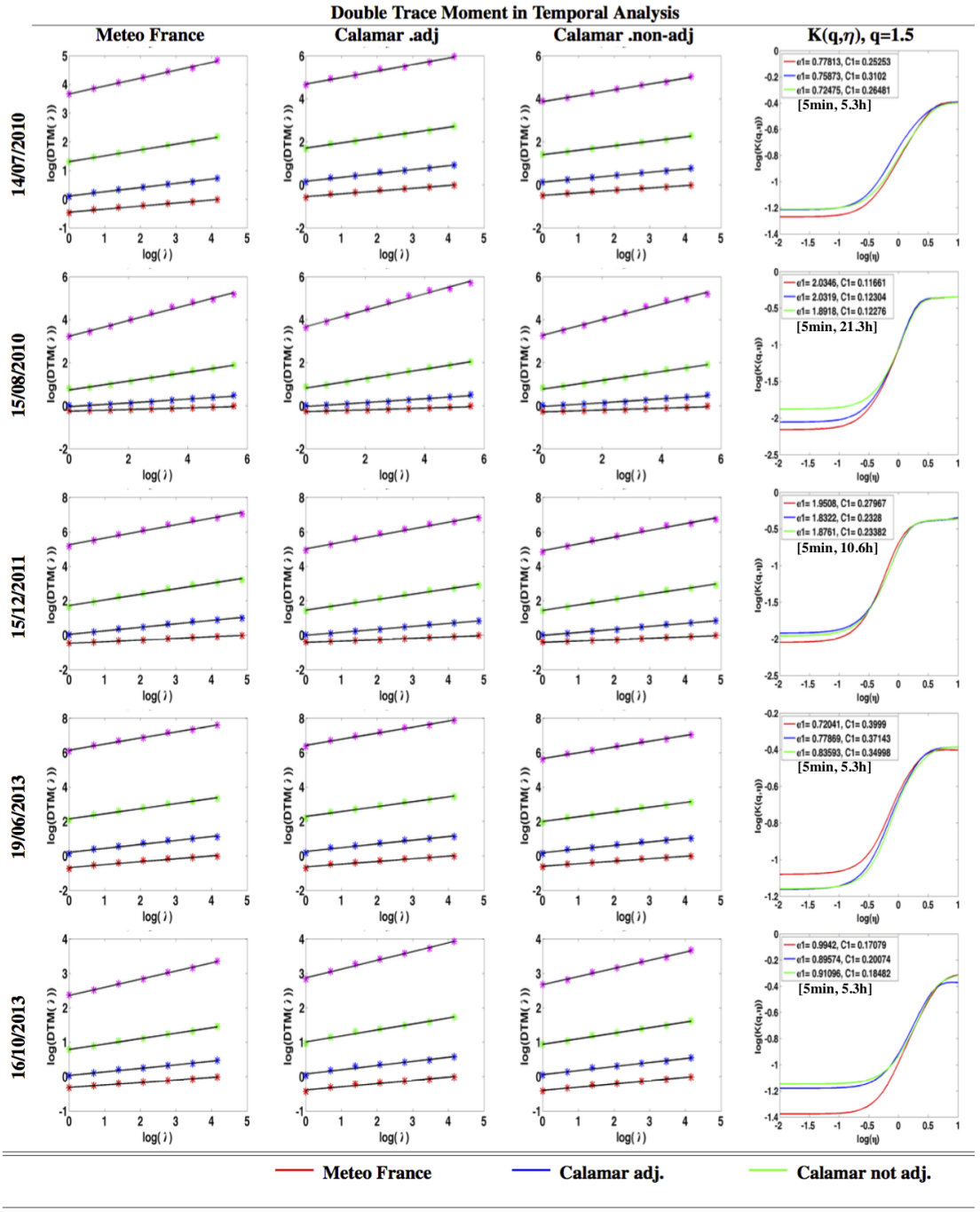

Figure 2.18: DTM analysis in temporal analysis for the three radar data and $K(q, \eta)$ function obtained in small scales

The contradiction noted in this study between the trace moment and the double trace moment analysis results confirms the remark already made on the possible stronger bias of α and C_1 estimations obtained with the TM analysis than with the DTM one due to a greater the sensitivity of this method to the numerous zero values observed on the data. More precisely, in the case of TM analysis α and

C_1 parameters are computed around $q = 1$, where $K(q)$ can still be influenced by zeros values whereas in the case of DTM analysis, the α and C_1 parameters are computed in the linear part of $K(q, \eta)$ which is far from the region affected by zeros.

- **Spatial analysis time step by time step :** Figure 2.19 displays the temporal evolution of fractal and multifractal parameters; α, C_1, the fractal dimension D_F and γ_s as well as the rain rate of all radar pixels, the average rain rate and the percentage of zero values. One can notice the higher rate of zero values observed in CALAMAR products compared to what is observed in Meteo-France except for the June 2013 event. The high rate of zero values observed for the first and the two last events is related to the fact that these events are very limited in space except for a short period (hence the higher percentage of zeros values -up to 90%- observed). The lower fractal dimension observed on the CALAMAR fields confirms the high rate of zeros values compared to Meteo-France data. These differences between the two products can be explained by the fact that CALAMAR uses a static method for the treatment of ground clutters, which involves the removal of these pixels and their replacement with extrapolation or zero value while Meteo-France replace ground clutter pixels with the average of the surrounding valid pixels (Figueras i Ventura and Tabary (2013)). It should also be noted that the difference observed in the mean rain intensity between CALAMAR adj. and CALAMAR not adj. data confirms the remark already mentioned that the adjustment process used by CALAMAR overestimate rainfall rate especially during the peak rainfall.

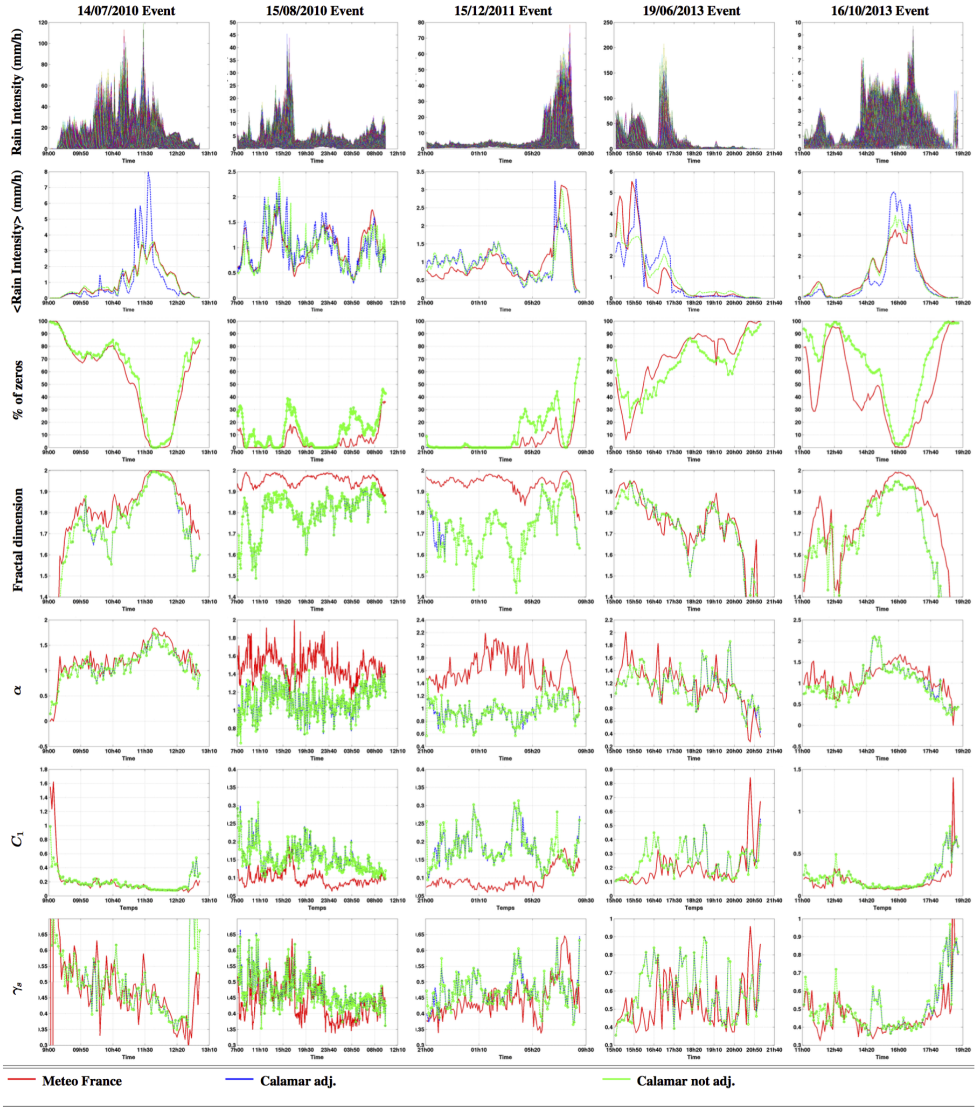

Figure 2.19: Temporal evolution of rain intensity, mean of rain intensity, the percentage of zero values, fractal dimension and universal multifractal parameters α, C_1 and γ_s for all events and for the three types of radar data.

Figure 2.19 shows clearly that the two products do not yield the same parameters in terms of temporal evolution; Meteo-France data exhibits the greatest values of α and the smaller values of C_1. No significant differences are found between the two CALAMAR products. This was expected since the adjustment process used by CALAMAR is based on a single calibration factor used for the entire 5 min radar image. It appears that the differences between the three fields are lower during the period with the heaviest rainfall (14h00-15h40 for the July 2010 event, 15h20-17h20 and 03h50-10h00 for the August 2010 event, 06h20-08h30 for 2011 event). This confirms what was mentioned in the event based analysis that

the CALAMAR process of zeros strongly affects the morphological features of the computed fields. Differences observed between the two products in terms of α and C_1 parameters are partially compensated in γ_s for which the three products exhibit similar values.

Table 2.3 represents the mean of α and C_1 parameters obtained in spatial analysis for small scales. As expected, values are consistence with those given by the ensemble DTM analysis in Figure 2.17.

	α			C_1		
	Meteo-France	CAL adj.	CAL non-adj.	Meteo-France	CAL adj.	CAL non-adj.
14/07/10	1.19	1.11	1.11	0.19	0.19	0.19
15/08/10	1.49	1.10	1.11	0.09	0.15	0.15
15/12/11	1.59	0.96	0.96	0.09	0.18	0.18
19/06/13	1.16	1.15	1.16	0.19	0.24	0.24
16/10/13	1.10	0.99	0.98	0.17	0.21	0.21

Table 2.3: Mean of α and C_1 parameters obtained in small scales for all events and the three types of radar data in spatial analysis

Table 2.3 shows a clear Difference between Meteo-France and RHEA products on term of variability with greatest values of α and smaller values of C_1 obtained for Meteo-France product.

- **Temporal analysis pixel by pixel :**

	α			C_1		
	Meteo-France	CAL adj.	CAL non-adj.	Meteo-France	CAL adj.	CAL non-adj.
14/07/10	0.74	0.72	0.69	0.27	0.33	0.29
15/08/10	1.8	1.73	1.63	0.11	0.12	0.12
15/12/11	1.8	1.69	1.72	0.23	0.20	0.20
19/06/13	1.16	1.19	1.14	0.26	0.28	0.23
16/10/13	0.96	0.78	0.75	0.17	0.21	0.20

Table 2.4: Mean of α and C_1 parameters obtained in small scales for all events and the three types of radar data in temporal analysis

In temporal analysis, Figure 2.20 shows maps describing the spatial variability of both α and C_1 parameters calculated using the DTM analysis, red color indicates a higher value while the blue one indicates a smaller value. This figure highlights the morphology of each field and describes the structure of the rainfall field as well as the movement of the storm cells. As an illustration, stripes obtained for the 15 December 2011 event reflect the movement of the storm cells. The succession of strips of strong intensity with those of lower intensity suggests that the revisit time radar is too large with regards to the rain cell movement, meaning the passage of the storm cell above some pixels is not recorded by the radar. The stripes pattern results from the complex interaction between the space-time variable field and the sampling strategy of the measuring device.

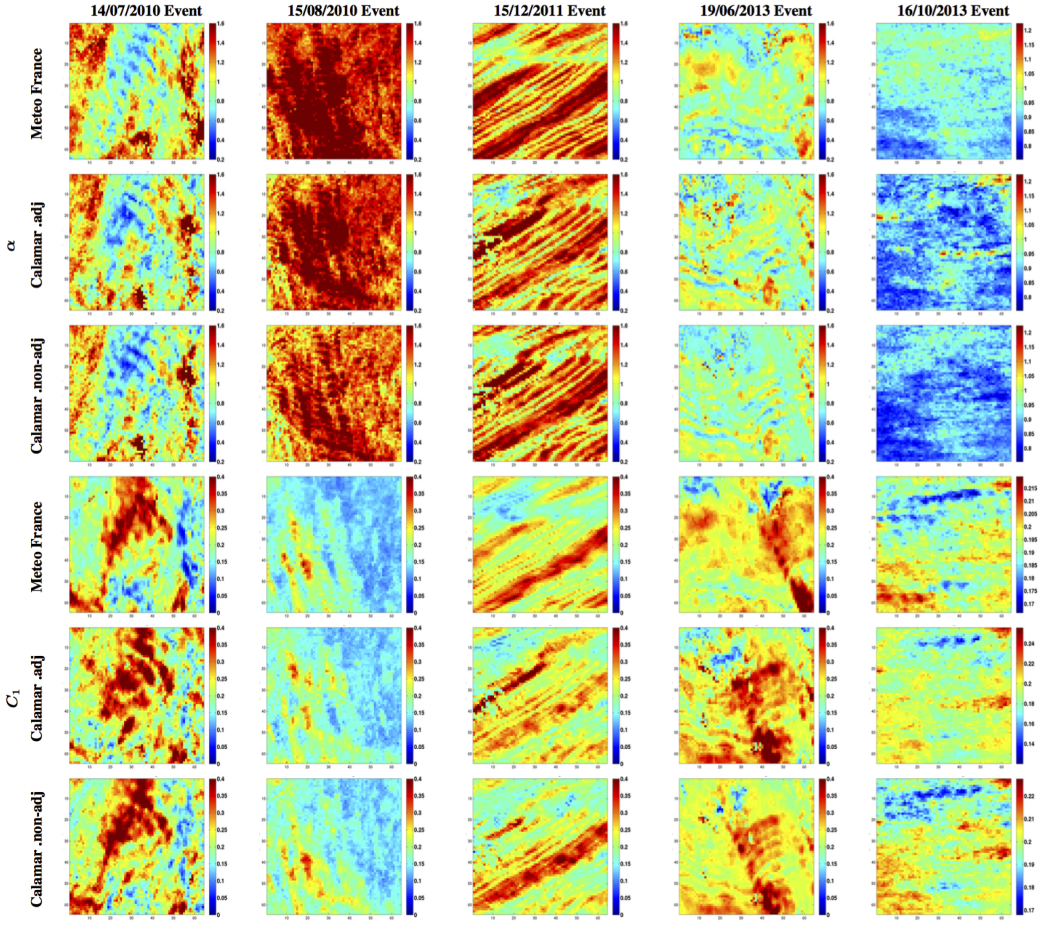

Figure 2.20: Maps of universal multifractal parameters α and C_1, for the three radar products and for all events. It shows clearly that the morphology of all fields is very comparable

Figure 2.20 indicates that Meteo-France and CALAMAR products exhibit the same parameters (with a slight difference observed for the 19 June event, for which

the structure of rainfall cells is different) which can be explained by the lower rates of zeros values observed in temporal analysis (less than 30%). A good match in the morphology is found between Meteo-France and CALAMAR non-adj. data. The adjustment process used by CALAMAR modifies slightly the structure of the rainfall product, and this issue will be studied more in depth with Figure 2.21.

Table 2.4 gives mean values of α and C_1 parameters obtained in temporal analysis; it highlights the slight difference noticed between Météo-France and RHEA products, this difference is less significant than that found in the spatial analysis.

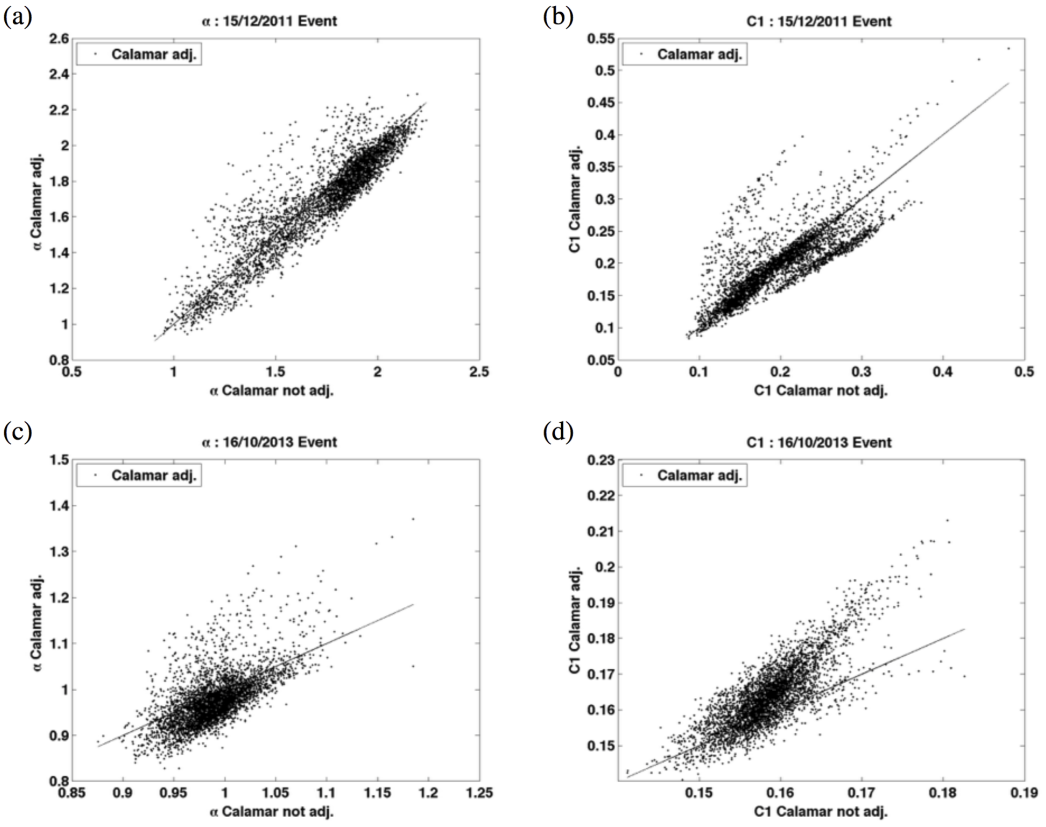

Figure 2.21: temporal UM parameters computed in both CALAMAR products, CALAMAR adj. product in the y-axis and CALAMAR not adj. product in the x-axis; (a) and (b) α and C_1 for the 2011 event and (c) and (d) α and C_1 for last event. The black line represents the bisector

Figure 2.21 compares the temporal UM parameters computed in both CALAMAR products for two rainfall events. For the 16 October 2013 event, the adjustment process furthermore tends to reduce values of α and to increase values of C_1. This effect is more pronounced for the fifth (16 October 2013) event which is not the heaviest one. The effect of the adjustment process on the multifractal behavior of

CALAMAR fields was not observed on the spatial analysis (Figure 2.19) because the correction factor is applied uniformly in space at a given time step. Since it changes in time, we observe a modification of the temporal variability (Figure 2.21).

- **Temporal analysis of rain gauges data** In this part, Multifractal temporal analysis is performed for the 27 rain gauges available, the scaling behavior is checked first with the power spectra analysis, β ranges from 0.53 to 2.4, with values above 1 for the first and the two last events. As noticed in the power spectra analysis of radar data, the analysis is very sensitive to the event length. Hence, the scaling behavior is clearer for the second event than for the other events.

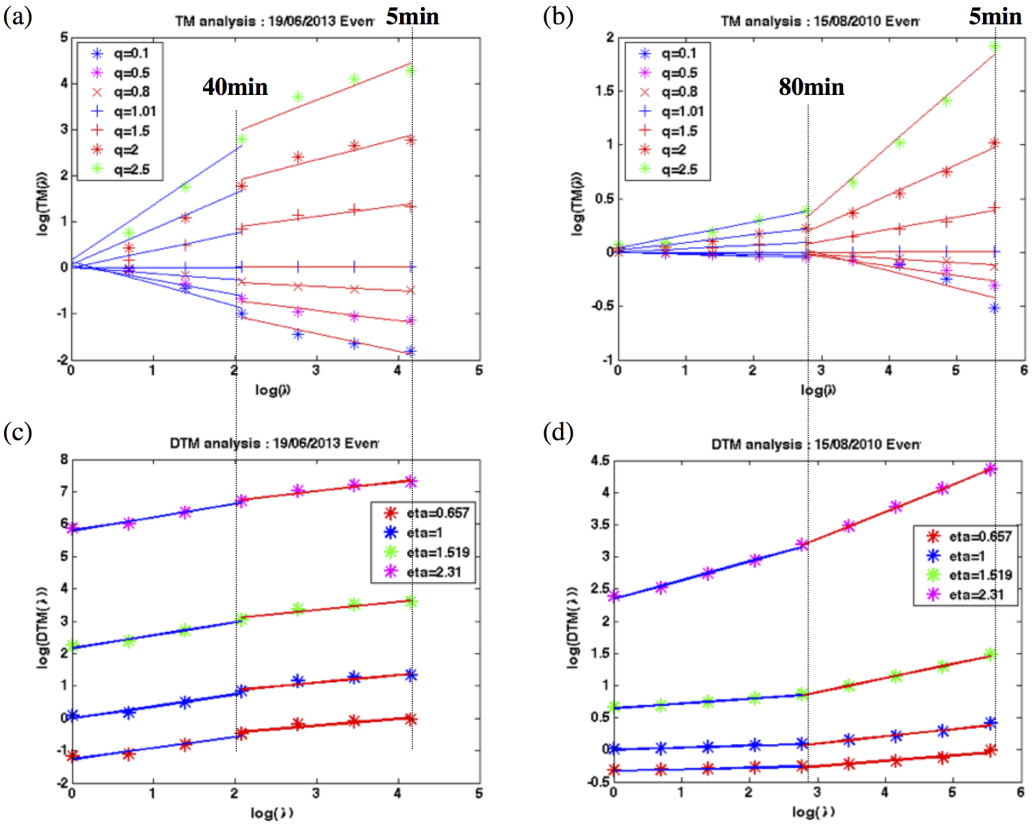

Figure 2.22: TM and DTM temporal analysis performed for all raingauges; (a) and (c) for the 19th of June 2013 and (b) and (d) for the 15 August 2010, results show clearly the two scaling regimes.

The TM analysis performed for rain gauges shows a break in the scaling behavior, indicating the need to considerer two scaling regimes. The break is found around 40 min for the 14th of July 2010 and the 19th of June 2013 events, and at 80 min for the other three events. An example of TM analysis performed for rain gauges is presented in Figure 2.22. The DTM analysis confirms the scaling break

noticed in the trace moment analysis. As a consequence, two scaling regimes will be considered when computing the UM parameters for rain gauges instead of one unique scaling observed in radar data. This difference between rain gauges and radar can be explained by the fact that these two devices are not affected by the same sources of errors, (raingauges are known of being more sensitive to their local environment perturbations especially during severe events (wind, losses...), and furthermore discretize data due to the the recording of the buckets' tips), or do not sample the same area / volume.

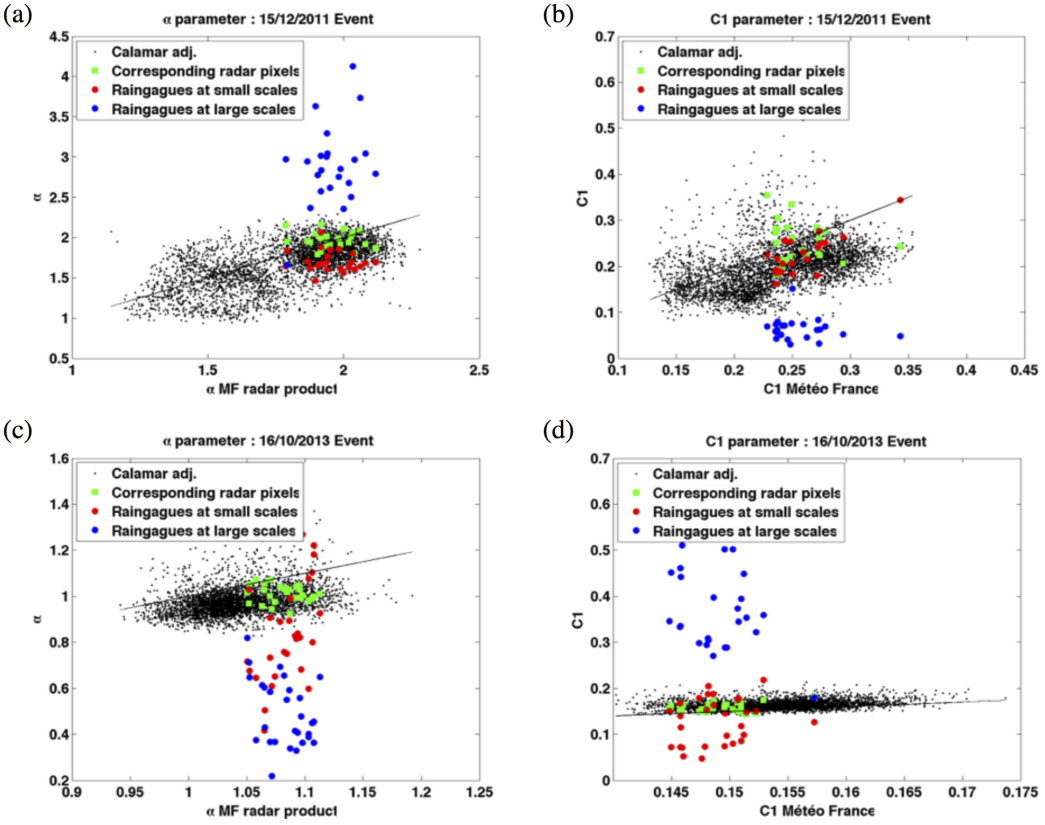

Figure 2.23: Radar-rain gauge comparison; the 4096 (64*64) UM parameters computed on CALAMAR adj. radar data are plotted (black point) as well as those computed in rain gauges at small scales (red circle) and at large scales (blue circle) as function of Meteo-France UM parameters, the corresponding CALAMAR adj. pixels are highlighted. The black line represents the bisector

Results of this rain gauges-radar comparison show two different behaviors presented in Figure 2.23. The 4096 (64*64) UM parameters computed on each CALAMAR adj. radar pixel are plotted (black point) as well as those computed for rain gauges at small scales (red circle) and at large scales (blue circle) as a function

of Meteo-France UM parameters, the corresponding CALAMAR adj. pixels are highlighted with green square.

The first three events exhibit the same behavior (first row), indicating that rain gauges at small scales exhibit similar temporal variability as radar data, but not at large scales (at small scales, raingauges are within the scatter plot, but not at large scales) for both UM parameters α, C_1. The two last events exhibit the second behavior (second row), raingauges at both small and large scales do not yield the same parameters as radar data (α and C_1 computed for raingauges are lower than what is obtained for radar data), this is more pronounced for the last event which is a not heavy rainfall (max rain intensity about 10 mm/h). A potential explanation could be that rain gauges are struggling to represent temporal variability due to intrinsic errors for some events. Indeed the 4^{th} event is an extreme event (several years return period over 30 min) meaning that the rain gauges are likely to be affected by uncounted water, and the last event was the more common one meaning that the discretisation associated with the tipping of the bucket might introduce a bias. The radar-rain gauges comparison result, confirms also conclusions of standard scores comparison (Subsubsection 2.4.2.1)in particularly the fact that the correlation between radar and raingauges is worse for the last two events, and it is not improved when changing the time resolution.

In this section, a new innovative comparison method of rainfall radar products has been developed. This new method relies on the Universal Multifractal framework and enables the comparison of products' structures by comparing their scaling behavior and the distribution in both space and time of their Universal Multifractal parameters α and C_1.

The two products are Meteo-France radar data and RHEA product in both adjusted with rain gauges and not adjusted radar data types. Both products use raw data from the same C-band radar but do not rely on the same QPE algorithms (one uses dual polarization capacities whereas the other not) and do not use the same rain gauge network in the adjustment phase. The comparison has been performed using five rainfall events that occurred in 2010, 2011 and 2013. Multifractal comparison method reveals significant differences between the two products parameters α and C_1 in term of temporal evolution and less significant in spatial distribution, results have been discussed with the

help of some field characteristics especially the rainfall rate and the percentage of zeros values. Principal results are summarized bellow:

In space, the power spectra analysis shows that the two products exhibit a good scaling behavior with a slope break at 8 km for the 2011 event. The scaling behavior was confirmed in the Trace Moment analysis with a break observed at 8 km for all events and all fields. Meteo-France field yield the greatest spectral slope β suggesting a shorter correlation range for this field in space. The scaling moment function $K(q)$ for small scales ([1 km-8 km]) comes out with a huge difference between the two products' multifractality. Meteo-France field exhibits a multifractal behavior with α ranging between (1.11 and 1.9) while both CALAMAR products exhibit almost a fractal behavior with much lower values for α. This has been related to the algorithms used by CALAMAR especially with the handling of ground clutters that changes the behavior of the field by introducing zeros values, the presence of these zero values on the data leads to a bias of the TM analysis estimation. The DTM analysis performed in spatial analysis gives a better estimation of Universal Multifractal parameters α and C_1, values obtained confirm the clear difference between the two products, and the fact that the variability of precipitation is better represented in Meteo-France product than in RHEA product. The temporal evolution of universal multifractal parameters α and C_1 confirms that the two products do not yield the same parameters except during the period with the heaviest rainfall when the structure of the two products becomes comparable, and the zero values much less numerous.

In time, the power spectra exhibits a slope break at 20 min, with a sign change of the non-conservativeness parameter H. The Trace Moment analysis confirms the scaling behavior and the need to take into account two distinct scaling regime with a break at 40 min for the four first events and 80 min for the last event while the scaling moment function $K(q)$ for small scales indicates the same behavior for the two products and for all events in temporal analysis. Thus, the two products behavior remains multifractal with comparable values of α and C_1 that can be explained by the lower rates of zeros values (less than 30%) observed in temporal analysis (calculated on the radar pixels) while it reaches 90% in spatial analysis (calculated on the radar images) for the same event. The DTM analysis performed in temporal analysis shows a clear scaling behavior but no break of this behavior was noticed, the difference observed between the two products in term of α and C_1 values are less significant than that found in spatial analysis.

It is also important to note that both CALAMAR products (adjusted and not adjusted) exhibit the same universal multifractal parameters α and C_1 in spatial analysis, the adjustment process changes slightly the temporal variability of CALAMAR radar data leading to a less variable field. Differences obtained between Meteo-France and CALAMAR products are due to the introduction of zeros values during the treatment of ground clutters process operated at each time step on a single radar image (meaning in space) which explains therefore the difference in term of zeros values observed between space and time and also the huge difference observed in space but not in time between the two products in term of universal multifractal parameters.

2.5 The new X-band polarimetric radar product

Figure 2.24: The new X-band polarimetric radar installed in the framework of RainGain project. © Rosa Vicari /HM&Co - ENPC

In the framework of the European research project RainGain, a new X-band polarimetric radar (Figure 2.24 and Section 1.2.1 for main technical characteristics) has been acquired

by Ecole des Ponts ParisTech and installed on its campus in Paris region. Since May 2015, this radar produces rainfall information at small space (up to 100 m) and time (up to 1 min) scales. The radar has both Dual polarization and Doppler capabilities that brings huge improvements in terms of rainfall measurement quality:

- **Doppler capability:**

  Doppler radars provide a measurement of targets velocity along a radial (V_r) from the radar in a direction either towards (velocity positive) or away (velocity negative) from the radar using the Doppler principle. In fact the velocity of the targets can be derived from the shift Δf observed between the frequency of the transmitted signal f_{trans} and the reflected one $f_{received}$ (Equation 2.30).

$$f_{received} = f_{trans}(1 - \frac{2V_r}{c}) \tag{2.30}$$

  However, at the standard velocity of meteorological targets, the frequency shift is relatively small compared to the radar frequency and is very difficult to measure. Another way to estimate raindrops velocity is to use the phase shift $\Delta\phi$ noticed between the transmitted pulse and the received one, instead of the frequency shift Δf. The velocity can be derived than from this pulse shift.

  The shift phase can only have values between $+\pi$ and $-\pi$ ($\pm 180°$). So velocity can be estimated correctly only if its absolute value doesn't exceed the maximum unambiguous velocity V_{max}.

  V_{max} depends on the radar wavelength λ, and the PRF (Pulse repetition frequency) and can be expressed as:

$$V_{max} = \pm\frac{PRF.\lambda}{4} \tag{2.31}$$

  In the meantime, it is known that the maximum radar range r_{max} can be expressed as:

$$r_{max} = \frac{c}{PRF.2} \tag{2.32}$$

  These two equations both depend on the PRF. Their combination leads to Equation 2.33.

$$r_{max}.V_{max} = \pm\frac{\lambda.c}{8} \tag{2.33}$$

This relationship (Equation 2.33) shows limits imposed by the selection of the wavelength λ and PRF. In fact, a high PRF is desirable to increase the unambiguous velocity V_{max} (Equation 2.31), while a low PRF is desirable to increase the radar range r_{max} (Equation 2.32). This problem is known as the Doppler Dilemma. A compromise solution consists in performing two scans; the first one with high PRF to retrieve good estimation of the reflectivity factor Z over a large range and the second one with small PRF to retrieve a reliable estimation of raindrops velocity. From Equation 2.33, one can notice the dependency of this Doppler Dilemma on the wavelength of the radar which is less important for S-band radars while it is dominant for X-band ones.

- **Dual polarization capability :**

  By transmitting both horizontally and vertically polarized signals, Dual polarization radars increase information available about the shape of raindrops, which can be used to improve the data processing step, in particular for the reflectivity to rain rate conversion and during the identification and removal of non precipitation echoes. The information about the shape of raindrops increases the knowledge of both the drop size distribution (DSD) and the precipitation types.

  It is assumed that spherical raindrops become elliptical with a major axis in the horizontal direction when falling in the atmosphere. The oblateness level of the drop is related to its size. Therefore, the backscattered signal is much stronger for a horizontal wave than for a vertical one. Hence a more accurate distribution of the drop size may be inferred resulting in a more accurate estimate of the precipitation rate.

  The differential reflectivity, called Z_{DR}, is retrieved from the ratio of the horizontally polarized reflectivity Z_h and the vertically polarized one Z_v. Comparisons of the equivalent reflectivity factor Z_e and the differential reflectivity Z_{DR} suggest a better identification of precipitation types (Seliga and Bringi (1978)).

$$Z_{DR} = 10 \log \frac{Z_h}{Z_v} \tag{2.34}$$

  The oblateness of raindrops has consequences on the phase of the backscattered signal. Indeed, a difference between the vertical and horizontal phase components

depends on the oblateness of the target and can be expressed as a specific differential phase (K_{dp}, the gradient of the phase shift along the beam path). According to English et al. (1991) the use of $K_{dp} - R$ relationship for rainfall estimation instead of $Z - R$ relationship is justified for rainfall rates greater than about 20 $mm.hr^{-1}$.

2.5.1 X-band data processing

The Radar is currently equipped with the Rainbow software developed by SELEX. The software ensures the data acquisition, pre and post processing as well as data visualization. Several options are included within this processing chain, some of them are presented below :

1. **Reflectivity correction :** Various corrections can be performed by the Rainbow software, the large list includes *Bright Band correction , Vertical Profile correction, Attenuation correction, Echo classification, Sea and Ground Clutter identification and correction, ...* All details included in this section were elaborated from the Rainbow software manual provided by SELEX (`http://www.de.selex-es.com/capabilities/meteorology/products/components/rainbow5`) :

   - **Z-based attenuation correction :** The attenuation correction based on single polarization data relies on method developed by Hitschfeld and Bordan (1954) which is based on the estimation of the specific attenuation $A(r)$ used to correct the measured reflectivity dBZ at distance r : $dBZ_{Corr}(r) = dBZ(r) + A(r)$.

     The estimation of the specific attenuation $A(r)$ is performed using relationship similar to the Z-R one used for the reflectivity to rain rate conversion (Marshall and Palmer (1948)). Thus, $A(r)$ (in dB/km) can be related to the rain intensity R (in mm/h) using coefficients α and β and the following relationship : $\delta A/\delta r = \alpha R^{\beta}$ (Battan (1973)).

     Where, α and β are user defined parameters and should be specified. Default values defined by (Battan (1973)) are included with the Rainbow software.

   - **Dual-Pol based attenuation correction :** In addition to the algorithm, decribed before, used to correct reflectivity for attenuation, which is based on the reflectivity data only; Rainbow software includes another algorithm for

attenuation correction in case of fully polarimetric radar system and based on the differential phase shift Φ_{dp} that provides more stable measurement of the attenuation. The correction of attenuation and differential attenuation using dual-polarization data follows the procedures described in the Gematronik Dual-Polarization Handbook (Bringi et al. (2005)) $dBZ_{Corr}(r) = dBZ(r) + \alpha.\Phi_{dp}(r)$.

The default value of the proportionality factor α is 0.25 dB/deg.

Other methods are also included within the Rainbow software.

2. **Reflectivity to rain rate conversion :** The reflectivity Z to rain rate R conversion can be performed either by using the classical $Z - R$ relationship or a combined $Kdp - R$ relationship for polarimetric radars.

   - For a single polarization product, the conversion is performed by the $Z - R$ relationship (Equation 2.9).
     with Z in $[mm^6/m^3]$ and R in $[mm/h]$. Typical values for a are 150 to 500, and for b 1.3 to 1.8.
   - The polarimetric measurements are used to calculate a rainfall intensity R based on a combined $Kdp - R$ relationship : $R = 19.63 \mid (K_{dp}) \mid^{0.823}$

2.5.2 X band & C band radar data analysis

First rainfall events available from the new X-band polarimetric radar were retrieved and used to here to perform a first analysis and comparison with the corresponding C-band data.

Unfortunately only two rainfall events could be selected for this analysis, X-band data, CALAMAR adjusted and non adjusted data as well as the corresponding rain gauges data were collected for the needs of this work.

The new comparison methodology presented in the previous section will be used to perform a multifractal comparison between the new X-band and CALAMAR radar products. Such methodology will allow to identify differences in terms of data quality and the measured rainfall spatio-temporal variability.

However, it is important to note that the X-band polarimetric radar is currently entirely devoted to research activities and not yet fully operational. Intensive tests and validation work are going on to test all processing options included within the Rainbow

software. It is important to note that no calibration with raingauges was performed for the X-band polarimetric radar data. This point is still a subject of debate regarding the usefulness of such calibration with respect to improvements provided by the Dual polarization capability, in particular the full new knowledge on raindrops shape.
The analysis of X band C band radar will follow the same steps presented in the new developed methodology presented above:

2.5.2.1 Rainfall data

Two rainfall events were selected for this analysis of X band C band radar data. They occurred in September 2015:

- The first event occurred in 12/09/2015, its total duration is 13 hr. The total rainfall depth is 40 mm.
- The second event occurred in 16/09/2015, its total duration is 12 hr and 45 min. The total rainfall depth is 35 mm.

It is important to note that data types involved in this comparison do not have the same spatio-temporal resolution (250 m - 3.41 min for X-band data and 1 km - 5 min for CALAMAR data). Indeed, they have different length and no transformation were used to get the data at the same spatio-temporal resolution. Thus a difference will be noticed in the results of the analysis performed here in terms of number of samples available. Figure 2.25 displays maps of total rainfall depth calculated within each radar product for the two rainfall events selected. One can notice the greater variability observed for X-band polarimetric radar data especially for the second event. This is due to the small scale rainfall information available. CALAMAR non adjusted data appears to underestimate rainfall depth; and the radar - rain gauges adjustment process applied in real time by CALAMAR system improves the total rainfall depth.
Figure 2.26 shows a comparison between the three radar products and the available 27 gauge data in terms of cumulative rainfall depth. Figure 2.26 confirms that CALAMAR non adjusted data underestimates rainfall depth with respect to point measurements for the two rainfall events. The adjustment process improves radar quality with respect to measurements. The X band product shows a slight underestimation for the first event and a significant overestimation for the second event. This is due to the fact that the

radar is under test and parameters of $Z - R$ and $Z - K_{dp} - R$ relationship not fully determined.

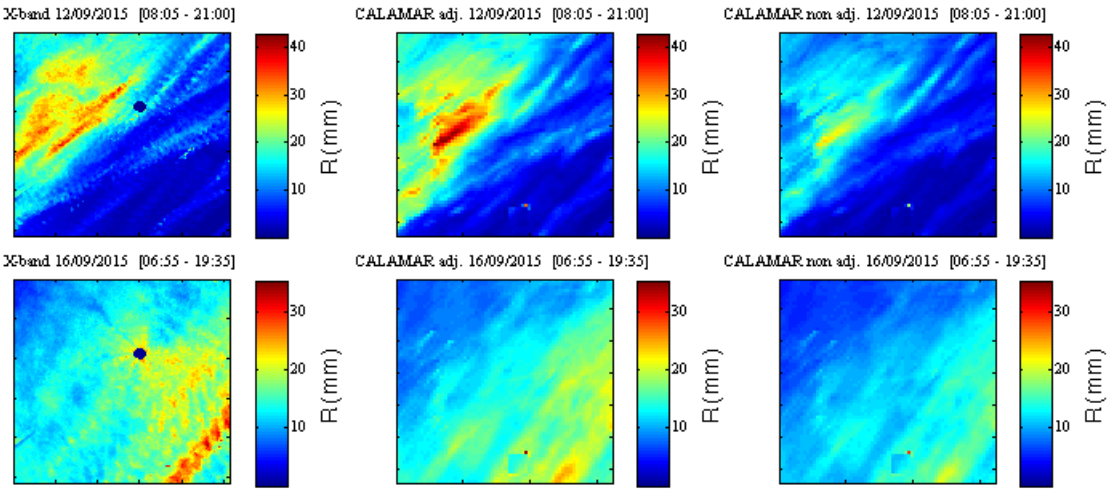

Figure 2.25: Maps of the total rainfall depth computed on the whole radar image (64*64 km^2 data) involved in this analysis part.

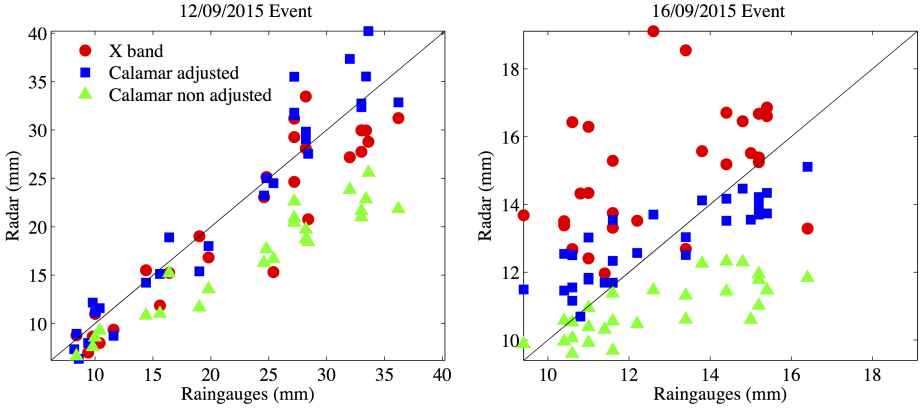

Figure 2.26: Radar-rain gauge comparison in terms of the cumulative rainfall depth computed on rain gauges and the corresponding radar pixels.

2.5.2.2 Spectral analysis

The spectral analysis was performed in both space and time to check the scaling behavior of the three radar products involved in this work (X band, CALAMAR adj. and CALAMAR non adj data).

- *Spatial analysis :* the spectral analysis performed for the two rainfall events, indicates that the three radar products exhibit a clear scaling behavior. In fact,

for the first event (12/09/2015) a clear break of this scaling was retrieved for the three products at $f \approx 12$ which correspond to $\approx 5km$. No break was noticed for the second event. β values obtained for the two events range between 2 and 3, which is greater than the dimension of the field (2 here) and means that it is non-conservative. Thus, a fluctuation analysis must be conducted and the corresponding field will be denoted $\Delta R - 2D$ as for the previous study. The $\Delta R - 2D$ new fields still exhibit a scaling behavior on the range of scales available with lower values of β (Figure 2.27). The scaling behavior is less clear in CALAMAR products for the 12/09/2015 event and no break of was considered for the $\Delta R - 2D$ fields. β values retrieved for the 12/09/2015 event are 1.2 for the X-band field and 1.4 for both CALAMAR products. For the 16/09/2015 event, β values are 1.3 for X-band product and 1.4 for both CALAMAR fields.

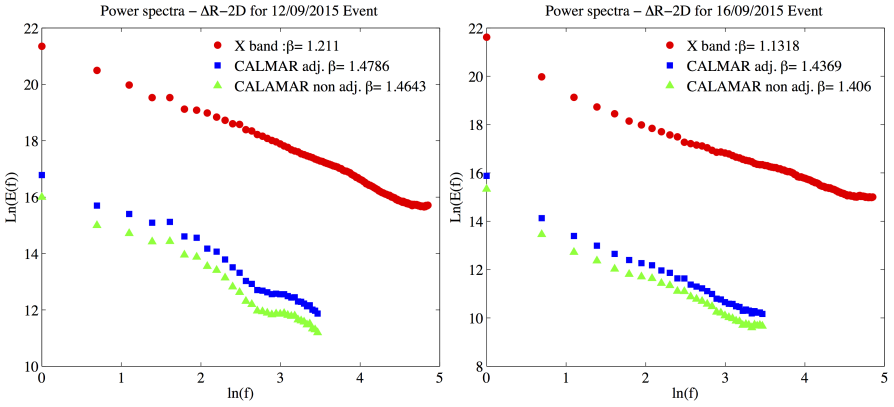

Figure 2.27: Power spectra in spatial analysis performed for the two rainfall events with the spectral slope β obtained for small scales using the $\Delta R - 2D$ data for the three radar products.

- *Temporal analysis :* the spectral analysis performed in temporal analysis indicates that the three radar products exhibit a scaling behavior with β values higher than the dimension of field (1 here). Hence, a fluctuation analysis was performed and the obtained $\Delta R - 1D$ fields were analyzed. As noticed in the previous analysis, the spectra of the rainfall fluctuations $\Delta R - 1D$ (Figure 2.28) exhibits a sign change of the non-conservativeness parameter, visible on the two rainfall events and the three fields (a clear break is observed between $f \approx 55$ for X band data and $f \approx 35$ for both CALAMAR products, which corresponds to a time break located between 18 min and 23 min). As a result of this spectral analysis the TM and

DTM analysis will be performed on the rainfall fluctuations fields $\Delta R - 2D$ and $\Delta R - 1D$.

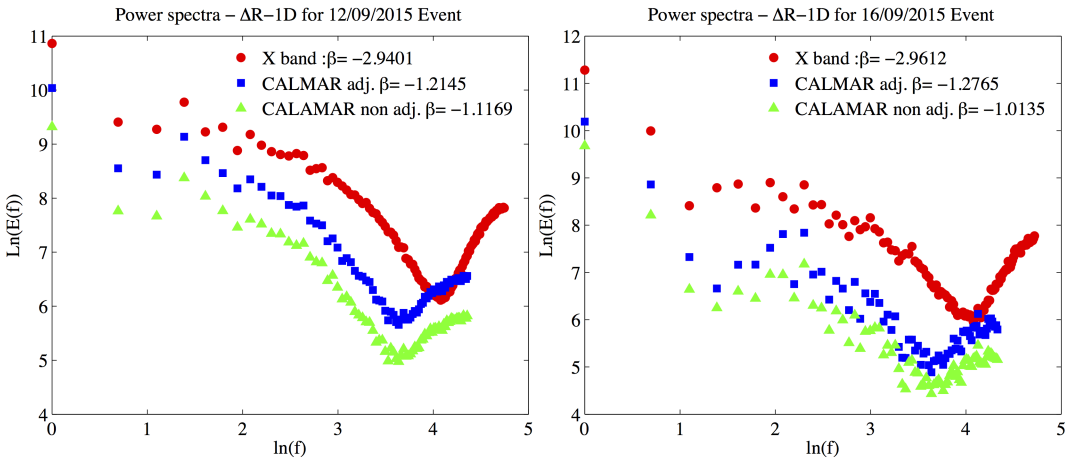

Figure 2.28: Power spectra in temporal analysis performed for the two rainfall events with the spectral slope β obtained for small scales using the $\Delta R - 1D$ data for the three radar products.

2.5.2.3 Trace moment analysis

- *Spatial analysis :* the TM analysis performed in space for the three radar products is displayed in Figure 2.29 where (Equation 2.15) is plotted in a log-log plot for the rainfall fluctuations $\Delta R - 2D$ for q=1.5. One can notice that a good scaling behavior was retrieved for the three products over two ranges of scales. In fact, a break is noticed as in the previous analysis at roughly 8 km for CALAMAR product and 2 km for the X band product, indicating the necessity to considered two distinct ranges of scales: small scales ([1 km - 8 km] and [250 m - 2 km] for C band and X band data respectively) and large scales ([8 km - 64 km] and [2 km - 64 km] for C band and X band data respectively). This finding shows a significant difference between the scaling characteristics of C band and X band products due to the available small variability measured by the X-band polarimetric radar. Values of α retrieved for the two selected events are around 1.8 and 0.6 for X band and C band radar data respectively. Values of C_1 for the first event are 0.14, 0.25 and 0.26 respectively for X band and both CALAMAR products. For the second event, C_1 values are 0.11, 0.15 and 0.16 respectively for X band and both CALAMAR products. Indeed, X band field exhibits greater values of α and smaller values of

C_1 than C band data.

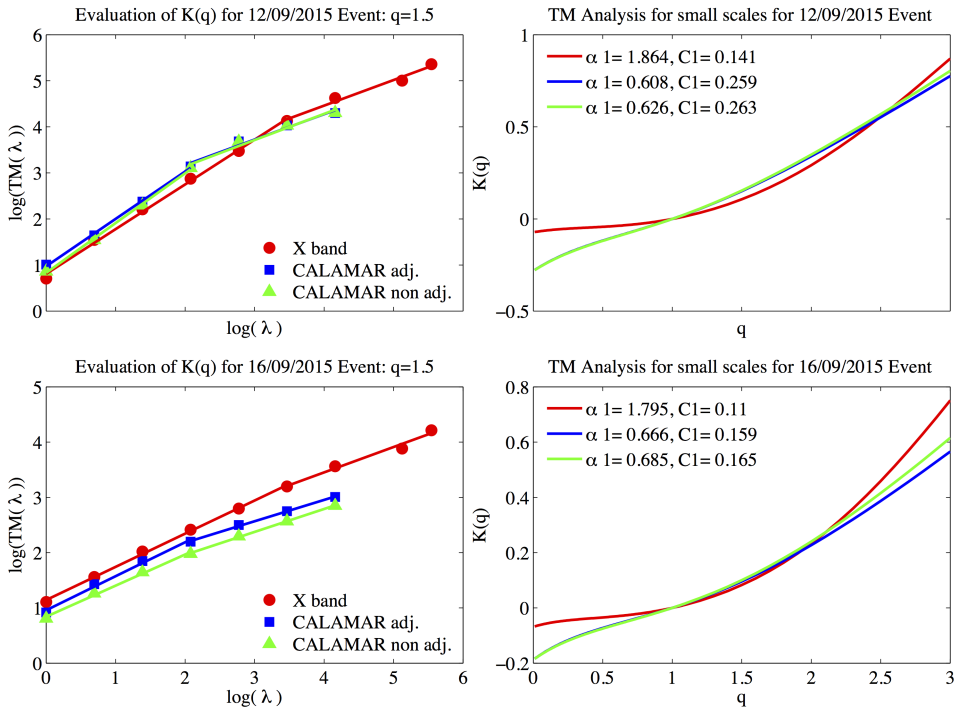

Figure 2.29: TM analysis (Equation 2.15 in log-log plot) for q=1.5 and scaling moment function $K(q)$ obtained in spatial analysis for small scales for $\Delta R - 2D$ field.

The scaling moment function K(q) estimated over the small-scale range in space ([1 km – 8 km] for C band data and [250 m – 2 km] for X band product)) are displayed in Figure 2.29. As already mentioned, the curvature of the K(q) functions reflects the multifractal nature of the studied field. For both events, K(q) is more affected by high rate of zero values in CALAMAR field, and exhibit almost a linear behavior with smaller values of α. This is more pronounced for the first event. The high rate of zero values that will be confirmed latter is due to the methodology applied by CALAMAR system for the identification and removal of ground clutters (GC). In fact, all pixels identified as GC are removed from the current radar image and replaced by extrapolation or zero values, while various options (interpolation and extrapolation) are included within the Rainbow software used for X-band polarimetric radar data processing.

- *Temporal analysis :* TM analysis performed in time for the three radar products is displayed in Figure 2.30 where (Equation 2.15) is plotted in a log-log plot for

the rainfall fluctuations $\Delta R - 1D$ for q=1.5. A scaling behavior was retrieved for all the three products with a break at roughly 40 min for CALAMAR field and 27 min, 20 sec for X band data. Indeed, two ranges of scales should be considered: small scales ([5 min – 40 min] for C band data and [3.41 min – 27.33 min] for X band data) and large scales. The scaling moment function K(q) estimated in temporal analysis over the small-scale range for the three products are displayed in Figure 2.30. The difference between C band and X-band polarimetric radar data is more pronounced for the first event, for which the K(q) function retrieved for CALAMAR product exhibits an almost a linear behavior with smaller values of α (between 0.55 and 0.6) while $\alpha = 1.19$. For the second event, values obtained for α are 1.2, 0.86 and 0.76 respectively for X band and both CALAMAR products. Values of C_1 are between 0.21 and 0.25. It is important to note that the estimation of the UM parameters α and C_1 using the TM analysis performed here is much more sensitive to zero values. This point was discussed in the previous section in the framework of the comparison between CALAMAR and Meteo France radar product. The DTM analysis will be performed below and allow a better estimation of the UM parameters α and C_1.

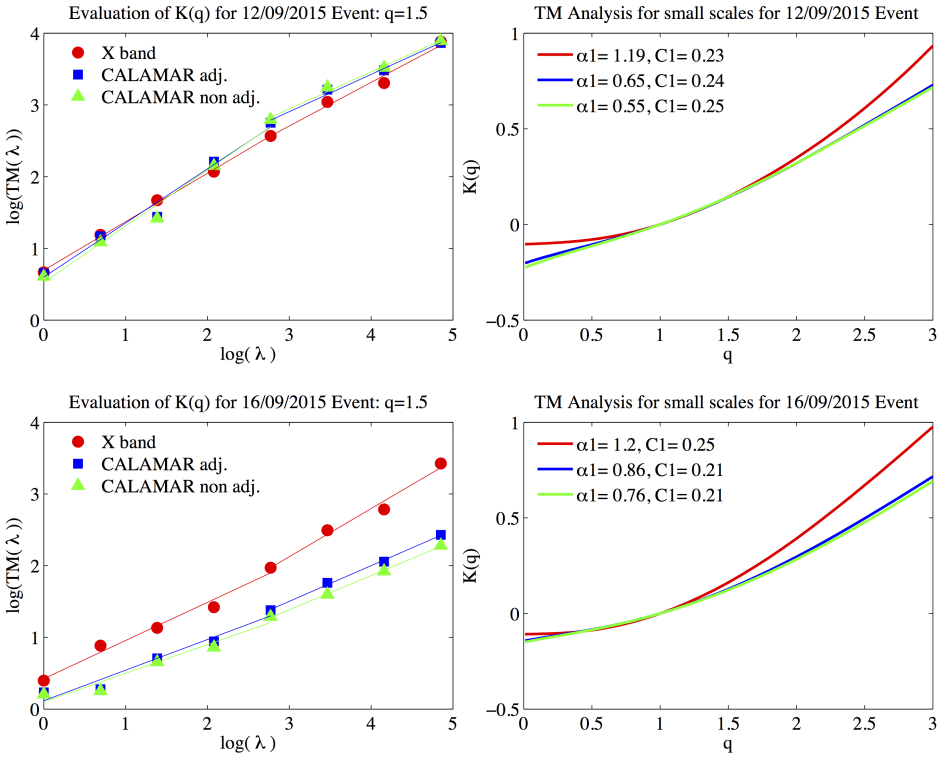

Figure 2.30: TM analysis (Equation 2.15 in log-log plot) for q=1.5 and scaling moment function $K(q)$ obtained in temporal analysis for small scales for $\Delta R - 1D$ field.

2.5.2.4 Double trace moment analysis

The DTM analysis was performed in both space and time. In space a clear scaling behavior was retrieved as noticed with the TM analysis for the three radar products. A break was noticed at roughly 8 km for C band data and 2 km for X band one. In Figure 2.31 are displayed the scaling moment functions $K(q,\eta)$ obtained in spatial analysis at small scales for the three products. The differences between C band and X band products in terms of UM parameters estimation α and C_1 is still important. In fact, X band field exhibits greater values of α (between 1.8 and 1.9) but smaller values of C_1 (between 0.11 and 0.15). In C band data α values range between 1.07 and 1.34 whereas values of C_1 range between 0.15 and 0.25. It is important to notice that the adjustment process performed by CALAMAR system does not change the UM parameters significantly.

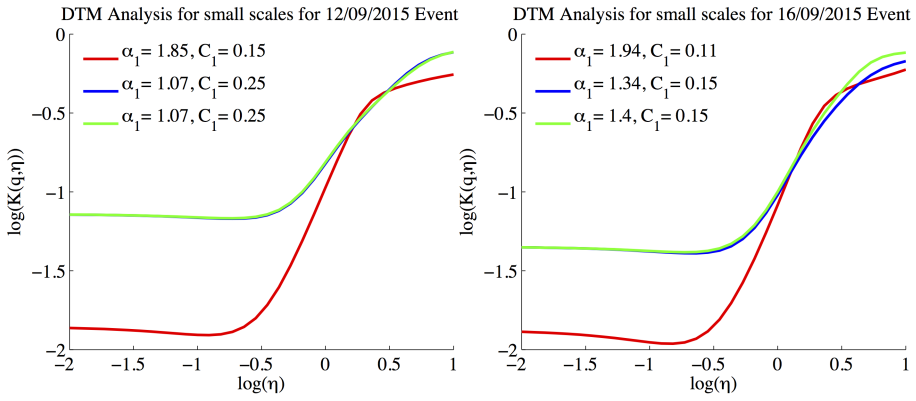

Figure 2.31: DTM analysis in spatial analysis; the $K(q,\eta)$ function obtained for the three radar data ($\Delta R - 2D$) at small scales for X band product (red line), CALAMAR adj. data (blue line) and CALAMAR non adj. data (green line)

In temporal analysis Figure 2.32, the difference between three radar products is less pronounced than in the spatial analysis. α values range between 0.85 and 1.27 and C_1 values are around 0.2. The impact of the radar - rain gauge adjustment process performed by CALAMAR is more pronounced in temporal analysis than in the spatial one. In fact this processes is performed in real time on each radar image and consists in the adjustment of the entire radar image using a single calibration factor, which explain the absence of difference between UM parameters computed for both CALAMAR products in space. The effect on such calibration process is more visible on the temporal rainfall variations.

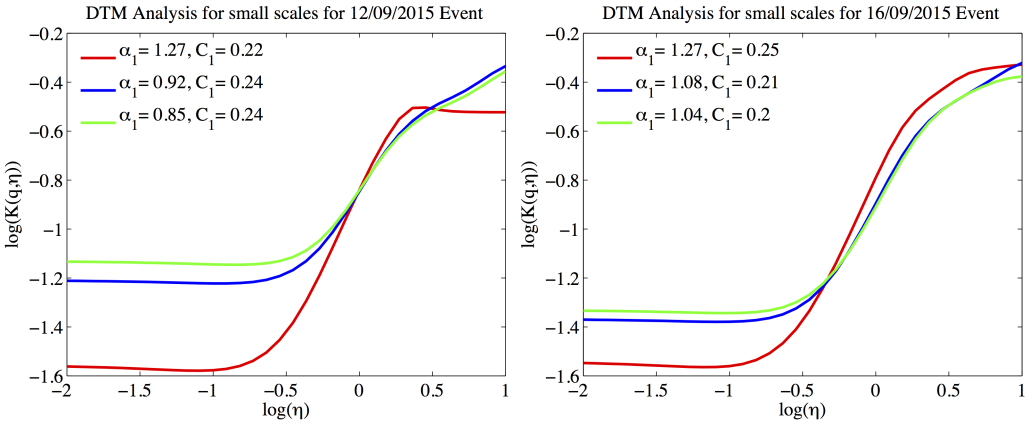

Figure 2.32: DTM analysis in temporal analysis; the $K(q,\eta)$ function obtained for the three radar data ($\Delta R - 1D$) at small scales for X band product (red line), CALAMAR adj. data (blue line) and CALAMAR non adj. data (green line)

2.5.2.5 Spatial analysis time step by time step

The step by step analysis will be performed first in space and consists in computing the UM parameters α and C_1 for each single radar image. The temporal evolution of these parameters will be plotted and discussed with the help of other parameters (the fractal dimension D_f, the maximum observable singularity γ_s as well as the rate of zero values). In Figure 2.33, are plotted the temporal evolution of the rainfall intensity mean (calculated within each single radar image) as well as the ratio of zero values observed in space. From Figure 2.33, one can notice, the high difference observed between X band and C band radar products in terms of zero values. In fact, CALAMAR field exhibits high rate of zero values especially for the first half of the first event and the second half of the second event. This difference is mainly related, as discussed previously, to the methodology applied by CALAMAR for the treatment of ground clutters.

Figure 2.33 indicates that the rainfall means estimated on CALAMAR and X band products are comparable. Slight difference is observed for the first event.

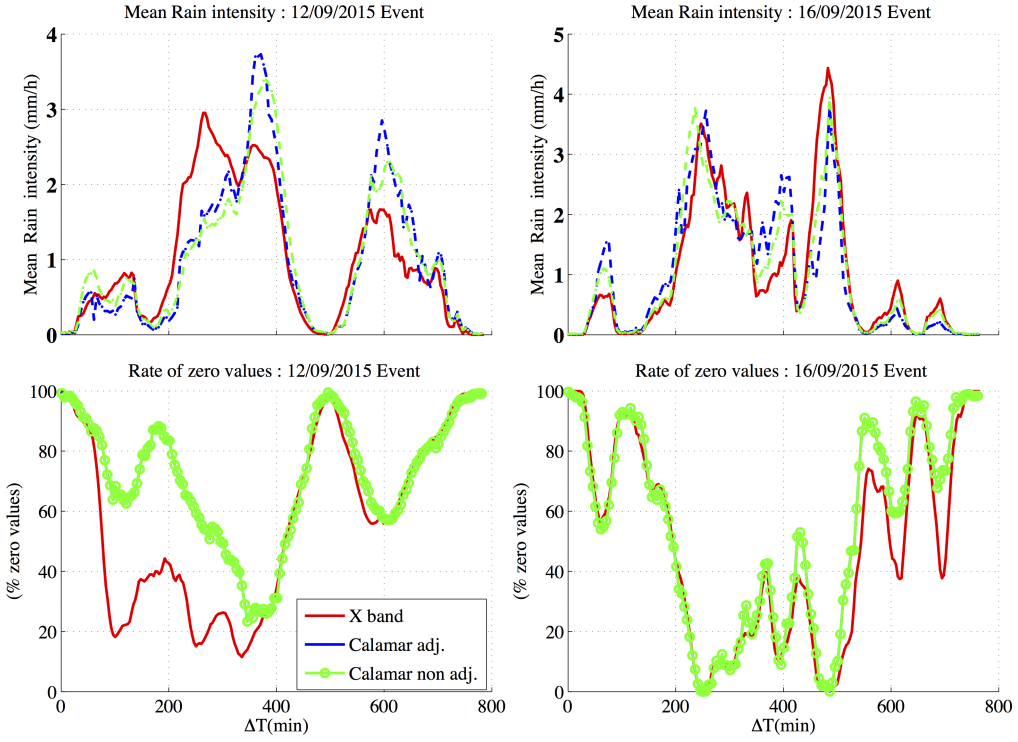

Figure 2.33: Rate of zero values and the rainfall intensity mean calculated in space on each single radar image.

The temporal variations of UM parameters α and C_1 estimated in spatial analysis are displayed in Figure 2.34. From this figure, the difference observed between C band and X-band polarimetric radar data in terms of the spatial structure is visible. In fact, X-band polarimetric radar data exhibits greater values of α and smaller values of C_1. This difference is not related to the rate of zero values observed within CALAMAR data, because the difference remains significant even during the last half of the first event (during which the two products exhibit a comparable rate of zero values).

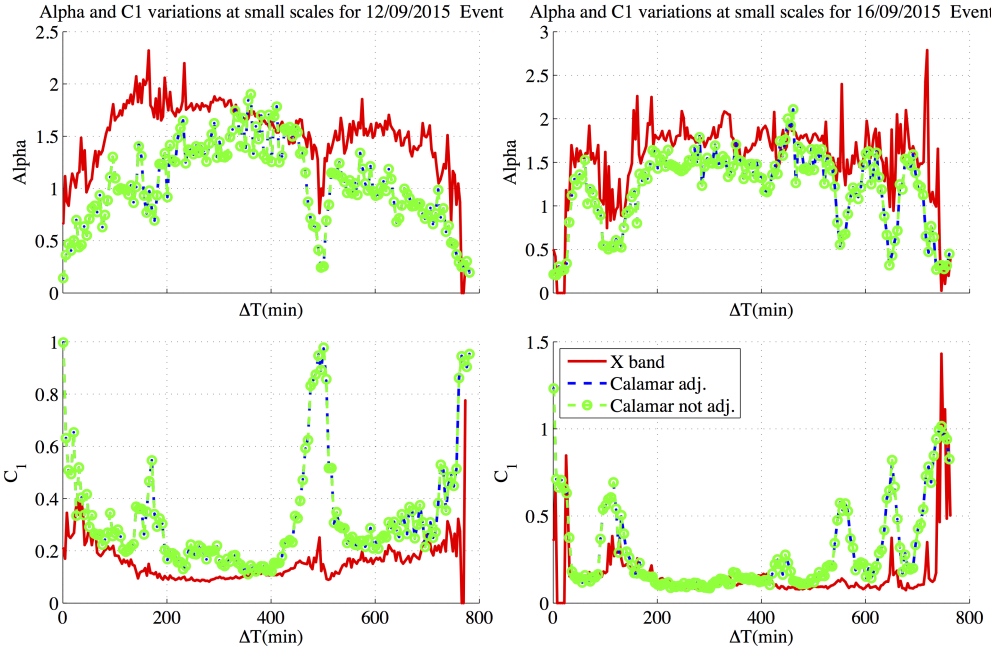

Figure 2.34: Temporal evolution of UM parameters α and C_1 estimated in spatial analysis.

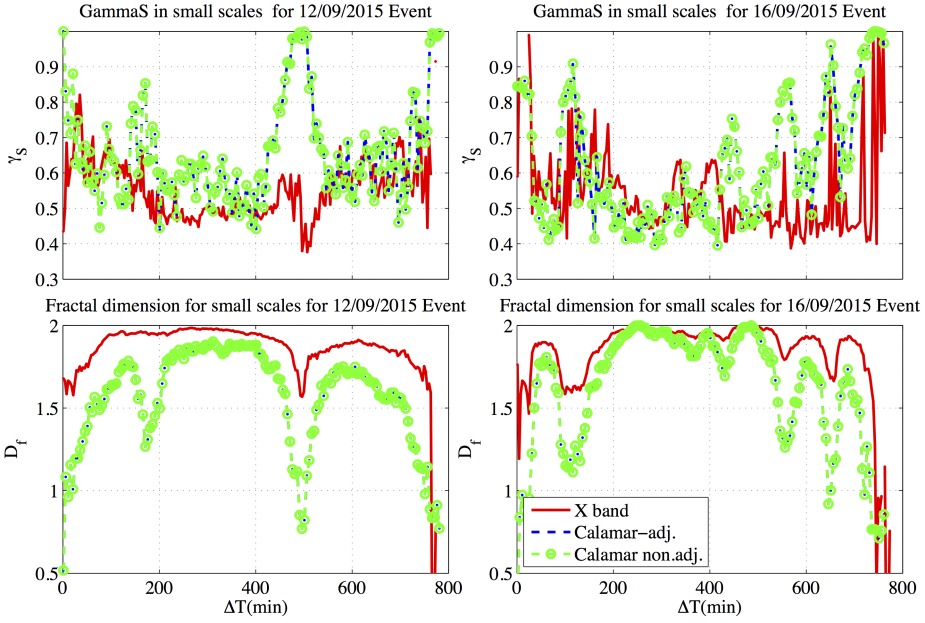

Figure 2.35: The fractal dimension D_f and the maximum observable singularity γ_s were computed in space and their temporal variations are plotted here.

Figure 2.35 displays the temporal variation of the fractal dimension D_f and the maximum observable singularity γ_s computed in space. From these results it appears clearly that the difference observed between the two radar products in terms of UM parameters

is more related to their fractal dimension, so to their spatial structure. In fact, the fractal dimension concept is used to characterize spatial patterns of the field which reflect mainly on the structure identified within the data. Indeed, the difference observed between C band and X band data in terms of UM parameters reflects a profound difference on their spatial structure.

2.5.2.6 Temporal analysis pixel by pixel

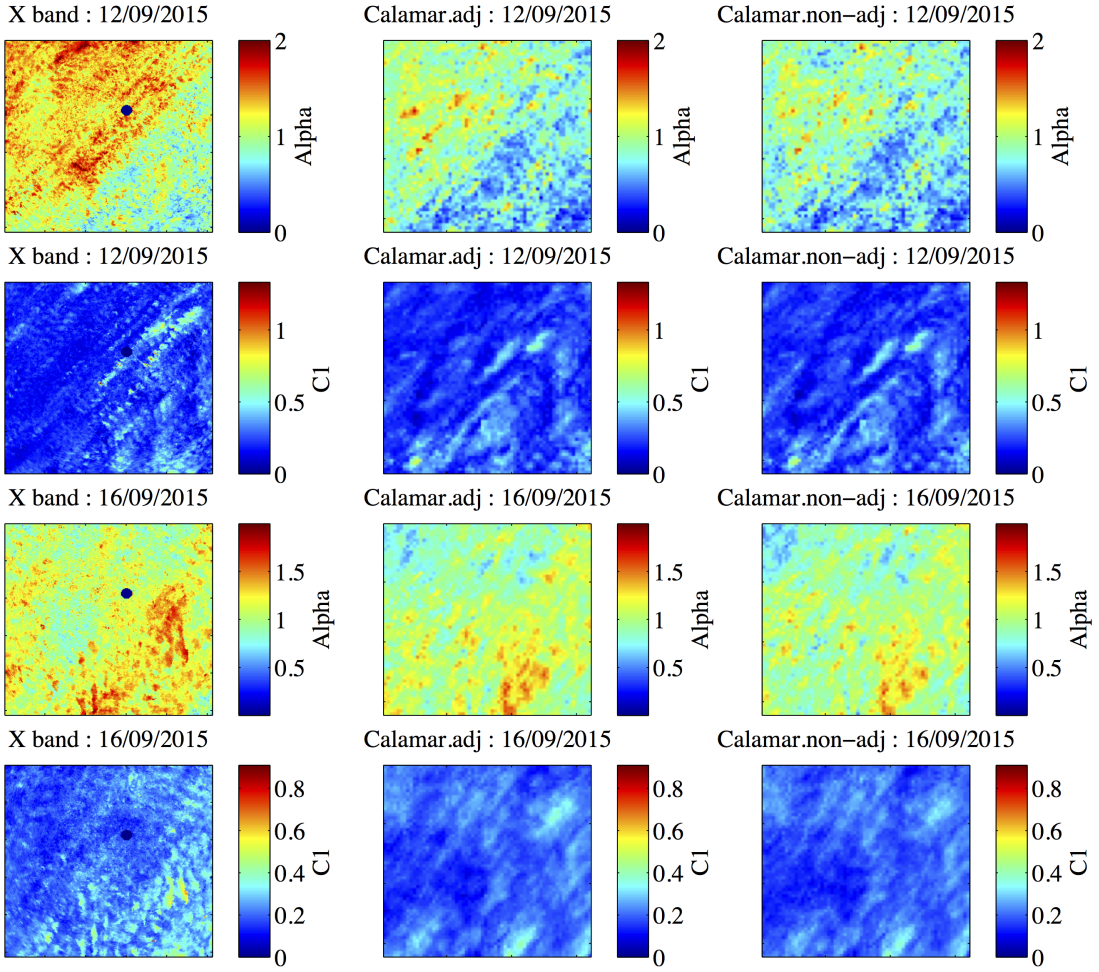

Figure 2.36: Maps of universal multifractal parameters α and C_1, for the three radar products and for the two rainfall events.

In temporal analysis, Figure 2.36 shows maps describing the spatial variability of both α and C_1 parameters calculated using the DTM analysis, red color indicates a higher value while the blue one indicates a smaller value. This figure highlights the morphology of each field and describes the structure of the rainfall field observed for the three radar

products involved in this work. Contrarily to the previous study (i,e the comparison between Meteo France and CALAMAR radar products), maps obtained in Figure 2.36 indicate a significant difference between C band and X-band polarimetric radar field in terms of rainfall temporal variability observed at small scales. In fact, higher values of α are obtained for X-band polarimetric radar data and indicate a better representation of the small scale rainfall variability than in the C band data. The difference is noticed for the two rainfall events.

For the first event, it should be mentioned that both radar products exhibit the same morphology with high variability observed within the new X band product. However, for the second event, a clear difference is observed in the obtained morphology suggesting that the two radars do not probably catch the same rainfall structure which can be related to a difference in the elevation of the radar site or scanning strategy that should be verified.

It appears also from Figure 2.36 that the adjustment process applied by CALAMAR modifies slightly the morphology of the field, it actually increases the variability observed with rainfall time series.

2.6 Intermediate conclusions on Chapter 2

This chapter is dedicated completely to the analysis of rainfall data. Various radar products were involved as well as rain gauges data. The analysis was conducted in both space and time and performed across spatio-temporal scales to enable a characterization of the structure of rainfall fields as well as their morphology.

The developed methodology is fully based on the Universal Multifractal framework and can be used to conduct an indepth analysis of radar data and to perform comparison between radar products and point measurement data. This new methodology overcomes some limitations of the classical radar - rain gauge comparison technique widely used for QPE validation and radar data comparison but involves a very limited number of radar pixels and does not provide any information about the rainfall structure.

For the first study, a comparison between CALAMAR and Meteo France products was performed. The main goal is to identify the influence of raw data processing on the quality of the obtained rainfall measurement. In fact, both Meteo France and CALAMAR products use the same raw data coming from a Meteo France C band radar located in

Paris region. However they do not rely on the same QPE algorithms which has significant effect on their measurement quality. The comparison confirms a clear difference between CALAMAR and Meteo France products in terms of UM parameters.

In spatial analysis, the scaling behavior was identified and confirmed in the Trace Moment analysis with a break observed at 8 km for all events and all radar products. The obtained scaling moment function K(q) for small scales ([1 km-8 km]) comes out with a great difference between the two products multifractality. Meteo France field exhibits a multifractal behavior with α ranging between (1.11 and 1.9) while both CALAMAR products exhibit almost a mono-fractal behavior with much lower values for α. This was related to the high rate of zero values noticed for CALAMAR fields, due to the methodology applied for the treatment of ground clutters. The DTM analysis gives a better estimation of Universal Multifractal parameters α and C_1; values obtained confirm the clear difference between the two products, and the fact that the variability of precipitation is better represented in Meteo France product than in RHEA product. The temporal evolution of UM parameters α and C_1 confirms that the two products do not yield the same parameters except during the period with the heaviest rainfall when the structure of the two products becomes comparable.

In temporal analysis, the difference observed between the two products in term of α and C_1 values are less significant than what is observed in the spatial analysis.

The same comparison methodology was used for the analysis of the new X-band polarimetric radar data and to perform a comparison between C band and X-band polarimetric radar products in terms of rainfall spatio-temporal variability. Only two rainfall events were selected for this study, further analysis will be conducted depending on the availability of X-band polarimetric radar data.

As a result of this comparison, both radar products exhibit a scaling behavior with a clear break noticed in spatial analysis around 8 km for C band data and 2 km for the X band product. In temporal analysis the break was noticed around 40 min and 27 min respectively for C band and X band products. A clear difference was noticed in terms of the rate of zero values. In fact, CALAMAR products exhibit greater rate of zero values than the X band product, and this was related to GC identification and removal technique.

The UM parameters α and C_1 retrieved indicate that the X band product represent better variability for small scale rainfall information. The structure of the two products become comparable when they represent the same fractal dimension D_f, which

means that the structure of rainfall support was caught by the two radars. However, a clear difference is observed in temporal analysis between X band and C band product, the X band data shows clearly more variability of rainfall information. The developed methodology was applied in the framework of this dissertation for the comparison of radar products. However, it can also be applied for other radar data analysis, including QPE validation or radar -rain gauge comparison. It has the advantage of providing much more information about rainfall fields' structure. Such information and details would be very difficult to obtain with the help of the conventional methods largely used until now, for which only a very limited number of radar pixels (only those containing rain gauges) are involved into the comparison of the radar and rain gauge data.
Further extensions of the proposed methodology open new horizons for the rainfall data merging.

Chapter 3

Hydrological modeling of urban catchments

A significant part of this work was devoted to urban hydrology modeling and various investigations were performed in the framework of RainGain project related to this topic. Three complementary studies were conducted in the framework of this work with the aim of providing answers to various questions related to the use of high resolution rainfall data for modeling applications. (i) The first study analyze the ability of urban storm models to integrate small scale rainfall information provided by X-band radars. A sensitivity analysis of hydrological models to rainfall spatio-temporal variability was conducted in this context. (ii) The second work concerns improvements and modifications that should be implemented on urban storm models to increase their ability to integrate small scale rainfall information. (iii) The last investigated point is about the implementation strategies of gridded-based models, and how performance of such models can be improved by analyzing scaling effects noticed on land use data used to describe urban catchments behavior.

All these studies are based on the use of huge and complete data set prepared for the needs of such investigations. Indeed, two urban storm models involving two different modeling approaches will be used for all investigations carried out. Rainfall data include point measurements data, C-band radar data and high resolution X-band data, some of the data was made available in the framework of RainGain project.

Consequently, this chapter includes four sections devoted each to a specific modeling study:

- The first part includes basic introduction of urban hydrology modeling and the water cycle processes in urban environment. It will be followed by the presentation of the two urban storm models used in this work. Their implementation for Sucy-en-Brie case study and their validation using real flow measurements will be discussed as well.

- In the second part, spatial scale issues in urban hydrology modeling will be investigated using fractal tools with the aim of highlighting scaling effects noticed on urban catchments data. The effects of such dependency on gridded-based model performance will be analyzed as well.

- The third part will be focusing on sensitivity of urban storm models to rainfall spatio-temporal variability with a deep analysis of both modeling approaches capabilities to integrate small scale rainfall information and what improvements should be implemented on urban storm models to increase their ability to take full advantage of small scale rainfall data.

- Finally, first high resolution rainfall events provided by the newly installed ENPC X-band dual polarization radar will be used to conduct first modeling analysis using high resolution rainfall data.

3.1 Urban storm models

Nowadays, hydrological models are extensively used in urban water management, research activities and decision-making, following advances noticed in recent few decades in terms of computing capabilities, remote sensing devices and also the increased need to understand the interaction between urban environments as a very complex system and the movement of water in such areas. The growing threat on urban population caused by water management issues especially flooding disasters and water resources pollution has the effect of broadening the scope of application of models to real time use in order to improve the understanding of natural processes or response to management questions. In the meantime, modeling constitute the only way to get an idea about what happened and indeed to enhance the given technical solution, given the difficulty for urban water managers to get distributed measurements at all critical points of the catchment.

Urban environments are very complex systems due to their extreme variability, the interference between human activities and natural processes, but also the effect of the ongoing urbanization process that changes the landscape and strongly influences the hydrological behavior of urban catchments. Urban models are mainly used to simulate the portion of the water cycle in urban environment. However these processes are just very complex and not yet fully understood by the scientific community. There are also some new processes specific for urban and semi-urban catchments that were neglected or not taken into account in rural environments. "The circulation of rainwater within urban areas has not yet been described in a detailed manner, as studies on this topic often remain limited to the runoff on impervious surfaces" (Rodriguez et al. (2008)).

Many research works were carried out recently (Refsgaard and Knudsen (1996), Tech University of Darmstadt and Ostrowski (2002), Salvadore et al. (2015), Hromadka (1987), Daniel et al. (2011), Elliott and Trowsdale (2007), Sarma et al. (1973), Blöschl and Sivapalan (1995)) to elaborate the state of the art of urban hydrological modeling, starting from the complex task of listing and representing all urban processes that define the water cycle in urban areas and determine the movement of pluvial water in urban areas. They were also focusing on the understanding of different modeling approaches used in urban hydrology. A brief overview of these works will be given in this section.

3.1.1 Water cycle in urban areas

The water cycle in urban areas includes all physical processes that govern the movement of water in urban areas, from the moment it falls as precipitation to the moment it leaves the catchment. In urban areas, main processes often considered in the water cycle, are the precipitation, evapotranspiration, infiltration, depression storage, interception and the drainage modeling. Evapotranspiration, depression storage, interception and infiltration are usually grouped as losses because they represent the portion of precipitation that does not participates to the runoff.

- **Precipitation modeling:**

  Rainfall constitute the principal input for hydrological models, it is the driving force behind all hydrological processes. Rainfall information is generally derived from rain gauge networks in the form of point measurements, or weather radars in a gridded format.

Most of hydrological models, can deal with both types of rainfall data. However, the way they take into account the rainfall information varies according to the modeling approach used. Semi-distributed models considered rainfall as homogeneous at the sub-catchment scale deleting thus the spatial variability that can be effectively measured at small scales. Fully distributed models allow taking into account the measured spatial variability of rainfall data. Spatio-temporal resolution needs for urban modeling is a subject of debate and exchange between the scientific community and urban water managers. The debate is motivated by recent advances noticed in rainfall measurement techniques especially radars that are increasingly integrated in urban areas and much more oriented towards specific urban hydrology applications. This point was also of a big interest for this work which contributed to this debate through several research works presented in this chapter.

Rainfall that falls in urban areas can have many destinations. A first part will be intercepted by the vegetation cover, another part will be stored by the depressions. Some will infiltrate and a small part will return to the atmosphere by evaporation. The remaining part called the rainfall excess or the effective rainfall will generate the surface runoff. Indeed, the first step of any runoff calculation consists in the estimation of the effective rainfall, which is defined as the rate of the gross rainfall minus the rate of all losses. However the estimation of losses rate is often complex, especially for urban environments and needs a huge and detailed information describing all urban catchment components (soil, landscape, vegetation cover, ...).

- **Evapotranspiration:**

  Evaporation quantifies the precipitated water that returns to the atmosphere due to the effect of temperature. A precise estimation of the evapotranspiration rate is highly complex and even impossible in urban areas because it requires a large amount of information for its estimation. The process that occurs along the water-air or soil-air interface depends on the vegetation density, season, soil characteristics, and meteorological conditions. In urban hydrology, it is widely assumed that the evapotranspiration rate is very small and can be justifiably neglected especially during severe events. However, unlike the event-based models, continuous-based events models should integrate an estimation of the evapotranspiration rate as the period simulated is long enough so that the evapotranspiration becomes significant.

- **Infiltration:**

  Infiltration is the process of water movement into the subsurface under gravity or capillary forces. The rate at which infiltration occurs may be affected by several physical factors including hydraulic conductivity, capillary action and gravity.

  The part of precipitation that finds its way to the ground is considered in urban hydrology as a loss because it does not contribute to the surface runoff. Unlike rural areas, the infiltration is decreasing in urban environments because of the increased imperviousness of urban surfaces. In the meantime, the existence of dense drainage network reduces the duration of stay of water at the surface, limiting thereby infiltration.

  Two approaches can be used in urban hydrology for the estimation of the infiltration rate that depends on the infiltration capability of the subsurface. One physical approach based on detailed soil properties (e.g., hydraulic conductivity, capillary tension and moisture content) and an hydrological approach based on the use of a parametric lumped model to estimate infiltration rate. Several models exist for infiltration estimation and modeling (Horton, Green-Ampt approaches), see El-Kadi et al. (1983) for a review.

  - **Green-Ampt approach :** the Green and Ampt relationship (Heber Green and Ampt (1911)) is widely used in urban models because of its ease of application and its robust estimation of the infiltration rate. In fact, the empirical equation of Green and Ampt has physical significance because its parameters have physical basis. Distributed and physically based models often relay on this approach.

    An additional advantage of the method is that its parameters have been determined and verified for soil textural classification (Rawls et al. (1983)). However, further investigations of the soil structure can be performed in order to validate parameters estimation.

    The general equation showing the Green and Ampt relationship can be expressed as (Li et al. (1976)):

$$f = K_h(1 + \frac{H_c(1 - S_e).\theta_e}{F}) \tag{3.1}$$

where f is the infiltration rate (m/s), K_h the effective hydraulic conductivity (m/s), H_c the capillary suction (m), θ_e the effective soil porosity, S_e the effective soil saturation and F the cumulative infiltrated water depth (m).

– **Horton model :** Horton model relies on a conceptual approach to simulate the infiltration rate. It is widely used by semi-distributed and conceptual models. The approach that was developed in 1933, indicates that if rainfall exceeds the infiltration capacity of the soil, then the infiltration tends to decrease exponentially.

$$f_p = f_c + (f_o - f_c)e^{-kt} \tag{3.2}$$

where f_p is the infiltration capacity or potential infiltration rate, f_c the final constant infiltration rate, f_o the initial infiltration capacity and k a soil parameter.

The Horton model needs to be calibrated and all parameters f_c, k, and f_o must be evaluated using measured infiltration data.

- **Interception:**

Interception quantifies the amount of precipitation that adheres to the vegetation until it evaporates or reaches the ground later. This phenomenon is significant at the beginning of the rainfall event since the vegetation loses its ability to capture raindrops. Interception rate is influenced by the characteristics of rainfall events, the vegetation species and meteorological factors (temperature, relative humidity, net radiation, and wind speed).

Several formulas are used in hydrology to estimate the interception as a function of rainfall and vegetation characteristics (Chow (1964)), However, in urban environments, the interception is reduced and less significant in the water balance because of the high imperviousness and low vegetation cover.

- **Depression storage:**

Depression storage or surface storage accounts for water that is trapped in small depressions on the catchment surface and retained until it infiltrates or evaporates. Depression storage depends mainly on catchment surface shape and slope. On impervious urban surfaces, depression storage ranges from 0.2 mm (smooth asphalt pavement) to 2.8 mm (an average value for small urban areas); on permeable

surfaces, depression storage ranges from 0.5 mm (bare clay) to 15 mm (wooded areas and open fields). A detailed listing of depression storage values for more than 25 types of surfaces can be found in W. F. Geiger J. Marsalek W. J. Rawls F. C. Zuidema (1987).

3.1.2 Urban modeling approaches

Hydrological models include often two basic components: (1) rainfall-runoff modeling to estimate the effective precipitation or rainfall excess that will participates to the runoff and (2) the routing modeling that simulates the transport of stormwater in urban water infrastructures. Indeed, various modeling approaches were developed for urban hydrology to simulate these components. They can be classified based on the nature of the employed algorithms: empirical, conceptual or physically-based approaches. They can also be classified based on their spatial resolution and how they represent the complexity of urban hydrology processes (lumped models, semi-distributed and fully-distributed). A recent (Salvadore et al. (2015)) review about urban hydrological modeling identifies and lists 5 most used modeling approaches in urban hydrology; (1) the first category is the lumped models. Lumped models consider the whole catchment as a single unit in which all physical and hydrological information are assumed to be homogeneous, processes are based usually on the Unit Hydrogram (UH) model which is defined based on hydrological data available (rainfall and corresponding flow), such models are used especially for catchment where the lack of data does not allow to go further in the description of the catchment.

The second category is the semi-distributed models using sub-catchments; sub-catchments are areas where parameters describing the rainfall-runoff function are considered to be uniform. Each sub-catchment outlet is connected to the drainage system and we can distinguish two sub-categories based on how sub-catchments are defined. (2) In HRU models (Hydrological Response Units) sub-catchments have same soil and land use type. (3) In the other sub-category, the identification is based often on the same drainage area concept which assumes based on the topography and/or the sewer network that all rainfall occurred in the area is routed to the same outlet point without worrying about the land use distribution.

(4) The fourth category is the fully distributed or grid-based models, which are considered to be more sensitive to the urban catchment variability and the scale issues.

(5) The last category is Urban Hydrological Element (UHE) models that are based on the identification of an object or a unit of calculation small enough to represent the urban heterogeneity and to be homogeneous (block of buildings, ...)

- **Physically based models :** Physically based models aim to describe as accurately as possible the internal mechanisms of the urban water system based on the best possible knowledge of the physical processes and using all existing physical laws such as the conservation of mass, of energy and of momentum. In theory, these models rely on real physical and measurable on site parameters and don't need thus to be calibrated. However, they are highly dependent of the model spatio-temporal resolution.

  Fully distributed and gridded-based models often rely on this approach. Indeed, the spatial distribution of all urban catchment components (topography, land use, sewer system, rainfall) are presented in a distributed manner using pixels for which the spatial resolution can be adapted to the quality of the data available and the expected goal.

- **Conceptual models :** Because of the high complexity of urban processes, conceptual models rely on a simplification of the system behavior. They attempt to integrate the complexity of processes by reproducing in a simple manner the physical concept of the system behavior. This type of models keeps the same physical meaning but not the accurate description of all involved processes. Due to their principal, conceptual models often use conceptual approaches involving no physical parameters and need therefore to be carefully calibrated.

  Semi-distributed models often rely on this conceptual approach. For these models, the catchment is divided to several entities called sub-catchments. The architecture of these models is based usually on two functions that describe the hydrological response of the catchment:

  - The production function used to estimate the effective rainfall Hyetograph from the gross rainfall one by quantifying all urban water losses.

– The routing function used to derive the hydrograph from the effective rainfall by considering meteorological, physical and hydrological characteristics of the catchment considered. It relies often either on the unit hydrograph model that is based on the hypothesis of linear rainfall-runoff relationship, or on the use of a cascade of linear reservoirs where the output of each reservoir is considered as the input for the next one.

- **Empirical models :** Empirical models do not refer to urban water processes. They attempt to establish a direct relationship between the input (rainfall) and the output (overland flow, sewer flow) in order to reconstruct a series as closest as possible to the observed one. They are most often based on a statistical approach and can therefore be stochastic or probabilistic.

3.1.3 Multi-Hydro model

Multi-Hydro (3.1 Giangola-Murzyn (2013)) is a fully distributed and physically based model developed at Ecole des Ponts ParisTech. It is an interacting core between four open source software packages, each of them representing a portion of the water cycle in urban environments. Multi-Hydro involves a modeling approach that consists in rasterizing the urban domain at a specific spatial resolution chosen by the user, each pixel is then affected by a unique land use class for which hydrological and physical properties are specified.

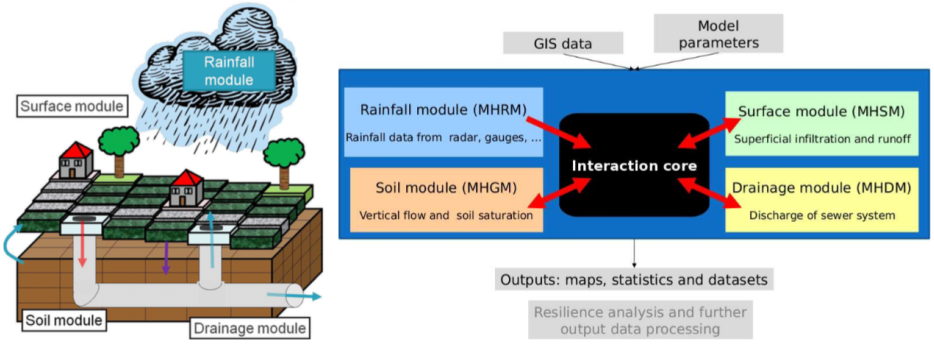

Figure 3.1: Multi-Hydro model is an interacting core between four modules, each of them representing a portion of the water cycle in urban environments. ©Giangola-Murzyn (2013)

The four modules that make up the core of Multi-Hydro are presented in the following points:

- The surface component (MHSC) is based on the existing TREX model (Two-dimensional Runoff, Erosion, and Export model) developed by Colorado State University and used in Multi-Hydro only for rainfall-runoff modeling (England et al. (2007), Velleux et al. (2008)). The integration of contaminants transport and sedimentation is in progress. The surface module computes interception, storage and infiltration occurred at each pixel according to its land use class, and properties defined for this class. The net (effective) rainfall P_e is then calculated by subtracting the interception from the gross rainfall P_g and overland flow can occur after satisfying the depression storage threshold, it is governed by the conservation of mass (continuity) and of momentum equations. This flow depends on the surface properties as well as the elevation, and computed using the diffusive wave approximation of Saint-Venant equations. Multi-Hydro integrates also the simulation of 1D channel flow.

- The rainfall module has been developed at Ecole des Ponts ParisTech, it is used to manage different types of rainfall data (rain gauges, radar data,...) and to process them in the correct input format needed for Multi-Hydro model. The module performs also some data analysis and can be used for radar data downscaling. The data analysis part relies on the Multifractal framework (Lovejoy and Schertzer (1990), Schertzer and Lovejoy (1987b)) and has been widely validated at Gires et al. (2012a).

- The Drainage module (MHDC) is based on the 1D SWMM (James et al. (2010)) model (Storm Water Management Model) developed by the US Environmental Agency. It is widely used for urban drainage and modeling purposes. The flow in the sewer network is given by a numerical solution of Saint-Venant equations. This module requires a detailed description of the sewer network (nodes, pipes characteristics, gullies, outlet...).

- The infiltration module relies on VS2DT model developed by the U.S. Geological Survey and it is used to simulate the infiltration into the unsaturated subsurface zone (Healy (1990), Lappala et al. (1987)). This module uses the infiltration depth

calculated by the surface module as input, and simulates a 2D infiltration (vertical and 1D horizontal) into the subsurface.

Multi-Hydro core ensures the connection, interaction and data exchange between these four modules after each time loop. Indeed, the surface module outputs are used as inputs for the soil and the drainage modules and in the same way the sewer overflow is taking into account on the overland depth for the next step. Multi-Hydro produces a large set of outputs that describe the catchment response. Indeed, the overland water depth maps are available at each time step as well as the overland discharge flow and the velocity profile at any point of the catchment. Saturation profile of the subsurface zone and the sewer flow are also computed. The model provides also a detailed volume balance at each time step.

3.1.3.1 Process modeling

The modeling approach involved in Multi-Hydro model, relies on the resolution of physical equations that describe the catchment behavior. Seven processes are simulated; (1) precipitation, (2) interception and storage, (3) infiltration, (4) overland flow, (5) sewer flow, (6) infiltration into the subsurface zone and (7) the sewer overflow.

- **Precipitation :** Multi-Hydro deals with three types of rainfall input; precipitation can be considered as homogeneous for the whole catchment if only one rain gauge is available or interpolation can be performed if more than one are used (for these two cases, the user should specify the number of rain gauges used, their locations and the corresponding rainfall intensity time series). The last choice is a gridded radar rainfall data, for which the spatio-temporal resolution may be different from those of the model. In this case, the rainfall module will process the data and do the necessary conversion to get the corresponding grid at the correct spatial resolution. Downscaling of radar data can also be performed to get a better resolution from the classical (1 km^2, 5 min) radar image. Whatever the type of selected inputs, a single value of precipitation will be affected to each pixel at the end of this process.

- **Interception :** The volume of precipitation intercepted by the vegetation cover is computed for each green pixel. In fact, the portion of gross rainfall held by the vegetation cover depends on the interception depth (mm) set by the user. It is

important to note that during rainfall events, the intercepted rainfall may reach the land surface or return to the atmosphere by evaporation, these two processes are neglected in Multi-Hydro model for single storm event modeling.

- **Depression storage :** It is a threshold set by the user for each land use class, it indicates the depth (mm) of water that can be stored before the beginning of the overland flow.

- **Infiltration :** Infiltration rate $f(m/h)$ into the subsurface is computed at each pixel using the Green and Ampt relationship (Equation 3.1) and according to physical properties assigned for each land use (hydraulic conductivity $K_h(m/s)$, capillary suction $H_c(m)$ and the moisture deficit θ_r), all these parameters are set by the user during the rasterazation phase.

  The infiltration into the unsaturated subsurface zone is modeled using the fluid mass conservation law and a non-linear form of the Darcy equation.

- **Overland flow :** The 2D overland flow can occur after satisfying the depression storage threshold, it is governed by the conservation of mass (continuity) and of momentum equations. This flow depends on the surface properties (Manning roughness coefficient $n(s.m^{-1/3})$ as well as the slope, and computed using the diffusive wave approximation of Saint Venant equations.

- **Sewer flow :** In Multi-Hydro model, the whole sewer system is modeled, and the sewer flow is computed using the dynamical wave approximation of the de Saint-Venant equations.

- **Sewer overflow :** Overflow occurs usually during flooding events, it is a consequence of the strong pressure on urban sewer networks. In fact, the amount of water generated during a short period of time can exceed the capacity of the sewer system and water exits the sewer network through gullies and reaches the surface. This phenomenon is complex to take into account in urban storm models and is neglected in most cases. However, the structure of Multi-Hydro model based on the interaction and data exchange between the four modules after each time loop simplifies the integration of this process. Indeed, after each time step, the sewer module outputs indicate the amount of the overflowing water and this information is taken into account in the initial water overland for the next step.

3.1.3.2 Model implementation

Multi-Hydro is a gridded-based model that needs a detailed description of the catchment behavior as well as the sewer network and the subsurface zone. The implementation process is performed on two steps:

1. **Data collection and validation :** The first step of the model implementation consists in data collection and validation. GIS data (Geographic Information System) describing the topography and the catchment land use must be collected at a high resolution, available satellite images are often used to validate the land cover data.

   Information about the sewer network should also be available. Details about all the system components are necessary for the drainage module. Such information are usually available for urban areas and can be obtained from the local authority in charge of the water management. Details about all pipes (geometry, length, diameter as well as inlet and outlet nodes) should be carefully validated as well as all the system nodes (coordinates and elevation). Identification of gullies is of high importance because they ensure the connection between the surface and the drainage modules. Finally, subsurface structure must be described as well if there is a need to simulate the infiltration to the unsaturated subsurface zone. The analysis of drilling data archived can help on building an acceptable description of the subsurface area.

2. **Rasterazation phase :** Once all needed data are available and validated, a special build in module MH-AssimTool (Multi-Hydro) can be used to perform the rasterazation process and to build all inputs needed for Multi-Hydro model. During this phase, the user should specify the spatial-temporal resolution of the model, and also physical properties set for various land cover classes. The module integrates a database about classical land cover characteristics (road, house, grass, forest, water, ...). The user can chose whether to use this database or to set up new parameters. The rasterazation process can take a few minutes or a few hours depending on the spatial resolution chosen and the catchment size. At the end of this process, Multi-Hydro is implemented and ready to be used for modeling applications. If all needed data is available and validated, the implementation of

Multi-Hydro model is much more easier than similar urban storm models.

As a part of this work, a deep reflection was conducted about the implementation approach involved in Multi-Hydro model. In fact, the original approach is based on a priority order set by the user during the rasterazation process. This order was defined in such a way to represent the catchment behavior observed on site during rainfall events, especially the "preferential water path" concept that makes that water circulates primarily in roads. Indeed, the priority order was chosen in order to keep the continuity of roads whatever the spatial resolution of the model is. Therefore, the obtained behavior exhibits usually a high rate of impervious surfaces which have important consequences on the model performance. This implementation approach is challenging in terms of Multi-Hydro performance, because it imposes additional constraints and makes that high resolution modeling (small pixel size) is the only way to get a better catchment behavior and to obtain acceptable model performance. However performing such small scale modeling investigation is not an easy task, and depends highly on the quality of the data used and it is also a very time consuming.

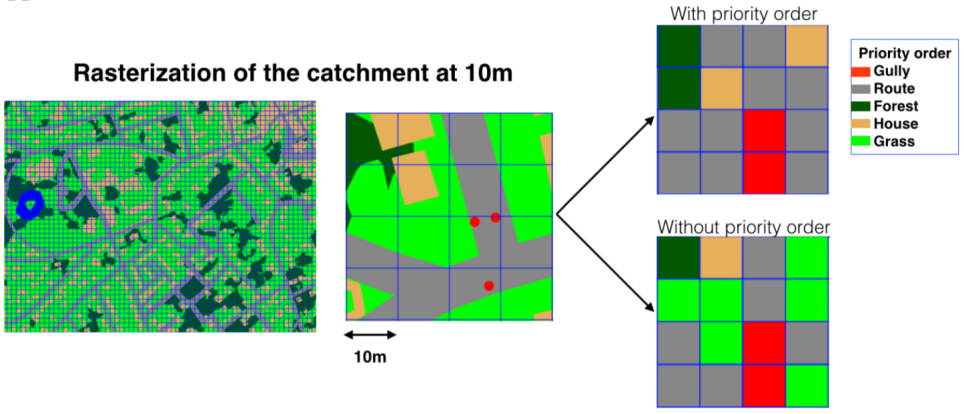

Figure 3.2: Comparison between the two implementation approaches. The original one is based on a priority order whereas the new one is based on a predominant criterion.

A new implementation approach (Figure 3.2) was developed in the framework of this work as a result of a lot of modeling investigations and a deep reflection about the manner the rasterazation process should be conducted to have a good representation of the heterogeneity of the catchment behavior. This new approach relies on two steps and it is not based any more on any priority order except for sewer inlet points that should be identified in priority because they ensure the connection between the surface and the drainage modules:

(a) The first step consists in rasterizing the land cover data using very small pixel size (up to 20 cm). Such rasterizing can be performed using the built in module MH-AssimTool or using a GIS software.

(b) The small scale land use distribution obtained in the first step will then be used to obtain land use data for coarser pixel size by considering the predominant land use observed within the small scale data. At 10 m pixel size for example, the land use attributed to each pixel will be the majority one observed within the 2500 (50 x 50 pixels) 20 cm small pixels included in the 10 m pixel.

The new approach was applied in the framework of a MSc Thesis I supervised (Elektra (2016)) for the small peri urban catchment of Perreux-sur-Marne (12.47 ha Figure 3.3) located in Val-de-Marne county. Rainfall data is derived from the rain gauge located at the center of the catchment. Modeling results are analyzed with respect to the observed flow measured by the flow sensor located at the catchment outlet (Elektra (2016)). Only results related to two rainfall events are presented here, please refer to Elektra (2016) for further details and analysis. The data was collected in the framework of ANR Trafipollu project.

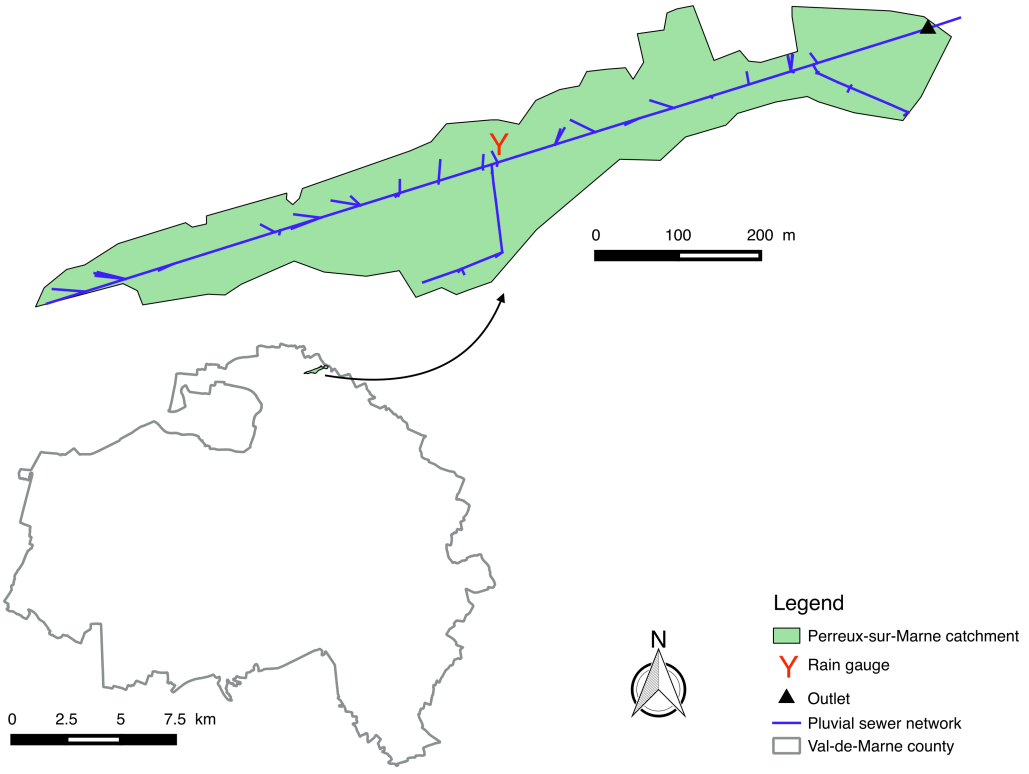

Figure 3.3: Perreux-sur-Marne catchment (12.47 ha) located in Val-de-Marne county. Rainfall data is derived from the rain gauge located at the center of the catchment. Sewer Flow data are measured by the flow sensor located at the outlet (Elektra (2016)).

Results obtained at different spatial scales in terms of land cover heterogeneity are presented in Figure 3.4 for the case study of Perreux-sur-Marne. The coefficient of imperviousness estimated for this case study is around 53% for both 10 m and 5 m scales while it is around 88% at 10 m scale when considering the priority order.

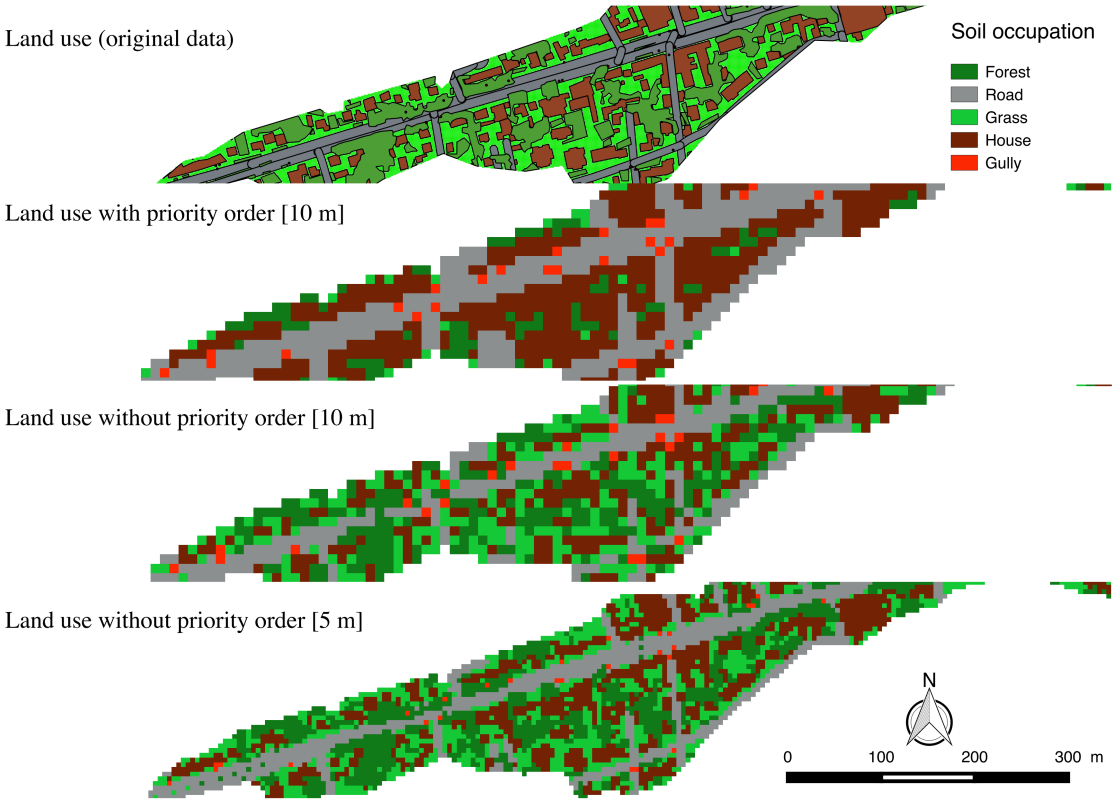

Figure 3.4: Multi-Hydro land cover data obtained for the Perreux-sur-Marne catchment (only a part of the catchment is visible here) with and without considering the priority order. One should notice the high coefficient if impervious areas (88%) obtained at 10 m when considering the priority order. The new implementation approach allows a better presentation of the catchment heterogeneity.

Results obtained with this new implementation approach are very interesting and show clearly the benefit of taking into consideration the heterogeneity of the land cover observed in urban environments. Modeling outputs obtained for the Perreux-sur-Marne case study are presented in Figure 3.5 and Figure 3.6 for two rainfall events. Those related to Sucy-en-Brie catchment will be presented later in this work. From these results, one can notice the high improvement noticed in Multi-Hydro performance when applying the new implementation approach. In fact, modeling outputs obtained at 10 m scale with the new approach are even better then those obtained at 5 m with the priority order. Nash indicator (NSE) is improved for the 15/11/2014 event (Figure 3.5) from -1.76 at 10 m and -0.45 at 5 m when applying the priority order to 0.73 at 10 m and 0.85 at 5 m with the new implementation approach. For the second event (Figure 3.6), NSE is improved from -1.33 to 0.82 when applying the new approach at 10 m.

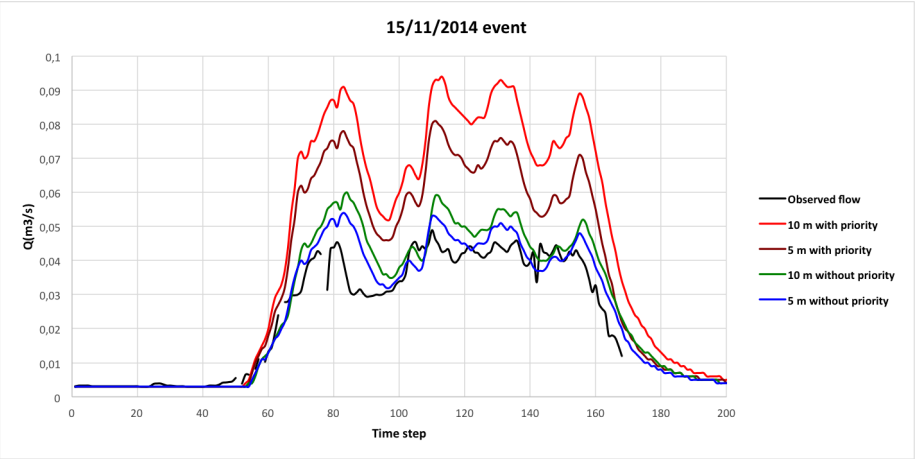

Figure 3.5: The impact of the new implementation approach on Multi-Hydro performance obtained at 10 m and 5 m scale for the 15/11/2014 event.

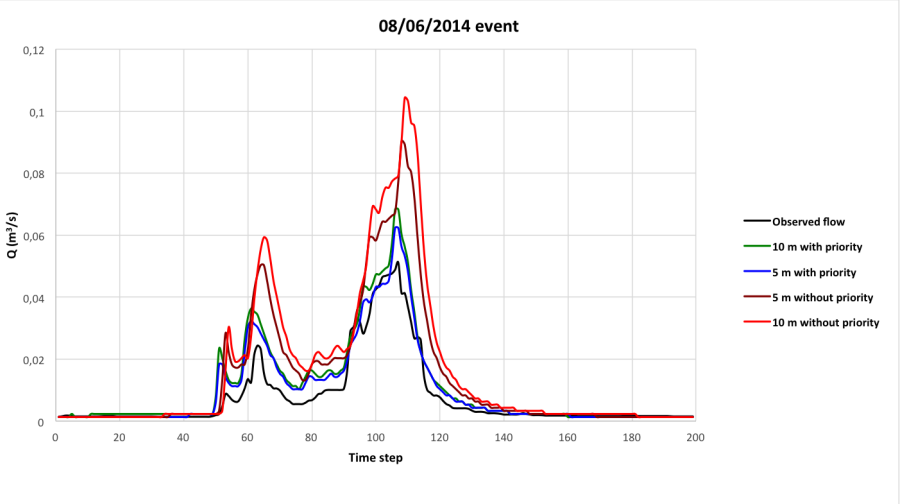

Figure 3.6: The impact of the new implementation approach on Multi-Hydro performance obtained at 10 m and 5 m scale for the 08/06/2014 event.

Consequently, all modeling investigations conducted in this work for Sucy-en-Brie catchment have been processed with this new implementation approach.

3.1.4 CANOE model

CANOE is a semi-distributed and conceptual model developed by INSA of Lyon and SOGREAH (now ARTELIA) (Insa-Valor (1999)) and widely used in France by practitioners of urban hydrology modeling and urban water management. It is best known for its ease of use, its fast computation time but it is hard to set up and needs to be carefully calibrated. The County Council of Val-de-Marne, which is a partner in the model

development, uses CANOE model as the primary model for all case studies, including the Sucy-en-Brie one.

The modeling approach involved in CANOE model is based on the decomposition of the urban catchment into several sub-catchments, each of them connected to the sewer network at its outlet. The rainfall-runoff transformation is modeled using a production function and a transfer one. The flow in the sewer is provided by Barre-Saint-Venant equations (it is also possible to use Muskingum model for simple cases without downstream influence). The model takes into account a changing runoff coefficient based on the rainfall intensity and allows the distinction between surfaces directly and indirectly connected to the network. Unfortunately, this type of model does not take into consideration the whole variability of physical properties since sub-catchments are considered as homogeneous. The delimitation of CANOE sub-catchments can be done based on the drainage system, the topography or according to the degree of imperviousness. Generally CANOE takes into account three types of sub-catchment :

- Strict urban catchments : urbanized areas equipped with a sewer network. Impervious area greater than 30%.
- Strict rural catchments : impervious areas is less than 5%.
- Mixed catchments : partially urbanized areas. Imperviousness coefficient is between 5 and 30%.

For each sub-catchment, three types of surfaces should be specified :

- Impervious surfaces directly connected to the network (S_1), where the flow to the network is fast (parking, road, roof,...).
- Impervious surfaces indirectly connected to the network (S_2), where the flow is delayed (roof, ...).
- Permeable surfaces (S_3).

3.1.4.1 Process modeling

Various modeling options are available within CANOE model and can be used depending on the characteristics of the catchment. The modeling calculation relies on two part performed by two functions:

1. **The production function :** defines the part of the precipitated rain that will effectively reach the sub-catchment outlet. The result of this first transformation is a net rainfall hyetograph. Net rainfall (H_R) is calculated as the difference between the gross rainfall (H_P) and losses (P_i) due to evaporation, vegetation retention, storage in depressions and infiltration (Equation 3.3) :

$$H_R = C_R.(H_P - P_i) \tag{3.3}$$

where C_R is the runoff coefficient.

CANOE model propose two types of the runoff coefficient C_R :

(a) **Constant runoff coefficient model :** it is the simplest and most classical modeling approach in urban hydrology. It consists in a runoff coefficient C_R which is constant during the whole period of the rainfall event and independent of the type of event. In this case, C_R is equal to the percentage of impervious surfaces directly connected to the network. This model is suitable for highly urbanized and homogeneous sub-catchments. Initial losses are considered null in this model ($H_R = C_R.H_P$).

(b) **CANOE standard model :** the standard model is applied equally to the three surface types (impervious surfaces directly connected to the sewer network, those indirectly connected and permeable surfaces), and assumes a different behavior depending on the precipitation rate.
The runoff coefficient C_R is defined as follow :

$$C_R = \alpha.CS_1 + \beta.CS_2 + \gamma.CS_3 \tag{3.4}$$

where α, β and γ represent the contribution of each type of surface (S_1, S_2 and S_3) to the runoff and depend on the rainfall event type (low to medium rain, heavy to very strong rain and exceptional rain). CS_1, CS_2 and CS_3 are respectively the percentage of the three types of surface S_1, S_2 and S_3.
In the standard model, α, β and γ coefficients as well as the criteria for the distinction between the types of rainfall are general parameters of the project that must be set by the user.
The initial constant losses P_I are defined according to the slope of the sub-catchment as follow :

- For impervious surfaces :
  - P_I = 2 mm, if the slope is $\leq$ 1.5% .
  - P_I = 0.5 +(3-S) mm, if slope is $\geq$ 1.5% & $\leq$ 3%.
  - P_I = 0.5 mm if slope is $\geq$ 3%
- For permeable surfaces :
  - P_I = 12 mm, if the slope is $\leq$ 0.5% .
  - P_I = 2 + 4.(3-S) mm, if slope is $\geq$ 0.5% & $\leq$ 3%.
  - P_I = 2 mm if slope is $\geq$ 3%

(c) **Horton model :** Horton model (Section 3.1.1, Equation 3.2) is widely used in urban hydrology for the estimation of the infiltration capacity of the soil, it is known for providing a good approximation of infiltration curves in saturated soil, or in a highly vegetated soil. However the obtained results are much less interesting in case of a bare or dry soil where water/air interface issues are more important (Insa-Valor (1999)). The main difficulty of this model is to properly assess the three parameters f_0, f_c and k. They greatly vary with soil physical characteristics (porosity) but also with its initial moisture content, its plant cover, the size of raindrops, temperature, etc. They can be measured in the laboratory or estimated from the literature, they can also be calibrated using available measurements database.

2. **The transfer function :**

The transfer function aims to convert the net rainfall rate obtained to a flow rate at the outlet of the sub-catchment (the entrance of the sewer system). This function represents the transformation that the net rainfall hyetograph will undergo as it passes across the catchment. Two models are available in CANOE model :

(a) **Linear reservoir model :**

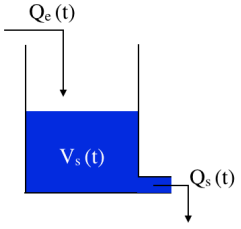

Figure 3.7: Linear reservoir model

The linear reservoir model is widely used in urban hydrology due to its simplicity, its low number of parameters (only one parameter) and its good performance in small catchment (up to 100 hectares). It is based on the combination of two equations; the continuity equation (Equation 3.5) and a storage linear relationship that link the volume stored in the catchment V_s (m^3) to the Outflow Q_s (m^3/s) (Equation 3.6).

$$dV_s/dt = Q_e(t) - Q_s(t) \tag{3.5}$$

$$V_s(t) = K.Q_s(t) \tag{3.6}$$

This model can be represented by a single reservoir for which the law defining the storage and the discharge varies linearly as a function of the water depth. Indeed, the flow rate $Q_{s,t}$ for a given time step t (s) can be obtained from the net rainfall $Q_{e,t}$ using :

$$Q_{s,t} = e^{\frac{-\Delta t}{K}}.Q_{s,t-1} + (1 - e^{\frac{-\Delta t}{K}}).Q_{e,t} \tag{3.7}$$

One of the major advantages of this model is that the catchment response time parameter K can be estimated for each sub-catchment according to its characteristics (area, slope, length of the water path and the imperviousness coefficient).

For urban catchments, it can be calculated from (Insa-Valor (1999)) :

$$K = 0.254A^{-0.0076}C_{imp}^{-0.512}S^{-0.401}L^{-0.6}. \tag{3.8}$$

where K is the sub-catchment response time expressed in minutes, A is the area in hectares, C_{imp} the imperviousness coefficient, S is the slope (m / m), and L is the water path length (m).

(b) **Nash model :** The model consists in a cascade of identical linear reservoirs discharging into each other. It is a two-parameters model (the lag time parameter K and the number of reservoir n). The number n of reservoirs depends mainly on the surface of the catchment and its imperviousness coefficient. The model is more interesting in the case of a slightly urbanized

catchments or large areas (over 50 hectares) because it further delays the output.

3. **Hydraulic modeling :** In CANOE model, the hydraulic simulation can be performed in two manners, depending on the complexity of the sewer network:

   (a) **Muskingum model :** The Muskingum model is a non physical model based on a storage equation relating the volume stored in the sewer to a linear combination of the inflow and outflow. It represents the time shift and the damping of the sewer network. This simplified models is hardly ever used now, since the growth of the computer calculation speed allows to use systematically the Barre-Saint-Venant equations.

   (b) **Barre-Saint-Venant equations :** Flow calculations in the sewer pipes are carried out using Barre-Saint-Venant equations; one reflects the conservation of mass and the other one is a dynamic equation expressing conservation of momentum also called the fundamental law of mechanics. Head losses in the pipe are estimated using a roughness coefficient that depends on the nature of the pipe. This coefficient is indicated in the model for each pipe (Manning coefficient).

   Barre-Saint-Venant equations are solved following the Preissmann scheme using an implicit finite difference method with discretisation in space and time. The values of the time and space steps can be set up by the user (Insa-Valor (1999)).

3.1.4.2 CANOE implementation

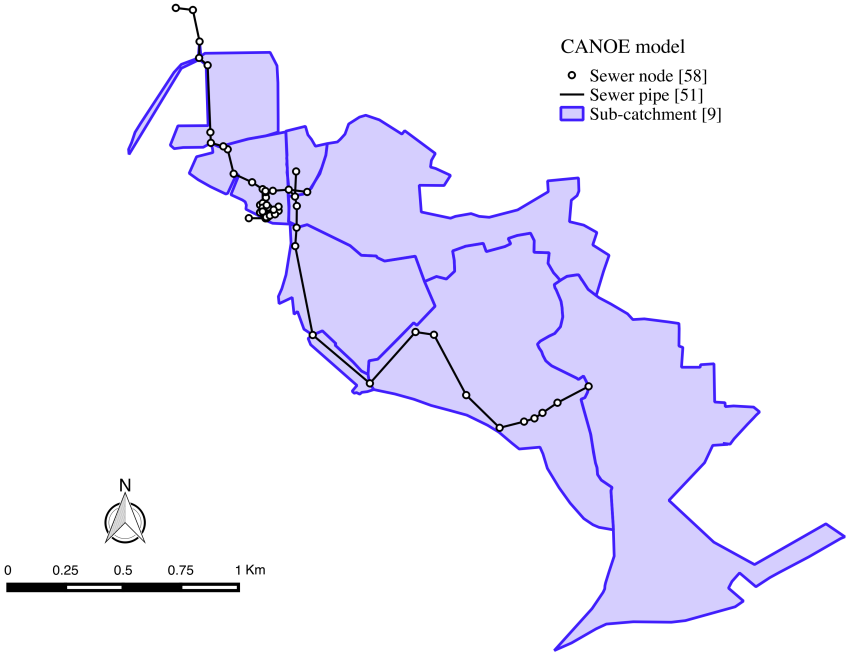

Figure 3.8: CANOE model implemented for Sucy-en-Brie catchment. It consists of 9 sub-catchments and 51 sewer pipes

CANOE model was implemented for Sucy-en-Brie case study by the CD94 (County Council of Val-de-Marne) and made available for this work. The catchment (Figure 3.8) was divided to 9 sub-catchments with size ranging from 1 ha to 76 ha. Their imperviousness coefficient ranges between 30% and 60%. Only a part of the pluvial sewer system is modeled, it consists of 58 nodes and 51 elements of pipe representing a total length about 4 km and having a mean slope about 0.0116 m/m. Main characteristics of each sub-catchment are presented in Table 3.1.

Sub-catchment	Area (ha)	S (m/m)	C_{imp}	CS_1	Lag time (min)	P_i (mm)
1	76.44	0.00225	35%	15%	37	2
2	43.88	0.03155	32%	15%	15	0.5
3	59.05	0.00756	30%	18%	27	2
4	24.79	0.00575	35%	15%	22	2
5	2.32	0.09253	35%	15%	4	0.5
6	3.74	0.00720	35%	15%	9	2
7	10.66	0.00279	60%	35%	12	2
8	13.07	0.00299	30%	15%	43	0
9	1.08	0.00055	40%	20%	38	2

Table 3.1: Main characteristics of sub-catchments considered in CANOE model. C_{imp}, P_i, and S represent respectively the imperviousness coefficient, the initial losses for impervious surfaces and the average slope.

In term of models used for the rainfall-runoff transformation, the second and the third sub-catchments are considered as mixed areas (urban + rural) and therefore Horton model was set up as the production function for these two sub-catchments with a constant of time $k = 1$, initial infiltration rate $f_0 = 40$ mm/h, final infiltration rate $f_c = 10$ mm/h and the initial losses P_i is equal to 2 mm and 6 mm respectively for the second and the third sub-catchment. The other sub-catchments are considered as urban areas and modeled using the standard model as the production function. Parameters α, β and γ of the runoff coefficient C_R used in the standard CANOE model ware calibrated using real flow measurements and were set up as follow:

low rain ($\leq$ 20 mm)			medium rain ($\leq$ 22 mm)			strong rain ($\geq$ 22 mm)		
α	β	γ	α	β	γ	α	β	γ
85	40	5	90	80	20	95	90	40

Table 3.2: Parameters α, β and γ of the runoff coefficient C_R set up for standard CANOE model

3.1.4.3 CANOE model refinement

One of the purposes of this work is to investigate improvements that should be implemented on urban storm models in such a way to increase their ability to consider the available small scale rainfall information measured by X-band radars. The current CANOE model configuration presented above and used by the CD94 for modeling applications includes sub-catchments with large size. This choice is fully appropriate and meets the CD94 requirements in terms of modeling; it is also coherent with the spatial variability of the rainfall data available. In fact the CD94 engineers rely often on point measurement rainfall data provided by rain gauges or on radar data provided by the forecasting system CALAMAR which is 1 km^2 resolution. Indeed, the small size of the catchment makes that it is only covered by 9 radar pixels (3*3 km^2) which is so far from presenting any spatial variability of rainfall structure.

However the use of high resolution rainfall data provided by the new ENPC X-band polarimetric radar with this model configuration may have a very limited effect on the model response since the latter considers the average of rainfall information over each sub-catchment. This is why we decided to improve the CANOE model resolution and to consider smaller sub-catchments. This choice was furthermore motivated by the availability of a large set of data including data describing the whole pluvial drainage system and the land cover of Sucy-en-Brie catchment (Figure 3.9).

It is important to note that it was not within the scope of this work to improve the performance of CANOE model that will be discussed during the validation step. The main objective of this refinement process is to increase the ability of CANOE model to take into account small scale rainfall information.

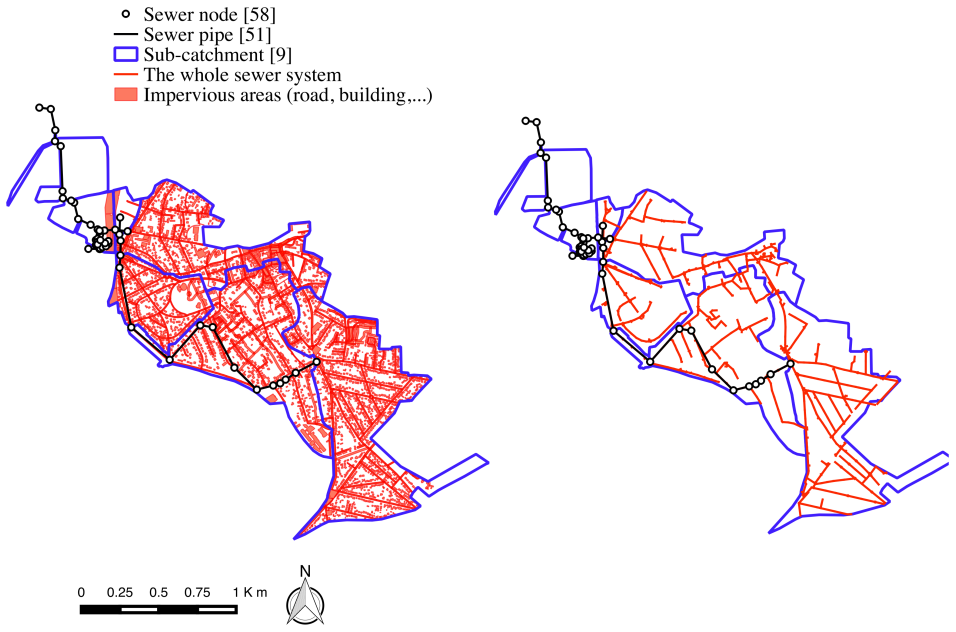

Figure 3.9: Data available for the refinement of CANOE model; the whole pluvial drainage system and a detailed land cover were available

The refinement process was performed following three steps:

1. Delimitation of new sub-catchments was done based primarily on the sewer network and the land use. Each new sub-catchment includes a part of the sewer network which is connected to the sub-catchment outlet.

2. Characteristics of new sub-catchments (surface, outlet point, main water path,..) were determined. The topography was used to estimate the mean slope whereas the imperviousness coefficient was calculated using the land cover (Figure 3.9). For simplification reasons, only roads are assumed to be directly connected to the sewer network, roofs are indeed considered as indirectly connected to the sewer system.

3. A calibration process was performed using a huge data set available to determine new parameters. As a results α, β and γ parameters were set up as follow:

low rain ($\leq$ 20 mm)			medium rain ($\leq$ 22 mm)			strong rain ($\geq$ 22 mm)		
α	β	γ	α	β	γ	α	β	γ
75	27	3	90	80	20	100	100	50

Table 3.3: Parameters α, β and γ of the runoff coefficient C_R set up in the new CANOE-2

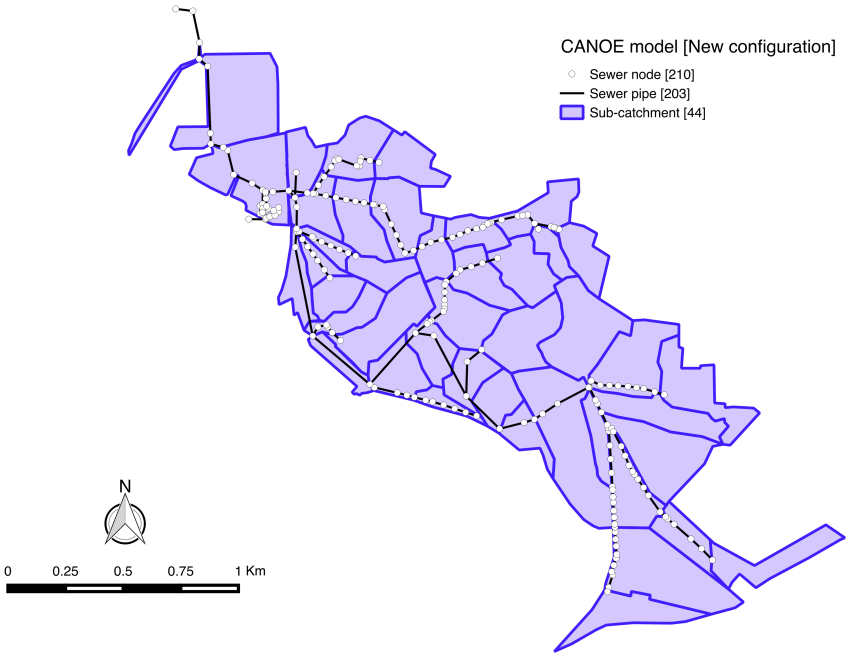

Figure 3.10: The new configuration of CANOE model implemented for Sucy-en-Brie catchment. It consists of 44 sub-catchments and 203 sewer pipes

The new CANOE model configuration consists of 44 sub-catchments instead of only 9. Their size ranges from 1 to 14 ha and 203 elements of pipe representing 9.7 km are considered instead of only 53 pipes representing 4 km in the previous configuration. The two CANOE model configurations will be used for various investigations performed in the framework of this work, and will be denoted CANOE-1 and CANOE-2 respectively.

3.1.5 Validation of urban storm models

The validation of both CANOE and Multi-Hydro models was performed using real flow measurements made available by the CD94. The aim of this part is to address the performance of each model and to perform a first comparison between the two modeling

approaches involved in this work. This validation step is also of extreme importance especially for Multi-Hydro model since its modeling approach is not based on any calibration protocol.

3.1.5.1 Selected rainfall events

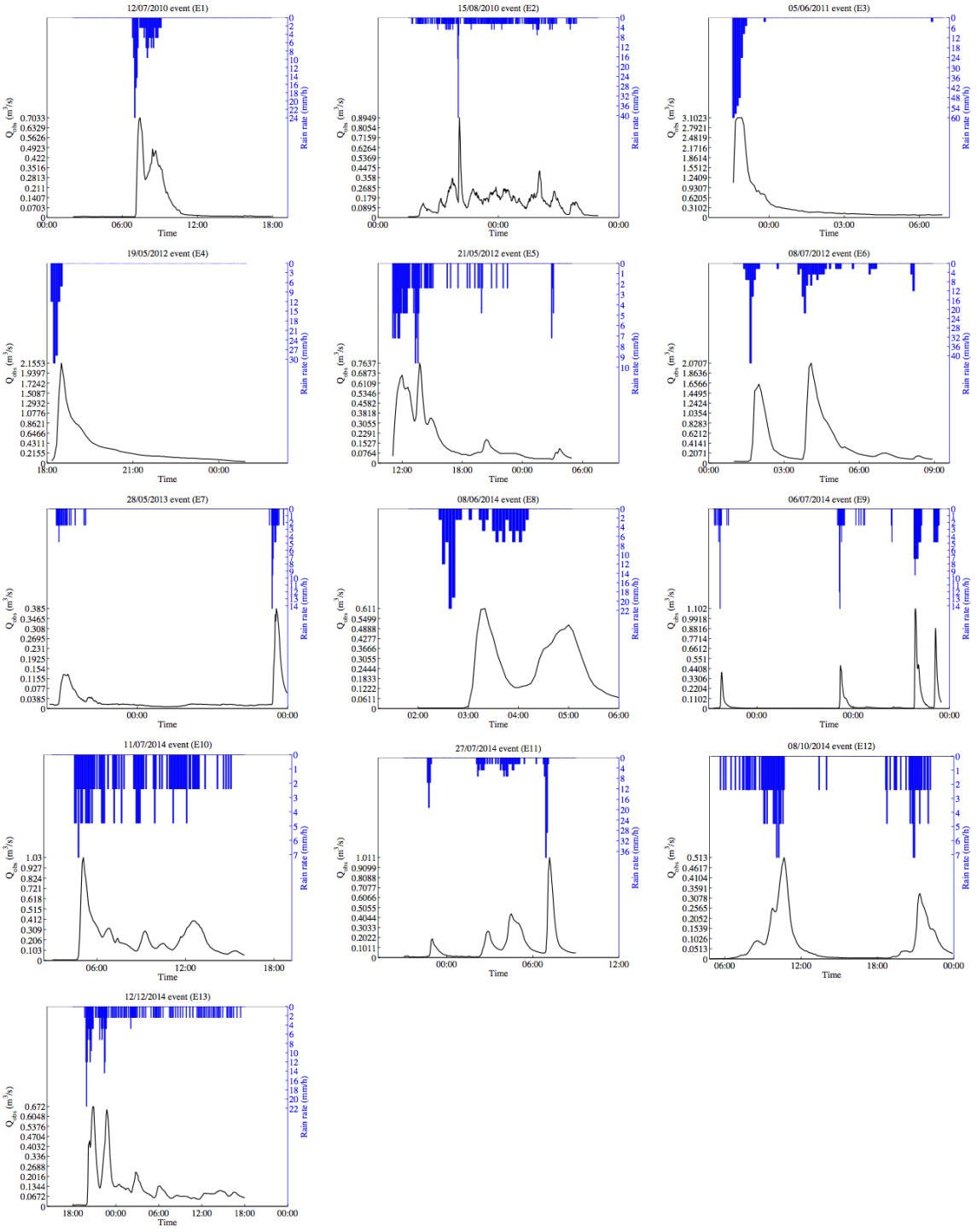

Figure 3.11: Hyetograph and hydrograph for the 13 rainfall events selected to perform the validation of Multi-Hydro and CANOE models

Figure 3.11 represents the 13 rainfall events occurred between 2010 and 2014 selected for the validation of MutiHydro and CANOE models. Their main characteristics and

details are given in Table 3.4. In this step, only rain gauge data coming from the Sucy gauge was available. Radar data will be used later in this work to perform further modeling analysis. The corresponding observed flow was sensed by the Sucy-171 flow sensor, located upstream of the entrance to the retention basin. So only one point measurement was available and no measurement campaign was carried out to collect distributed data in various points of the sewer system.

Event	Date	Duration	I^{max} (mm/h)	P (mm)	Q^{obs} (m^3/s)
1	12/07/2010	15h55'	24.0	14.2	0.7033
2	15/08/2010	38h	40.8	54.6	0.8949
3	05/06/2011	8h25'	60.0	21.8	3.1023
4	19/05/2012	6h50'	31.2	7.6	2.1553
5	21/05/2012	17h55'	9.6	19.2	0.7637
6	08/07/2012	8h	43.2	19.2	2.0707
7	28/05/2013	38h	14.4	10.4	0.3850
8	08/06/2014	4h5'	21.6	11.4	0.6110
9	06/07/2014	57h5'	14.4	27.2	1.1020
10	11/07/2014	13h5'	7.2	19.8	1.0300
11	27/07/2014	12h5'	38.4	19.8	1.0110
12	08/10/2014	19h	7.2	17.8	0.5130
13	12/12/2014	24h5'	21.6	33.2	0.6720

Table 3.4: Main characteristics of the 13 rainfall events selected for the validation of Multi-Hydro and CANOE models. I^{max} (mm/h) is the maximum rainfall intensity, P is the total rainfall depth (mm) and Q^{obs} (m^3/s) is the maximum observed flow at the outlet of the drainage system.

It is important to note that no selection criterion was used for the selection of these rainfall events. Moreover, no distinction between event types in terms of intensity or spatial pattern was set in this work. The main aim was to perform a first validation step, especially for MutiHydro model newly implemented and not calibrated as well as the new configuration of CANOE model. Such validation is important and will allow the use of both models to perform more modeling works and analysis.

3.1.5.2 Methodology

The validation of hydrological models has been a point of interest of various research studies over the years (Khakbaz et al. (2012), Refsgaard (1997), Bennett et al. (2013), Biondi et al. (2012)). Their aim was to investigate a universal strategy that can be applied for the validation of urban models and to define parameters that can be used to address performance of models with respect to flow measurements.

Biondi et al. (2012), Bennett et al. (2013) proposed both a validation protocol of hydrological models, that relies first of all on a better knowledge of the modeling approach involved. The use of a large input data with different characteristics is desired (i,e different rainfall events including low, medium and severe events. If available the use of different rainfall sources (point measurements and radar gridded data) is advisable), the identification of sources of uncertainties and finally the use of graphical techniques and metric parameters to asses and discuss the model performance.

Generally, model evaluation is performed in two manners: (1) graphical techniques evaluation remain the first step in any validation process. They are based in most cases on a graphic comparison of observed and simulated data. This allows a quick and efficient inspection of the model results, a verification of the obtained temporal dynamic and the identification of possible sources of errors. (2) Performance evaluation can be performed using a set of parameters carefully identified based on the desired modeling goal. They are often based on squared deviations to quantify performance from different points of view: (i) the correlation coefficient is usually used to analyze the hydrodynamic of the model,(ii) the coefficient of determination R^2 is used in urban hydrology to assess the quality of the model fit with respect to observed data. (iii) Additional parameters are used to quantify specific errors in simulated data (i,e errors in the peak flow (δr) or in the total volume (δV)). A review of these parameters can be found in (Biondi et al. (2012), Bennett et al. (2013)).

As previously discussed, the quantification of uncertainties is of crucial interest in urban hydrology and should be a part of any validation protocol. Several sources of uncertainties were reported in the literature: they are related to the model formulation itself or to the data used for the calibration and validation steps (Butts et al. (2004), Rochester (2010), Surfleet and Tullos (2013), Bastola et al. (2011), Lee et al., Knoche et al. (2014),

Li et al. (2010), Hossain et al. (2004), Stransky et al. (2007a), Wu et al. (2014), Villarini and Krajewski (2010), Deletic et al. (2012), McMillan et al. (2012), Stransky et al. (2007b)).

1. *Uncertainty related to the model parameters :* the estimation of hydrological model parameters is the most important step during the model implementation. It is a very complex and time consuming task, that may require huge investigations whether on input data or on site for direct measurements. Uncertainty related to model parameters can be estimated in the framework of a sensitivity analysis. However, this uncertainty often remains and urban models usually rely on calibration protocol to minimize it.

   Sensitivity of hydrological models to the fluctuation of their parameters depends mainly on the modeling approach involved. In CANOE model, an estimation of the ratio of each type of surface (permeable, impervious directly connected and impervious indirectly connected to the sewer network) is of crucial interest because the runoff coefficient (Equation 3.4) depends on such estimations. However, an accurate estimation is impossible and Equation 3.4 parameters α, β and γ should be calibrated using real flow measurements.

   For physical based model, the problem related to parameters estimation is different. In fact, these models rely on physical equations that involve physical properties. Such parameters were widely analyzed and defined for each type of soil (Rawls et al. (1983)). In this work all physical parameters used in Multi-Hydro were estimated from the literature and no real site measurements were done. Calibration is not performed for Multi-Hydro model, for which the classical calibration approach that consists in forcing the model to reproduce observed data as accurate as possible by changing its parameters cannot be applied here. In fact gridded based model performance are highly dependent on the spatial scale of the model. So taking into account the high scale dependency of urban catchment patterns can improve the model performance. This point will be investigated in more details later in this work.

2. *Uncertainties related to rainfall :* uncertainties related to rainfall were well discussed in the literature and many studies demonstrate that rainfall uncertainties remain and propagate in the model outputs (Lee et al., Hossain et al. (2004),

Stransky et al. (2007a,b)). Uncertainties due to rainfall can have two sources; (1) uncertainties in rainfall measurements themselves and (2) uncertainties due to the way the model consider rainfall information (sub-catchment based model usually consider an average of the rainfall information at the sub-catchment scale). The first point was discussed in the previous chapter while the second one will be investigated later in this chapter in the framework of a sensitivity analysis of Multi-Hydro and CANOE models to rainfall spatio-temporal variability. Such investigations was already performed by Gires et al. (2015) using downscaled radar data.

In this validation step, performance of urban storm models will be analyzed using four parameters estimated based on observed Q_{obs} and modeled flow Q_{mod} time series :

- **Nash criterion :** Nash-Sutcliffe efficiency coefficient *NSE* (Equation 3.9) is the most used parameters in urban hydrology to quantify performance of urban models. It is also widely used for model validation and calibration. *NSE* measures how well the model describes the variance in the observations in comparison with a model that only uses the mean of the observed data. *NSE* values range from $-\infty$ to $+1$. A value of 1 indicates a perfect model, while a value of zero indicates performance no better than simply using the mean. A negative value indicates even worse performance than using just the mean. The efficiency of Nash criterion was discussed in the literature, and many attempts were conducted in order to improve the *NSE* coefficient (Gupta et al. (2009)).

$$NSE = 1 - \frac{\sum_{t=0}^{n}(Q_{obs}^{t} - Q_{mod}^{t})^2}{\sum_{t=0}^{n}(Q_{obs}^{t} - \bar{Q}_{obs}^{t})^2} \tag{3.9}$$

- **Correlation coefficient :** The correlation coefficient r (Equation 3.10) measures the strength and the direction of the linear relationship between the model output and the observed data, r values range from -1 to $+1$, positive value of r indicates that the two time series describe the same dynamic (they increase and decrease at the same moment). A correlation greater than 0.8 is generally described as strong, whereas a correlation less than 0.5 is generally described as weak.

$$r = Cor(Q_{mod}, Q_{obs}) = \frac{cov(Q_{mod}, Q_{obs})}{\sigma_{mod}.\sigma_{obs}} \tag{3.10}$$

- **The Volume error (δV) and the relative peak flow error (δr) :** The volume error δV (Equation 3.11) is used here to set the error between the simulated and the observed flow in terms of the total volume. The relative error δr (Equation 3.12) will assess error observed in the peak flow between modeled and observed data.

$$\delta V = \frac{\sum_{t=0}^{n} Q_{mod}^{t} - \sum_{t=0}^{n} Q_{obs}^{t}}{\sum_{t=0}^{n} Q_{obs}^{t}} \tag{3.11}$$

$$\delta r = \frac{Q_{mod}^{max} - Q_{obs}^{max}}{Q_{obs}^{max}} \tag{3.12}$$

3.1.5.3 Results and discussions

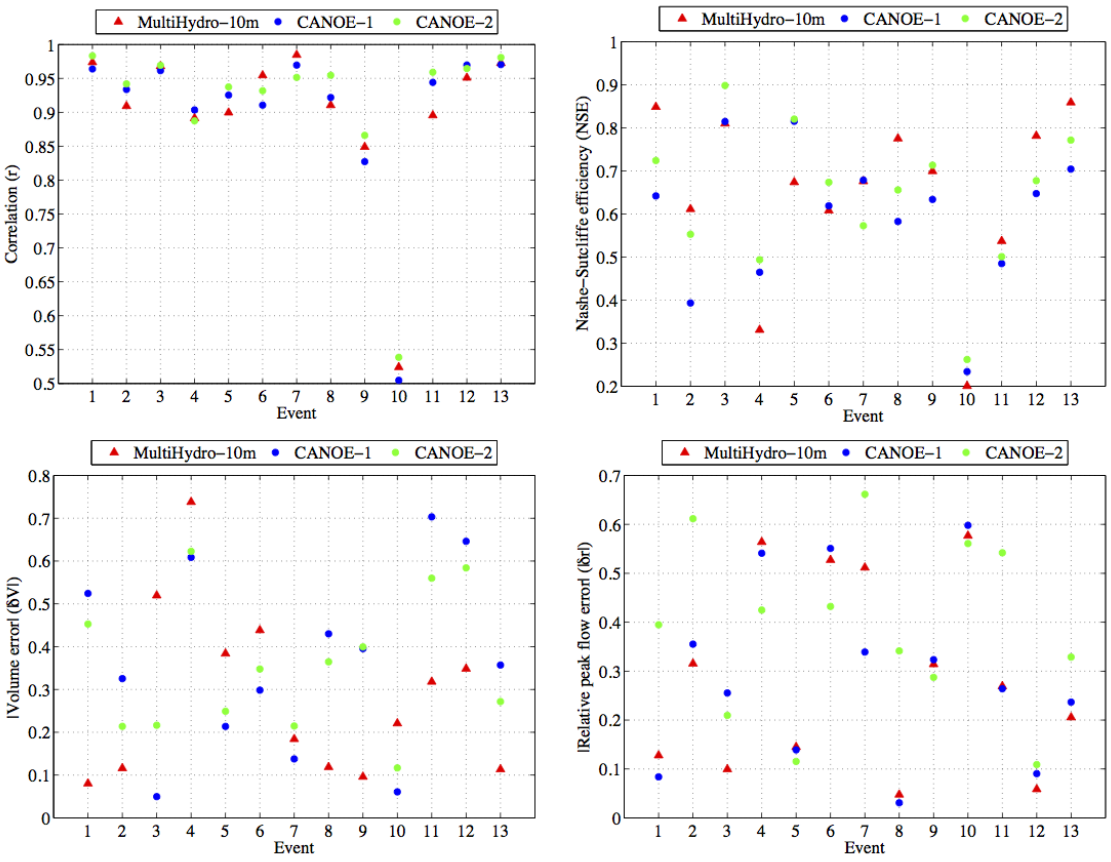

Figure 3.12: Performance analysis of Multi-Hydro, CANOE-1 and CANOE-2 models; the correlation coefficient r was computed as well as NSE coefficient, the volume error δV and the relative error in the peak flow δr.

In Figure 3.13 are compared modeled and observed data for the 13 rainfall events selected (black line represents the observed flow while red, blue and green ones represent Multi-Hydro, CANOE-1 and CANOE-2 modeled flow respectively).

One can notice, that the observed flow dynamic is in general well reproduced by both CANOE and Multi-Hydro models; peaks flow occur at the exact time except for E4, E6 and E10 events. Small and highly variable flow dynamic observed in the E2, E10 and E13 events are reproduced in a good manner as well. However, results show that the magnitude observed at the peak flow is not too accurate with respect to measurements, especially in the case of CANOE-2 model. This is probably related to the calibration issues of the new configuration.

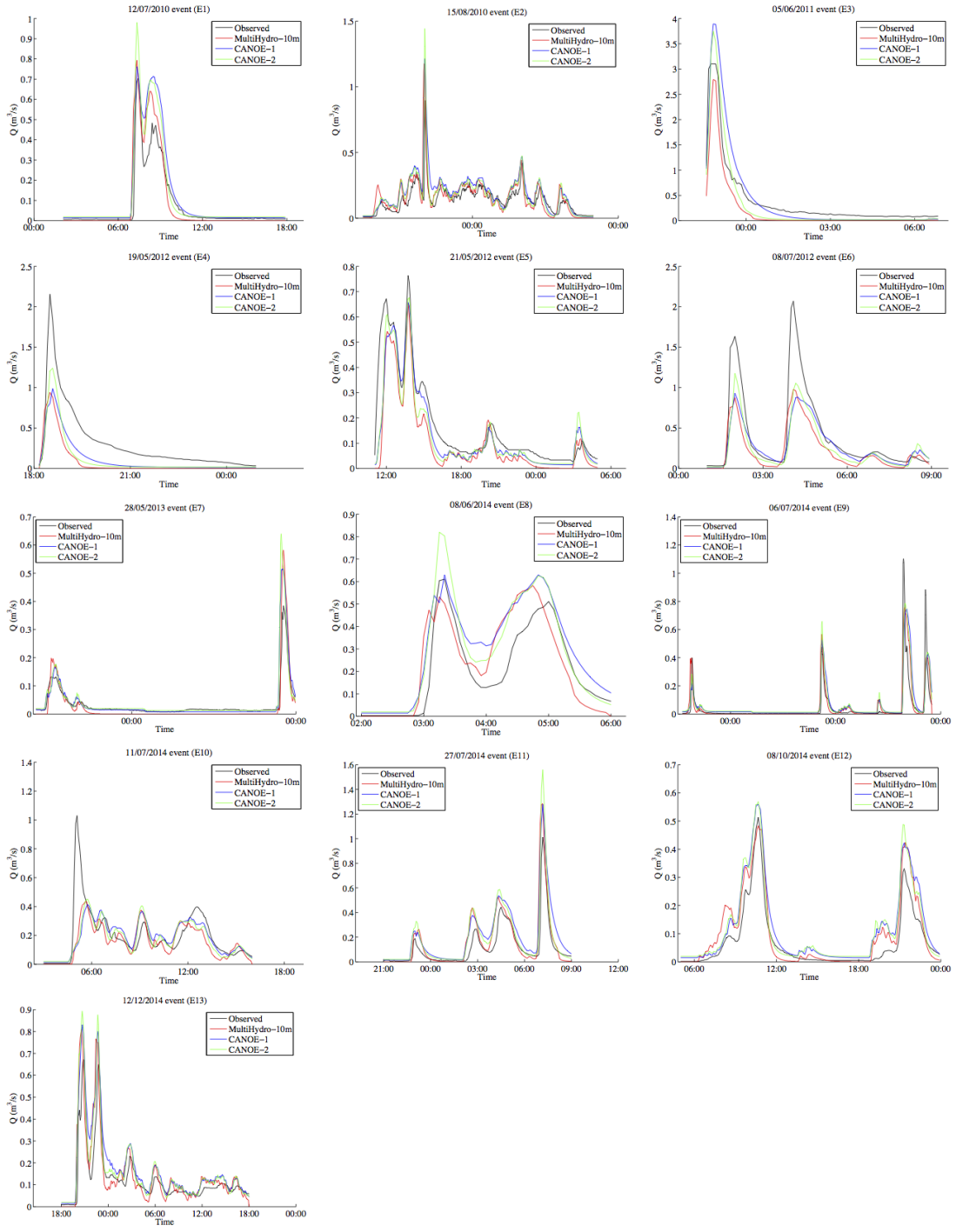

Figure 3.13: Simulated flows obtained are plotted as well as the corresponding observations; black line represent the observed flow while red, blue and green ones represent Multi-Hydro, CANOE-1 and CANOE-2 modeled flow respectively

The underestimation of peaks flow observed in the E4, E6 and E10 events is certainly due rainfall measurement issue. In fact, only point measurement data was involved in this work which explain the difference observed here.

The last observation that should be made, concerns the base flow observed in the modeled data. In fact Multi-Hydro tends to decrease rapidly compared to CANOE model, and its base flow is null while it is 0.0145 m^3/s in case of CANOE model. This flow corresponds to the leakage rate due to bad connections observed in the pluvial drainage network (people connect their waste water system to the pluvial drainage network instead of the sewer network) and it is not considered in Multi-Hydro model. This point should be improved in future version of the model.

Figure 3.12 shows performance analysis of models with respect to flow measurements. As expected, the correlation coefficient is higher except for the E10 event indicating that the modeled flow dynamic is in a good agreement with the observed one. If we do not consider the E10 event, r averages are 0.93, 0.93 and 0.94 respectively for Multi-Hydro, CANOE-1 and CANOE-2 models.

NSE performance indicator shows a better performance for Multi-Hydro model, *NSE* retrieved means are 0.65, 0.59 and 0.64 respectively for Multi-Hydro, CANOE-1 and CANOE-2 models. However when not considering the E4, E6 and E10 events, *NSE* means are improved to 0.73, 0.64 and 0.69 respectively. High values of *NSE* are observed for the E3, E5 and the E13 events.

One can notice also the slight improvement noticed between CANOE-1 and CANOE-2 performance, but difficult to relate this improvement to the refinement of CANOE model resolution. In fact the calibration protocol applied after the refinement process makes it difficult to relate improvements on CANOE model performance to the improved model spatial resolution.

In terms of the ability to reproduce the peak flows, the mean of $|\delta r|$ is 21% for Multi-Hydro and CANOE-1 models while it is 0.35 for CANOE-2 model. The new configuration of CANOE model is clearly overestimating peaks flow between 0.10 and 0.70 noticed for the E7 event whereas Multi-Hydro model underestimates peaks flow between 0.5 and 0.30 observed for the E9 event, and sometimes overestimates the peaks flow between 0.10 and 0.50.

In terms of the total volume error, the mean of $|\delta V|$ is 0.23, 0.38 and 0.35 respectively for Multi-Hydro, CANOE-1 and CANOE-2 models. A part of this volume error noticed in Multi-Hydro model is due to the fact that leakage flows are not considered in the current version of the model.

It is important to note that Multi-Hydro was implemented and validated in this work at 10 m spatial scale. The configuration of the model at this scale shows an impervious

coefficient about 37% which is coherent with what is estimated from the GIS data and CANOE model. However Figure 3.14 shows a high sensitivity of the model response to the spatial scale [100 m, 5 m]. Indeed, it will be important to analyze how the performance of the model changes when changing the model spatial scale. This point will be investigated in the next section from two points of view; (i) first of all, scale dependency observed within input data will be highlighted using fractal tools, then (ii) huge multi-scale modeling investigations will be performed and Multi-Hydro response will be analyzed at various spatial scales ranging from 100 m to 5 m.

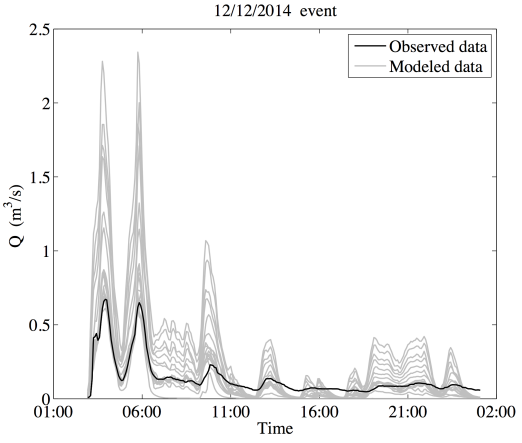

Figure 3.14: Sensitivity of Multi-Hydro model hydrological response to the spatial resolution of the model [100 m, 5 m]

3.2 Scale dependency in urban hydrology

The effect of scaling still remains a serious issue in urban hydrology especially for fully distributed and gridded based models. The choice of an appropriate spatial resolution is a crucial problem, and the obtained model performance depends highly on the chosen implementation scale. The appropriate spatial resolution is obviously linked to the quality of data available, their spatial resolution and the modeling goal (Dehotin and Braud (2008)). Very few works were reported in the literature Dehotin and Braud (2008), Hardy et al. (1999), Ostrowski (2002) about scaling effects in urban hydrology, much less are based on real modeling investigations of scaling effects on models performance. The scale dependency observed in urban areas, is first of all due to the high heterogeneity observed in such areas, scaling effects are much more important in urban areas than rural ones. They are the consequences of the high heterogeneity observed in all

geophysical factors such as topography and land use. The impact of scale dependency on modeling outputs depends mainly on the modeling approach involved. In fact, semi-distributed models and in general conceptual based models are not affected by scaling effects, parameters used in such models are usually calibrated and considered as uniform at sub-catchment scale. On the contrary, fully distributed and physically based models are based mainly on a full consideration of the catchment heterogeneity. Such models show more flexibility on changing the implementation scale, depending on the availability of the data and its quality.

In this work, we propose to investigate scaling issues in urban hydrology modeling. The investigation will be performed in two steps: in the first part, fractal tools will be used to characterize the scale dependency observed within GIS data used as input for urban storm models. Then multi-scale modeling investigations will be carried out using Multi-Hydro model to analyze the effect of this scale dependency on model performance. To achieve this investigation, huge works were conducted to implement Multi-Hydro model at a wide range of scales from 100 m to 5 m.

3.2.1 Demonstration of scaling of urban catchment

The first stage of this work is to investigate and identify the scale dependency in GIS data used as input for urban modeling by computing its fractal dimension. In fact the complexity of urban sewer systems and the extreme variability of urban land use make that urban environments can be described with fractal geometry. Fractal tools (Section 2.3.1) are widely used in several science domains including geology, medicine, meteorology and finance. In hydrology, the fractal dimension concept has been used in many studies in the past for the various purposes (Gires et al. (2014a), Mesev et al. (1995), Use, Wu et al. (2013), Thibault and Crews (1995), Frankhauser (1998), Wu and He (2009), Sagar (2004), Jiang et al. (2012), Gires et al. (2013), Radziejewski and Kundzewicz (1997)).

In this work, the structure of the urban storm system, the distribution of impervious land use pixels as well as the distribution of gully surface points will be analyzed using fractal concept. Results of this fractal analysis will clearly highlight the scale dependency of urban catchment patterns, it should also increase our understanding of how gridded based urban storm models consider the high heterogeneity of urban catchments. Impacts

of this scale dependency on urban storm models outputs will be investigated later as well in the framework of a multi-scale modeling performance evaluation.

1. **Fractal dimension of urban sewer network :** Two areas have been selected to perform the fractal analysis for the storm system. The purpose of these selection is to minimize the effect of no data pixels by considering two well covered square areas for which the size is a power of 2. Figure 3.15 shows the 2 m pixel size original data available and the two selected zones. The small area is a 512 m size (l_0=512 m) and the bigger one is a 1024 m. In practice the data in these areas will be presented using different pixel sizes l starting from 2 m and multiplying the size by 2 at each step.

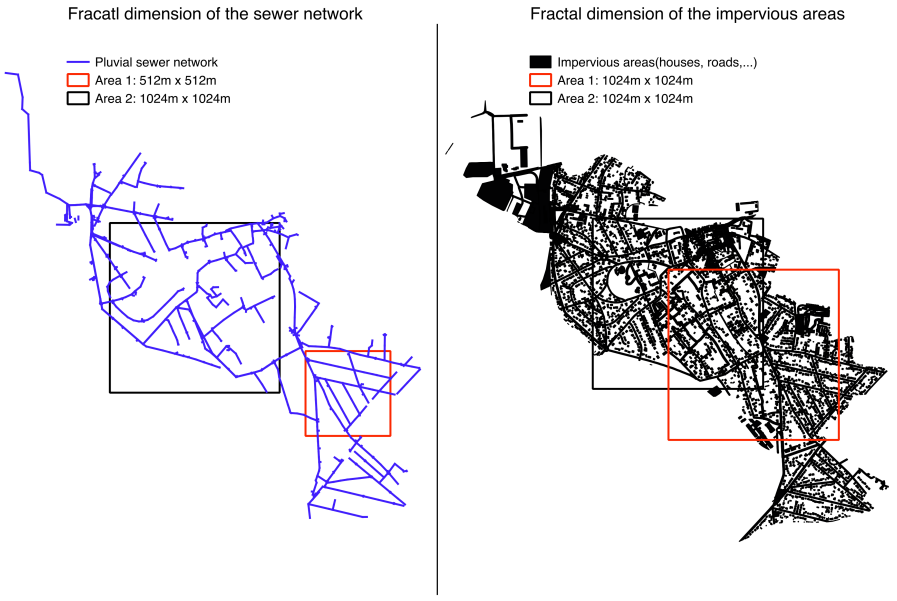

Figure 3.15: The original 2 m pixel size data used to perform the fractal analysis of the sewer system and impervious areas, two well covered areas were selected.

Figure 3.16 gives results obtained when plotting in a log-log plot the number of pixel N_λ needed at a given resolution λ to cover the storm network data as a function of λ. Results show a clear respect of the Equation 2.11 at two ranges of scale; indeed two scaling regimes should be considered with a clear break noticed at $\approx$ 64 m. For small scales [2 m, 64 m], the fractal dimension D_f is almost equal to 1 indicating the linear behavior of the sewer pipes structure observed at small scales. For large scales $l \geq$ 64 m the fractal dimension D_f is higher than 1.8 (1.82 for area 1 and 1.88 for area 2) suggesting that the pluvial network structure occupies almost

the whole 2D space. Thus it becomes difficult at large scales to identify the whole sewer structure (pipes, nodes,...). These results confirm similar conclusions of a multi-catchment work performed in the framework of RainGain project about fractal analysis of environments data of 5 pilot sites located in Europe. The break at 64 m was related according to this study to the distance between two roads in urban areas.

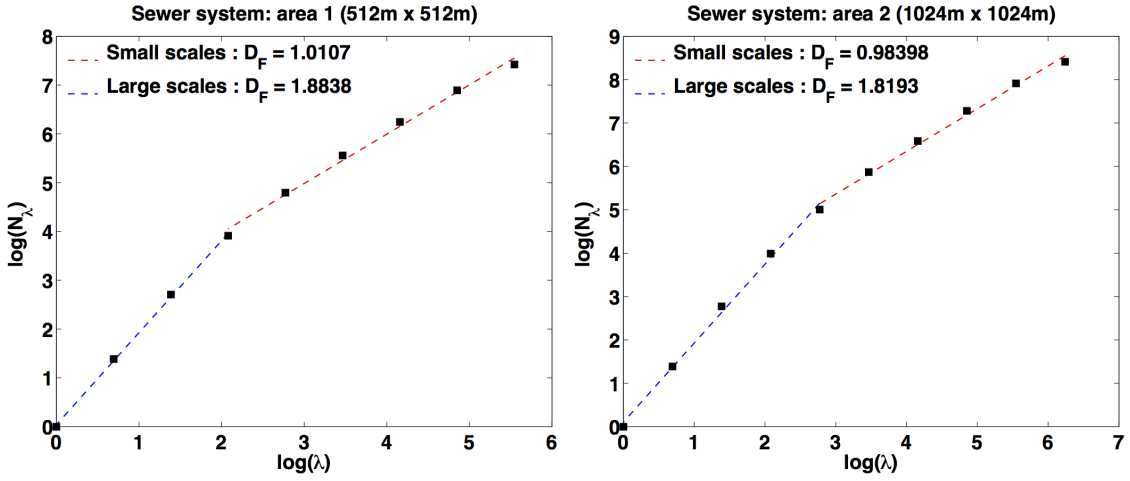

(a) (b)

Figure 3.16: Fractal analysis of the sewer structure. Two ranges of scale are identified on both areas; D_f is equal to 1 at small scales [2 m, 64 m] and 1.8 for large scales $l \geq 64$ m

2. **Fractal dimension of impervious areas :**

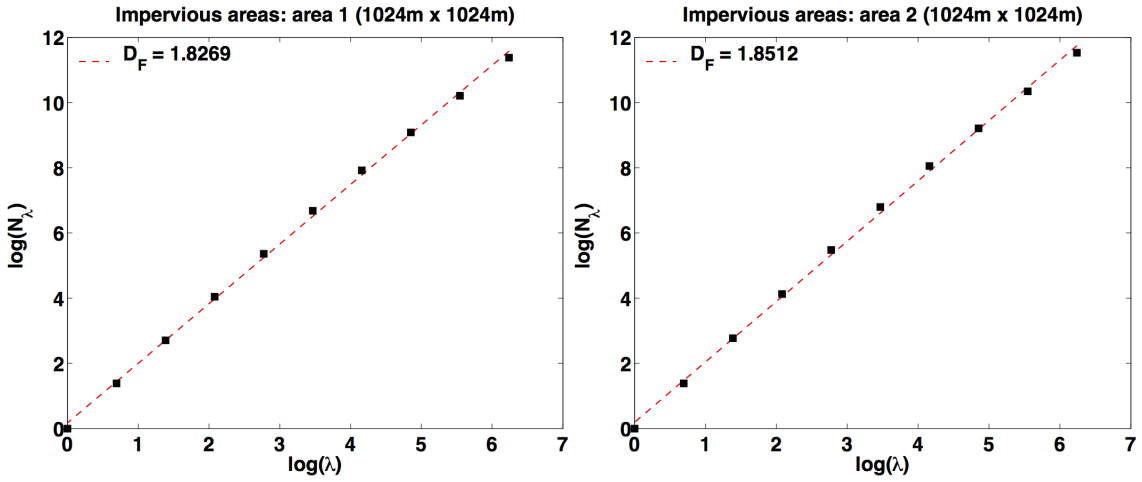

(a) (b)

Figure 3.17: Fractal analysis of the impervious data. one unique scaling regime is identified at the whole range of scale available [2 m, 1024 m]; D_f is greater than 1.8 for both areas.

For impervious data (Figure 3.15), two 1024 m size square areas were selected to perform the fractal analysis. Figure 3.17 shows results obtained. Indeed, both areas exhibit a clear and unique scaling regime at the whole range of scale available [2 m, 1024 m]. The fractal dimension D_f computed is greater than 1.82 (1.82 for Area 1 and 1.85 for Area 2) which is coherent with what was found for similar urban areas in Europe. Results obtained here are of extreme importance, they show clearly the high scale dependence of urban catchment patterns, such dependency will have significant effects on the catchment behavior and modeling outputs. Indeed, the imperviousness coefficient C_{imp} of the catchment (defined as the ratio between impervious surface and the total surface) depends highly on the spatial scale at which the model is implemented indicating that the model output will shows high scale dependency as well.

3. **Fractal dimension of gully network**

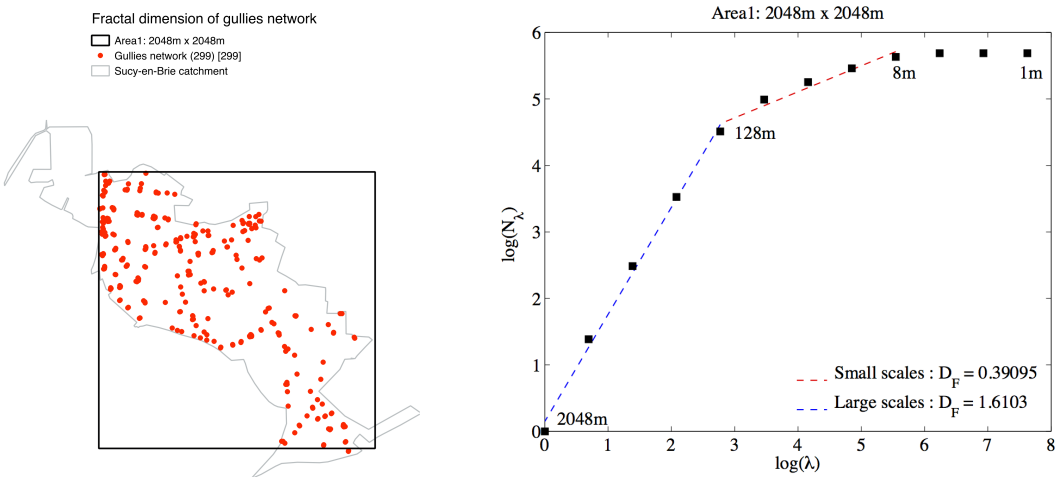

Figure 3.18: Fractal analysis of storm sewer inlet points network.

A significant advantage of gridded based model is their ability to consider the whole available sewer network, instead of only modeling a part as it is done by semi-distributed models. In the case of Multi-Hydro model, inlet points are the only connection available between the surface and the drainage module. So keeping the distribution of all these points whatever the spatial scale of the model is very important but unfortunately not possible due to the dense gully network available. In fact, the number of inlet points considered decreases as shown in Figure 3.18. Indeed, 292 gullies are considered at 2 m resolution while only 272 at 8 m. The

number decreases to 199 at 25 m and to only 113 when using 100 m pixel size. This change my have significant impacts on the hydrological response of the model and should be taken into consideration during modeling investigations.

4. **Effect on the urban catchment behavior :** Previous results show that the urban catchment configuration considered by gridded based models depends highly on the scale at which the model is implemented. In fact, spatial patterns observed in the land cover are quickly changed once we change the observation scale. The impervious coefficient C_{imp} which is widely used in urban hydrology to address hydrological behavior of urban catchments is indeed changing as well. In Figure 3.19 are displayed the distribution of four important land cover classes (Forest, road, grass and house) considered in Multi-Hydro model, as well as the variation of the impervious coefficient C_{imp} as function of the model spatial scale. Several key information emerge from this graph. The first one is that the impervious coefficient is highly sensitive to the model spatial resolution, three ranges of scale can therefore be clearly identified; large scales [100 m, 30 m] at which the impervious coefficient decreases significantly from 55% observed in 100 m to its minimum value of 27% at 30 m, this is due to a huge redistribution of land cover classes. At medium scales [30 m, 10 m], the impervious coefficient increases from 27% to 37% estimated at 10 m. The second important remark is that for small scales [10 m, 5 m], we observe what can be considered as the final configuration of the catchment, the most accurate and closer to the reality on the ground, the impervious coefficient remains stable around 38% which may suggests that the model response will be stable as well at this range of scale.

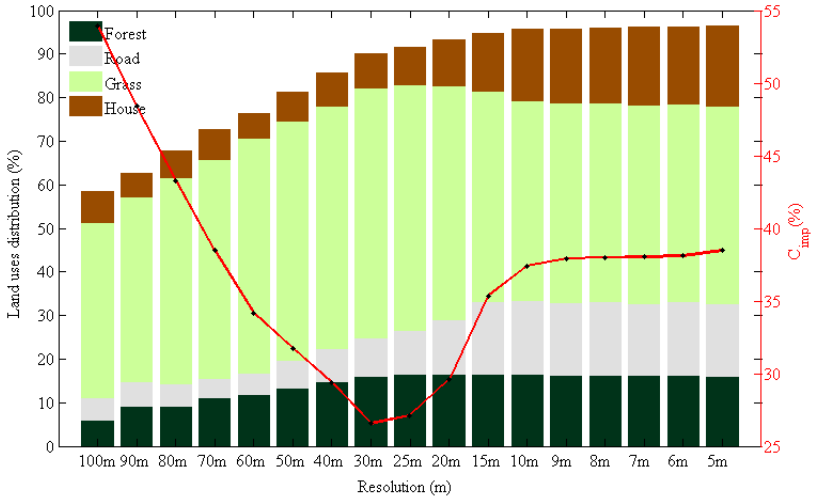

Figure 3.19: Scale dependency observed in the imperviousness coefficient C_{imp}, the distribution of impervious surfaces remain stable for small scales [10 m, 5 m], the white color corresponds to "gully".

In order to carry out the multi-scale modeling analysis, Multi-Hydro model was implemented at 17 spatial scales ranging from 100 m to 5 m. Fractal analysis presented above shows that all input data used for urban models is highly sensitive to the model resolution.

3.2.2 Study of sensitivity of urban storm models to spatial variability of the catchment

3.2.2.1 Selected rainfall events

8 rainfall events (Figure 3.20) that occurred between 2010 and 2014 were selected from the data set used for the validation part (see 3.1.5.1. Please note that only events for which the model shows better performance were selected here.), their main characteristics are summarized in Table 3.5. To avoid the effect of rainfall variability, the choice was made to use only uniform rainfall information provided by rain gauge. The corresponding flow measurement sensed by the flow sensor located upstream the entrance of the retention basin was available as well. Rain gauge data is coming from a tipping bucket rain gauge located at the center of the catchment, the data was available with 5 min time resolution.

Event	Date	Duration	Imax (mm/h)	Total depth (mm)
E1	12/06/2010	22:00 - 07:00 (+1)	19.2	16
E2	12/07/2010	06:00 - 14:00	24	14.2
E3	16/07/2011	19:00 - 05:00 (+1)	9.6	38.6
E4	05/08/2011	07:00 - 19:00	9.6	21.2
E5	21/05/2012	11:00 - 04:00 (+1)	43.2	19.2
E6	08/07/2012	01:00 - 09:00	21.6	11.6
E7	08/10/2014	06:00 - 15:00	21.6	33.2
E8	12/12/2014	18:00 - 18:00 (+1)	14.4	38.6

Table 3.5: Main characteristics of the 8 rainfall events selected to perform the scale dependency investigations

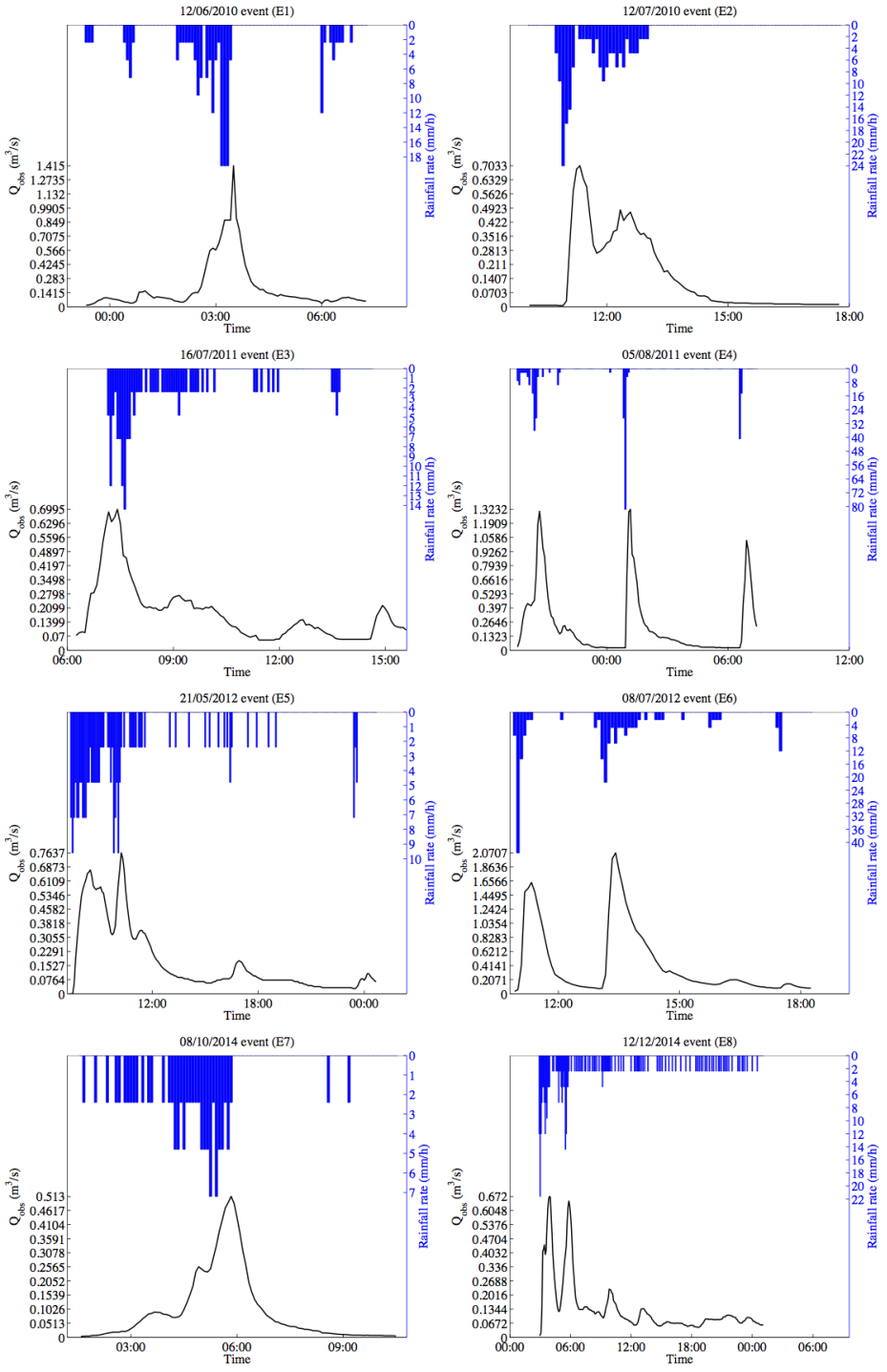

Figure 3.20: Rainfall data and the corresponding flow measurement available for the 8 rainfall events selected to perform the multi-scale modeling investigation.

3.2.2.2 Methodology

The fractal analysis of Multi-Hydro input data presented above, demonstrates how the catchment patterns are dependent on the spatial scale. The model response is therefore

expected to be so.

To address the sensitivity of Multi-Hydro modeling outputs to its spatial scale, the model was implemented at 17 spatial scales ranging from 100 m to 5 m and intensive modeling work was carried out. Results were analyzed with respect to real flow measurements from different points of view using performance indicators presented in Section 3.1.5.2

- **Hydrodynamic evaluation :** it is interesting in a first place to investigate the dynamic of the model and how it can be affected and modified when we change the implementation scale. In fact it is clear from previous results that the distribution of impervious and permeable surfaces is significantly changing every time we change the observed spatial scale leading to an over - or underestimation of water volumes.

  The correlation coefficient r (Equation 3.10) defined in Section 3.1.5.2 will be used to set this dynamic.

  As reported in Bennett et al. (2013), *spectral analysis* is one of the techniques that can be used in urban hydrology to compare the dynamic of modeled and observed data in the frequency domain. Indeed, the power spectrum of simulated flow Q_s time series will be computed as well and compared to the power spectrum of observed flow.

- **Qualitative evaluation :** the model performance and accuracy obtained at each spatial scale will be discussed with respect to observations. Indeed, two parameters will be used to achieve this analysis; (1) *Nash coefficient (NSE)* (Equation 3.9) will be used to set the efficiency of the model at each spatial scale. (2) We used *the coefficient of regression* β (Equation 3.13) to distinguish spatial scales for which the model overestimates and those for which the model underestimates the observed flow, β values range between $-\infty$ and $+\infty$, a value of $\beta = 1$ indicates a perfect match between the observed and simulated flows, if $\beta \leq 1$, then the model is underestimating the observed flow, otherwise it is overestimating the observed flow.

$$\beta = \frac{cov(Q_s, Q_{obs})}{var(Q_{obs})} \tag{3.13}$$

- **Peak flow analysis :** A special focus will be given to peak flows and how they are affected by changes on the model spatial scale. The relative error observed at the peak flow δr (Equation 3.12) will be used for this purpose.

All these parameters will be analyzed and results discussed in the next section, the analysis will help us to identify spatial resolutions for which the model shows good performance with respect to measurements.

3.2.2.3 Results and discussions

1. **General discussions :** For each of the 8 selected rainfall event, 17 simulations were carried out and the corresponding simulated flow time series were retrieved at the pipe located immediately at the upstream of the retention basin, the same point where the observed flow was sensed. Figure 3.21 represents all simulated flows Q_s obtained with Multi-Hydro model at 17 spatial scales involved. The first remark to be noticed from these results is the high sensitivity of the modeling output to the spatial scale of the model, two basic statistics parameters were used to analyze this sensitivity; the mean flow and the range of modeled flow defined as the difference between the maximum and the minimum obtained flow (Q_s) were computed. Considering these results, we can analyze three ranges of scale; large scales [100 m, 40 m] for which the model overestimates greatly the observed flow (for 100 m and 40 m, the mean flow (Q_s) is respectively 234% and 34% higher than the mean observed flow, the range is 281% and 44% respectively higher than what is observed). This result is expected given the distribution of urban surfaces noticed at this range of scale. at medium scales [30 m, 15 m], the model output variability is less important, the mean flow is very close to the observed one (between -2% and +8%), the range remains greater than the observed one (6% to 39% higher), high performance according to these two parameters are obtained at 15 m scale. For small scales [10 m, 5 m], the mean %Bias noticed for the mean flow remains stable between -11% and 23%, whereas the range mean %Bias still important (between 16% and 55%).

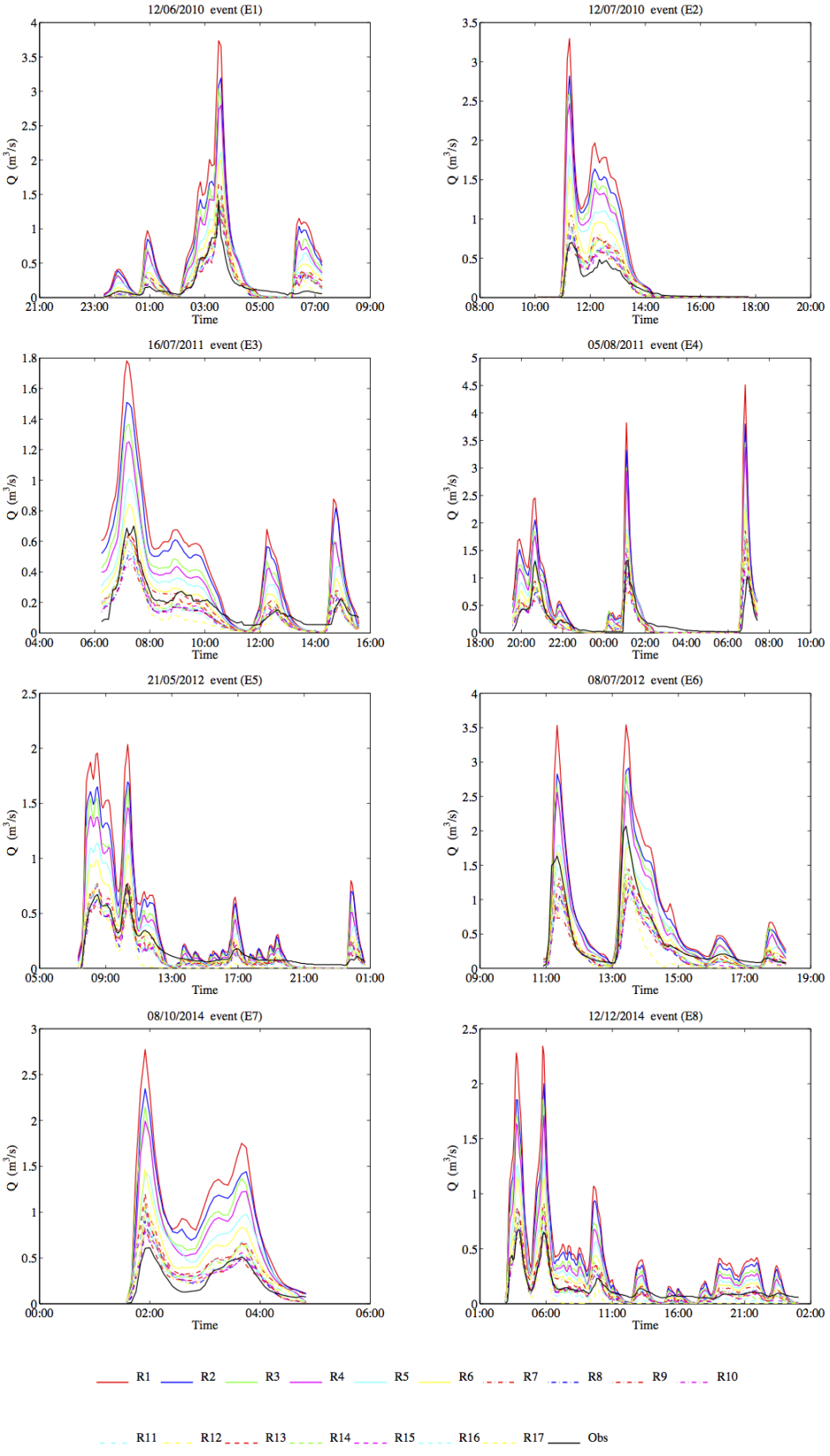

Figure 3.21: Multi-scale modeling outputs compared with observed flow, one can notice the high sensitivity of Multi-Hydro response to the spatial scale of the model.

All Boxes presented in the following sections were processed as follow:

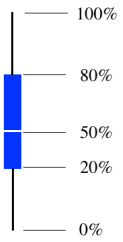

2. **Hydrodynamic evaluation :**

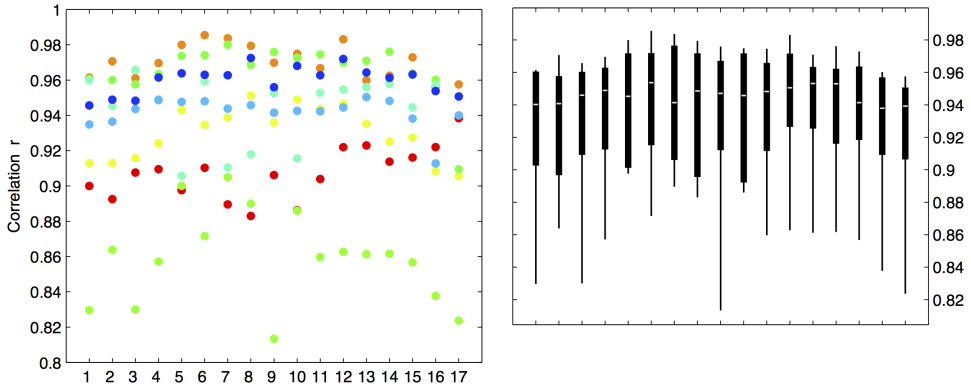

Figure 3.22: Results of model hydrodynamic evaluations; the correlation coefficient r was retrieved for each modeling outputs with respect to real measurements

The hydrodynamic evaluation of modeling outputs is based on the estimation of the correlation indicator r between modeled and observed data. Figure 3.22 shows results obtained. From Figure 3.22, one can notice the high performance of Multi-Hydro model to reproduce the observed flow dynamic at any spatial scale. In fact, *Nash* values range between 0.85 and 0.98 with an average between 0.94 and 0.98 indicating high correlation between modeled and observed data. This trend was also noticed from the graphical comparison (Figure 3.21) between modeling outputs and observed data.

The ability of Multi-Hydro model to reproduce such results demonstrates one of the advantages of physical-based models to reflect correctly the observed flow dynamic. It also indicates that physical parameters used for the implementation of the model are "corrects". The overestimation of the volume is due in fact to an overestimation of impervious areas observed at large scales.

Same conclusions were retrieved from the power spectra analysis of observed and simulated data. In Figure 3.23 are plotted in a log log plot, the power energy

spectrum of modeled and observed data as function of the time frequency. Results confirm the ability of Multi-Hydro model to reproduce the observed flow dynamic even at large scales.

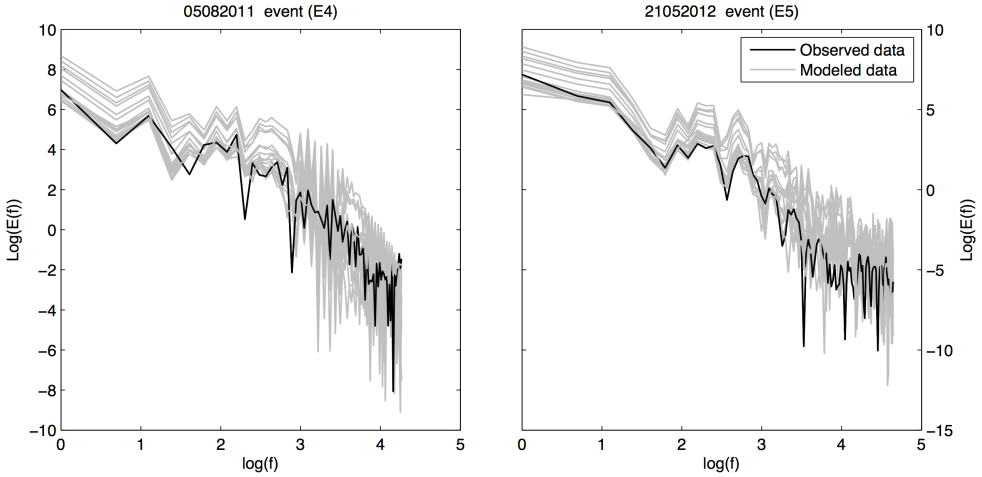

Figure 3.23: Power spectra analysis of modeling outputs; the power energy spectrum of modeled and observed data is plotted in a log log plot as function of the time frequency

3. **Performance evaluation :**

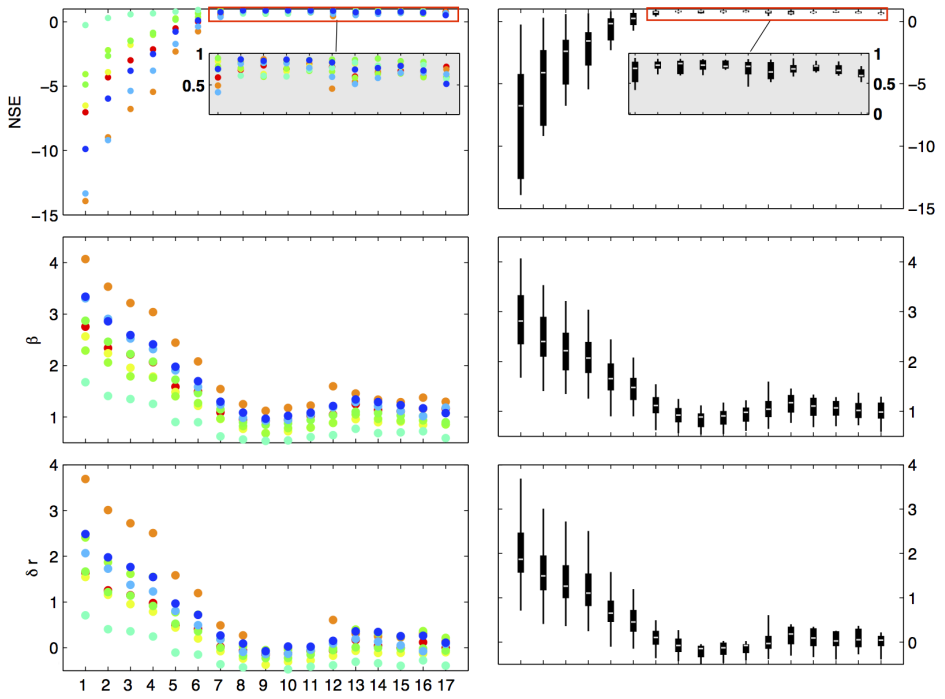

Figure 3.24: Performance indicators *NSE*, β and δr estimated from Multi-Hydro modeling outputs obtained at the 17 spatial scales with respect to observed data.

The multi-scale performance evaluation of Multi-Hydro model outputs is performed using three statistics presented earlier in this work; Nash-Sutcliffe efficiency *NSE*, the coefficient of regression β and the relative error at the peak flow δr. Obtained results are summarized in Figure 3.24. One can notice the high scale dependency of the obtained model performance. In fact all parameters adopt the same trends indicating lower performance at large scales and high performance retrieved at small scales. Model performances are indeed improved as the model resolution increases. From these results, the three ranges of scale previously identified during the fractal analysis (Figure 3.19) are also recognized in Figure 3.24. Consequently, performance evaluation will be analyzed at these three ranges of scale.

Range of scale	Performance indicators (min/max/mean)			
	Correlation	*NSE*	β	δr
[100 m - 40 m]	0.83/0.99	-13.92/0.92	0.62/4.07	-0.36/3.69
	/0.93	/-2.36	/1.99	/1.09
[30 m - 15 m]	0.81/0.98	0.63/0.91	0.54/1.25	-0.31/0.51
	/0.94	/0.79	/0.89	/0.17
[10 m - 5 m]	0.82/0.98	0.44/0.91	0.59/1.60	-0.39/0.61
	/0.93	/0.72	/1.06	/0.19

Table 3.6: Min/Max/Mean of performance indicators (*Correlation*, *NSE*, β and δr) calculated at three ranges of scale ([100 m - 40 m], [30 m - 15 m], [10 m - 5 m])

In Table 3.6 are summarized basic statistics (minimum, maximum and the average) of performance indicators *Correlation*, *NSE*, β and δr calculated at three ranges of scale [100 m - 40 m], [30 m - 15 m] and [10 m - 5 m].

- **At large scales [100 m - 40 m] :** the impervious coefficient C_{imp} of the catchment is very high, it ranges from 45% at 100 m to 30% at 40 m. The model flow obtained at this range of scale exhibits similar dynamic as observed flow. However performance indicators show very weak performances of the model at this range of scale; *NSE* values range from -13.92 observed at 100 m scale to 0.92 observed at 40 m scale, β indicator indicates that the model is highly overestimating observed flow, its values range from 4.07 observed at

100 m scale to a minimum value of 0.62 noticed at 40 m, the average at this range of scale is around 2. In terms of the peak flow analysis, the relative error indicator (δr) shows clear overestimation of the peak flow at this range of scale up to 369%.

All statistic indicators suggest very weak performances of the model at large scales [100 m - 40 m]. In fact, the catchment behavior at this range of scales exhibit high impervious coefficient which means that infiltration is limited and water is routed in majority to the sewer system.

- **At medium scales [30 m - 15 m] :** the model shows its better performances, *NSE* values range between 0.63 and 0.91, with an average around 0.79 demonstrating high performance of Multi-Hydro model. The β indicator takes values between 0.54 and 1.25, its mean is around 0.89 suggesting a good fit between modeled and observed data. The relative error indicator (δr) ranges from -0.31 to 0.51, its mean value is around 0.17. The model still indeed overestimating the peak flow by 17% on average. However, the overestimation of peak flow was already noticed during the validation step of Multi-Hydro model, it was estimated around 21%.
- **At small scales [10 m - 5 m] :** the model performances are just unclear even if they do not vary too much, trends observed at large and medium scales are changed. In fact, Table 3.6 indicates that *NSE* values range between 0.44 and 0.91, its mean value is around 0.72 demonstrating high performance of Multi-Hydro model. The β indicator takes values between 0.59 and 1.6, its mean is around 1.06. The relative error indicator (δr) ranges from -0.39 to 0.61, its mean value is around 0.19. Indeed, slight fluctuations of the model performance are observed at this range of scale and no improvement noticed in the model performance. The model loses even its performance for some rainfall events. These fluctuations observed at this range of scale highlight some specific issues that only take place at this range of scale and influence the model performance.

From the performance evaluation performed here, results noticed at medium scales are surprising because the impervious coefficient is between 27% and 35% noticed at 15 m. However, high performance were retrieved at 15 m scale and were expected to remain stable at small scales as well but starting from 10 m, other issues occur

and changes the model performance. The quality of GIS data is clearly identified as the major problem that only takes place at small scales and leads to fluctuations observed in the model performance at this range of scale.

4. **Specific modeling issues at small scales :** we found it important here to discuss performance of the model in a global framework, especially by taking into consideration some serious problems that one may face when performing high resolution modeling. In fact, as shown in Figure 3.24, previous results show that the model performances are indeed increasing with the spatial scale of the model decreasing, this is due to a better representation of the catchment behavior and the consideration of small scale heterogeneity. However 3 ranges of scales were clearly identified from previous results. At large scales [100 m, 40 m], the model shows a fast computation time (up to few minutes) but lower performances (the model reproduces the same flow dynamic, but the volume is overestimated up to 234%). At medium scales [30 m, 15 m], the model exhibits high performance (Table 3.6) and fast computation time. At small scales [10 m, 5 m] the urban catchment configuration remains unchanged (the impervious coefficient remains around 37%). However model performances at this range of scales are just unclear and some fluctuations of these performances are noticed). Such fluctuations are in fact related to some serious problems that only take place at small scales and should be considered when implementing urban storm models:

   (a) **GIS data quality :** urban hydrological models in general and fully-distributed ones in particular are highly demanding on distributed data for their implementation. A detailed description of the land use occupation is essential as well as distributed topography data. Such data are usually available and can be provided by GIS services. However, its quality is a big issue especially when used to perform high resolution modeling. Two main issues should be detailed here:

   - The spatial resolution of the topography data : the topography is the main driving force for surface water movements and the accuracy of this data has a lot of influence on gridded based models outputs. In our case, the topography data was available at 25 m resolution and interpolation was performed to obtain distributed data at small scales. However, the quality of obtained data below the 25 pixel grid is not fully reliable. The problem is even more striking

in small scale up to 2 m (not included in this work), where the movements of water in the surface were very limited.

- Land use occupation description: the description of the land use is also of extreme importance in urban hydrology and specifically for fully-distributed models. In fact, physical properties defined for each pixel depend exclusively on its land use. Such data are usually available especially after huge improvements noticed in the availability of satellite images and new technologies used in this field. However, one commonly and often faced issue of this data is the portion of unknown data, indicating unidentified land use occupation. This is not related to the data resolution, but depends on the processing of satellite images obtained. For the case of Sucy-en-Brie catchment, land use occupation data was available at very good resolution (25 cm), but the portion of unidentified data was about 20% and was filled in most cases by grass.

At large scales, the problem specific to "no data" pixels has no influence because large pixels size usually include a portion of a road, house,.... But at small scales, the catchment behavior will be affected by the land use attributed to these no data pixels, and the model response will not be the same if the unidentified areas were filled by grass or by impervious soil.

Fluctuation of the model performances observed at very small scales can be in fact related to this two issues that should be therefore considered when implementing hydrological models.

(b) **Numerical instabilities :** Fluctuation of the model performance noticed at small scales can also be the consequence of numerical instabilities. In fact, the numerical scheme used in Multi-Hydro model for the surface modeling calculations is sensitive to small scale variation and have effect on the model response. Further works should be conducted to quantify these instabilities.

(c) **Computation time :** it is important in urban hydrology to consider the computation time needed for a given model to simulate a given rainfall period. It is in fact one of the first criteria considered by urban water managers for the choice of urban storm models. Fast computation time is even crucial in case of models involved in real-time management processes. For fully-distributed models, the computation time depends on two factors; the size of

the catchment and the resolution of the model.

For the case of Sucy-en-Brie catchment, Multi-Hydro model shows fast computation time at large scales up to 10 m (few minutes), and huge computation time is needed at very small scales [5 m, 2 m] (several hours). This is due to the huge number and size of the model outputs kept saved for research needs. Improvements should be implemented in the model structure in order to enhance the model performance from this point of view.

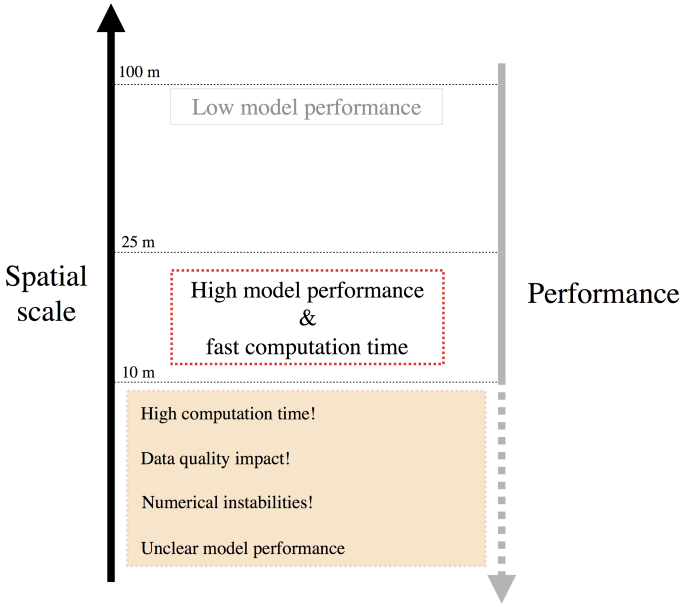

Figure 3.25: Model performance versus model implementation scale. Three ranges of scale are reported here. Specific attention should be devoted to small scale urban modeling needs in terms of data quality and computation time.

Figure 3.25 summarized main conclusions of this scale dependency investigation. In fact, fractal analysis of environment data used as input for urban storm models demonstrates the high scale dependency observed in such data. Urban catchment geophysical data appear to be modified every time the implementation scale changed. The effect of such scale dependency on gridded based models performance was investigated in the framework of a multi-scale modeling investigation performed using Multi-Hydro model at 17 spatial scales. Results show huge scale dependency of the models performance. Performance Multi-Hydro model increases as the model resolution increases. High performance are retrieved at starting from 30 m scale. "Good model" response with respect to flow measurements is obtained at 15 m scale. However some special issues related to data quality and resolution affect the model performance at very small scales. These

issues as well as model needs in terms of computation capabilities should be considered when performing high resolution modeling.

At the same time, analysis performed here demonstrates the difficulty to apply the classical calibration approach in the case of gridded based models. In fact, such approach, based on forcing the model to give a better performance by changing its parameters, cannot be applied for gridded based models because of this high scale dependency. A better consideration of such scale dependency allows to define an optimum scale, at which the model gives better performance with respect to measurements. It can be seen as a new approach of gridded based models calibration.

3.2.3 Sensitivity of urban storm models to rainfall spatio-temporal variability

One of the purposes of this work is to investigate the real needs for small scale rainfall information for modeling applications. Most of former research carried out in this direction (ten Veldhuis et al. (2014), Emmanuel et al. (2011), Bruni et al. (2012), Schilling (1991a), Gires et al. (2011a, 2013), Einfalt et al. (2004), Schilling (1991b), Berne et al. (2004), Bruni et al. (2015), Gires et al. (2015)), with often a hypothetical X-band polarimetric radar data, remains inconclusive about the advantage of such detailed rainfall information for modeling applications. Furthermore, most of these works involve only conceptually based models, originally designed for input of a uniform rainfall on sub-catchment or even catchment scales.

Berne et al. (2004), estimated the required space-time resolution of rainfall as a function of the surface of the catchments based on quantitative investigations of the space-time scales of urban catchments and rainfall structures. Recommendations coming out from this work, quantify the need for 1000 ha urban catchment about 5 min and 3 km spatio-temporal resolution. For small urban catchment, of the order of 100 ha, the needs in terms of rainfall spatio-temporal resolution are 3 min and 2 km. Bruni et al. (2015) investigated the sensitivity of urban hydrodynamic modeling to rainfall spatial and temporal resolution. Rainfall spatio-temporal resolutions used in this work were obtained by upscaling the original data in space between up to 2000 m and in time up to 10 min. The impact of rainfall spatio-temporal resolutions was analyzed on the modeling outputs of a semi-distributed sub-catchment based model. Main results show that model sensitivity to temporal resolution of rainfall was low compared to spatial resolution. The

impact was more pronounced at the peak flow of modeling outputs and finally. Gires et al. (2012a) investigated the impact on unmeasured small scale rainfall variability on urban flow using synthetic X-band polarimetric radar data obtained by downscaling the classical 1 km^2 - 5 min C band radar data. Two rainfall events types were involved: a convective and stratiform one. Gires et al. (2012a) results show a change in observed peak flow of modeling outputs between 3% and 20% when considering small scale rainfall data. Gires et al. (2015) conducted a complementary work about impact of small scale rainfall variability for two urban storm model outputs using synthetic X-band polarimetric radar data generated through downscaling of the classical 1 km^2 - 5 min C band radar data. Main result indicate that both fully and semi distributed models show an impact to small scale rainfall information. The fully distributed model was found to be more sensitive than the semi-distributed model.

We did participate in the framework of RainGain project, on an international work (Ochoa-Rodriguez et al.) involving seven case studies from four European countries. The aim of this work was to identify urban modeling needs in terms of rainfall spatio-temporal resolution. To achieve this work, 9 high resolution X band rainfall events were available at 100 m - 1 min space time scales. 16 spatio-temporal combinations up to 3 km and 10 min were retrieved from the original data. In fact coarser spatial resolutions were obtained by averaging the 100 m radar grid to 500 m, 1 km and 3 km radar grids. Coarser temporal resolutions were obtained by sampling the data at the desired rainfall resolution (3 min, 5 min and 10 min). Results obtained from this work are presented below:

- The impact of rainfall input resolution on hydraulic outputs was shown to decrease significantly as catchment drainage area increases. In an other way, small urban catchment show much more needs for small scale rainfall information.

- Urban storm models appear to be more sensitive to the temporal variability of rainfall than its spatial variability: this finding was related to the sampling methodology used for the selection of coarser temporal resolution. In fact, according to Ochoa-Rodriguez et al., when averaging the spatio-temporal rainfall information, models show comparable sensitivity to spatial and temporal variability of rainfall.

- One of the findings of Ochoa-Rodriguez et al., is the definition of urban modeling needs in terms of rainfall spatio-temporal resolution. In fact, for very small

drainage areas, below 1 ha, rainfall input resolutions of 100 m are required. For drainage areas between 1 ha and 100 ha, a spatial resolution of 500 m appears to be sufficient; for these areas, no significant improvement is observed when using finer spatial resolution rainfall estimates and acceptable hydraulic performance is still obtained for rainfall estimates at 1 km/1 min resolution. For drainage areas larger than 100 ha rainfall input spatial resolutions of 1 km appear to be sufficient.

- According to Ochoa-Rodriguez et al., a big part of the impact of rainfall input resolution on urban runoff estimates can be explained by the spatial–temporal characteristics of the storm events.

Further analysis were performed in the framework of this thesis in the case study catchment using the same rainfall data set as (Ochoa-Rodriguez et al.), made available in the framework of RainGain project. This work is presented here as a complementary study to Ochoa-Rodriguez et al. and aims to investigate some relevant questions raised by various studies performed in this direction. Both works allow to increase our understanding of how urban storm models deal with the small scale rainfall variability.

3.2.3.1 Scope of this work

The investigation performed in this work about the sensitivity of urban storm models to rainfall spatio-temporal resolution is of extreme importance. In fact, various scientific questions do exist about the real need for high resolution rainfall data for modeling applications, and improvements that should be implemented on urban storm models in order to increase their ability to integrate the detailed knowledge about the rainfall structure.

The scope of this work, is to carry out several modeling investigations on the sensitivity of urban storm models to rainfall variability and to quantify the gain in terms of performance related to the knowledge of the small scale rainfall structures. Investigations will be performed using two different modeling approaches implemented at various spatial scales.

The purpose of this investigation is to increase our knowledge about urban storm models needs in terms of rainfall spatio-temporal resolution from five perspectives:

- The relationship that may be retrieved between storm models sensitivity to rainfall variability and the modeling approach involved will be investigated through the comparison between Multi-Hydro and CANOE models. In fact, semi-distributed models are known for considering an average of the rainfall information at each sub-catchment scale whereas fully-distributed models consider distributed rainfall data at the scale of their pixel size.

- The effect of urban storm models spatial resolution on their ability to take into account the rainfall structure is a part of our interest. The purpose is to inspect whether or not improvements of urban storm models resolution can increase their ability to integrate the small scale rainfall information. To facilitate the investigation of this issue, huge works were performed in the framework of this thesis to implement CANOE and Multi-Hydro models at various spatial scales.

- The possible relationship between the catchment size and the sensitivity of urban storm models to rainfall spatio-temporal variability will be explored as well. In another way it will of be benefit to understand whether or not the need for small scale rainfall information increases with the size of the catchment decreasing.

- A distinction between the impact of rainfall temporal and spatial variability on urban storm models outputs will be performed here. The purpose is to confirm results coming out from new research works done related to this topic for which urban storm models are more sensitive to temporal variability rather than the spatial one.

- Finally, the dependence between storms characteristics and the impact of their rainfall spatio-temporal resolution on modeling outputs should be clarified.

A huge data set was available for the needs of this work, and a specific methodology was applied in order to investigate responses to various questions presented above.

3.2.3.2 Rainfall data

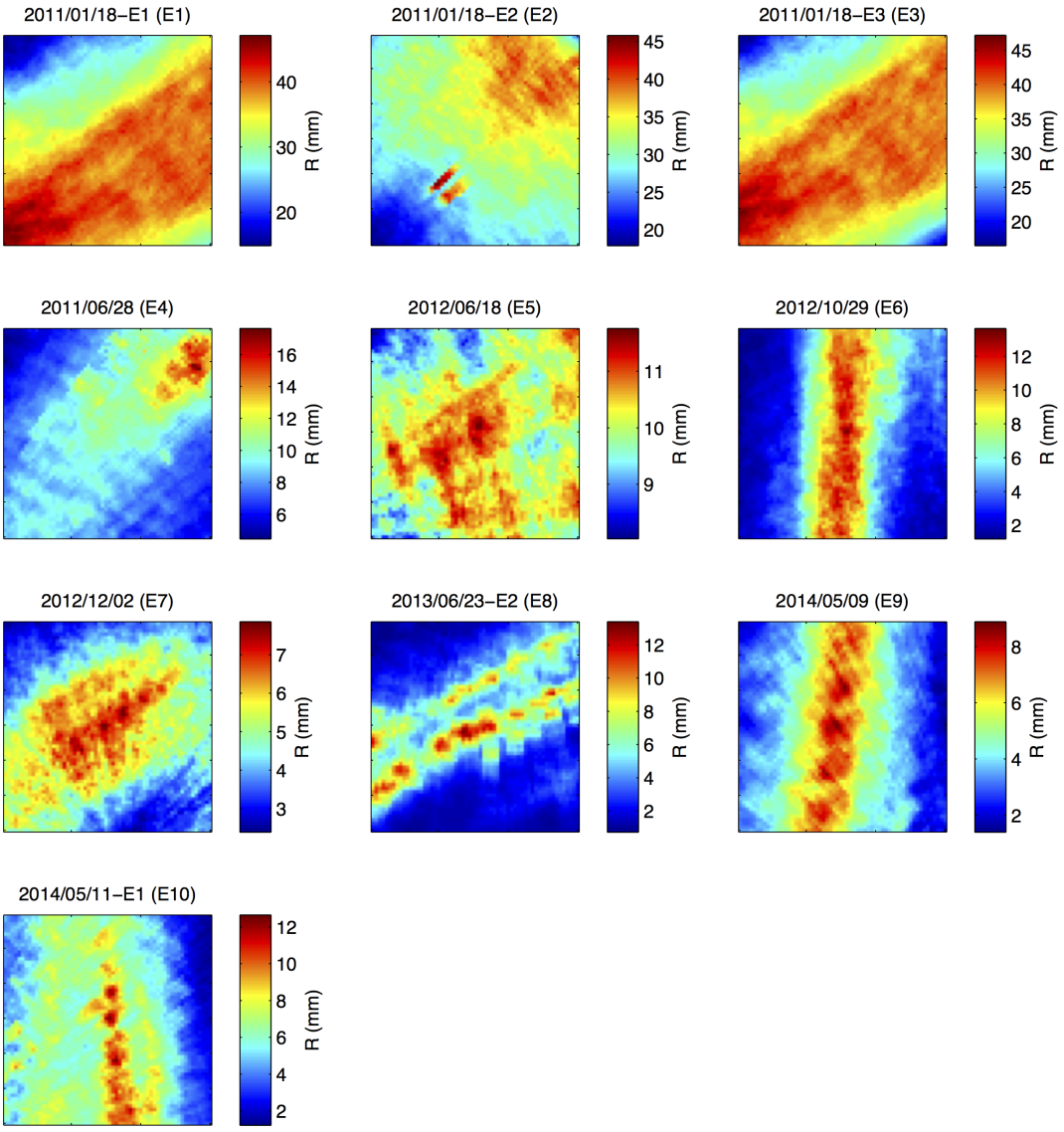

Figure 3.26: Total rainfall depth maps of the 10 selected rainfall events (6 km x 6 km) coming from the X-band weather radar located in the CESAR observatory of the Netherlands and used for the sensitivity analysis of urban hydrological models to rainfall spatio-temporal resolutions (Ochoa-Rodriguez et al.).

10 high resolution rainfall events (were made available in the framework of RainGain project and were selected to perform a multi-catchment investigation on the impact of rainfall spatio-temporal resolution (Ochoa-Rodriguez et al.). Same rainfall events were used here in this work. They were obtained by a dual-polarimetric X-band weather radar, located in the CESAR observatory of the Netherlands. The original available resolution is 100 m by 100 m grid and 1 min in time. 36 km^2 radar grid was available.

Readers should refer to (Ochoa-Rodriguez et al.) for further information about the data processing.

ID	spatio-temporal resolution
Ref	100 m - 1 min
1	100 m - 3 min
2	100 m - 5 min
3	100 m - 10 min
4	500 m - 1 min
5	500 m - 3 min
6	500 m - 5 min
7	500 m - 10 min
8	1000 m - 1 min
9	1000 m - 3 min
10	1000 m - 5 min
11	1000 m - 10 min

Table 3.7: 11 spatio-temporal combinations were selected by averaging the Ref data in space and time. The coarser resolution is 1000 m - 10 min

11 spatio-temporal combinations (see Table 3.7) were selected for this study. Coarser spatio-temporal resolutions rainfall data were obtained exclusively by averaging the 100 m, 1 min rainfall data to the needed spatio-temporal resolution (s,t) where s takes value in {100 m, 500 m, 1 km}, t takes value in {1 min, 3 min, 5 min, 10 min}. Given the small size of Sucy-en-Brie catchment (2.45 km^2), the 3 km^2 radar grid was not used here, because it does not represents any spatial variability at the scale of the catchment. This is the main difference between data used here and that one used in Ochoa-Rodriguez et al.. In fact, in Ochoa-Rodriguez et al., coarser spatial resolutions were obtained by averaging the original data in space whereas coarser temporal resolution were obtained by sampling the data at the desired rainfall resolution in such way to replicate the radar scanning strategies (Ochoa-Rodriguez et al.). However, some of Ochoa-Rodriguez et al. results, especially the high sensitivity of urban storm models to temporal variability of rainfall was explained by the sampling methodology used for the selection of coarser

temporal resolutions.

3.2.3.3 Methodology

The methodology applied in this work is similar to that one conducted in Ochoa-Rodriguez et al. and consists in performing various simulations using the 11 spatio-temporal rainfall combinations. The modeled flow was retrieved at four point locations in the sewer system, corresponding to four sub-catchments for which the drainage area size ranges from 44 ha to 215 ha (Figure 3.27). All simulations were performed at 1 min model time step.

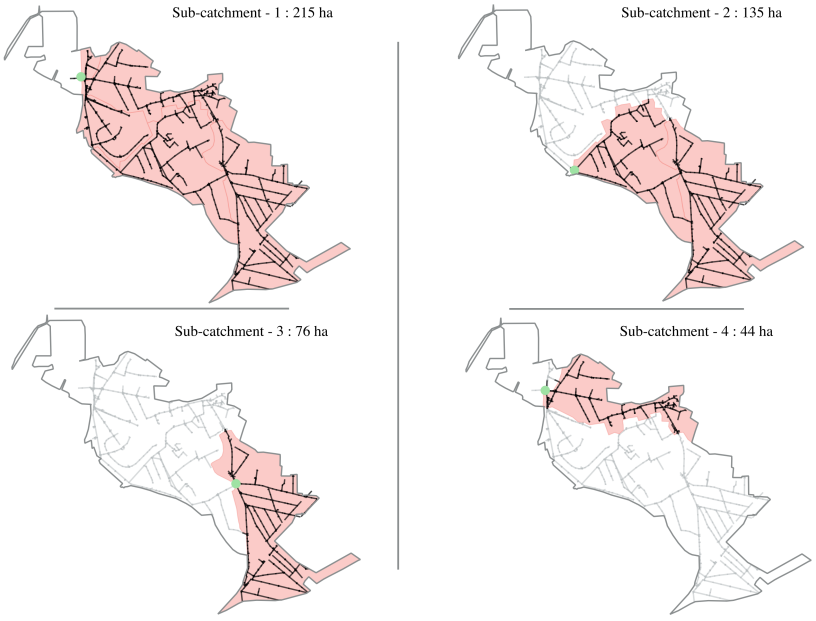

Figure 3.27: Modeled flow is retrieved at four point locations in the sewer system (green pints) corresponding to four drainage areas with size ranging from 44 ha to 215 ha

The impact of rainfall spatio-temporal variability on modeling outputs is quantified using three statistic parameters. They were estimated between the obtained modeled flow $Q_{s,t}$ and the reference modeling output Q_{ref} (modeled flow obtained for the reference rainfall data (100 m, 1 min) was considered as the reference one Q_{ref}).

- **Regression coefficient β** (Equation 3.13) is used to quantify the agreement between modeled flow $Q_{s,t}$ and the reference flow Q_{ref} time series. $\beta \approx 1$ indicates good agreement between $Q_{s,t}$ and Q_{ref}; $\beta \leq 1$ indicates that the model is

underestimating in the mean the *Reference* flow (Q_{ref}) and $\beta \geq 1$ indicates an overestimation of (Q_{ref}).

- **Nash-Sutcliffe efficiency *NSE*** (Equation 3.9) will be used in this work to quantify the impact of the rainfall spatio-temporal variability on the model performance.

- **The relative error at the peak flow δr** (Equation 3.12) will be used to analyze the impact of rainfall spatio-temporal variability on the modeled peak flow. $\delta r \approx 0$ will indicates no impact on the modeled flow whereas $\delta r \leq 0$ or $\delta r \geq 0$ indicate respectively an underestimation or overestimation of the *Ref* peak flow.

Results will be presented and analyzed following five steps in order to investigate the impact of rainfall spatio-temporal variability from different perspectives.

3.2.3.4 Results and discussions

All boxplots presented in the following sections were processed as in Section 3.2.2.3.

1. **Comparison between semi-distributed and fully distributed models sensitivity to rainfall variability :** a comparison between semi-distributed and fully-distributed models sensitivity to rainfall spatio-temporal resolution is presented here. This comparison will allow a better understanding of how different modeling approaches deal with the spatio-temporal variability and to identify the needs for high resolution rainfall information. Several works investigated this question. Gires et al. (2015) conducted a comparison between two urban storm models using downscaled C-band radar data generated through a Multifractal process. Their results indicate that the fully-distributed model is more sensitive to small scale rainfall information than the semi-distributed one.

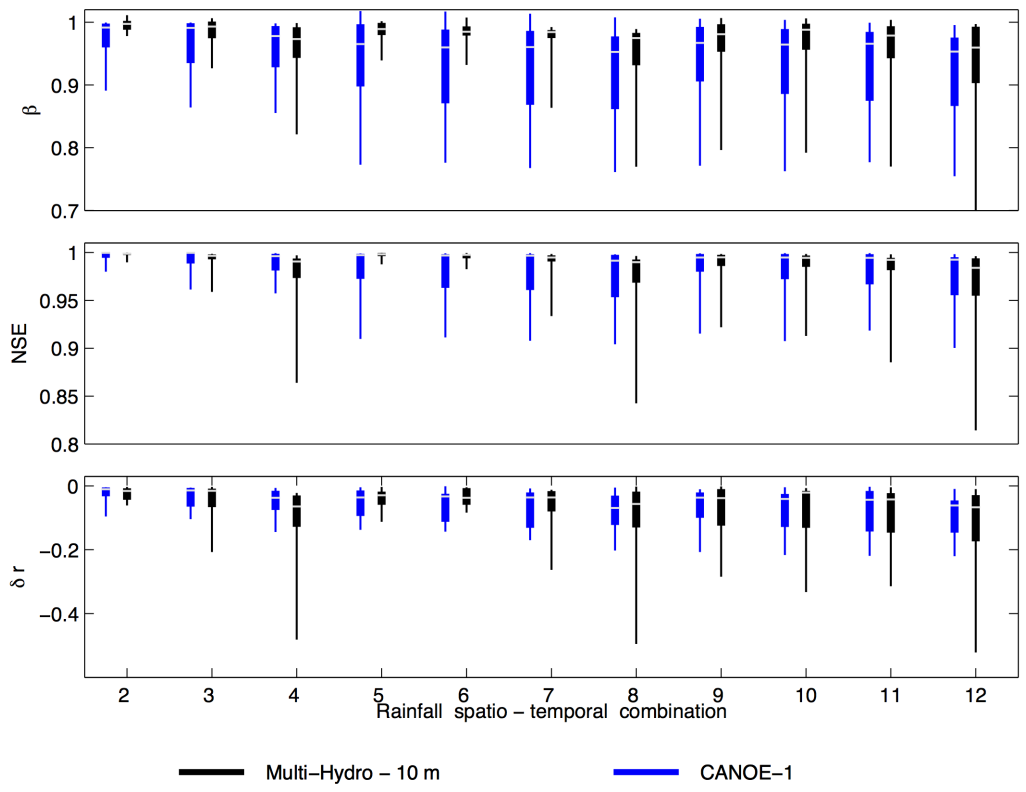

Figure 3.28: Boxplots, representing performance indicators retrieved for Multi-Hydro (black ones) model and CANOE -1 (blue ones) versus the 12 available spatio-temporal resolutions.

In Figure 3.28, are presented in boxplots parameters indicators retrieved for both Multi-Hydro (black ones) and CANOE-1 (blue ones) models for the 11 rainfall spatio-temporal resolutions. Three important remarks should be made here; (i) general trends demonstrate that urban storm models regardless of their modeling approaches are clearly losing performance when considering coarser spatio-temporal resolutions. They are in fact underestimating Q_{ref} up to 30%. β values decrease to 0.8 when considering the 1 km radar grid. *NSE* shows a decrease in the model performance up to 20%, whereas δr indicates that urban storm models are clearly underestimating the peak flow up to 40%. The underestimation noticed in modeling outputs $Q_{s,t}$ when considering coarser spatio-temporal resolutions is due to the fact that averaging rainfall data decreases the rainfall intensity and leads to an underestimation of Q_{ref}. (ii) The impact of considering coarser spatio-temporal resolutions is more pronounced in the peak flow. In fact, peaks flow are underestimated up to 40% reflecting the fact that peak rainfall intensity are more affected when averaging the small scale rainfall information. The same remark was

made in Bruni et al. (2015), Gires et al. (2015).

(iii) Figure 3.28 demonstrates that the impact of rainfall spatio-temporal resolution depends also on the modeling approach involved. In fact, gridded based models are clearly more sensitive to small scale rainfall information than sub-catchments based models that tend to reduce the effect of rainfall variability by considering an average of rainfall information at the sub-catchment scale. Discussions about the effect of improvement of semi-distributed models resolution on their sensitivity to small scale rainfall data will be discussed later in this work.

An important remark emerges also from the comparison between semi-distributed and gridded based models sensitivity. It reflects a huge difference in terms of their ability to integrate the small scale rainfall information. In fact, from Figure 3.28, one can notice that the impact of rainfall variability on the semi-distributed modeling outputs is more pronounced during the transition from 100 m radar grid to the 500 m one. After that, CANOE-1 model loses clearly its sensitivity for both the temporal and the spatial rainfall variability, the impact on CANOE-1 modeling outputs when considering the 1 km -1 min radar data instead of the 500 m - 1 min is not significant. Same remark can be made about the impact of temporal variability when considering the 500 m and the 1 km radar grid. On the contrary, Multi-Hydro model continues to show a decrease on its performance every time the spatial and temporal resolution of rainfall changes. In fact, the impact of Multi-Hydro modeling outputs when considering the 500 m - 10 min radar data instead of the 500 m - 1 min one is about 20% and the impact of rainfall variability observed on modeling outputs when considering the 1 km radar grid instead of the 500 m is more than 10%. So the semi-distributed model shows much more sensitivity to fine scale rainfall data below the 500 m grid, its sensitivity to temporal variability observed within large spatial scales is negligible. On the contrary, the fully distributed model shows a better sensitivity to the spatio-temporal variability observed below the classical 1 km^2 radar grid.

2. **Sensitivity versus the model spatial resolution :** a special focus was made in this work on the investigation of what will be the effect of improving urban storm models spatial resolution on their sensitivity to small scale rainfall variability. To achieve this goal, Multi-Hydro model was implemented at various spatial scales and the spatial resolution of CANOE model was improved as well by considering

smaller sub-catchments. The impact of such improvements on the urban models ability to consider small scale rainfall information will be analyzed in two steps; (i) a comparison between the two CANOE model configurations will be performed below and (ii) the sensitivity of Multi-Hydro model will be investigated at various spatial scales (100 m, 50 m and 10 m). Conclusions expected from this work should indicate enhancements to be made on urban storm models in order to increase their ability to integrate the small scale rainfall information.

- *Semi-distributed model:*

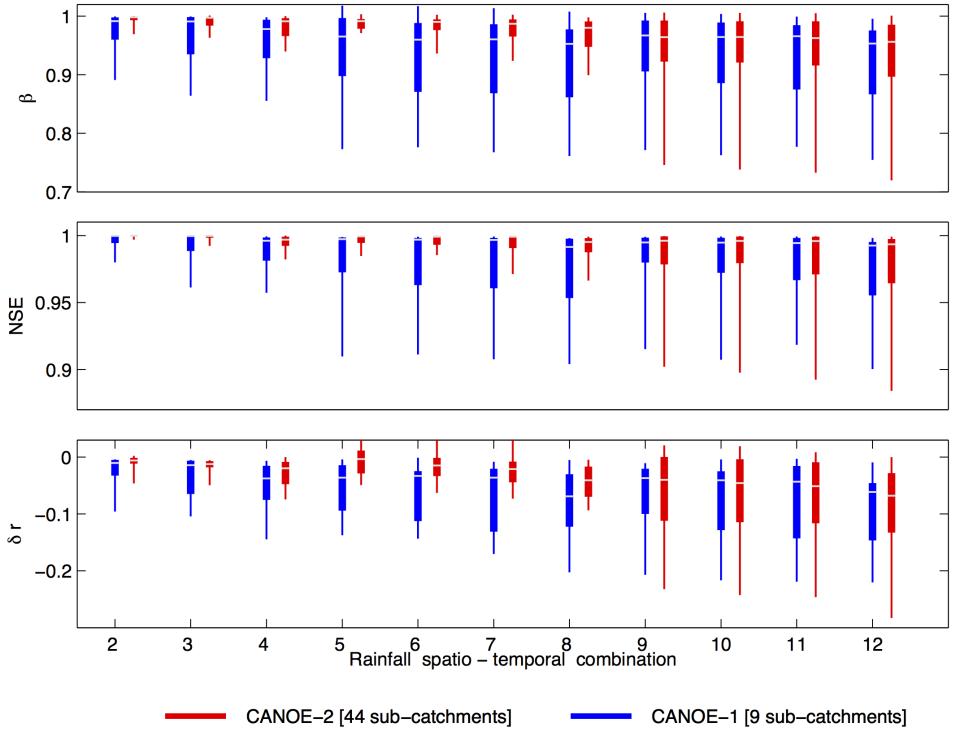

Figure 3.29: Impact of rainfall spatio-temporal resolution on modeling outputs of CANOE-1 (blue) and CANOE-2 (red) models

In Figure 3.29, are compared statistic parameters obtained for CANOE-1 and CANOE-2 models. Two significant changes were observed on the behavior of CANOE model. Indeed, an improvement of the model sensitivity to small scale rainfall variability is noticed, the impact of using the 1 km radar grid instead of the 500 m is more significant when considering smaller sub-catchments. The sensitivity to rainfall temporal variability was improved as well. Nevertheless, CANOE-1 still more sensitive to the transition from the 100 m radar grid to the 500 m one. However, there are some few rainfall

events for which the improved configuration is more sensitive to the spatio-temporal variability indicating that considering smaller sub-catchments increases specifically the impact of convective rainfall events (more localized storms with high spatial heterogeneity,...) while the impact of stratiform events remains unchanged. This point should be investigated later in this work.

- *Fully-distributed model:*

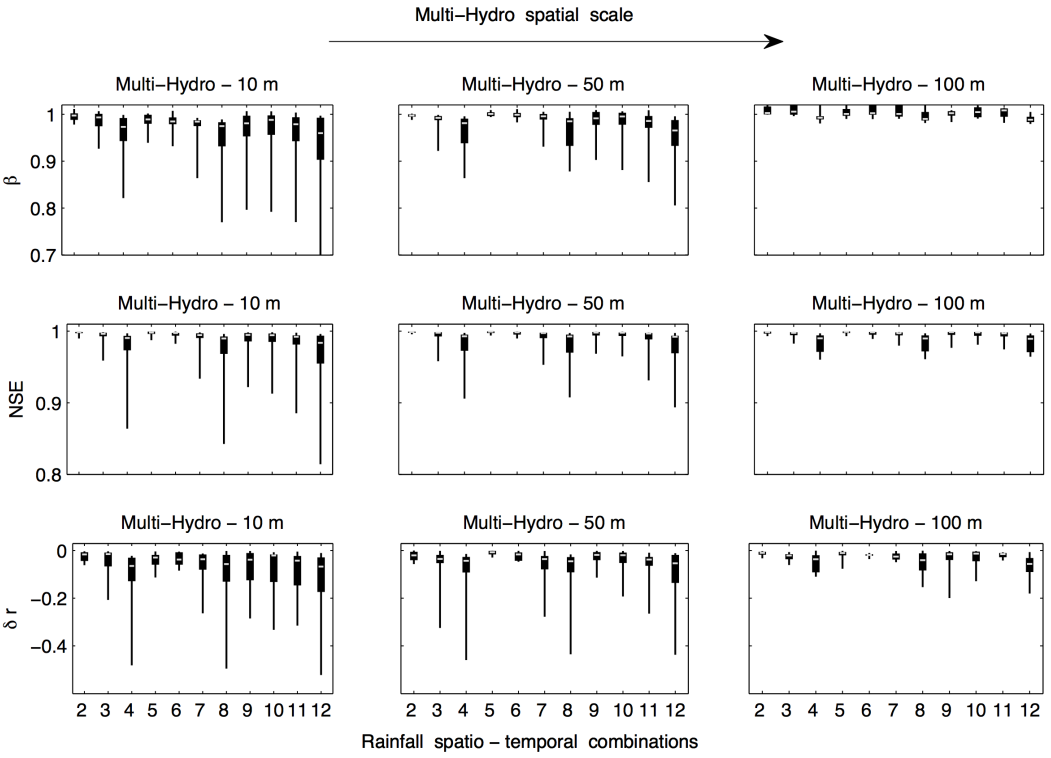

Figure 3.30: Impact of rainfall spatio-temporal resolution on modeling outputs versus model spatial resolution investigated here for three spatial scales of Multi-Hydro model; 100 m, 50 m and 10 m

In Figure 3.30 are displayed in boxplots performance statistics β, NSE and δr that indicate the impact of rainfall spatio-temporal variability on modeling outputs obtained using the gridded based model implemented at three spatial scales (100 m, 50 m and 10 m). As one may notice, the impact of small scale rainfall information depends significantly on the model resolution. It is clear that the ability of the model to integrate such information increases with model scale decreasing. This can be related to a better consideration of the spatial heterogeneity of the urban catchment especially the land use occupation. This result confirms the need to integrate a detailed description

of the catchment characteristics. So considering small size pixels increases the model sensitivity up to 20%. It may be noticed as well that improving the model resolution increases much more its sensitivity to spatial variability of rainfall rather than the temporal variability for which the model still responding partially even at large scales.

- **Sensitivity versus the size of the catchment**

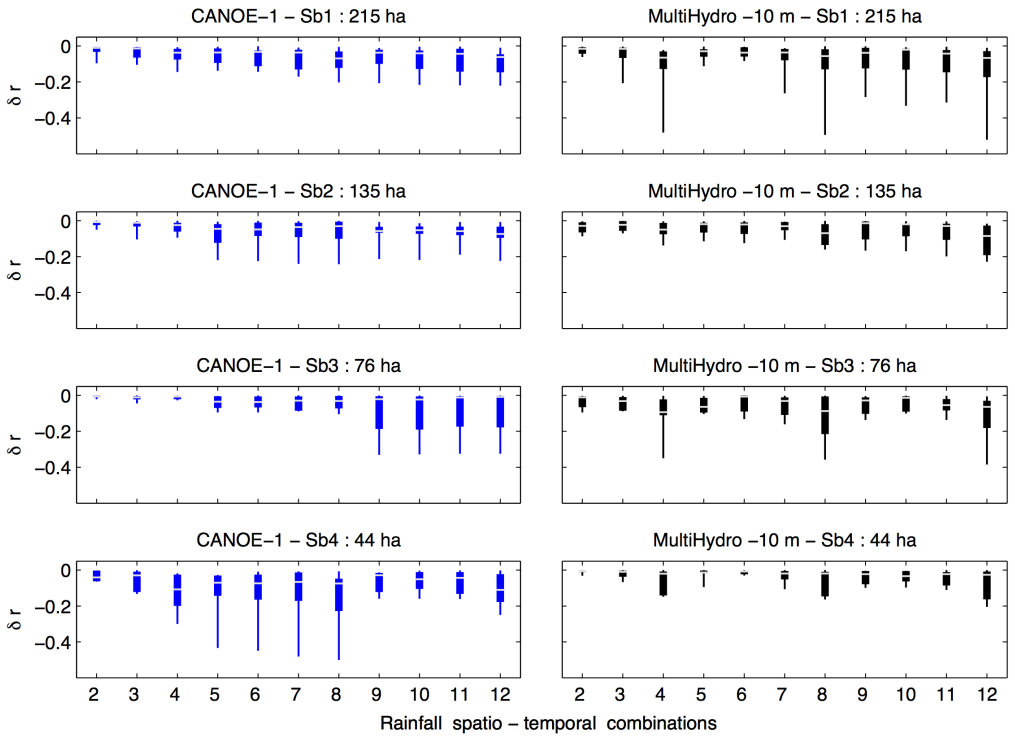

Figure 3.31: Impact of rainfall spatio-temporal variability on modeling outputs observed for four catchment size ranging from 44 ha to 215 ha. Only the relative error at the peak flow is presented here for both Multi-Hydro (black) and CANOE-1 models (blue).

In Figure 3.31 are presented in Boxplots, impacts of rainfall small scale variability on modeling performance analyzed at four sub-catchments with size ranging from 44 ha to 215 ha. From results obtained it is difficult to retrieve a possible impact of the catchment size on the need for small scale rainfall information. In fact, for CANOE model, the sensitivity appears to increase as the catchment size decreases. At large catchment size (the 215 ha sub-catchment) the model shows no spatio-temporal sensitivity of rainfall beyond the 500 m spatial scale. The impact of small scale rainfall information is more pronounced for small sub-catchments (using the 1 km -1 min radar data instead of the 500 m - 1 min decreases performance observed at the outlet of a

76 ha sub-catchment up to 10%, whereas no change in the model performance is noticed for the large catchment). This result is related to the modeling approach involving in CANOE model based on a uniform rainfall information within sub-catchments. For large sub-catchments, the model averages more radar pixels than for small sub-catchments, it deletes thus furthermore the spatio-temporal variability observed within the data.

For Multi-Hydro model, the modeling approach is different and the model integrates directly the rainfall information available at each pixel size. From Figure 3.31, the behavior of the model is not obvious. In fact, for the 44 ha sub-catchment, the model shows more sensitivity to temporal variability of rainfall especially when considering the 10 min radar grid. The sensitivity for spatio-temporal variability is noticed for the large sub-catchment where the impact of considering the 1 km radar grid instead of the 500 m one is more clear, more sensitivity to small scale temporal variability is noticed as well.

- **Sensitivity versus the rainfall characteristics**

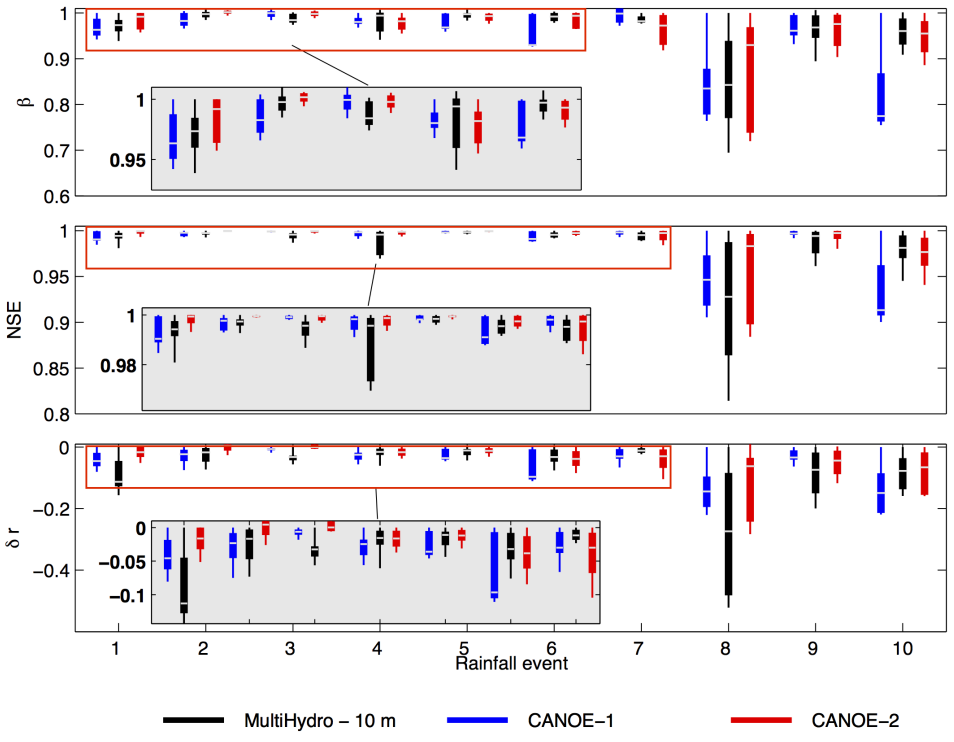

Figure 3.32: Boxplots of performance indicators β, *NSE* and δr versus storm event ID

Characteristics of rainfall events involved in this work were estimated in Ochoa-Rodriguez et al. in terms of the maximum singularity γ_s observed

within the radar field. γ_s is calculated in the framework of a multifractal analysis of radar data (Schertzer and Lovejoy (1987b, 1997)). Values of the maximum singularity γ_s observed at small scales range between 0.33 and 0.92. The maximum of γ_s is noticed for the 23/06/2013 (8) rainfall event.

In Figure 3.32 are displayed performance indicators β, *NSE* and δr retrieved for Multi-Hydro (black ones), CANOE-1(blue ones) and CANOE-2(red ones) models versus the storm ID. One should notice the clear dependency noticed in Figure 3.32 between the impact of rainfall spatio-temporal variability and storm characteristics. In fact, the magnitude of variations in the response of hydrological models vary significantly from one event to an other depending on the spatio-temporal variability observed within the original data. High sensitivity is noticed for the 23/06/2013 rainfall event for which γ_s exhibits it high value.

For this event, Multi-Hydro shows a high ability to integrate the small scale rainfall information than CANOE model. Improving the CANOE model configuration by considering smaller sub-catchments improves clearly the obtained sensitivity for such event. Indeed, for more localized rainfall storms urban storm models shows high sensitivity to the change in the spatio-temporal scale of the rainfall information. The impact of uniform storm events is very limited. This results indicates clearly that the need for high resolution rainfall information is more crucial for convective and localized rainfall cells, often behind major flooding disasters.

3. **Spatial sensitivity versus temporal sensitivity**

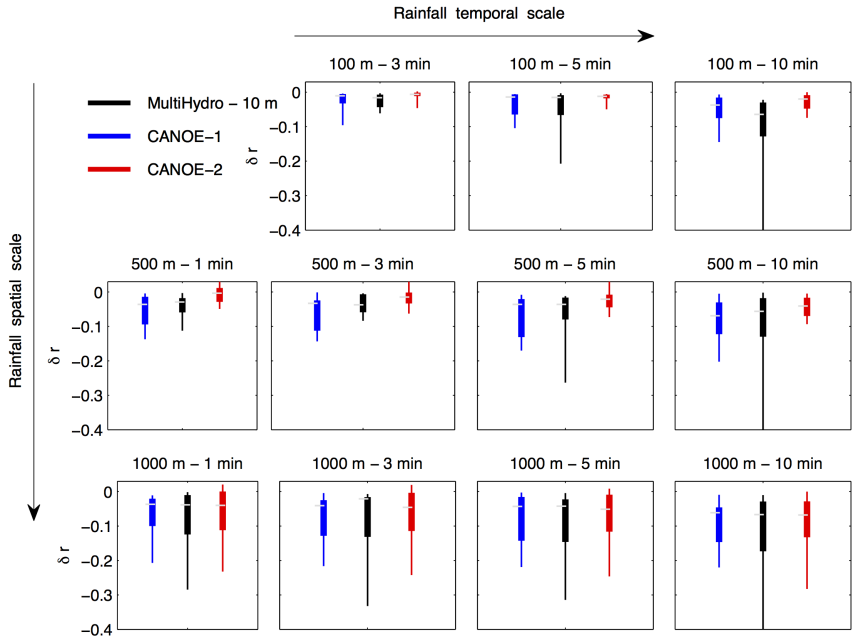

Figure 3.33: Comparison between small scale temporal and spatial variability impact on the peak flow of modeling outputs investigated for the 215 ha catchment

In Figure 3.33 are compared, the impact of temporal and spatial rainfall variability on the peak flow modeling outputs. Ochoa-Rodriguez et al. demonstrated that urban models are more sensitive to the temporal variability of rainfall than the spatial variability. This result was related to the sampling methodology used for the selection of coarser temporal resolution. In fact in Ochoa-Rodriguez et al., coarser spatial resolutions were obtained by averaging the original data in space whereas coarser temporal resolution were obtained by sampling the data at the desired rainfall resolution in such way to replicate the radar scanning strategies. This has consequences on the sensitivity of urban storm models, which confirmed in the framework of this thesis by considering exclusively the average of rainfall spatio-temporal information for the selection of coarser resolutions. From Figure 3.33, it appears that urban storm models are sensitive to both the spatial and the temporal variability, the impact of spatial rainfall variability appears to be more important than the impact of temporal variability. For small sub-catchment, the impact of temporal variability is more pronounced whereas large sub-catchments are more sensitive to the spatial variability of rainfall. One should also notice, that sensitivity of both models increases much more when considering the spatio-temporal variability instead of only considering the spatial or the temporal one.

The modeling work performed in this thesis about the sensitivity of urban storm models to small scale rainfall variability allows a better understanding of their needs in terms of rainfall spatio-temporal resolution. Results coming out from this work show that considering the small scale rainfall variability improves models performance up to 20% compared with the classical 1 km^2 - 10 min radar data. They are indeed in contradiction with Berne et al. (2004) recommendations especially for small catchment size. In fact, Berne et al. (2004) suggests that 3 min 2 km radar data is sufficient for small catchment size of order of 100 ha. However, modeling works performed in this thesis show that urban storm models still needs for small scale rainfall data below the 1 km radar grid. Results confirm also that urban models are more sensitive to spatial rainfall variability than the temporal variability. The high sensitivity to temporal variability observed in Ochoa-Rodriguez et al. is indeed due to the sampling methodology applied for the selection of temporal coarser resolutions.
Several conclusions can be made based on this work:

- All urban storm models exhibit a sensitivity to small scale scale rainfall variability. Their sensitivity depends upon on the modeling approach involved, on their spatial resolution and on the characteristics of storm events. Decrease noticed in models performance is estimated up to 20%.

- Fully-distributed models seem to be more sensitive to the spatio-temporal variability of rainfall information observed below the 1 km - 10 min radar data. In fact, their modeling approach allows a direct consideration of the rainfall variability at the scale of their pixel size.

- Taking into account the heterogeneity of geophysical data (land use distribution) with model higher space resolution increases the impact of small scale rainfall variability on gridded model performance.

- High dependency between the impact of rainfall variability on model performance and spatial characteristics of the storms is observed. In fact, localized storm events have more impact on models performance because of the high variability of their rainfall structures.

- Improvement of semi-distributed models resolution by considering smaller sub-catchment increases their ability to integrate the small scale rainfall variability,

especially for convective rainfall events (localized storm with high heterogeneity in space).

3.3 First applications with X-band polarimetric radar of Ecole des Ponts

The new ENPC X-band polarimetric radar was installed in later 2014 and inaugurated in June 2015. First rainfall events available were retrieved and will be used here to perform some modeling work and comparison between urban storm models. Unfortunately, only two storm events were selected and further analysis will be carried out based on future data available from the radar.

It is important to note that the radar is currently devoted fully for research activities and not yet operational. A lot of testing was carried out and will continue to be performed to define the scan strategy, and to investigate all processing options included within the SELEX software. Discussions are also going on with various local partners (local authorities, urban water managers and stakeholders) to build a platform around the radar, which will help to exchange knowledge about the use of high resolution X-band polarimetric radar data, and to implement new research output in local pilot sites in Paris region. A lot of research work should also be conducted to improve the processing chain and to develop new QPF products based on the use of small scale rainfall information.

In addition to selected X-band polarimetric radar data, rain gauge data were available as well as flow measurements and both CALAMAR adjusted (CALAMAR adj.) and non adjusted (CALAMAR non adj.) radar data. modeling outputs obtained when using all these types of rainfall information will be compared with respect to flow measurements.

3.3.1 Rainfall data available

Two rainfall events presented in Section 2.5.2.1 were used in this part. Figure 3.34 shows the total rainfall depth maps computed over the study catchment.

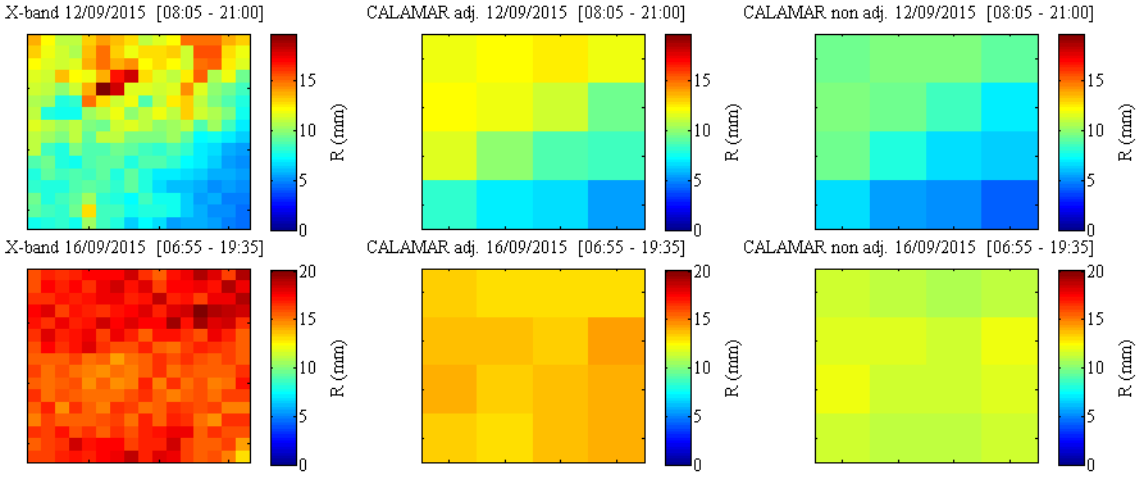

Figure 3.34: Total rainfall depth maps computed on the radar pixels used for modeling applications (4*4 km^2 C band data and 16*16 X-band data).

From Figure 3.34, one can notice the small scale rainfall variability observed at the scale of Sucy-en-Brie catchment within the X-band polarimetric radar data with respect to the classical 1 km^2 C-band gird. In fact a small and localized rainfall cell can be identified in the X-band map related to the 12/09/2015 event with a total rainfall depth around 25 mm and a maximum rainfall intensity around 143 mm/h.

One can also notice, that CALAMAR non adjusted data shows the lower cumulative rainfall depth (the maximum depth noticed in CALAMAR non adjusted map is 9 mm for the first event and 11 mm for the second event). The radar-rain gauge adjustment process performed by CALAMAR system improves the cumulative rainfall depth (12 mm and 13 mm for the first and the second rainfall events respectively). X-band polarimetric radar maps exhibit higher cumulative depth value (the maximum observed is around 25 mm for the first event and 20 mm for the second event).

In Figure 3.35, are displayed the cumulative rainfall depth calculated using rain gauge data (black line) and the corresponding pixel in the X-band polarimetric radar image (red line), CALAMAR adjusted data (blue line) and CALAMAR non adjusted data (green one). Figure 3.35 confirms that the new ENPC X-band product is overestimating rainfall with respect to point measurements and CALAMAR data. The non adjusted CALAMAR product underestimates clearly the rainfall depth. Figure 3.35 indicates also that the calibration process performed in real time by CALAMAR system improves the quality of CALAMAR data.

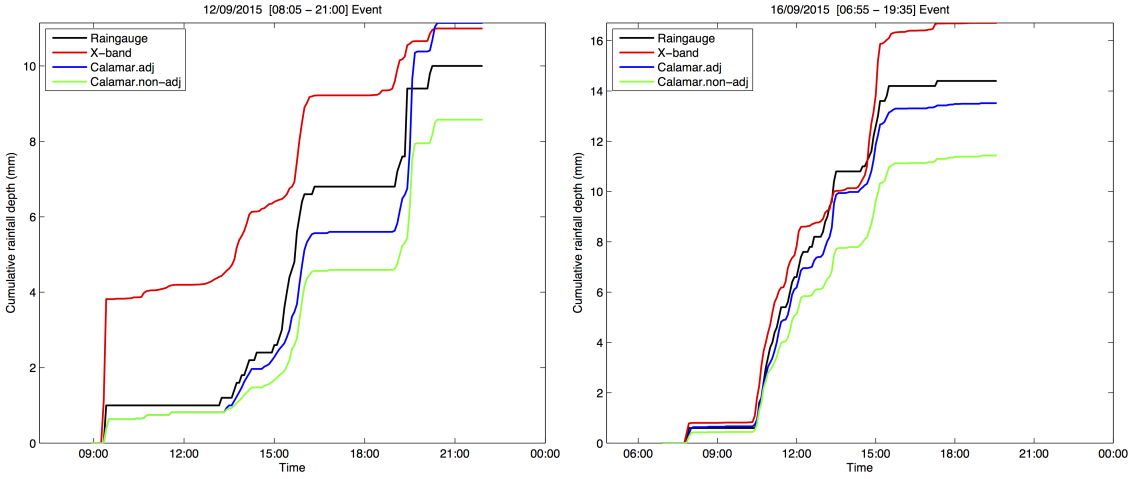

(a) **(b)**

Figure 3.35: Cumulative rainfall depth plot estimated in the rain gauge and the corresponding radar pixel for the first event (a) and the second event (b)

Modeling work will be performed using all available rainfall data and modeling outputs will be analyzed with respect to flow measurements. The three urban storm models available (Multi-Hydro, CANOE-1 and CANOE-2) are used for this work.

Figure 3.36 shows flow measurements available for the two selected events.

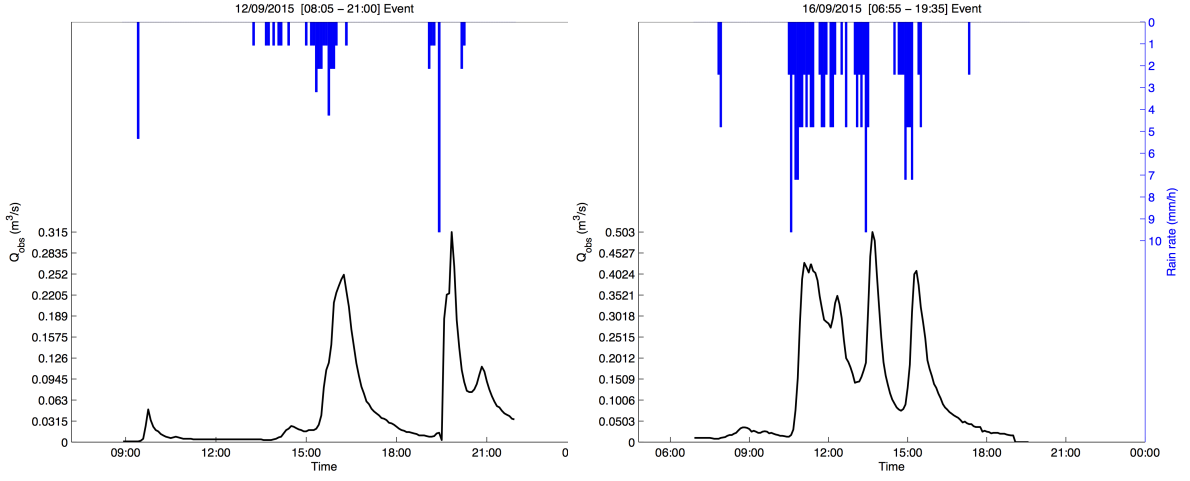

(a) **(b)**

Figure 3.36: Hyetograph and hydrograph recorder for; (a) 12/09/2015 and (b) 16/09/2015 events

3.3.2 Modeling analysis

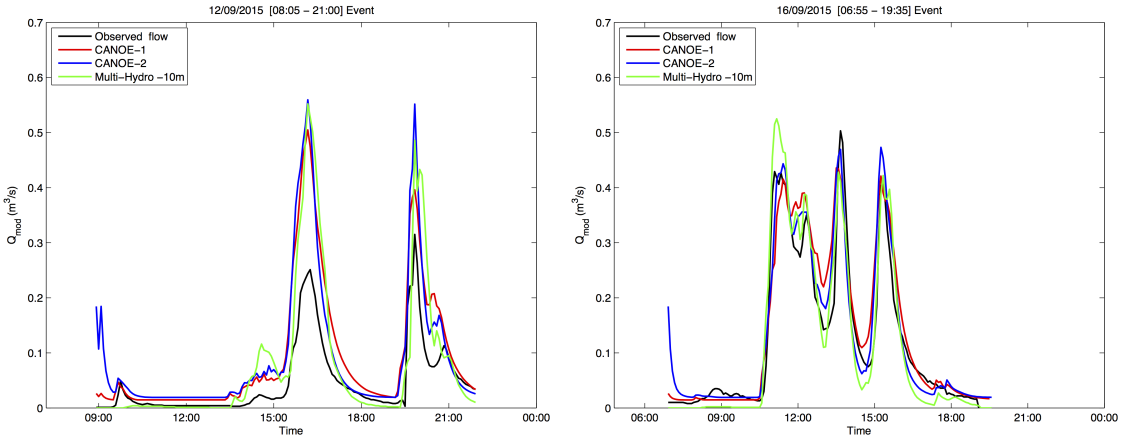

(a) **(b)**

Figure 3.37: Modeling outputs obtained by Multi-Hydro (green line), CANOE-1 (red line) and CANOE-2 (blue line) models when using only rain gauge data for the 12/09/2015 event (a) and the 16/09/2015 event (b). The corresponding observed flows are plotted in black line.

In Figure 3.37 are displayed modeling outputs obtained for the 12/09/2015 event (a) and the 16/09/2015 event (b) when using rain gauge information. Multi-Hydro outputs are presented with green line while CANOE-1 and CANOE-2 are presented by red and blue lines respectively. From Figure 3.37 it appears clearly that the three storm models shows good performance especially for the second event, *NSE* performance indicator is around 0.86 for CANOE-1, 0.89 for CANOE-2 and 0.91 for Multi-Hydro model. For the first event, modeled outputs are overestimating the observed flow, it appears that rain gauge data overestimates the rainfall rate.

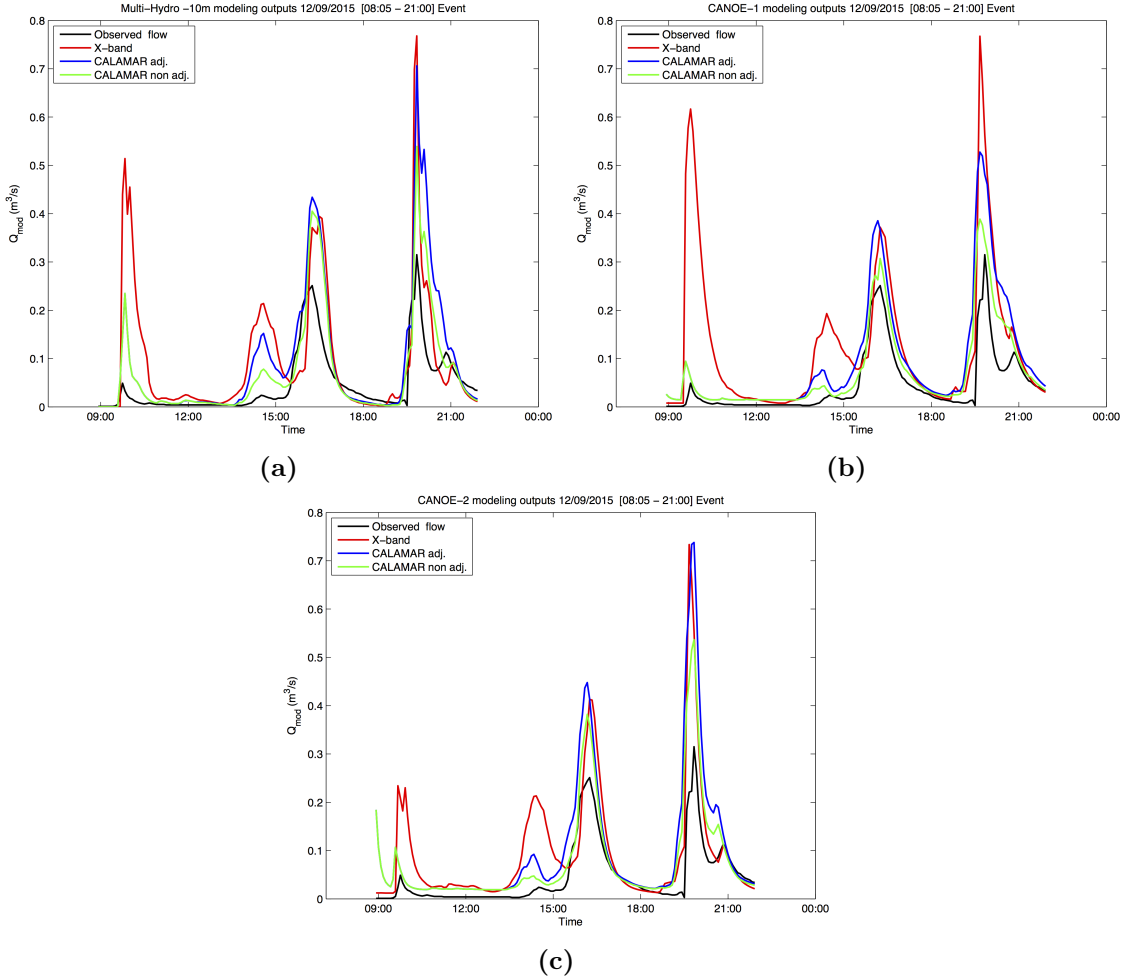

Figure 3.38: Modeling outputs obtained for the 12/09/2015 event, when using X-band polarimetric radar data (red line), CALAMAR adjusted data (blue line) and CALAMAR non adjusted data (green line). Multi-Hydro outputs are presented in figure (a) figures (b) and (c) represent CANOE-1 and CANOE-2 modeling outputs respectively.

In Figure 3.38 are presented models outputs obtained for the 12/09/2015 event, when using X-band polarimetric radar data (red line), CALAMAR adjusted data (blue line) and CALAMAR non adjusted data (green line). Multi-Hydro outputs are presented in figure (a) figures (b) and (c) represent CANOE-1 and CANOE-2 modeling outputs respectively. From Figure 3.38 one can notice important difference on modeling outputs obtained when using radar data. The overestimation of rainfall rate observed within the X-band polarimetric radar data is also observed here. For all urban storm models, obtained modeled flows show an overestimation of modeled flow with respect to observed data. A first peak flow is clearly observed in CANOE-1 and Multi-Hydro outputs but less pronounced in CANOE-2 model output, this is related to the sensitivity of urban storm models to rainfall variability observed within the new ENPC X-band polarimetric

radar data. The obtained modeling response obtained for CALAMAR adjusted data and X-band data is quite similar especially for Multi-Hydro and CANOE-2 models, the response obtained when using non adjusted CALAMAR data is much more lower. Results obtained for the second event are presented in Figure 3.39. It appears that the modeled flow obtained when X-band data is overestimating the observed flow. Modeled flow obtained when using CALAMAR non adjusted data underestimate the observed flow, the rain gauge-radar adjustment process improve obtained results.

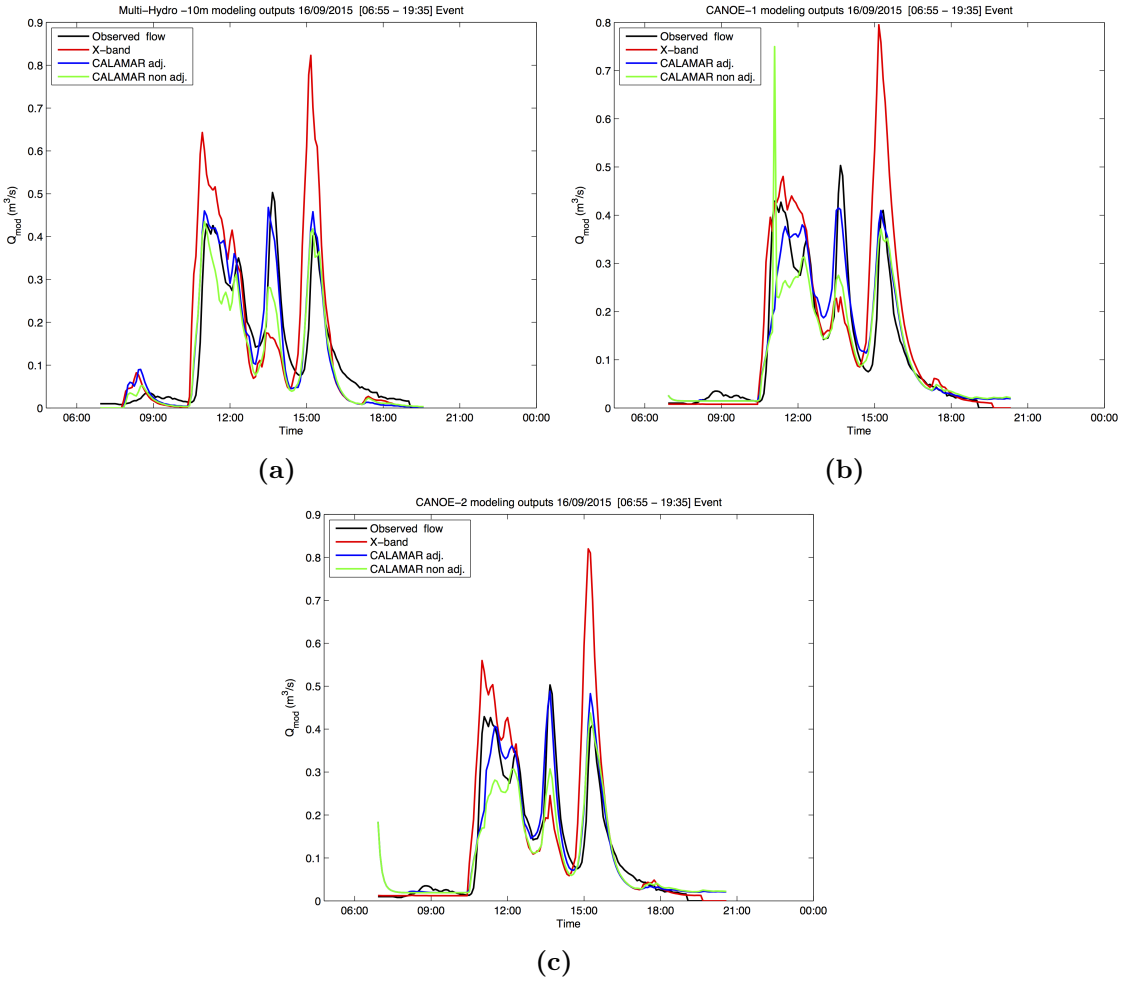

Figure 3.39: Modeling outputs obtained for the 16/09/2015 event, when using X-band polarimetric radar data (red line), CALAMAR adjusted data (blue line) and CALAMAR non adjusted data (green line). Multi-Hydro outputs are presented in figure (a) figures (b) and (c) represent CANOE-1 and CANOE-2 modeling outputs respectively.

The overestimation noticed in X-band polarimetric radar data is due to the fact that the $Z - R$ and K_{dp} parameters were not validated, they were just determined based on the literature. Various test and comparison with other radar products and rain gauges should be conducted to identify the correct parameters.

3.4 Intermediate conclusions on Chapter 3

This chapter was entirely devoted to hydrological modeling of urban catchments. Various investigations were performed in the framework of this thesis to understand the use of urban storm models with small scale rainfall information from several perspectives. Considerable works achieved in this thesis concern three axes:

1. The first part of our modeling investigations, concerns the implementation of urban storm models and their validation for the case study catchment of Sucy-en-Brie. Huge efforts were made in this direction to improve some aspects of urban hydrological models used in this thesis. Indeed, the approach used until now for the implementation of Multi-Hydro model was totally improved following a deep reflection and modeling investigations of the model performance and the way it takes into consideration the high heterogeneity of urban catchment. Results coming out from this work are huge and show a considerable improvement of the model performance. They changed significantly our understanding about the model functionality and raised several questions about the scale dependency of Multi-Hydro model performance. In addition to that, the semi-distributed CANOE model was improved as well in terms of its spatial resolution. The new model configuration includes smaller sub-catchments (44 sub-catchments instead of only 9 with the original configuration of the model). Such improvement was crucial and highly required not to improve the model performance but to understand the effect of such modification on the ability of the model to consider the small scale rainfall information.

2. The second point investigated in this thesis is the scale dependency on urban hydrology and its effects on gridded based models performance. Fractal tools were used in the first stage to highlight the scale dependency observed in geophysical data used as input for models implementation. The effect of such scale dependency on gridded based models performance was investigated in the framework of a multi-scale modeling investigation performed using Multi-Hydro model at 17 spatial scales. Results show huge scale dependency of the models performance. Indeed, performance of the model increases as the model resolution increases. High performance are retrieved starting from 30 m scale. Perfect model response with respect to flow measurements is obtained at 15 m scale. However some special

issues related to data quality and resolution affect the model performance at very small scales [10 m - 5 m] and should be considered when performing high resolution modeling.

3. Finally, a special focus was made on the investigation of urban models needs in terms on rainfall spatio-temporal resolution. This investigation was performed using two urban storm models involving two distinct modeling approaches. This allows a better understanding of their needs in terms of rainfall spatio-temporal variability. Results coming out from this work show that considering the small scale rainfall variability improves models performance up to 20% compared with the classical 1 km^2 - 10 min radar data. They are indeed in contradiction with Berne et al. (2004) recommendations especially for small catchment size. In fact, modeling works performed in this thesis show that urban storm models still needs for small scale rainfall data below the 1 km radar grid. Several conclusions can be made based on this work:

   - All urban storm models show a sensitivity to small scale scale rainfall variability. Their sensitivity depends upon on the modeling approach involved, on their spatial resolution and on the characteristics of storm events. Decrease noticed in models performance is estimated up to 20%.
   - Fully-distributed models appear to be more sensitive to the spatio-temporal variability of rainfall information observed below the 1 km - 10 min radar data. In fact, their modeling approach allows a direct consideration of the rainfall variability at the scale of their pixel size.
   - Considering the heterogeneity of urban catchments geophysical data (land use distribution) increases the impact of small scale rainfall variability on gridded based models performance. In fact, the impact of rainfall variability increases as the spatial resolution of the model increases.
   - High dependency between the impact of rainfall variability on models performance and spatial characteristics of the storms is retrieved here. In fact, localized storm events have more impact on models performance because of the high variability of their rainfall structures.

- Improvement of semi-distributed models resolution by considering smaller sub-catchment increases their ability to integrate the small scale rainfall variability, especially for convective rainfall events (localized storm with high heterogeneity in space).

All modeling works performed in this thesis represent an important step to meet the main goal of the thesis, which is to set up a new and reliable management tool based entirely on the use of High resolution rainfall data combined with powerful storm models that can take the whole advantages of small scale rainfall information. Such management tool should help to better manage urban flooding risk.

Conclusions and perspectives

In this dissertation we discussed the use of radar data for predictive management in urban hydrology. The relevant example of Sucy-en-Brie retention basin gives a sheer illustration of how complex and adverse could be various aspects of flood risk management. It pinpoints the specific needs of predictive management in terms of rainfall data reliability and quality.

The County Council of Val-de-Marne currently uses the forecasting system CALAMAR as a decision tool for the predictive management. It is a forecasting system combined with a warning system, both using single-polarization radar data, provided by Meteo-France radar network and processed with the help of the conventional Z-R relation. The results of this system were not considered as fully satisfactory due to a high rate of false early warnings. The predictive management had thus become difficult and was finally abandoned. The reliability of the warning system was brought into question, as well as the quality of the radar rainfall estimates, compared to those provided by local rain gauges. Therefore, a significant part of this dissertation has been devoted to the development of a new methodology for more meaningful comparison of radar rainfall products.

The comparison methodology of this dissertation has been developed in the framework of multifractals, more precisely of Universal Multifractals (UM) that have been somewhat extensively used in precipitation research. A few UM parameters, which have a strong physical meaning, enable us to proceed to an in-depth morphological comparison of the precipitation fields provided by different retrieval algorithms and/or by different measurements. This overcomes limitations of the classical radar - rain gauge comparison techniques widely used for Quantitative Precipitation Estimates (QPE) that unfortunately involve a very limited number of radar pixels and depends on the rain gauge network density.

A comparison between CALAMAR and Meteo-France products was thus performed and presented in this dissertation. The main goal was to identify the impacts of slightly distinct retrieval algorithms applied to the same radar data, provided in both cases by the Meteo France C band radar located in Trappes, located southwest of Paris. This comparison confirms a clear difference between CALAMAR and Meteo France products

in terms of Universal Multifractal parameters α and C_1.

In the spatial analysis, a scaling behavior was identified by a spectral analysis and confirmed by the Trace Moment analysis, as well as a scaling break observed at 8 km for all events and all radar products. The respective estimates of the scaling moment function $K(q)$ for small scales ([1 km-8 km]) point out a large difference of multifractality between the two products. Indeed, the Meteo France field exhibits a multifractal behavior with α ranging between 1.11 and 1.9 while both CALAMAR products exhibit almost a fractal behavior with much lower values for α. We showed that a large part of this difference is due to the high rate of zero values of the CALAMAR fields, mainly due to the ground clutter removal method. The DTM analysis, which provides more direct estimates of the UM parameters α and C_1, confirms a clear difference between the two products: the variability of precipitation seems to be better represented in the Meteo France product than by CALAMAR. The temporal evolution of UM parameters α and C_1 indicates that the two products do not yield the same parameters except during the heaviest rainfall period, when their structure becomes comparable. In temporal analysis, the difference observed between the two products in terms of α and C_1 values are less significant than what is observed in the spatial analysis.

The same methodology was used to analyse the X-band polarimetric radar data recently acquired by Ecole des Ponts ParisTech and installed on the Bienvenüe of the Descartes campus. building, and to compare them with the Meteo-France C band radar, with both the Meteo-France radar product and CALAMAR one. We selected two rainfall events that were also analysed on the Bièvre river basin. As a result of this comparison, both radar products exhibit a scaling behavior with a clear break noticed in spatial analysis around 8 km for C band data and 2 km for the X band product. the temporal analyses point out a break around 40 min and 27 min respectively for C band and X band products. A clear difference was noticed in terms of the rate of zero values. In fact, CALAMAR product still exhibits the highest rate of zero values and, as mentioned above, this is related to the ground clutter identification and removal technique.

The retrieved UM parameters α and C_1 indicate that the X band product displays a higher small scale variability. The structure of the two products become comparable only when they have the same fractal dimension D_f, which means that both radars

identify the same rainfall support. However, a clear difference is observed in temporal analysis between X band and C band products, the X band product clearly displays a higher small scale variability.

The developed methodology was applied in the framework of this dissertation for the comparison of radar products. However, it can also be applied for other rainfall data analysis, including QPE validation or radar-rain gauge comparison. It has the advantage of providing much more information about rainfall fields' structure. Such information and details would be very difficult to obtain by the conventional methods that are widely used for radar-rain gauge comparison until now but involve only a very limited number of radar pixels (those containing rain gauges).

An important goal of this dissertation is to estimate how high resolution rainfall data can improve urban storm model performance, i.e. how important is small scale rainfall information for urban hydrology. Various investigations reported in the literature are rather inconclusive on this issue, because they rely on conceptually based models, originally designed for input of a uniform rainfall over sub-catchment or even catchment scales.

1. The first part of our modeling investigations, concerns the implementation of urban storm models and their validation for the case study catchment of Sucy-en-Brie. To adequately deal with the small scale variability, we proceeded to several improvements of the urban hydrological models used in this thesis. The fully distributed model Multi-Hydro, developed by HM&Co, was adapted to run much more efficiently and be able to deal with larger resolutions. The space resolution of the semi-distributed CANOE model greatly improved with 44 sub-catchments instead of only 9 in the original configuration of the model.

2. The second investigated item is the scale dependency of urban hydrology variables and its effects on gridded model performance using Multi-Hydro model at 17 different space scales. Fractal tools were then used to highlight the scale dependency of the input geophysical data. Finally, the data assimilation was adapted to reduce this scale dependency, e.g. rather acceptable results were obtained with 30 m resolution simulations and quasi-perfect ones at 15m, in comparison with 5 m resolution runs.

3. Finally, we focus our investigation on the urban model needs in terms of rainfall spatio-temporal resolution with the help of both Multi-Hydro and CANOE. We have shown that high resolution data (100m, 1 min) improve model performance up to 20% compared to the classical 1 km^2 - 10 min radar data. Several conclusions can be made based on this work:

    - All urban storm models exhibit a sensitivity to small scale scale rainfall variability. Their sensitivity depends upon the modeling approach involved, on their spatial resolution and on the characteristics of storm events. Decrease noticed in models performance is estimated up to 20%.
    - Fully-distributed models seem to be more sensitive to the spatio-temporal variability of rainfall information observed bellow the 1 km - 10 min radar data. In fact, their modeling approach allows a direct consideration of the rainfall variability at the scale of their pixel size.
    - Taking into account the heterogeneity of geophysical data (land use distribution) with model higher space resolution increases the impact of small scale rainfall variability on gridded model performance.
    - High dependency between the impact of rainfall variability on model performance and spatial characteristics of the storms is observed. In fact, localized storm events have more impact on models performance because of the high variability of their rainfall structures.
    - Improvement of semi-distributed models resolution by considering smaller sub-catchment increases their ability to integrate the small scale rainfall variability, especially for convective rainfall events (localized storm with high heterogeneity in space).

As prospects, various tests and further analyses of the X-band polarimetric radar data should be conducted to confirm our insights on the small scale rainfall behaviour and implications. The developed methodology will be used to perform comparison between X band and other radar products available in the Paris region. It can also be used for the data validation with point measurements data. Further extensions of the proposed methodology should open new horizons for rainfall data merging and to predefine the conditions when the optimization may worsen the quality of rainfall estimates. An in-depth analysis should be performed to analyse improvements provided by the dual

polarisation and Doppler capabilities on the accuracy of rainfall measurements. We hope that the modeling developments performed in this dissertation represent a major step towards a new and reliable flood management. It will be designed to take the advantage of high resolution rainfall data at their full extent with the help of innovative urban hydrological models. in relation to the issue of management of Sucy-en-Brie retention basin, the research are going to continue in order to improve the process of managing both by using the new X-band radar that provides better data quality at high spatio-temporal resolution and by continuing the development of the high-resolution Multi-Hydro model. This should improve both the real-time management but also the replay of critical situation mode. In real time management mode, several solutions for the development of the forecasting model will be investigated (forecast based on the identification of rain cell and the extrapolation of their movement, ensemble forecast, multifractals forecast).In the replay mode, Multi-Hydro model will be used to replay critical situations in order to improve optimization scenarios (planning, optimization, resiliency).

Bibliography

AghaKouchak, A., E. Habib, and A. Bardossy

2010. Modeling radar rainfall estimation uncertainties: Random error model. *J. Hydrol. Eng.*, 15(4):265–274.

Alexander, L. V.

2016. Global observed long-term changes in temperature and precipitation extremes: A review of progress and limitations in IPCC assessments and beyond. *Weather and Climate Extremes*, 11:4–16.

Alexander, L. V., X. Zhang, T. C. Peterson, J. Caesar, B. Gleason, A. M. G. Klein Tank, M. Haylock, D. Collins, B. Trewin, F. Rahimzadeh, A. Tagipour, K. Rupa Kumar, J. Revadekar, G. Griffiths, L. Vincent, D. B. Stephenson, J. Burn, E. Aguilar, M. Brunet, M. Taylor, M. New, P. Zhai, M. Rusticucci, and J. L. Vazquez-Aguirre

2006. Global observed changes in daily climate extremes of temperature and precipitation. *J. Geophys. Res.*, 111(D5).

Ali, M., S. J. Khan, I. Aslam, and Z. Khan

2011. Simulation of the impacts of land-use change on surface runoff of lai nullah basin in islamabad, pakistan. *Landsc. Urban Plan.*, 102(4):271–279.

Anctil, F., N. Lauzon, V. Andréassian, L. Oudin, and C. Perrin

2006. Improvement of rainfall-runoff forecasts through mean areal rainfall optimization. *J. Hydrol.*, 328(3–4):717–725.

Badoche Jacquet, G. and F. Blanchet

1994. Procede de mesure de pluie. (FR2703472).

Badoche Jacquet, G., F. Blanchet, and B. Blanchet

1994. Procede et dispositif pour levaluation des precipitations sur une zone de terrain. (FR2693557).

Balica, S. and N. G. Wright

2010. Reducing the complexity of the flood vulnerability index. *Environ. Hazards*, 9(4):321–339.

Barnsley, M. and A. J. Hurd

1989. Fractals everywhere. *Am. J. Phys.*, 57(11):1053–1053.

Barraqué, B.

2014. The common property issue in flood control through land use in france. *J. Flood Risk Manage.*

Bastola, S., C. Murphy, and J. Sweeney

2011. The role of hydrological modelling uncertainties in climate change impact assessments of irish river catchments. *Adv. Water Resour.*, 34(5):562–576.

Battan, L. J.

1973. *Radar observation of the atmosphere.*

Bech, J., B. Codina, J. Lorente, and D. Bebbington

2003. The sensitivity of single polarization weather radar beam blockage correction to variability in the vertical refractivity gradient. *J. Atmos. Ocean. Technol.*, 20(6):845–855.

Bell, V. A. and R. J. Moore

1998. A grid-based distributed flood forecasting model for use with weather radar data: Part 2. case studies. *Hydrol. Earth Syst. Sci. Discuss.*, 2(2/3):283–298.

Bellon, A. and G. L. Austin

1984. The accuracy of short-term radar rainfall forecasts. *J. Hydrol.*, 70(1–4):35–49.

Bellon, A., I. Zawadzki, A. Kilambi, H. C. Lee, Y. H. Lee, and G. Lee

2010. McGill algorithm for precipitation nowcasting by lagrangian extrapolation (MAPLE) applied to the south korean radar network. part i: Sensitivity studies of the variational echo tracking (VET) technique. *Asia-Pacific J Atmos Sci*, 46(3):369–381.

Bennett, N. D., B. F. W. Croke, G. Guariso, J. H. A. Guillaume, S. H. Hamilton, A. J. Jakeman, S. Marsili-Libelli, L. T. H. Newham, J. P. Norton, C. Perrin, S. A. Pierce, B. Robson, R. Seppelt, A. A. Voinov, B. D. Fath, and V. Andreassian

2013. Characterising performance of environmental models. *Environmental Modelling & Software*, 40:1–20.

Benzi, R., G. Paladin, G. Parisi, and A. Vulpiani

1984. On the multifractal nature of fully developped turbulence. *Journal of Physics A*, 17:3521–3531.

Berenguer, M., C. Corral, R. Sánchez-Diezma, and D. Sempere-Torres

2005. Hydrological validation of a Radar-Based nowcasting technique. *J. Hydrometeorol.*, 6(4):532–549.

Berenguer, M., D. Sempere-Torres, C. Corral, and R. Sánchez-Diezma

2006. A fuzzy logic technique for identifying nonprecipitating echoes in radar scans. *J. Atmos. Ocean. Technol.*, 23(9):1157–1180.

Bergue, J.-M. and Y. Ruperd

2000. *Stormwater Retention Basins*. CRC Press.

Bernardara, P., D. Schertzer, E. Sauquet, I. Tchiguirinskaia, and M. Lang

2007. The flood probability distribution tail: how heavy is it? *Stochastic Environmental Research and Risk Assessment*, 22(1):107–122.

Berne, A.

2005. A stochastic model of range profiles of raindrop size distributions: Application to radar attenuation correction. *Geophys. Res. Lett.*, 32(10).

Berne, A., G. Delrieu, J.-D. Creutin, and C. Obled

2004. Temporal and spatial resolution of rainfall measurements required for urban hydrology. *J. Hydrol.*, 299(3–4):166–179.

Berne, A. and R. Uijlenhoet

2006. Quantitative analysis of x-band weather radar attenuation correction accuracy. *Nat. Hazards Earth Syst. Sci.*, 6(3):419–425.

Biondi, D., G. Freni, V. Iacobellis, G. Mascaro, and A. Montanari

2012. Validation of hydrological models: Conceptual basis, methodological approaches

and a proposal for a code of practice. *Physics and Chemistry of the Earth, Parts A/B/C*, 42–44:70–76.

Blong, R. J.

1996. Volcanic hazards risk assessment. In *Monitoring and Mitigation of Volcano Hazards*, Pp. 675–698. Springer Berlin Heidelberg.

Blöschl, G. and M. Sivapalan

1995. Scale issues in hydrological modelling: A review. *Hydrol. Process.*, 9(3-4):251–290.

Borja, A., J. Franco, V. Valencia, J. Bald, I. n. Muxika, M. J. Belzunce, and O. Solaun

2004. Implementation of the european water framework directive from the basque country (northern spain): a methodological approach. *Mar. Pollut. Bull.*, 48(3-4):209–218.

Brandes, E. A., G. Zhang, and J. Vivekanandan

2002. Experiments in rainfall estimation with a polarimetric radar in a subtropical environment. *J. Appl. Meteorol.*, 41(6):674–685.

Braud, I., P. Breil, F. Thollet, M. Lagouy, F. Branger, C. Jacqueminet, S. Kermadi, and K. Michel

2013. Evidence of the impact of urbanization on the hydrological regime of a medium-sized periurban catchment in france. *J. Hydrol.*, 485:5–23.

Brémaud, P. J. and Y. B. Pointin

1993. Forecasting heavy rainfall from rain cell motion using radar data. *J. Hydrol.*, 142(1):373–389.

Bringi, V. N. and V. Chandrasekar

2001. *Polarimetric Doppler weather radar: principles and applications*. Cambridge University Press.

Bringi, V. N., V. Chandrasekar, J. Hubbert, E. Gorgucci, W. L. Randeu, and M. Schoenhuber

2003. Raindrop size distribution in different climatic regimes from disdrometer and Dual-Polarized radar analysis. *J. Atmos. Sci.*, 60(2):354–365.

Bringi, V. N., M. Thurai, and R. Hannesen

2005. *Dual-Polarization Weather Radar Handbook*. Selex-Gematronik, Neuss, Germany,.

Browning, K. A.

1980. Review lecture: Local weather forecasting. *Proceedings of the Royal Society of London A: Mathematical, Physical and Engineering Sciences*, 371(1745):179–211.

Bruni, G., R. Reinoso, N. C. van de Giesen, F. H. L. R. Clemens, and J. A. E. ten Veldhuis

2015. On the sensitivity of urban hydrodynamic modelling to rainfall spatial and temporal resolution. *Hydrol. Earth Syst. Sci.*, 19(2):691–709.

Bruni, G., J. ten Veldhuis, T. Otto, and H. Leijnse

2012. TOWARDS THE USE OF X-BAND DUAL POLARIMETRIC RADAR RAINFALL ESTIMATES IN URBAN HYDROLOGY.

Burlando, P., A. Montanari, and R. Ranzi

1996. Forecasting of storm rainfall by combined use of radar, rain gages and linear models. *Atmos. Res.*, 42(1–4):199–216.

Butts, M. B., J. T. Payne, M. Kristensen, and H. Madsen

2004. An evaluation of the impact of model structure on hydrological modelling uncertainty for streamflow simulation. *J. Hydrol.*

Chandrasekar, V.

1987. *Some Uncertainties in the Multiparameter Radar Measurement of Rainfall.*

Chandrasekar, V. and V. N. Bringi

1988. Error structure of multiparameter radar and surface measurements of rainfall part II: X-Band attenuation. *J. Atmos. Ocean. Technol.*, 5(6):796–802.

Chen, D., T. Ou, L. Gong, C.-Y. Xu, W. Li, C.-H. Ho, and W. Qian

2010. Spatial interpolation of daily precipitation in china: 1951–2005. *Adv. Atmos. Sci.*, 27(6):1221–1232.

Chen, X., C. Tian, X. Meng, Q. Xu, G. Cui, Q. Zhang, and L. Xiang

2015. Analyzing the effect of urbanization on flood characteristics at catchment levels. *Proc. IAHS*, 370:33–38.

Chow, V. T.

1964. Handbook of applied hydrology.

Ciach, G. J.

2003a. Local random errors in Tipping-Bucket rain gauge measurements. *J. Atmos. Ocean. Technol.*, 20(5):752–759.

Ciach, G. J.

2003b. Local random errors in Tipping-Bucket rain gauge measurements. *J. Atmos. Ocean. Technol.*, 20(5):752–759.

Ciach, G. J. and W. F. Krajewski

1999. Radar-rain gauge comparisons under observational uncertainties. *J. Appl. Meteorol.*, 38(10):1519–1525.

Clark, R. H., I. C. on Irrigation, and Drainage

1981. *Flood Control in Relation to Land Use Planning and Water Management.*

Crichton, D.

2007. What can cities do to increase resilience? *Philosophical Transactions of the Royal Society of London A: Mathematical, Physical and Engineering Sciences*, 365(1860):2731–2739.

Cyr, I.

2014. *Estimation of Z-R relationship and comparative analysis of precipitation data from colocated rain-gauge, vertical radar and disdrometer.* PhD thesis.

Daniel, E. B., J. V. Camp, E. J. LeBoeuf, J. R. Penrod, J. P. Dobbins, and M. D. Abkowitz

2011. Watershed modeling and its applications: A state-of-the-art review. *Open Hydrology Journal*, 5(2).

Dasgupta, S., A. Zaman, S. Roy, M. Huq, S. Jahan, and A. Nishat

2015. *Urban Flooding of Greater Dhaka in a Changing Climate: Building Local Resilience to Disaster Risk.* World Bank Publications.

Dehotin, J. and I. Braud

2008. Which spatial discretization for distributed hydrological models? proposition of

a methodology and illustration for medium to large-scale catchments. *Hydrol. Earth Syst. Sci. Discuss.*, 12(3):769–796.

Deletic, A., C. B. S. Dotto, D. T. McCarthy, M. Kleidorfer, G. Freni, G. Mannina, M. Uhl, M. Henrichs, T. D. Fletcher, W. Rauch, J. L. Bertrand-Krajewski, and S. Tait
2012. Assessing uncertainties in urban drainage models. *Physics and Chemistry of the Earth, Parts A/B/C*, 42–44:3–10.

Delrieu, G., H. Andrieu, and J. D. Creutin
2000. Quantification of Path-Integrated attenuation for X- and C-Band weather radar systems operating in mediterranean heavy rainfall. *J. Appl. Meteorol.*, 39(6):840–850.

Dimitriadis, P. and D. Koutsoyiannis
2015. Climacogram versus autocovariance and power spectrum in stochastic modelling for markovian and Hurst–Kolmogorov processes. *Stoch. Environ. Res. Risk Assess.*, Pp. 1–21.

Easterling, D. R.
2008. Observed changes in the global distribution of daily temperature and precipitation extremes. In *Climate Extremes and Society*, H. F. Diaz, R. J. Murnane, H. F. Diaz, and R. J. Murnane, eds., Pp. 24–34, Cambridge. Cambridge University Press.

Easterling, D. R., J. L. Evans, P. Y. Groisman, T. R. Karl, K. E. Kunkel, and P. Ambenje
2000. Observed variability and trends in extreme climate events: A brief review*. *Bull. Am. Meteorol. Soc.*, 81(3):417–425.

Eccles, P. J. and E. A. Mueller
1971. X-Band attenuation and liquid water content estimation by a Dual-Wavelength radar. *J. Appl. Meteorol.*, 10(6):1252–1259.

Einfalt, T.
1988. *Recherche d'une méthode optimale de prévision de pluie par radar en hydrologie urbaine.* PhD thesis, Ecole Nationale des Ponts et Chaussées.

Einfalt, T., K. Arnbjerg-Nielsen, C. Golz, N.-E. Jensen, M. Quirmbach, G. Vaes, and B. Vieux
2004. Towards a roadmap for use of radar rainfall data in urban drainage. *J. Hydrol.*, 299(3–4):186–202.

Einfalt, T., T. Denoeux, and G. Jacquet

1990. A radar rainfall forecasting method designed for hydrological purposes. *J. Hydrol.*, 114(3–4):229–244.

El-Kadi, A. I., P. K. M. van der Heijde, I. G. W. M. Center, H. R. Institute, T.-D. I. of Applied Geoscience, and B. University

1983. *A Review of Infiltration Models: Identification and Evaluation*, IGWMC ground water modeling reprints. International Ground Water Modeling Center, Holcomb Research Institute.

Elektra, S. P.

2016. Modelisation hydrologique de bassin urbain a haute resolution. Technical report, AgropariTech.

Elliott, A. H. and S. A. Trowsdale

2007. A review of models for low impact urban stormwater drainage. *Environmental Modelling & Software*, 22(3):394–405.

Ellis, J. B.

2013. Sustainable surface water management and green infrastructure in UK urban catchment planning. *J. Environ. Planning Manage.*, 56(1):24–41.

Ellis, J. B. and D. M. Revitt

2010. The management of urban surface water drainage in england and wales. *Water Environ. J.*, 24(1):1–8.

Emmanuel, I., H. Andrieu, and P. Tabary

2012. Evaluation of the new french operational weather radar product for the field of urban hydrology. *Atmos. Res.*, 103(0):20–32.

Emmanuel, I., E. Leblois, H. Andrieu, and B. Flahaut

2011. Variabilité spatio-temporelle des précipitations aux échelles de l'hydrologie urbaine. *La Houille Blanche*, (4):31–36.

England, Jr., J. F., M. L. Velleux, and P. Y. Julien

2007. Two-dimensional simulations of extreme floods on a large watershed. *J. Hydrol.*, 347(1–2):229–241.

English, M., B. Kochtubajda, F. D. Barlow, A. R. Holt, and R. McGuinness

1991. Radar measurement of rainfall by differential propagation phase: A pilot experiment. *Atmosphere-Ocean*, 29(2):357–380.

Fankhauser, R.

1997. Measurement properties of tipping bucket rain gauges and their influence on urban runoff simulation. *Water Sci. Technol.*, 36(8-9):7–12.

Fankhauser, R.

1998. Influence of systematic errors from tipping bucket rain gauges on recorded rainfall data. *Water Sci. Technol.*, 37(11):121–129.

Feder, J.

1988. Fractals plenum press new york 283.

Ferreira Carneiro, P. R. and M. Gomes

2012. A flood control approach integrated with a sustainable land use planning in metropolitan regions. In *Environmental Land Use Planning*, S. Appiah-Opoku, ed. InTech.

Figueras i Ventura, J., A.-A. Boumahmoud, B. Fradon, P. Dupuy, and P. Tabary

2012. Long-term monitoring of french polarimetric radar data quality and evaluation of several polarimetric quantitative precipitation estimators in ideal conditions for operational implementation at c-band. *Q.J.R. Meteorol. Soc.*, 138(669):2212–2228.

Figueras i Ventura, J. and P. Tabary

2013. The new french operational polarimetric radar rainfall rate product. *J. Appl. Meteorol. Climatol.*, 52(8):1817–1835.

Fišer, O.

2004. ZR (radar Reflectivity-Rain rate) relationships derived from czech distrometer data. In *Proceedings of ERAD*, volume 233.

Förster, M., D. Thévenot, G. Geldof, G. Svensson, P. S. Mikkelsen, M. Revitt, E. Aftias, J. Krejcik, H. Sieker, M. Legret, and Others

2004. Urban stormwater source control management in european countries: DayWater project. In *Conference internationale sur les nouvelles technologies en assainissement pluvial*. cat.inist.fr.

Frankhauser, P.

1998. The fractal approach. a new tool for the spatial analysis of urban agglomerations. *Population: An English Selection*, 10(1):205–240.

French, M. M., H. B. Bluestein, D. C. Dowell, L. J. Wicker, M. R. Kramar, and A. L. Pazmany

2008. High-Resolution, mobile doppler radar observations of cyclic mesocyclogenesis in a supercell. *Mon. Weather Rev.*, 136(12):4997–5016.

Gebremichael, M., T. M. Over, and W. F. Krajewski

2006. Comparison of the scaling characteristics of rainfall derived from Space-Based and Ground-Based radar observations. *J. Hydrometeorol.*, 7(6):1277–1294.

Germann, U. and I. Zawadzki

2002. Scale-Dependence of the predictability of precipitation from continental radar images. part i: Description of the methodology. *Mon. Weather Rev.*, 130(12):2859–2873.

Giangola-Murzyn, A.

2013. *Modelisation et parametrisation hydrologique de la ville, resilience aux inondations*. PhD thesis, Université Paris-Est.

Gires, A., A. Giangola-Murzyn, J.-B. Abbes, I. Tchiguirinskaia, D. Schertzer, and S. Lovejoy

2015. Impacts of small scale rainfall variability in urban areas: a case study with 1D and 1D/2D hydrological models in a multifractal framework. *Urban Water J.*, 12(8):607–617.

Gires, A., S. Ochoa Rodriguez, J. Van Assel, G. Bruni, D. Murla Tulys, L. Wang, R. Pina, J. Richard, A. Ichiba, P. Willems, I. Tchiguirinskaia, M. C. ten Veldhuis, and D. J. M. Schertzer

2014a. Fractal analysis of urban environment: land use and sewer system. *AGU Fall Meeting Abstracts*.

Gires, A., C. Onof, C. Maksimovic, D. Schertzer, I. Tchiguirinskaia, and N. Simoes

2012a. Quantifying the impact of small scale unmeasured rainfall variability on urban runoff through multifractal downscaling: A case study. *J. Hydrol.*, 442–443:117–128.

Gires, A., D. Schertzer, I. Tchiguirinskaia, S. Lovejoy, C. Onof, C. Maksimovic, and N. Simoes

2011a. Impact of small scale rainfall uncertainty on urban discharge forecasts. *Weather radar and hydrology*, 400:400–406.

Gires, A., I. Tchiguirinskaia, D. Schertzer, and S. Lovejoy

2011b. Analyses multifractales et spatio-temporelles des precipitations du modele meso-nh et des donnees radar. *Hydrological Sciences Journal–Journal des Sciences Hydrologiques*, 56(3):380–396.

Gires, A., I. Tchiguirinskaia, D. Schertzer, and S. Lovejoy

2012b. Influence of the zero-rainfall on the assessment of the multifractal parameters. *Adv. Water Resour.*, 45(0):13–25.

Gires, A., I. Tchiguirinskaia, D. Schertzer, and S. Lovejoy

2013. Multifractal analysis of a semi-distributed urban hydrological model. *Urban Water J.*, 10(3):195–208.

Gires, A., I. Tchiguirinskaia, D. Schertzer, A. Schellart, A. Berne, and S. Lovejoy

2014b. Influence of small scale rainfall variability on standard comparison tools between radar and rain gauge data. *Atmos. Res.*, 138(0):125–138.

Girons Lopez, M., H. Wennerström, L.-A. Nordén, and J. Seibert

2015. Location and density of rain gauges for the estimation of spatial varying precipitation. *Geogr. Ann. Ser. A. Phys. Geogr.*, 97(1):167–179.

Goodrich, D. C., J.-M. Faurès, D. A. Woolhiser, L. J. Lane, and S. Sorooshian

1995. Measurement and analysis of small-scale convective storm rainfall variability. *J. Hydrol.*, 173(1–4):283–308.

Goonetilleke, A., E. Thomas, S. Ginn, and D. Gilbert

2005. Understanding the role of land use in urban stormwater quality management. *J. Environ. Manage.*, 74(1):31–42.

Groisman, P. Y. and R. W. Knight

2008. Prolonged dry episodes over the conterminous united states: New tendencies emerging during the last 40 years. *J. Clim.*, 21(9):1850–1862.

Groisman, P. Y., R. W. Knight, D. R. Easterling, T. R. Karl, G. C. Hegerl, and V. N. Razuvaev

2005. Trends in intense precipitation in the climate record. *J. Clim.*, 18(9):1326–1350.

Gu, G., R. F. Adler, G. J. Huffman, and S. Curtis

2007. Tropical rainfall variability on Interannual-to-Interdecadal and longer time scales derived from the GPCP monthly product. *J. Clim.*, 20(15):4033–4046.

Gupta, H. V., H. Kling, K. K. Yilmaz, and G. F. Martinez

2009. Decomposition of the mean squared error and NSE performance criteria: Implications for improving hydrological modelling. *J. Hydrol.*, 377(1–2):80–91.

Gupta, K.

2007. Urban flood resilience planning and management and lessons for the future: a case study of mumbai, india. *Urban Water J.*, 4(3):183–194.

Haberlandt, U.

2011. Interpolation of precipitation for flood modelling. In *Flood Risk Assessment and Management*, Pp. 35–52. Springer Netherlands.

Habib, E., W. Krajewski, and A. Kruger

2001. Sampling errors of Tipping-Bucket rain gauge measurements. *J. Hydrol. Eng.*, 6(2):159–166.

Habib, E. H., E. A. Meselhe, and A. V. Aduvala

2008. Effect of local errors of Tipping-Bucket rain gauges on Rainfall-Runoff simulations. *J. Hydrol. Eng.*, 13(6):488–496.

Halsey, T. C., M. H. Jensen, L. P. Kadanoff, I. Procaccia, and B. Shraiman

1986. Fractal measures and their singularities: the characterization of strange sets. *Physical Review A*, 33:1141–1151.

Hamilton, P. M.

1960. *Radar Attenuation Estimates from Rain-gauge Statistics*, McGill theses. publisher not identified.

Hardy, R. J., P. D. Bates, and M. G. Anderson

1999. The importance of spatial resolution in hydraulic models for floodplain environments. *J. Hydrol.*, 216(1–2):124–136.

He, S., S. V. Raghavan, N. S. Nguyen, and S.-Y. Liong

2013. Ensemble rainfall forecasting with numerical weather prediction and radar-based nowcasting models. *Hydrol. Process.*, 27(11):1560–1571.

Healy, R. W.

1990. *Simulation of solute transport in variably saturated porous media with supplemental information on modifications to the US Geological Survey's computer program VS2D.* Department of the Interior, US Geological Survey.

Heber Green, W. and G. A. Ampt

1911. Studies on soil phyics. *J. Agric. Sci.*, 4(01):1–24.

Hentschel, H. G. E. and I. Procaccia

1984. Relative diffusion in turbulent media: the fractal dimension of clouds. *Physical Review A*, Pp. 1461–1470.

Hitschfeld, W. and J. Bordan

1954. ERRORS INHERENT IN THE RADAR MEASUREMENT OF RAINFALL AT ATTENUATING WAVELENGTHS. *J. Meteorol.*, 11(1):58–67.

Hoang, C. T., I. Tchiguirinskaia, D. Schertzer, P. Arnaud, P. Laveau, and S. Lovejoy

2012. Assessing the high frequency quality of long rainfall series. *Journal of Hydrology*, 438-439:39–51.

Hoang, C.-T., I. Tchiguirinskaia, D. Schertzer, and S. Lovejoy

2014. Caracteristiques multifractales et extremes de la precipitation a haute resolution, application a la detection du changement climatique. *Revue des sciences de l'eau*, 27(3):205.

Hollis, G. E.

1975. The effect of urbanization on floods of different recurrence interval. *Water Resour. Res.*, 11(3):431–435.

Hossain, F., E. N. Anagnostou, T. Dinku, and M. Borga

2004. Hydrological model sensitivity to parameter and radar rainfall estimation uncertainty. *Hydrol. Process.*, 18(17):3277–3291.

Hromadka, II, T. V.

1987. The state-of-the-art in hydrologic models. *Environmental Software*, 2(1):29–36.

Hubbert, J. C., M. Dixon, and S. M. Ellis

2009. Weather radar ground clutter. part II: Real-Time identification and filtering. *J. Atmos. Ocean. Technol.*, 26(7):1181–1197.

Hubert, P., Y. Tessier, S. Lovejoy, D. Schertzer, F. Schmitt, P. Ladoy, J. P. Carbonnel, S. Violette, and I. Desurosne

1993. Multifractals and extreme rainfall events. *Geophys. Res. Lett.*, 20(10):931–934.

Huffman, G. J., R. F. Adler, D. T. Bolvin, and G. Gu

2009. Improving the global precipitation record: GPCP version 2.1. *Geophys. Res. Lett.*, 36(17).

Humphrey, M. D., J. D. Istok, J. Y. Lee, J. A. Hevesi, and A. L. Flint

1997. A new method for automated dynamic calibration of Tipping-Bucket rain gauges. *J. Atmos. Ocean. Technol.*, 14(6):1513–1519.

Illingworth, A. J. and T. M. Blackman

2002. The need to represent raindrop size spectra as normalized gamma distributions for the interpretation of polarization radar observations. *J. Appl. Meteorol.*, 41(3):286–297.

Insa-Valor, S.

1999. Canoe: logiciel d'hydrologie urbaine, conception et evaluation de reseaux d'assainissement, simulation des pluies, des ecoulements et de la qualite des eaux. *Manuel de l'utilisateur*.

James, W., L. A. Rossman, and W. R. C. James

2010. User's guide to SWMM 5:[based on original USEPA SWMM documentation].

Jha, A. K., R. Bloch, and J. Lamond

2012. *Cities and flooding: a guide to integrated urban flood risk management for the 21st century*. World Bank Publications.

Jiang, S., J. Shiguo, and L. Desheng

2012. Box-Counting dimension of fractal urban form. *International Journal of Artificial Life Research*, 3(3):41–63.

Jongman, B., S. Hochrainer-Stigler, L. Feyen, J. C. J. H. Aerts, R. Mechler, W. J. W. Botzen, L. M. Bouwer, G. Pflug, R. Rojas, and P. J. Ward

2014. Increasing stress on disaster-risk finance due to large floods. *Nat. Clim. Chang.*, 4(4):264–268.

Kaika, M.

2003. The water framework directive: A new directive for a changing social, political and economic european framework. *European Planning Studies*, 11(3):299–316.

Kang, I. S., J. I. Park, and V. P. Singh

1998. Effect of urbanization on runoff characteristics of the On-Cheon stream watershed in pusan, korea. *Hydrol. Process.*, 12(2):351–363.

Karl, T. R. and K. E. Trenberth

2003. Modern global climate change. *Science*, 302(5651):1719–1723.

Khakbaz, B., B. Imam, K. Hsu, and S. Sorooshian

2012. From lumped to distributed via semi-distributed: Calibration strategies for semi-distributed hydrologic models. *J. Hydrol.*, 418–419:61–77.

Kittinger, C., E. Marth, F. F. Reinthaler, G. Zarfel, F. Pichler-Semmelrock, W. Mascher, G. Mascher, and F. Mascher

2013. Water quality assessment of a central european river — does the directive 2000/60/EC cover all the needs for a comprehensive classification? *Sci. Total Environ.*, 447:424–429.

Klein Tank, A. and G. P. Können

2003. Trends in indices of daily temperature and precipitation extremes in europe, 1946-99. *J. Clim.*, 16(22):3665–3680.

Knoche, M., C. Fischer, E. Pohl, P. Krause, and R. Merz

2014. Combined uncertainty of hydrological model complexity and satellite-based forcing data evaluated in two data-scarce semi-arid catchments in ethiopia. *J. Hydrol.*, 519, Part B:2049–2066.

Knowles, N., M. D. Dettinger, and D. R. Cayan

2006. Trends in snowfall versus rainfall in the western united states. *J. Clim.*, 19(18):4545–4559.

Krajewski, W. F., B. Vignal, B.-C. Seo, and G. Villarini

2011. Statistical model of the range-dependent error in radar-rainfall estimates due to the vertical profile of reflectivity. *J. Hydrol.*, 402(3–4):306–316.

Krajewski, W. F., G. Villarini, and J. A. Smith

2010a. RADAR-Rainfall uncertainties. *Bull. Am. Meteorol. Soc.*, 91(1):87–94.

Krajewski, W. F., G. Villarini, and J. A. Smith

2010b. Radar-rainfall uncertainties: Where are we after thirty years of effort? *Bull. Am. Meteorol. Soc.*, 91(1):87–94.

Kyznarová, H. and P. Novák

2009. CELLTRACK—Convective cell tracking algorithm and its use for deriving life cycle characteristics. *Atmos. Res.*, 93(1):317–327.

Labat, D., C.-T. Hoang, J. Masbou, A. Mangin, I. Tchiguirinskaia, S. Lovejoy, and D. Schertzer

2013. Multifractal behaviour of long term karstic discharge fluctuations. *Hydrological Processes*, 27(25):3708–3717.

Lahaie, P. and M. Lecours

. Attenuation by rain at 30 GHz: relationship between weather radar echoes and microwave attenuation. In *Proceedings 1995 Canadian Conference on Electrical and Computer Engineering*, volume 2, Pp. 897–900. IEEE.

Lang, T. J., S. W. Nesbitt, and L. D. Carey

2009. On the correction of partial beam blockage in polarimetric radar data. *J. Atmos. Ocean. Technol.*, 26(5):943–957.

Lappala, E. G., R. W. Healy, E. P. Weeks, and Others

1987. *Documentation of computer program VS2D to solve the equations of fluid flow in variably saturated porous media*. Department of the Interior, US Geological Survey.

Lavallée, D., S. Lovejoy, D. Schertzer, and P. Ladoy

1993. Nonlinear variability and landscape topography: analysis and simulation. *Fractals in geography*, Pp. 171–205.

Lavallée, D., S. Lovejoy, D. Schertzer, and F. Schmitt

1992. On the determination of universal multifracal parameters in turbulence. In

Topological aspects of the dynamics of fluids and plasmas, K. Moffat, M. Tabor, and G. Zalslavsky, eds., Pp. 463–478. Kluwer.

Lee, H., D. Balin, and M. Rode.

. Sensitivity analysis of rainfall uncertainties in rainfall runoff model - extended GLUE concept.

Lee, J.

2000. Characterization of urban stormwater runoff. *Water Res.*, 34(6):1773–1780.

Legates, D. R. and C. J. Willmott

1990. Mean seasonal and spatial variability in gauge-corrected, global precipitation. *Int. J. Climatol.*, 10(2):111–127.

Li, R.-M., D. B. Simons, and M. A. Stevens

1976. Solutions to green amptinfiltration equation. *Journal of the Irrigation and Drainage Division*, 102(2):239–248.

Li, Z., Q. Shao, Z. Xu, and X. Cai

2010. Analysis of parameter uncertainty in semi-distributed hydrological models using bootstrap method: A case study of SWAT model applied to yingluoxia watershed in northwest china. *J. Hydrol.*, 385(1–4):76–83.

Lilley, M., S. Lovejoy, N. Desaulnier-Soucy, and D. Schertzer

2006. Multifractal large number of drops limit in rain. *J. Hydrology*, 328:20–37.

Lovejoy, S., M. Duncan, and D. Schertzer

1996. Scalar multifractal radar observer's problem. *J. Geophys. Res.*, 101(D21):26479–26492.

Lovejoy, S. and D. Schertzer

1990. Multifractals, universality classes and satellite and radar measurements of cloud and rain fields. *J. Geophys. Res.*, 95(D3):2021.

Lovejoy, S. and D. Schertzer

1992. Multifractals and Rain. In *New Uncertainty Concepts in Hydrology and Water Resources*, Z. W. Kunzewicz, ed., Pp. 62–103, Cambridge UK. Cambridge University Press.

Lovejoy, S. and D. Schertzer

2013. *The Weather and Climate: Emergent Laws and Multifractal Cascades.*, volume (in press). Cambridge U.K.: Cambridge Univeristy Press.

Lovejoy, S., D. Schertzer, and V. Allaire

2008. The remarkable wide range spatial scaling of TRMM precipitation,. *J. Atmos. Research,*, 90:10–32.

Löwe, R., S. Thorndahl, P. S. Mikkelsen, M. R. Rasmussen, and H. Madsen

2014. Probabilistic online runoff forecasting for urban catchments using inputs from rain gauges as well as statically and dynamically adjusted weather radar. *J. Hydrol.*, 512:397–407.

Luyckx, G. and J. Berlamont

2001. Simplified method to correct rainfall measurements from tipping bucket rain gauges. In *Urban Drainage Modeling*, Pp. 767–776, Reston, VA. American Society of Civil Engineers.

Macor, J., D. Schertzer, and S. Lovejoy

2007a. Méthodes multifractales appliquées à la prévision de pluie en utilisant des données radar. *La Houille Blanche*, (4):92–98.

Macor, J., D. Schertzer, and S. Lovejoy

2007b. Multifractal methods applied to rain forecast using radar data. *HOUILLE BLANCHE-REVUE INTERNATIONALE DE L'EAU*, (4):92–98.

Macor, J. L.

2007. *Developpement de techniques de prevision de pluie basees sur les proprietes multi-echelles des donnees radar et satellites.* PhD thesis, Ecole des Ponts ParisTech.

Makepeace, D. K., D. W. Smith, and S. J. Stanley

1995. Urban stormwater quality: Summary of contaminant data. *Crit. Rev. Environ. Sci. Technol.*, 25(2):93–139.

Mandapaka, P. V., U. Germann, L. Panziera, and A. Hering

2012. Can lagrangian extrapolation of radar fields be used for precipitation nowcasting over complex alpine orography? *Weather Forecast.*, 27(1):28–49.

Mandelbrot, B.

1967. How long is the coast of britain? statistical self-similarity and fractional dimension. *Science*, 156(3775):636–638.

Mandelbrot, B.

1977. Fractals form, chance, and dimension, WH freeman and co. *San Francisco MATH.*

Mandelbrot, B. B.

1983. *The fractal geometry of nature*, volume 173. Macmillan.

Mandelbrot, B. B.

1989. Multifractal measures, especially for the geophysicist. *Pure and Applied Geophysics*, 131(1-2):5–42.

Mapiam, P. P. and N. Sriwongsitanon

2008. Climatological ZR relationship for radar rainfall estimation in the upper ping river basin. *Sci. Asia.*, 34(2):215–222.

Marquis, J., Y. Richardson, J. Wurman, and P. Markowski

2008. Single- and Dual-Doppler analysis of a tornadic vortex and surrounding Storm-Scale flow in the crowell, texas, supercell of 30 april 2000. *Mon. Weather Rev.*, 136(12):5017–5043.

Marsan, D., D. Schertzer, and S. Lovejoy

1996. Causal space-time multifractal processes: Predictability and forecasting of rain fields. *J. Geophy. Res.*, 101(D21):26,326–333,346.

Marshall, J. S. and W. M. K. Palmer

1948. THE DISTRIBUTION OF RAINDROPS WITH SIZE. *J. Meteorol.*, 5(4):165–166.

Martin, C., Y. Ruperd, and M. Legret

2007. Urban stormwater drainage management: The development of a multicriteria decision aid approach for best management practices. *Eur. J. Oper. Res.*, 181(1):338–349.

Mc Cuen, R. H., Z. Knight, and A. Gillian Cutter

2006. Evaluation of the Nash–Sutcliffe efficiency index. *J. Hydrol. Eng.*, 11(6):597–602.

McMillan, H., T. Krueger, and J. Freer

2012. Benchmarking observational uncertainties for hydrology: rainfall, river discharge and water quality. *Hydrol. Process.*, 26(26):4078–4111.

Mecklenburg, S., J. Joss, and W. Schmid

2000. Improving the nowcasting of precipitation in an alpine region with an enhanced radar echo tracking algorithm. *J. Hydrol.*, 239(1-4):46–68.

Merz, R. and G. Blöschl

2004. Regionalisation of catchment model parameters. *J. Hydrol.*, 287(1–4):95–123.

Mesev, T. V., P. A. Longley, M. Batty, and Y. Xie

1995. Morphology from imagery: Detecting and measuring the density of urban land use. *Environment and Planning A*, 27(5):759–780.

Messer, H., A. Zinevich, and P. Alpert

2006. Environmental monitoring by wireless communication networks. *Science*, 312(5774):713.

Milly, P. C. D., R. T. Wetherald, K. A. Dunne, and T. L. Delworth

2002. Increasing risk of great floods in a changing climate. *Nature*, 415(6871):514–517.

Moberg, A., P. D. Jones, D. Lister, A. Walther, M. Brunet, J. Jacobeit, L. V. Alexander, P. M. Della-Marta, J. Luterbacher, P. Yiou, D. Chen, A. M. G. Klein Tank, O. Saladié, J. Sigró, E. Aguilar, H. Alexandersson, C. Almarza, I. Auer, M. Barriendos, M. Begert, H. Bergström, R. Böhm, C. J. Butler, J. Caesar, A. Drebs, D. Founda, F.-W. Gerstengarbe, G. Micela, M. Maugeri, H. Österle, K. Pandzic, M. Petrakis, L. Srnec, R. Tolasz, H. Tuomenvirta, P. C. Werner, H. Linderholm, A. Philipp, H. Wanner, and E. Xoplaki

2006. Indices for daily temperature and precipitation extremes in europe analyzed for the period 1901–2000. *J. Geophys. Res.*, 111(D22).

Mote, P. W.

2003. Trends in snow water equivalent in the pacific northwest and their climatic causes. *Geophys. Res. Lett.*

Mulholland, M. and W. N. Z. . E. Waikato

2006. *The Effect of Land Use Change on the Flood Hydrology of Pumice Catchments*, Environment Waikato technical report. Environment Waikato.

Multi-Hydro

. Multi-Hydro. *protected by the Agence de Protection des Programmes (French Agency for software protection). Official number: IDDN FR 001 340017 000 S C 2015 0000 31235.*

Nardi, F., A. Annis, and C. Biscarini

2015. On the impact of urbanization on flood hydrology of small ungauged basins: the case study of the tiber river tributary network within the city of rome. *J. Flood Risk Manage.*

Nash, J. E. and J. V. Sutcliffe

1970. River flow forecasting through conceptual models part I — a discussion of principles. *J. Hydrol.*, 10(3):282–290.

Neumann, A.

1991. *Introduction d'outils de l'intelligence artificielle dans la prévision de pluie par radar.* PhD thesis, Ecole Nationale des Ponts et Chaussées.

Nešpor, V. and B. Sevruk

1999. Estimation of Wind-Induced error of rainfall gauge measurements using a numerical simulation. *J. Atmos. Ocean. Technol.*, 16(4):450–464.

Newson, M.

1991. Catchment control and planning. *Land use policy*, 8(1):9–15.

Niemczynowicz, J.

1999. Urban hydrology and water management ± present and future challenges. *Urban Water*, 1:1–14.

Novák, P., L. Březková, and P. Frolík

2009. Quantitative precipitation forecast using radar echo extrapolation. *Atmos. Res.*, 93(1–3):328–334.

Nykanen, D. K.

2008. Linkages between orographic forcing and the scaling properties of convective rainfall in mountainous regions. *J. Hydrometeorol.*, 9(3):327–347.

Nystuen, J. A., J. R. Proni, P. G. Black, and J. C. Wilkerson

1996. A comparison of automatic rain gauges. *J. Atmos. Ocean. Technol.*, 13(1):62–73.

Ochoa-Rodriguez, S., L.-P. Wang, A. Gires, R. D. Pina, R. Reinoso-Rondinel, G. Bruni, A. Ichiba, S. Gaitan, E. Cristiano, J. van Assel, S. Kroll, D. Murlà-Tuyls, B. Tisserand, D. Schertzer, I. Tchiguirinskaia, C. Onof, P. Willems, and M.-C. ten Veldhuis

. Impact of spatial and temporal resolution of rainfall inputs on urban hydrodynamic modelling outputs: A multi-catchment investigation. *J. Hydrol.*, (0).

O'connell, E., J. Ewen, and G. O'donnell

2010. Strategic overview of land use management in the context of catchment flood risk management planning. In *Flood Risk Science and Management*, Pp. 17–38. Wiley-Blackwell.

Ostrowski, M. W.

2002. Modeling urban hydrological processes and management scenarios at different temporal and spatial scales. *Best Modeling Practices for Urban Water Systems, Monograph*, 10:27.

Otto, T. and H. W. J. Russchenberg

2010. Attenuation correction for a high-resolution polarimetric x-band weather radar. *Adv. Radio Sci.*, 8:279–284.

Pandey, G., S. Lovejoy, and D. Schertzer

1998. Multifractal Analysis Including Extremes of Daily River Flow Series for Basins one to a million square kilomemeters. *J. Hydrology*, 208(1-2):62–81.

Parisi, G. and U. Frisch

1985. On the singularity structure of fully developed turbulence. In *Turbulence and predictability in geophysical fluid dynamics and climate dynamics*, M. Ghil, R. Benzi, and G. Parisi, eds., Pp. 84–88, Amsterdam. North Holland.

Pecknold, S., S. Lovejoy, and D. Schertzer

1996. The morphology and texture of anisotropic multifractals using generalized

scale invariance. In *Stochastic Models in Geosystems*, W. A. Woyczynski and S. S. Molchanov, eds., Pp. 269–311, New-York. Springer-Verlag.

Pessoa, M. L., R. L. Bras, and E. R. Williams

1993. Use of weather radar for flood forecasting in the sieve river basin: A sensitivity analysis. *J. Appl. Meteorol.*, 32(3):462–475.

Peterson, T. C., M. A. Taylor, R. Demeritte, D. L. Duncombe, S. Burton, F. Thompson, A. Porter, M. Mercedes, E. Villegas, R. Semexant Fils, A. Klein Tank, A. Martis, R. Warner, A. Joyette, W. Mills, L. Alexander, and B. Gleason

2002. Recent changes in climate extremes in the caribbean region. *J. Geophys. Res.*, 107(D21):4601.

Pflug, K., S. Lovejoy, and D. Schertzer

1992. Generalized Scale Invariance and differentially rotating cloud rariances. *Physica A*, 185(1-4):121–128.

Porter, E., A. Santorelli, and M. Popovic

. Measurement uncertainties in differential radar applied to breast imaging. In *2014 IEEE Sensors Applications Symposium (SAS)*, Pp. 6–10. IEEE.

Price, K., S. T. Purucker, S. R. Kraemer, J. E. Babendreier, and C. D. Knightes

2014. Comparison of radar and gauge precipitation data in watershed models across varying spatial and temporal scales. *Hydrol. Process.*, 28(9):3505–3520.

Puhakka, T.

1974. *On the Variability of the Z-R Relationship in Rainfall Related to Radar Echo Pattern*. University of Helsinki, Department of Meteorology.

Qureshi, A. A.

. MICROBIOLOGICAL STUDIES ON THE QUALITY OF URBAN STORMWATER RUNOFF IN SOUTHERN.

Raay, V. and V. P. Thevenet Leprevost Amelie, Jacquet Guy

2008. Procede et dispositif d'aide ala gestion en temps reel de risques d'inondations.

Radziejewski, M. and Z. W. Kundzewicz

1997. Fractal analysis of flow of the river warta. *J. Hydrol.*, 200(1-4):280–294.

Ramesh, A.

2013. *Response of Flood Events to Land Use and Climate Change: Analyzed by Hydrological and Statistical Modeling in Barcelonnette, France*, Springer Theses. Springer Netherlands.

Rawls, W. J., D. L. Brakensiek, and N. Miller

1983. Green and ampt infiltration parameters from soils data. *J. Hydraul. Eng.*

Refsgaard, J. C.

1997. Parameterisation, calibration and validation of distributed hydrological models. *J. Hydrol.*, 198(1–4):69–97.

Refsgaard, J. C. and J. Knudsen

1996. Operational validation and intercomparison of different types of hydrological models. *Water Resour. Res.*, 32(7):2189–2202.

Reyniers, d. M.

2008. Quantitative precipitation forecasts based on radar observations: principles, algorithms and operational systems.

Robinson, M., M. Scholz, N. Bastien, and J. Carfrae

2010. Classification of different sustainable flood retention basin types. *J. Environ. Sci.*, 22(6):898–903.

Rochester, R. E. L.

2010. *Uncertainty in hydrological modelling: a case study in the tern catchment, Shropshire, UK*. PhD thesis, UCL (University College London).

Rodriguez, F., H. Andrieu, and F. Morena

2008. A distributed hydrological model for urbanized areas–model development and application to case studies. *J. Hydrol.*, 351(3):268–287.

Rosenfeld, D.

1987. Objective method for analysis and tracking of convective cells as seen by radar. *J. Atmos. Ocean. Technol.*, 4(3):422–434.

Royer, J. F., Biaou, F. Chauvin, D. Schertzer, and S. Lovejoy

2008a. Multifractal analysis of the evolution of simulated precipitation over France in a climate scenario. *C.R. Geoscience*, 340(431-440).

Royer, J.-F., A. Biaou, F. Chauvin, D. Schertzer, and S. Lovejoy

2008b. Multifractal Analysis of Rainfall Change Over France in a Climate Scenario. In *American Geophysical Union, Fall Meeting 2008*, Pp. Ng33a–1216–Ng33a–1215, San Francisco, United States.

Sagar, B. S. D.

2004. Fractal dimension of non-network space of a catchment basin. *Geophys. Res. Lett.*, 31(12).

Salvadore, E., J. Bronders, and O. Batelaan

2015. Hydrological modelling of urbanized catchments: A review and future directions. *J. Hydrol.*, 529, Part 1:62–81.

Salvadori, G., D. Schertzer, and S. Lovejoy

2001. Multifractal objective analysis: conditioning and interpolation. *Stoch. Environ. Resear. and Risk Analysis*, 15(4):261–283.

Sánchez-Diezma, R., D. Sempere-Torres, G. Delrieu, I. Zawadzki, and M. i Ambiental

2001. P7. 5 AN IMPROVED METHODOLOGY FOR GROUND CLUTTER SUBSTITUTION BASED ON a PRE-CLASSIFICATION OF PRECIPITATION TYPES.

Sands, P. and P. a. Galizzi

2006. Directive 2000/60/EC of the european parliament and of the council of 23 october 2000 establishing a framework for community action in the field of water policy (*oj* l 327 22.12.2000 p. 1). Pp. 879–969.

Sarma, P. B. S., J. W. Delleur, and A. R. Rao

1973. Comparison of rainfall-runoff models for urban areas. *J. Hydrol.*, 18(3–4):329–347.

Sauvageot, H.

1994. Rainfall measurement by radar: a review. *Atmos. Res.*, 35(1):27–54.

Schellart, A. N. A., M. A. Rico-Ramirez, S. Liguori, and A. J. Saul

2009. QUANTITATIVE PRECIPITATION FORECASTING FOR a SMALL URBAN AREA: USE OF RADAR NOWCASTING.

Scherger, D. A. and J. A. Davis

1982. Control of stormwater runoff pollutant loads by a wetland and retention basin.

Schertzer, D., P. Bernardara, A. Biaou, I. Tchiguirinskaia, M. Lang, E. Sauquet, H. Bendjoudi, P. Hubert, S. Lovejoy, and J. M. Veysseire

2006. Extremes and multifractals in hydrology : results, validation and prospects. *Houille Blanche*, 5:112–119.

Schertzer, D. and S. Lovejoy

1983. On the Dimension of Atmospheric motions. In *6th Symposium Turbulence and Diffusion*, T. Tatsumi, ed., volume 5, Pp. 69–72, Amsterdam. Elsevier Science Publishers B. V.

Schertzer, D. and S. Lovejoy

1987a. Physical modeling and analysis of rain and clouds by anisotropic scaling multiplicative processes. *J. Geophys. Res. D: Atmos.*, 92(D8):9693–9714.

Schertzer, D. and S. Lovejoy

1987b. Physical modeling and analysis of rain and clouds by anisotropic scaling multiplicative processes. *J. Geophys. Res. D: Atmos.*, 92(D8):9693–9714.

Schertzer, D. and S. Lovejoy

1992. Hard and Soft Multifractal processes. *Physica A*, 185(1-4):187–194.

Schertzer, D. and S. Lovejoy

1997. Universal multifractals do exist!: Comments on "a statistical analysis of mesoscale rainfall as a random cascade". *J. Appl. Meteorol.*, 36(9):1296–1303.

Schertzer, D. and S. Lovejoy

2004. Space-time Complexity and Multifractal Predictability. *Physica A*, 338(1-2):173–186.

Schertzer, D. and S. Lovejoy

2011. Mulitfractals, generalized scale invariance and complexity in geophysics. *International Journal of Bifurcation and Chaos*, 21(12):3417–3456.

Schertzer, D., S. Lovejoy, and P. Hubert

2002a. An Introduction to Stochastic Multifractal Fields. In *ISFMA Symposium on Environmental Science and Engineering with related Mathematical Problems*, A. Ern and W. Liu, eds., volume 4, Pp. 106–179, Beijing. High Education Press.

Schertzer, D. and I. Tchiguirinskaia

2015. Multifractal vector fields and stochastic clifford algebra. *Chaos*, 25:123127.

Schertzer, D., I. Tchiguirinskaia, S. Lovejoy, and P. Hubert

2010. No monsters, no miracles: in nonlinear sciences hydrology is not an outlier! . *Hydrological Sciences Journal*, 55(6):965–979.

Schertzer, D., I. Tchiguirinskaia, S. Lovejoy, P. Hubert, and H. Bendjoudi

2002b. Which chaos in the rain-runoff process? *J. Hydrological Sciences*, 47(1):139–148.

Schilling, W.

1991a. Rainfall data for urban hydrology: what do we need? *Atmos. Res.*, 27(1–3):5–21.

Schilling, W.

1991b. Rainfall data for urban hydrology: what do we need? *Atmos. Res.*, 27(1–3):5–21.

Schulz, E. F. and C. S. U. D. of Civil Engineering

1976. *Research on the Effect of Urbanization on Flood Response.* Colorado State University.

Scolobig, A. and B. D. Marchi

. Dilemmas in land use planning in flood prone areas. In *Flood Risk Management: Research and Practice*, Pp. 1185–1192.

Scuri, S., M. Torrisi, M. Cocchioni, and A. Dell'Uomo

2006. The european water framework directive 2000/60/EC in the evaluation of the ecological status of watercourses. case study: the river chienti (central apennines, italy). *Acta Hydrochim. Hydrobiol.*, 34(5):498–505.

Sébastian, C., S. Barraud, C. Gonzalez-Merchan, Y. Perrodin, and R. Visiedo

2014. Stormwater retention basin efficiency regarding micropollutant loads and ecotoxicity. *Water Sci. Technol.*, 69(5):974–981.

Sebastianelli, S., F. Russo, F. Napolitano, and L. Baldini

2010. Comparison between radar and rain gauges data at different distances from radar

and correlation existing between the rainfall values in the adjacent pixels. *Hydrol. Earth Syst. Sci. Discuss.*, 7(4):5171–5212.

Sebastianelli, S., F. Russo, F. Napolitano, and L. Baldini

2013. On precipitation measurements collected by a weather radar and a rain gauge network. *Nat. Hazards Earth Syst. Sci.*, 13(3):605–623.

Seed, A. W.

2003. A dynamic and spatial scaling approach to advection forecasting. *J. Appl. Meteorol.*, 42(3):381–388.

Seliga, T. A. and V. N. Bringi

1978. Differential reflectivity and differential phase shift: Applications in radar meteorology. *Radio Sci.*, 13(2):271–275.

Seo, D.-J., J. Breidenbach, R. Fulton, D. Miller, and T. O'Bannon

2000. Real-Time adjustment of Range-Dependent biases in WSR-88D rainfall estimates due to nonuniform vertical profile of reflectivity. *J. Hydrometeorol.*, 1(3):222–240.

Serre, D., B. Barroca, and R. Laganier

2012. *Resilience and urban risk management*. CRC Press.

Sevruk, B. and W. R. Hamon

1984. *International comparison of national precipitation gauges with a reference pit gauge*. Secretariat of the World Meteorological Organization.

Snyder, J. C., H. B. Bluestein, G. Zhang, and S. J. Frasier

2010. Attenuation correction and hydrometeor classification of High-Resolution, x-band, Dual-Polarized mobile radar measurements in severe convective storms. *J. Atmos. Ocean. Technol.*, 27(12):1979–2001.

Sokol, Z.

2006. Nowcasting of 1-h precipitation using radar and NWP data. *J. Hydrol.*, 328(1–2):200–211.

Stransky, D., V. Bares, and P. Fatka

2007a. The effect of rainfall measurement uncertainties on rainfall–runoff processes modelling. *Water Sci. Technol.*, 55(4):103–111.

Stransky, D., V. Bares, and P. Fatka

2007b. The effect of rainfall measurement uncertainties on rainfall-runoff processes modelling. *Water Sci. Technol.*, 55(4):103–111.

Strecker, E., M. Quigley, B. Urbonas, J. Jones, J. Clary, and J. O'BRIEN

2004. Urban stormwater BMP performance: Recent findings from the international stormwater BMP database project. In *Conference internationale sur les nouvelles technologies en assainissement pluvial*. cat.inist.fr.

Su, Y.-S.

2015. Urban flood resilience: A chronology of policies to prevent flooding in taipei.

Sugier, J., J. P. du Chatelet, P. Roquain, and A. Smith

2002. Detection and removal of clutter and anaprop in radar data using a statistical scheme based on echo fluctuation. *Proceedings of ERAD (2002)*, Pp. 17–24.

Surfleet, C. G. and D. Tullos

2013. Uncertainty in hydrologic modelling for estimating hydrologic response due to climate change (santiam river, oregon). *Hydrol. Process.*, 27(25):3560–3576.

Tabary, P.

2007. The new french operational radar rainfall product. part i: Methodology. *Weather Forecast.*, 22(3):393–408.

Tabary, P., A.-A. Boumahmoud, H. Andrieu, R. J. Thompson, A. J. Illingworth, E. L. Bouar, and J. Testud

2011. Evaluation of two "integrated" polarimetric quantitative precipitation estimation (QPE) algorithms at c-band. *J. Hydrol.*, 405(3–4):248–260.

Tabary, P., J. Desplats, K. Do Khac, F. Eideliman, C. Gueguen, and J.-C. Heinrich

2007. The new french operational radar rainfall product. part II: Validation. *Weather Forecast.*, 22(3):409–427.

Tchiguirinskaia, I., D. Schertzer, and S. Lovjeoy

2014. *Multifractals and Physically Based Estimates of Extreme Floods*. CEATI International Inc.

Tech University of Darmstadt and M. Ostrowski

2002. Modeling urban hydrological processes and management scenarios at different temporal and spatial scales. *JWMM*.

ten Veldhuis, M.-C., S. Ochoa-Rodriguez, G. Bruni, A. Gires, J. Van Assel, L. Wang, R. Reinoso Rodinel, S. Kroll, D. Schertzer, C. Onof, and Others

2014. Weather radar for urban hydrological applications, lessons learnt and research needs identified from 4 pilots in North-West europe. In *International Symposium on Weather Radar and Hydrology*, Pp. 1–10.

Tessier, Y., S. Lovejoy, and D. Schertzer

1993. Universal multifractals: Theory and observations for rain and clouds. *J. Appl. Meteorol.*, 32(2):223–250.

THE EUROPEAN PARLIAMENT AND THE COUNCIL OF THE EUROPEAN UNION

2000. *Directive 2000/60/EC of the European Parliament and of the Council of 23 October 2000 Establishing a Framework for Community Action in the Field of Water Policy*, Official Journal of the European Communities. Legislation. Office for Official Publications of the European Communities.

Thibault, S. and J. Crews

1995. The morphology and growth of urban technical networks: a fractal approach. *flux*, 11(19):17–30.

Travis, Q. B. and L. W. Mays

2008. Optimizing retention basin networks. *Journal of Water Resources Planning and Management*, 134(5):432–439.

Trenberth, K. E., P. D. Jones, P. Ambenje, R. Bojariu, D. Easterling, A. Klein, D. Tank, D. Parker, J. Renwick, F. Rahimzadeh, and Others

2007. Observations: Surface and atmospheric climate change, inclimate. *Change*.

Uijlenhoet, R.

2001. Raindrop size distributions and radar reflectivity–rain rate relationships for radar hydrology. *), Raindrop size distributions and radar reflectivity-rain rate relationships for radar hydrology*, 61:5–627.

United Nations

2014. World urbanization prospects: The 2014 revision, highlights (ST/ESA/SER.A/352).

Use, L.

. The morphology of urban.

Velleux, M. L., J. F. England, Jr, and P. Y. Julien

2008. TREX: spatially distributed model to assess watershed contaminant transport and fate. *Sci. Total Environ.*, 404(1):113–128.

Vignal, B. and W. F. Krajewski

2001. Large-Sample evaluation of two methods to correct Range-Dependent error for WSR-88D rainfall estimates. *J. Hydrometeorol.*, 2(5):490–504.

Villarini, G. and W. F. Krajewski

2010. Sensitivity studies of the models of Radar-Rainfall uncertainties. *J. Appl. Meteorol. Climatol.*, 49(2):288–309.

Villarini, G., F. Serinaldi, and W. F. Krajewski

2008. Modeling radar-rainfall estimation uncertainties using parametric and non-parametric approaches. *Adv. Water Resour.*, 31(12):1674–1686.

Vogl, S., P. Laux, W. Qiu, G. Mao, and H. Kunstmann

2012. Copula-based assimilation of radar and gauge information to derive bias corrected precipitation fields. *Hydrol. Earth Syst. Sci. Discuss.*, 9(1):937–982.

W. F. Geiger J. Marsalek W. J. Rawls F. C. Zuidema, C.

1987. Manual on drainage in urbanized areas; studies and reports in hydrology; vol.:43; 1987.

Wanyu Li, D. Willie, and V. Chandrasekar

. Attenuation statistics for X band radar design. In *Proceedings. 2005 IEEE International Geoscience and Remote Sensing Symposium, 2005. IGARSS '05.*, volume 7, Pp. 5077–5080. IEEE.

Wheater, H. S., C. Ballard, N. Bulygina, N. McIntyre, and B. M. Jackson

2012. Modelling environmental change: Quantification of impacts of land use and

land management change on UK flood risk. In *System Identification, Environmental Modelling, and Control System Design*, Pp. 449–481. Springer London.

Wibben, H. C.

1976. *Effects of Urbanization on Flood Characteristics in Nashville-Davidson County, Tennessee*, Water resources investigations - United States Geological Survey, Water Resources Division. U.S. Geological Survey, Water Resources Division.

Wilson, J. W. and E. A. Brandes

1979. Radar measurement of rainfall-a summary. *Bull. Am. Meteorol. Soc.*, 60(9):1048–1058.

WMO

2008. CIMO_Guide-7th_Edition-2008.pdf. Technical report.

Wood, S. J., D. A. Jones, and R. J. Moore

2000. Accuracy of rainfall measurement for scales of hydrological interest. *Hydrol. Earth Syst. Sci.*, 4(4):531–543.

Wu, H., Y. Sun, W. Shi, X. Chen, and D. Fu

2013. Examining the Satellite-Detected urban land use spatial patterns using multi-dimensional fractal dimension indices. *Remote Sensing*, 5(10):5152–5172.

Wu, J. and C. He

2009. Experimental and modeling investigation of sewage solids sedimentation based on particle size distribution and fractal dimension. *Int. J. Environ. Sci. Technol.*, 7(1):37–46.

Wu, S.-J., C.-T. Hsu, H.-C. Lien, and C.-H. Chang

2014. Modeling the effect of uncertainties in rainfall characteristics on flash flood warning based on rainfall thresholds. *Nat. Hazards*, 75(2):1677–1711.

Xu, H., C.-Y. Xu, H. Chen, Z. Zhang, and L. Li

2013. Assessing the influence of rain gauge density and distribution on hydrological model performance in a humid region of china. *J. Hydrol.*, 505:1–12.

Yang, D., B. E. Goodison, J. R. Metcalfe, V. S. Golubev, R. Bates, T. Pangburn, and C. L. Hanson

1998. Accuracy of NWS 8“ standard nonrecording precipitation gauge: Results and application of WMO intercomparison. *J. Atmos. Ocean. Technol.*, 15(1):54–68.

Yu, B., C. Ciesiolka, C. W. Rose, and K. J. Coughlan

1997. A note on sampling errors in the rainfall and runoff data collected using tipping bucket technology. *Trans. ASAE*, 40(5):1305–1309.

Yuter, S. E.

2003. RADAR — precipitation radar. In *Encyclopedia of Atmospheric Sciences*, Pp. 1833–1851. Elsevier.

Zhang, J., Y. Qi, K. Howard, C. Langston, and B. Kaney

2011. Radar quality index combined measure of beam blockage and VPR effects in a national network. In *Proc. Eighth Int. Symp. on Weather Radar and Hydrology*, Pp. 388–393.

Zhang, Y., T. Adams, and J. V. Bonta

2007. Subpixel-Scale rainfall variability and the effects on separation of radar and gauge rainfall errors. *J. Hydrometeorol.*, 8(6):1348–1363.